Thèse

Présentée pour obtenir le grade de docteur
de l'École Nationale Supérieure des Télécommunications

Spécialité : **Signal et Images**

par

Nadir Castañeda Palomino

Titre :

Géo-localisation et poursuite dans un réseau mobile

Soutenue le 4 juillet 2008 devant le jury composé de :

M. Philippe	LOUBATON	Président
M. Jean-François	GIOVANNELLI	Rapporteur
M. Randal	DOUC	Rapporteur
M. David	CULTRU	Examinateur
M. Eric	MOULINES	Directeur de thèse
M. Maurice	CHARBIT	Co-directeur de thèse

To Margarita, Rosa and Michel

Extrait

Nous proposons et évaluons des méthodes de localisation et de poursuite des cibles non-coopératives en exploitant des mesures passives réalisées sur leurs émissions. L'étude comporte ainsi deux grandes parties : la première concerne la localisation aussi bien de stations de base que de stations mobiles dans des systèmes de communication sans fil, la seconde s'intéresse à la poursuite d'une ou plusieurs cibles évoluant sur un réseau routier en présence de fouillis d'échos (clutter). Ce travail s'inscrit à la fois dans le développement d'algorithmes novateurs d'inférence statistique pour la localisation et l'utilisation du filtrage particulaire dans des situations où les contraintes des routes sont incorporées dans le modèle d'évolution de la cible. Ces thématiques sont explorées avec le souci constant de développer une méthodologie qui tient compte aussi bien des erreurs dans les mesures que des a priori sur le déplacement de cibles (cas de la poursuite). Le résultat de cette recherche a permis l'éclosion d'algorithmes robustes dont certains sont déjà utilisés à des fins industrielles.

Abstract

We propose and evaluate methods for the localization and tracking of non-cooperative targets from passive measurements of its radio emissions. This study is divided into two main parts: the first one concerns about the localization of mobile stations or base stations in wireless communication systems and the second one concerns about tracking a single or several targets moving along a road network in presence of clutter. More specifically, we propose novel algorithms based on statistical inference for the localization and use particle filters for the situations in which road constraints are incorporated into the dynamic model of the target. These issues are studied with the objective to propose a methodology able to take into account errors in the radio measurements as well as a priori information one may have about the target dynamics (tracking case). The result of this research has permitted the development of robust algorithms, some of which are already being used in the industry.

Acknowledgements

I would like to thank Eric MOULINES and Maurice CHARBIT, my advisors, for their support during this research.

I wish to thank all my friends for being with me all these years in France.

Of course, I am grateful to my mother and sisters for believing in me.

Finally, I would like to thank the "Consejo Nacional de Ciencia y Tecnología (CONACYT)" for its financial support to perform my doctoral studies in France, as well as the "Secretaría de Educación Pública (SEP)" for its financial aid.

Nadir

Contents

Extrait i

Abstract iii

Acknowledgements v

Contents vii

Résumé en Français xiii

General introduction 1

I Localization in radiocommunication systems 5

Introduction to part I 7

1 Measurement model 13
1.1 Localization system classification 13
1.1.1 Self-localization 14
1.1.2 Remote localization 14
1.2 Measurements and localization techniques 14
1.2.1 Time based techniques 15
1.2.2 Angle-Of arrival (AOA) 16
1.2.3 Received signal strength (RSS) 16
1.2.4 Hybrid techniques 17
1.3 Sources of error 17
1.3.1 Noise measurement 17
1.3.2 Multipath 19
1.3.3 Non-line-of-sight propagation 20
1.3.4 Systematic offsets 21
1.3.5 Quantization 22

1.4 Measurement model proposal 23
1.5 Parameter estimation via the EM algorithm 24
1.5.1 Expectation-Maximization algorithm outline 24
1.6 Conclusions 25

2 TABLA: Timing Advance-Based Localization Algorithm[1] 27
2.1 Problem statement 27
2.2 Preliminary study 28
2.2.1 Radio link 28
2.2.2 Timing Advance 29
2.2.3 Localization based on timing advance measurements . . 30
2.3 Proposed approach 33
2.3.1 Observation model 33
2.3.2 Likelihood of the observations 34
2.3.3 Identifiability 36
2.3.4 3D BS position estimation issue 36
2.3.5 Timing Advance-Based Localization Algorithm (TABLA) derivation 37
2.3.6 Initialization 41
2.3.7 Cramer-Rao bound (CRB) 43
2.4 Simulations results 46
2.4.1 Asymptotic confidence region 47
2.4.2 Effects of μ, σ, P_D on the BS position estimation . . . 47
2.4.3 Dependence on the MS trajectory 49
2.5 Real experiments 52
2.5.1 Measurement system description 52
2.5.2 Tests 52
2.6 Conclusions 54

3 ADABLA: Angle and Delay of Arrival-Based Localization Algorithm[1] 67
3.1 Problem statement 67
3.2 Preliminary study 68
3.2.1 Discrete Channel Model 69
3.2.2 JADE Method 70
3.2.3 Algorithms for Parameter Estimation and asymptotical behavior of the estimators 72
3.2.4 Conditions for identifiability 74
3.3 Proposed approach 74
3.3.1 Observation model 77
3.3.2 Likelihood of the observations 78

3.3.3 Algorithm derivation . . . 79
3.3.4 Initialization . . . 81
3.4 Simulations results . . . 82
3.4.1 Asymptotic behavior of JADE-ML and JADE-MUSIC estimates . . . 83
3.4.2 ADABLA in a controlled simulation scenario . . . 88
3.4.3 ADABLA in a realistic simulation scenario . . . 91
3.5 Conclusions . . . 93

Conclusions of part I **99**

Appendices **101**

A TABLA: Fisher information matrix derivation **103**
A.1 Derivatives . . . 103
A.1.1 Derivative w.r.t x_s . . . 104
A.1.2 Derivative w.r.t μ . . . 104
A.1.3 Derivative w.r.t σ . . . 105
A.1.4 Derivative w.r.t P_D . . . 105
A.2 FIM's elements computation . . . 105

B UTM system and conversion formulae **107**
B.1 UTM longitude zone . . . 107
B.2 UTM latitude zone . . . 108
B.3 Locating a position using UTM coordinates . . . 108
B.4 Latitude, longitude to UTM conversion (or vice versa) . . . 108
B.4.1 Latitude, longitude to UTM conversion formulae . . . 109
B.4.2 UTM to Latitude, longitude conversion formulae . . . 110

C Derivation of maximum likelihood for JADE **113**
C.1 Stochastic maximum likelihood: a separable solution . . . 113
C.1.1 Proof . . . 114
C.2 Fisher information matrix computation . . . 118
C.2.1 Derivatives . . . 118

D Asymptotical behavior of JADE-MUSIC estimator **121**
D.1 JADE-MUSIC estimates . . . 121
3.2 JADE-MUSIC covariance matrix deduction . . . 122
3.2.1 $\mathrm{cov}(\mathbf{\Pi}_{lp}, \mathbf{\Pi}_{l'p'})$ deduction . . . 123

II Terrain-aided target tracking 125

Introduction to part II 127

4 Terrain aided tracking 131
4.1 Digital maps . . . 131
4.1.1 Hospitability maps . . . 132
4.1.2 Road maps . . . 133
4.1.3 Hospitability versus road maps for ground target tracking 134
4.2 Problem description and basic formulation . . . 135
4.2.1 Unconstrained target tracking problem . . . 135
4.2.2 Description of road map-aided tracking problem . . . 136
4.3 Methods to include road map information . . . 137
4.3.1 Projection methods . . . 137
4.3.2 Incorporating road map information into the dynamic model . . . 138
4.3.3 Road information as a pseudo-measurement . . . 141
4.4 Further issues on ground target tracking . . . 142
4.4.1 A single target in clutter . . . 142
4.4.2 Multiple targets in clutter . . . 143
4.5 Bayesian estimation . . . 144
4.5.1 Recursive Bayesian estimation . . . 144
4.5.2 Particle filters . . . 146
4.6 Conclusions . . . 152

5 Single target tracking with road constraints[1] 155
5.1 Road Constrained Target Dynamics and Measurement Models 156
5.1.1 Modified polar coordinate system . . . 156
5.1.2 Constrained Dynamic Model Formulation . . . 157
5.1.3 Measurement Equations . . . 160
5.2 Algorithm implementation . . . 162
5.2.1 Particle filter implementation . . . 162
5.2.2 ML Method for Track Initialization . . . 164
5.2.3 Finding the nearest road segment . . . 166
5.2.4 Drawing an Epanechnikov random variable . . . 167
5.3 Simulation results . . . 168
5.4 Conclusions . . . 170

6 Multiple target tracking with road constraints 177
6.1 Exploiting road network information for tracking ground moving targets . . . 178

6.2 Road Constrained Target dynamics 179
6.3 Model description for multiple-observer multiple-target tracking with road constraints 181
6.3.1 State-space of constrained targets 181
6.3.2 Measurements 183
6.3.3 Association Prior 186
6.4 Monte Carlo JPDAF 187
6.4.1 JPDAF framework 188
6.4.2 Implementation of the JPDAF with particles 192
6.5 Simulations 194
6.6 Conclusions 197

Conclusions of part II **205**

Appendices **207**

E Constrained dynamic model derivation **209**
E.1 State space, dynamic models, and velocity constraint 209
E.2 Relative target dynamics in MP: URM case 211
E.3 Relative target dynamics in MP: UAM case 212

General conclusions and future work **215**

Bibliography **219**

Résumé en Français

Les problèmes de localisation et poursuite ont été largement étudié ces dernières années [8, 37, 38, 44, 64, 65, 71, 74] grâce à leurs applications civiles et militaires. L'objectif de notre étude est de localiser et de poursuivre des cibles non-coopératives en exploitant des mesures passives réalisées par des intercepteurs mobiles. L'étude comporte ainsi deux grandes parties : la première concerne la localisation aussi bien de stations de base (BS) que de stations mobiles (MS) dans des systèmes de communication sans fil, la seconde s'intéresse à la poursuite d'une ou plusieurs cibles évoluant sur un réseau routier en présence de fouillis d'échos (clutter). Ce travail s'inscrit à la fois dans le développement d'algorithmes novateurs d'inférence statistique pour la localisation, l'utilisation du filtrage particulaire dans des situations où les contraintes de déplacement de la cible sont incorporées dans le modèle d'évolution, des techniques d'association de données dans le cadre de poursuite multi-cibles. Ces thématiques sont très actuelles et sont explorées avec le souci constant de développer une méthodologie basée sur des mesures facilement accessibles tout en proposant une modélisation qui tient compte aussi bien des défauts dans la transmission des données que des a priori sur le déplacement de cibles, dans le cas de cibles mobiles. Cet effort constant de validation dans des scénarios complexes a permis l'éclosion d' algorithmes robustes dont certains sont déjà utilisés à des fins industrielles.

Ce résumé suit le plan suivant : La partie I présente la méthodologie de localisation proposée (section 1.1) ainsi que son application pour la localisation d'une BS (section 1.2) et d'une MS (section 1.3). La partie II présente le problème de la poursuite à l'aide de l'information de terrain (section 1.4) et propose deux méthodes pour exploiter l'information d'une carte du réseau routier dans le problème de poursuite mono-cible (section 1.5) et multi-cible (section 1.6). Finalement, dans la section 1.7 nous donnons les conclusions.

Partie I : Localisation dans un réseau GSM

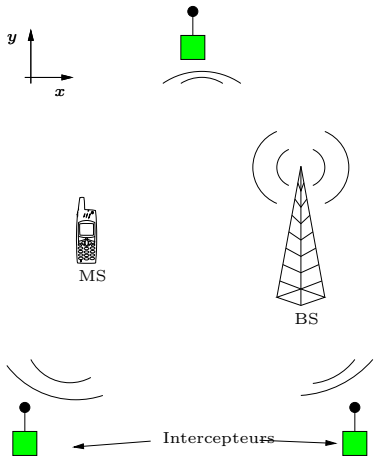

FIG. 1 – Localisation

1.1 Approche statistique proposée

Nous nous intéressons à la localisation passive et non-coopérative de stations de base (BS) et de stations mobiles (MS) d'un réseau GSM à partir de mesures radio effectuées par des intercepteurs mobiles, voir figure 1. Typiquement, les mesures radio sont : le temps d'arrivée (TOA), la différence de temps d'arrivée (TDOA), l'angle d'arrivée (AOA) ou le niveau de puissance reçue (RSS). De façon générale, la mesure radio effectuée par un intercepteur à l'i-ème position d'interception peut s'écrire par

$$z_i = h(p_c, p_i)$$

où p_c est la position inconnue de la cible (MS ou BS) et p_i la position connue de l'intercepteur.

1.1.1 Sources d'erreurs et de bruit

En pratique, les mesures radio présentent des erreurs dues :

Au bruit additif introduit principalement par l'équipement de mesure

$$z_i = h(p_c, p_i) + e_i$$

où $e_i \sim \mathcal{N}(0, \sigma^2)$ est un bruit additif blanc Gaussian de moyenne nulle et de variance σ^2.

Aux offsets systématiques introduits, par exemple dans des systèmes basés sur le TOA ou le AOA, par les temps de réponse non nulle des

MSs ou BSs ou bien par des mauvaises calibrations de l'équipement de mesure

$$z_i = h(p_c, p_i) + \mu + e_i$$

où μ prend en compte l'offset systématique.

A la quantification liée aux bandes passantes réduites du système de communications et/ou à une précision finie du système de mesure

$$y_i = Q(z_i)$$

où $Q(\cdot)$ dénote le quantificateur.

A la propagation à trajets multiples occasionnée par les divers obstacles rencontrés par les signaux transmis lors de leurs propagations vers l'intercepteur

$$Y_i = \left[\begin{array}{cccc} y_i^1 & y_i^2 & \cdots & y_i^{M_i} \end{array} \right]^T$$

où y_i^j pour $j = 1 : M_i$ sont les mesures liées aux M_i trajets de propagation arrivant à la position d'interception i.

A la propagation en non ligne de vue (NLOS) occasionnée par des obstacles obstruant la ligne de vue (LOS) entre la cible et l'intercepteur.

1.1.2 Modèle de mesure

Sans perte de généralité et sous les hypothèses faites précédemment, on peut considérer que l'ensemble de mesures proviennent d'un seul intercepteur. Dans ce cas, l'observation à l'i-ème position d'interception s'écrit :

$$Y_i = \begin{bmatrix} y_i^1 & y_i^2 & \cdots & y_i^{M_i} \end{bmatrix} \tag{1}$$

où

$$y_i^j = \begin{cases} Q(z_i), & \text{si} \quad \psi_i = j \\ u_i, & \text{si} \quad \psi_i \neq j \quad \text{ou} \quad \psi_i = 0 \end{cases}$$

et où

- $z_i = h(p_c, p_i) + \mu + e_i$ représente la mesure en LOS en présence de bruit additif $e_i \sim \mathcal{N}(0, \sigma^2)$ et d'un offset systématique μ,
- $u_i \sim \mathcal{U}(\mathcal{E})$ représente la mesure en NLOS, considéré par simplicité comme une variable aléatoire uniforme dans l'espace de mesure $\mathcal{E}$,

– ψ_i est une variable aléatoire à valeurs dans $\{0, 1, \ldots, M_i\}$ qui indique l'index de la mesure en LOS si $\psi_i \neq 0$ avec

$$p(\psi_i = k) = \begin{cases} 1 - P_D & \text{si} \quad k = 0 \\ P_D/M_i & \text{si} \quad k \neq 0 \end{cases}$$

où $P_D \in [0, 1]$ est la probabilité de détection de la cible.
– M_i est le nombre de mesures issues des M_i trajets de propagation. Il peut être : i) connu et fixe ou ii) une variable aléatoire suivant une loi de Poisson.

1.1.3 Estimation de la position de la cible

La position de la cible est estimée à partir de n mesures indépendantes en utilisant le maximum de vraisemblance

$$\hat{\theta} = \underset{\theta \in \Theta}{\operatorname{argmax}} \left(\sum_{i=1}^{n} \log p(Y_i; \theta) \right) \tag{2}$$

où

– l'on suppose que le modèle est dominé par une mesure λ et $p(Y_i; \theta)$ désigne la pdf par rapport à λ
– θ est l'ensemble de paramètres associés à $p(Y_i; \theta)$, par exemple la position de la cible, ainsi que d'autres paramètres nuisibles.

Comme la maximisation en (2) est analytiquement compliquée et que le modèle est un "mélange", nous avons utilisé l'algorithme "**Expectation-Maximization (EM)**" pour explorer les maxima de la log-vraisemblance.

1.2 Algorithme de localisation basé sur le temps d'arrivée

La méthodologie de localisation présentée précédemment est appliquée au problème de la localisation d'une BS du système GSM à partir des mesures d'avance temporelle (TA). La mesure de TA est disponible à la MS lors d'un appel et elle se renouvelle chaque 480ms.

1.2.1 Principe de l'avance temporelle

Le GSM utilise dans son interface radio le multiplexage en fréquence (FDMA) et en temps (TDMA). Chaque porteuse, dans le sens montant

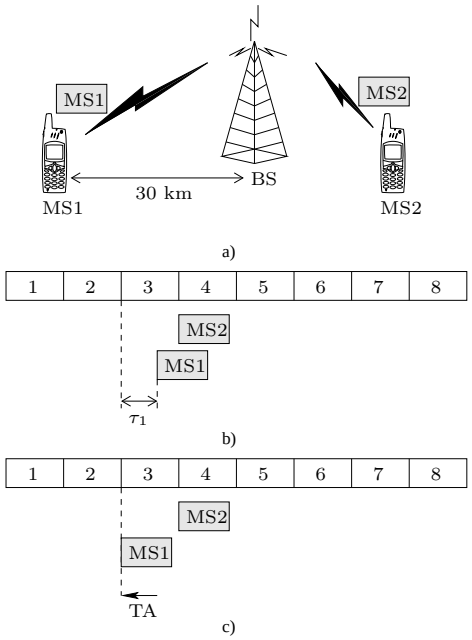

FIG. 2 – Le concept de l'avance temporelle : a) deux MSs situées à des distances différentes par rapport leur BS, b) chevauchement des bursts dû aux différents temps de propagation, c) la mesure de TA est utilisée pour éviter le chevauchement.

comme descendant, est divisée en 8 canaux logiques (appelés slots) utilisant le mode TDMA. Pour que le TDMA fonctionne, les signaux envoyés par les MSs (appelés bursts) doivent arriver à la BS de façon synchrone, c'est-à-dire dans leurs slots correspondants, voir figure 2. Afin d'éviter le chevauchement de bursts dû aux différents temps de propagation MSs-BS, le concept d'avance temporelle est employé. Ceci consiste à indiquer à chaque MS le temps qu'elle doit avancer sa transmission pour recevoir ses bursts dans le slot assigné. La mesure de TA est effectuée par la BS qui l'envoie à la MS sous un chiffre codé sur 6 bits. Le TA est donc un nombre entier entre 0 et 63 représentant le nombre de temps symbole ($T_b = 3,7\mu$s) que la MS doit avancer sa transmission.

1.2.2 Localisation par TA

La distance MS-BS, z, comme fonction du TA est donnée par

$$\max\left\{0, \left(TA - \frac{1}{2}\right) q\right\} \leq z < \left(TA + \frac{1}{2}\right) q$$

où $q = 554$m est la résolution des distances due à la quantification et $TA \in \{0, \ldots, 63\}$.

En l'absence de bruit de mesure, d'écarts systématiques et de données aberrantes, les valeurs du TA en trois positions permettent de localiser la BS à l'intérieur de l'intersection des trois couronnes (voir figure 3 a)). Il est à noter que, *malgré la quantification*, il est possible, en l'absence de bruit, d'estimer la position de la BS avec une précision aussi grande que l'on veut. Il suffit, en effet, de déplacer la MS avec un pas suffisamment petit dans n'importe quelle direction ; on observe un changement de la valeur du TA, ce qui réduit la couronne à un cercle. En répétant cette opération trois fois, on obtient la position de la BS à l'intersection de trois cercles.

En pratique les valeurs des distances obtenues à partir des TAs sont : bruitées, avec un offset, quantifiées et quelques unes diffèrent considérablement de leurs vraies valeurs, voir figure 3 a). Cependant, il est encore possible d'affiner la mesure de distance en utilisant l'approche statistique proposée précédemment. Le résultat est un algorithme que nous appelons **"Algorithme de Localisation Basé sur le Temps d'Arrivée (TABLA)"**.

1.2.3 Initialisation de TABLA

Quatre paramètres doivent être initialisés dans TABLA : la probabilité de détection de la cible P_D, la valeur de l'offset systématique μ, la variance du bruit additif σ^2 et la position de la BS x_s.

Nous utilisons de l'information a priori [72, 96] pour l'initialisation de $\tilde{\mu} = 550$ m et $\tilde{\sigma} \geq 277$ m. On pose $\tilde{P}_D = 0.5$ ce qui représente l'incertitude maximale pour savoir si ce que l'on observe est une mesure en LOS ou en NLOS. Finalement, on prend pour $\tilde{x}_s$ plusieurs initialisations d'une grille située sur la zone de surveillance, voir figure 4. Chacune de ces initialisations donne un estimé correspondant à un maximum local de la fonction de vraisemblance. Cependant, on garde l'estimé qui donne la valeur de la vraisemblance plus grande.

1.2.4 Résultats

TABLA a été testé avec des données réelles. Les données on été collectées lors des campagnes de mesure réalisées dans des environnements du type urbain, semi-urbain et rural. Les résultats de 6 campagnes se présentent

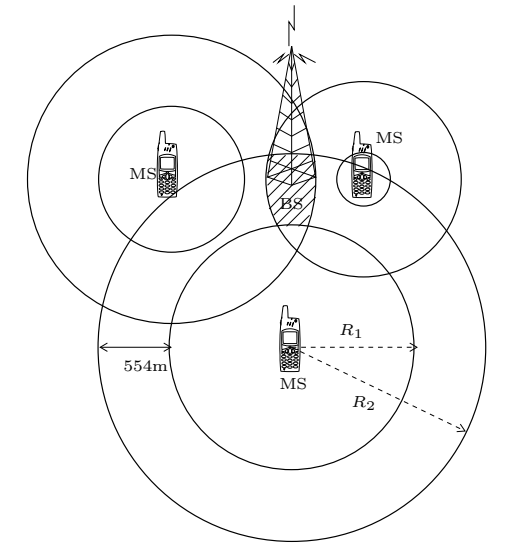

a)

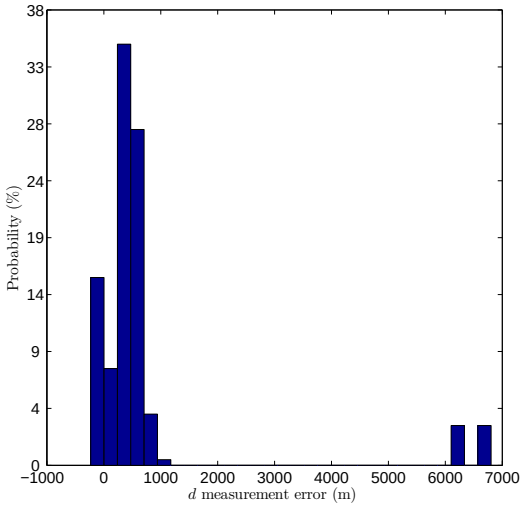

b)

FIG. 3 – a) Localisation par avance temporelle : trois valeurs de TA en positions distinctes permettent de localiser la BS. b) Histogramme des différences entre la vraie position de la BS et la position centrale de la couronne de quantification.

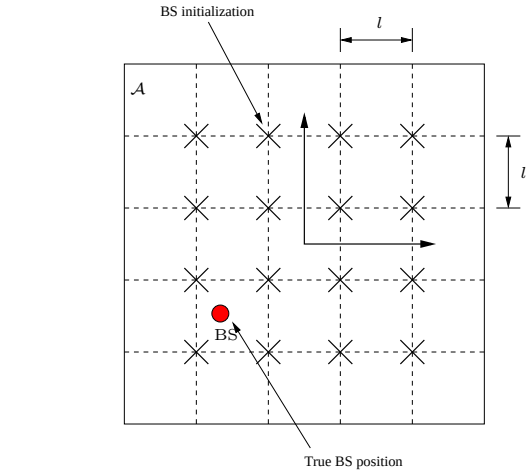

a)

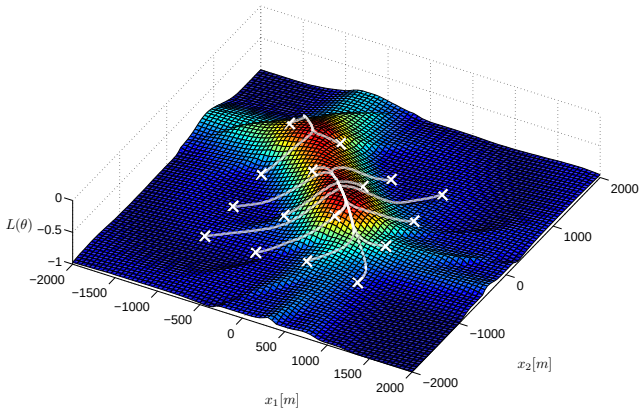

b)

FIG. 4 – a) Grille d'initialisation. b) Convergence de TABLA vers un maximum local.

Terrain	n	d_e [m]
rural	1148	93
semi-urbain	745	173
semi-urbain	244	237
semi-urbain	340	163
urbain	252	84
urbain	207	378

TAB. 1 – Résultats obtenues par TABLA lors de six campagnes de mesure. La première colonne indique le type d'environnement, la deuxième le nombre de TAs collectés et la troisième la distance entre la position estimée et la vraie position de la BS.

dans le tableau 1.

Il est a remarquer que la précision d'estimation est en dessous du pas de quantification (554 m).

1.3 Algorithme de localisation basé sur l'angle et le retard d'arrivée

Le problème abordé ici est celui de la localisation d'une cible à partir des mesures de TOA et AOA issues d'une estimation du canal. Le canal est à trajets multiples (avec ou sans LOS), ce qui occasionne la présence de multiples mesures (chacune associée à un trajet de propagation) au niveau de l'intercepteur. Le canal introduit également du bruit et des évanouissements Rayleigh. D'autre part, chaque intercepteur est équipé d'un réseau de capteurs ainsi que d'une chaîne complète de démodulation.

1.3.1 Principe de l'estimation conjointe de TOAs et AOAs

Suivant [81], l'estimation conjointe des AOAs et TOAs (JADE[1]) consiste à :

- estimer la réponse du canal à l'aide de séquences d'apprentissage
- et à exploiter l'expression de la réponse du canal.

[1]De l'anglais Joint Angle and Delay Estimation.

On démontre que cette expression peut s'écrire

$$\mathbf{y}^{(s)} = \mathbf{U}(\boldsymbol{\theta}, \boldsymbol{\tau})\mathbf{b}^{(s)} + \mathbf{v}^{(s)} \tag{3}$$

où $\mathbf{U}(\cdot)$ est la matrice de réponse spatio-temporelle, fonction des Q TOAs $\boldsymbol{\tau} = [\tau_1 \dots \tau_Q]^T$ et AOAs $\boldsymbol{\theta} = [\theta_1 \dots \theta_Q]^T$ qui caractérisent la propagation à trajets multiples entre la cible et l'intercepteur. $\mathbf{b}^{(s)} = [b_1^{(s)} \dots b_Q^{(s)}]$ et $\mathbf{v}^{(s)}$ sont respectivement des termes nuisibles liées aux évanouissements et au bruit d'estimation.

Le problème JADE consiste à estimer $\boldsymbol{\theta}$ et $\boldsymbol{\tau}$ à partir d'une suite d'estimations de canal $\{\mathbf{y}^{(1)}, \dots \mathbf{y}^{(S)}\}$ et en utilisant le modèle (3). On peut donc envisager l'utilisation de méthodes telles que **MUSIC** ou **ML** pour estimer $\boldsymbol{\theta}$ et $\boldsymbol{\tau}$.

1.3.2 Fonction d'estimation

Nous proposons d'utiliser la loi asymptotique de $\hat{\boldsymbol{\eta}} = [\hat{\boldsymbol{\theta}} \quad \hat{\boldsymbol{\tau}}]$ issue des méthodes MUSIC et ML pour obtenir une fonction d'estimation de la position de la cible. Comme la loi asymptotique dépend des paramètres à estimer nous avons adopté une façon classique de procéder qui consiste à remplacer les paramètres par des estimations consistantes.

Plus formellement, après l'estimation des TOAs et AOAs via MUSIC ou ML nous avons deux types de mesures : celles issues d'une propagation en LOS ou NLOS. Par la suite, nous détaillons la modélisation pour chaque type.

Mesures en LOS

La distribution asymptotique du TOA et AOA associée au q_i trajet en LOS à l'i-ème position d'interception est donnée par

$$\sqrt{S}(\hat{\boldsymbol{\eta}}_{i,q_i}^{LOS} - \boldsymbol{\eta}_{i,q_i}) \longrightarrow \mathcal{N}(0, \boldsymbol{\Gamma}_{i,q_i}) \tag{4}$$

où $q_i \in \{1, 2, \dots, Q_i\}$ est l'indice pour les trajets à la position i, $i \in \{1, 2, \dots, I\}$ est l'indice de positions et

- $\boldsymbol{\eta}_{i,q_i} = [\theta_{i,q_i} \quad \tau_{i,q_i}]^T$ est la vraie valeur des paramètres en LOS et
- $\boldsymbol{\Gamma}_{i,q_i}$ est la covariance asymptotique de $\hat{\boldsymbol{\eta}}_{i,q_i}^{\text{MUSIC}}$ ou $\hat{\boldsymbol{\eta}}_{i,q_i}^{\text{ML}}$

En théorie,

$$\boldsymbol{\Gamma}_{i,q_i} = \mathbf{f}(\boldsymbol{\eta}_i, \mathcal{B}_i)$$

est une fonction définie par MUSIC ou ML qui dépend de paramètres inconnus tels que les vraies valeurs de TOAs et AOAs du canal à trajets multiples $\boldsymbol{\eta}_i = [\boldsymbol{\eta}_{i,q_1} \dots \boldsymbol{\eta}_{i,q_i}]$ et des paramètres nuisibles $\mathcal{B}_i$.

En pratique, on utilise des estimations consistantes pour $(\hat{\boldsymbol{\eta}}_i, \hat{\mathcal{B}}_i)$ afin d'obtenir :

$$\hat{\boldsymbol{\Gamma}}_{i,q_i} = \mathbf{f}_{q_i}(\hat{\boldsymbol{\eta}}_i, \hat{\mathcal{B}}_i)$$

En vue d'une relation directe entre $\boldsymbol{\eta}^{\mathrm{LOS}}$ et la position de la cible $X = [x \quad y]^T$ donnée par une transformation connue $\boldsymbol{\eta}^{LOS} \longmapsto X^{LOS}$, on peut réécrire (4) en utilisant la méthode delta comme

$$\sqrt{S}(\hat{X}^{\mathrm{LOS}}_{i,q_i} - X) \longrightarrow \mathcal{N}(0, \hat{\boldsymbol{\Sigma}}_{i,q_i})$$

avec

$$\hat{\boldsymbol{\Sigma}}_{i,q_i} = \nabla_\eta J(X) \hat{\boldsymbol{\Gamma}}_{i,q_i} \nabla_\eta J(X)^H$$

où $\nabla_\eta J(X)$ est le Jacobian de la transformation.

Mesures en NLOS

Pour les mesures de position $X^{\mathrm{NLOS}}_{i,q_i}$ issues d'une mesure $\boldsymbol{\eta}^{\mathrm{NLOS}}$ nous considérons

$$\hat{X}^{\mathrm{NLOS}}_{i,q_i} \sim \mathcal{U}(\mathcal{R})$$

où $\mathcal{U}(\mathcal{R})$ désigne une distribution uniforme sur la zone de surveillance $\mathcal{R}$.

1.3.3 Algorithme de localisation et initialisation

Afin d'estimer la position de la cible, nous avons traité les mesures de position $\hat{X}^{\mathrm{LOS}}$ et $\hat{X}^{\mathrm{NLOS}}$ ainsi que leurs matrices de covariance asymptotique $\hat{\boldsymbol{\Sigma}}$ obtenues à un certain nombre I de positions d'interception avec l'approche statistique proposée. Le résultat est un algorithme que nous appelons **"Algorithme de Localisation Basé sur l'Angle et le Retard d'Arrivée (ADABLA)".**

Deux paramètres doivent être initialisés dans ADABLA : la probabilité de détection de la cible $\tilde{P}_D$ et sa position $\tilde{X}$. Pour les initialiser nous avons employé la procédure décrite dans la section 1.2.

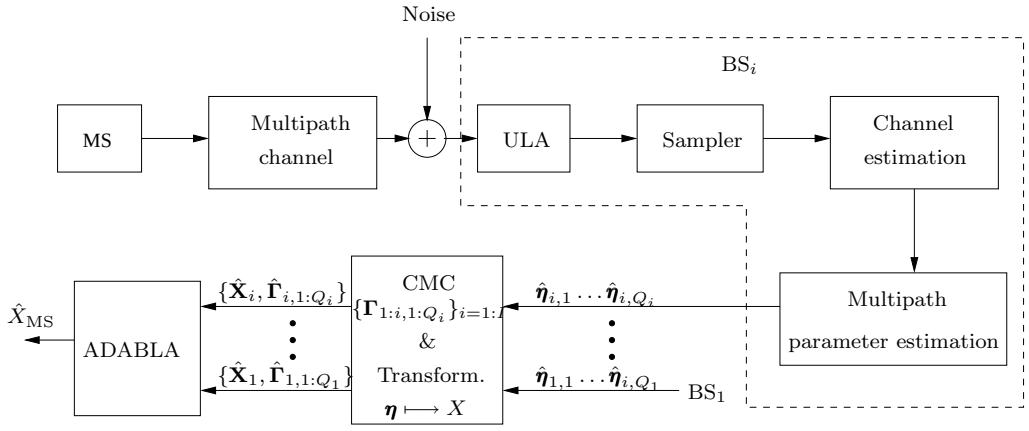

FIG. 5 – Diagramme conceptuel des simulations pour ADABLA.

1.3.4 Résultats des simulations

Nous avons testé ADABLA dans un scénario de simulation réaliste où la cible représente la MS et les intercepteurs 3 BSs. La MS transmet des signaux numériques à une cadence $T_b = 3.7\mu$ s sur un canal à trajets multiples. Les signaux se propagent sur trois trajets dominants qui introduisent du bruit et des évanouissements Rayleigh. A chaque BS les signaux sont reçus à l'aide d'un réseau multi-capteurs avec 5 capteurs. La sortie du réseau est ensuite échantillonnée en temps à une cadence de $T = T_b/2$. Les échantillons et les séquences d'apprentissage sont utilisés pour estimer le canal via moindres carrées. 20 estimations de canal sont employées pour estimer les TOAs et les AOAs via les méthodes JADE-MUSIC et JADE-ML. Finalement, les estimations sont exploitées par ADABLA afin d'estimer la position de la MS. Le diagramme conceptuel des simulations ainsi que les résultats sont donnés respectivement par les figures 3.16 et 6.

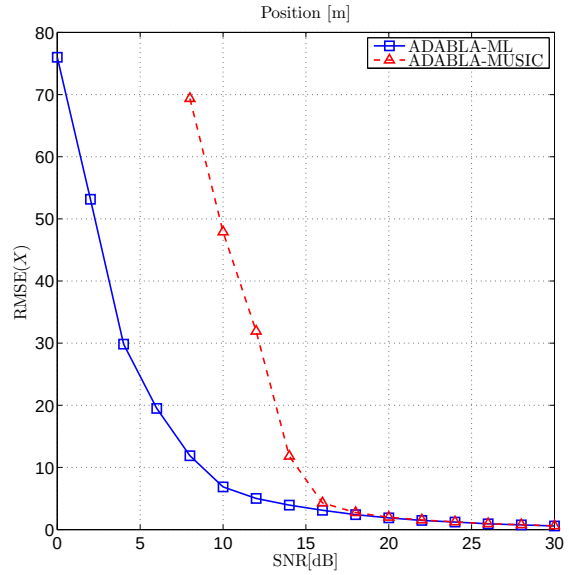

a)

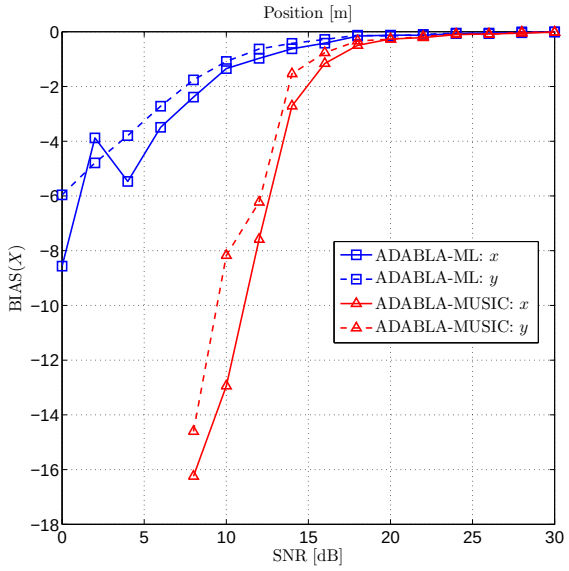

b)

FIG. 6 – a) Courbes de RMSE et b) BIAIS de l'estimation de la position de la MS en fonction du SNR (dB), obtenues à partir des 500 simulations Monte Carlo. ULA avec 5 capteurs. Nombre de slots = 20. Nombre de BS = 3. Nombre de trajets à chaque BS = 3. En bleu ADABLA-ML. En rouge ADABLA-MUSIC

Partie II : Poursuite à l'aide d'un réseau routier

1.4 Description du problème

De façon générale, les seules entrées aux systèmes de poursuite sont les mesures effectuées par un ou plusieurs capteurs. Cependant, la connaissance de l'environnement dans lequel la cible se déplace peut être exploitée dans un cadre Bayesian.

Dans le contexte de la poursuite de cibles terrestres [45, 65], nous nous intéressons à la poursuite par mesure d'angle seul d'un nombre connu de cibles que se déplacent sur un réseau routier. Dans ce contexte, l'information a priori à exploiter par le système de poursuite est la carte du réseau routier.

Les principales considérations que nous faisons sont :

- Le réseau routier (voir figure 4.2) est décrit par un graphe orienté $G = (V, E)$ où V désigne l'ensemble des sommets représentant les intersections des routes et E l'ensemble des arêtes orientées, à savoir un ensemble de couples ordonnés de sommets, représentant les routes. On note $(i, j) \in E$ l'arête qui va du sommet i au sommet j. Les routes peuvent être à double sens de circulation, dans ce cas les arêtes (i, j) et (j, i) appartiennent à E. On note $\lambda_{i,j}$ la longueur de l'arête (i, j). Chaque sommet i possède un ensemble de descendants Children(i) auquel on associe une distribution de probabilité ζ_i.
- Les mesures d'angle, effectuées par un groupe d'intercepteurs mobiles, s'écrivent suivant le modèle (1).
- Les cibles suivent un mouvement rectiligne uniforme (MRU) perturbé donné par :

$$\mathbf{x}_k = F\mathbf{x}_{k-1} + G\epsilon_{k-1} \tag{5}$$

où $\mathbf{x}_k = \begin{bmatrix} x & y & \dot{x} & \dot{y} \end{bmatrix}$ est le vecteur d'état de la cible à l'instant k composé par sa position et sa vitesse. F et G sont des matrices de transition et ϵ_k est un procès de bruit additif.

1.5 Poursuite mono-cible à l'aide d'un réseau de routes

Nous proposons un algorithme à deux étapes pour la poursuite d'une cible mouvant dans un réseau routier. Dans la première étape (étape batch), l'algorithme emploie une procédure peu coûteuse basée sur le maximum de vraisemblance pour estimer l'angle en LOS. Dans la seconde étape (étape

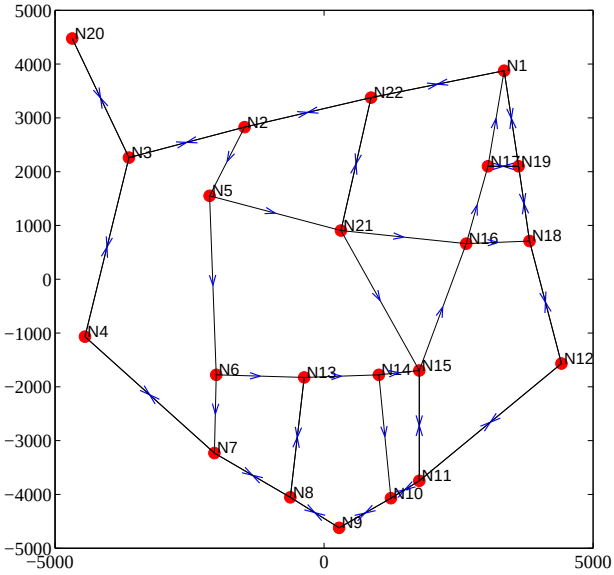

FIG. 7 – Exemple de réseau routier.

récursive), l'algorithme exploite l'estimé de l'angle en LOS pour initialiser un filtre particulaire régularisé qui maintient la poursuite de la cible en estimant de façon récursive son vecteur d'état.

1.5.1 Méthode pour l'exploitation du réseau routier

Afin d'exploiter l'information du réseau routier dans le système de poursuite nous proposons de :

1. Contraindre la direction du vecteur vitesse de la cible à ce qu'elle soit parallèle à la direction de la route dans laquelle la cible est supposée se déplacer [60]. Ceci peut s'écrire comme

$$\vec{n}_s \cdot \vec{v} = 0$$

où $\vec{n}_s$ est un vecteur normal à la route s et $\vec{v} = [\dot{x} \quad \dot{y}]^T$ est le vecteur vitesse de la cible.

2. Contraindre la position de la cible en utilisant le concept de la pseudo-mesure [22,37,77]. La pseudo-mesure que nous introduisons est donnée par

$$d_k = h(p_k, s) + w_{2,k}$$

où p_k est la position de la cible à l'instant k, s est la route la plus proche à la cible, $h(p_k, s)$ est la distance Euclidienne entre p_k et s et $w_{2,k} \sim \mathcal{N}(0, \sigma_d^2)$ est le bruit de mesure.

3. Modéliser le procès de bruit additif comme un *procès de bruit directionnel* [44]. Ceci consiste à considérer pour ϵ_k dans le modèle (5) une matrice de covariance donnée par

$$\mathbf{Q}_s = \begin{bmatrix} -\cos\alpha_s & \sin\alpha_s \\ \sin\alpha_s & \cos\alpha_s \end{bmatrix} \begin{bmatrix} \sigma_o^2 & 0 \\ 0 & \sigma_a^2 \end{bmatrix} \begin{bmatrix} -\cos\alpha_s & \sin\alpha_s \\ \sin\alpha_s & \cos\alpha_s \end{bmatrix}$$

avec $\sigma_a^2 \gg \sigma_o^2$ et où α_s est l'angle entre la route s et l'axe x.

1.5.2 Modèle d'évolution

Dans le contexte de la poursuite par mesure d'angle seul (BOT[2]), on a démontré [2] que l'utilisation des coordonnées polaires modifiées (CPM) pour représenter le vecteur d'état de la cible produit des algorithmes plus stables que ceux basés sur une représentation Cartésienne. Suivant ces résultats nous utilisons par la suite les CPM.

Dans ces conditions le modèle d'évolution relatif contraint peut s'écrire

$$\boldsymbol{\chi}_{k+1} = \boldsymbol{f}_s(\boldsymbol{\chi}_k) - \boldsymbol{\varrho}_k + \boldsymbol{\upsilon}_k$$

où

- $\boldsymbol{\chi}_k = \begin{bmatrix} \theta_k & \dot{\theta}_k & \xi_k & r_k \end{bmatrix}'$ est le vecteur d'état de la cible en CPM,
- $\boldsymbol{f}_s(\boldsymbol{\chi}_k)$ décrit l'évolution relative de la cible dans la direction de s par rapport à un intercepteur non-manœuvrant
- $\boldsymbol{\varrho}_k$ prend en compte une **accélération constante** de l'intercepteur
- $\boldsymbol{\upsilon}_k \sim \mathcal{N}(\mathbf{0}, \mathbf{Q}_k)$ est le procès de bruit additif construit à partir du modèle de procès de *bruit directionnel*.

1.5.3 Implementation : Filtre particulaire régularisé

L'estimation récursive du vecteur d'état de la cible a été réalisée par le filtre particulaire régularisé (FPR) [56]. A la différence du filtre particulaire standard (FPS), dans le FPR les nouvelles particules sont engendrées à partir d'une approximation continue de la distribution a posteriori $p(\boldsymbol{\chi}_k|\mathbf{Z}_k)$ (voir figure 8). Cette approximation a été réalisée à l'aide des noyaux de

[2]De l'anglais Bearings-Only Tracking.

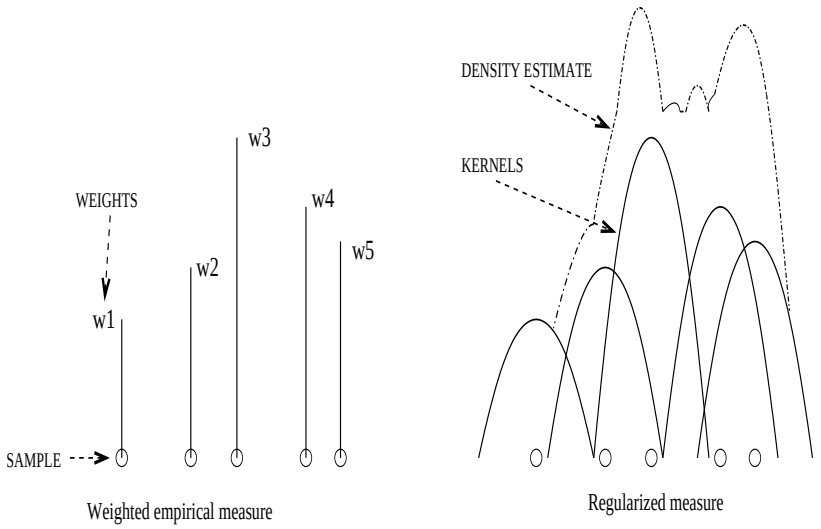

FIG. 8 – Étape de régularisation dans le filtre particulaire régularisé

Epanechnikov.

L'initialisation du filtre particulaire s'effectue en utilisant une procédure batch où l'objectif principal est d'estimer la direction en LOS afin d'initialiser les particules du FPR sur cette direction.

1.5.4 Simulations et résultats

Le scénario de simulation consiste en une cible et un intercepteur mouvant sur le réseau routier montré dans la figure 9. La cible se déplace à une vitesse de 54 km/h et décrit la trajectoire rouge. La vitesse de l'intercepteur est de 60 km/h et décrit la trajectoire bleue. L'intercepteur obtient des mesures d'angle chaque 0.5 s avec une précision de 0.5 deg. Le nombre de particules utilisé par le filtre particulaire est 1000 et la loi de proposition est la loi a priori.

Les résultats de 100 simulations Monte Carlo en utilisant un FPS et un FPR sont donnés respectivement par les figures 10 et 11.

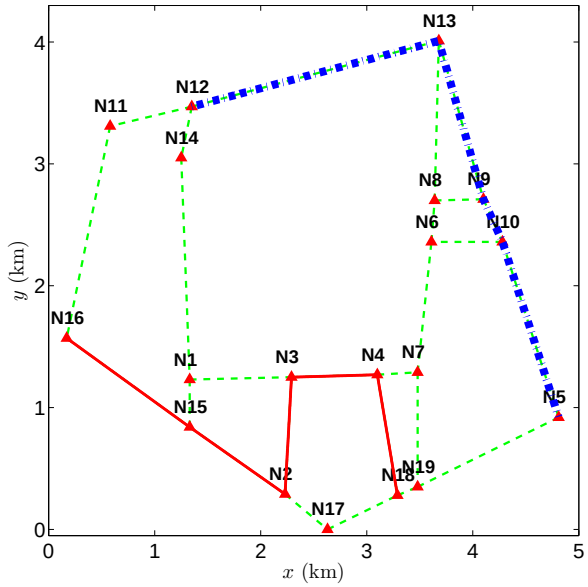

FIG. 9 – Scénario de simulation : en bleu, trajectoire de l'intercepteur. En rouge, trajectoire de la cible. En vert-pointillé, réseau routier.

1.6 Poursuite multi-cible à l'aide d'un réseau de routes

Nous proposons une procédure originale pour contraindre l'évolution des cibles terrestres mouvant sur un réseau routier. Plus précisément, nous proposons une représentation du vecteur d'état et un algorithme d'évolution qui permettent d'exploiter l'information du réseau routier. D'autre part, nous exploitons deux caractéristiques supplémentaires inclues dans les cartes routières : 1) les sens des routes ainsi que 2) la probabilité d'emprunter une route quelconque lors du passage de la cible sur une intersection (préférence de trafic).

La procédure proposée est testée dans un cadre de poursuite multi-cible en utilisant le "Monte Carlo Joint Probabilistic Data Association Filter (MC-JPDAF)" [87].

1.6.1 Espace d'états

On propose de modéliser l'état de la cible à l'instant k par

$$\mathbf{x}_k = \begin{bmatrix} (i,j)_k \\ d_k \\ v_k \end{bmatrix}$$

où

- $(i,j)_k$ définit le segment de route allant du i au j,
- $d_k \in \mathbb{R}^+$ est la distance de la cible par rapport à i et
- $v_k \in \mathbb{R}^+$ est le module de la vitesse de la cible

Par la suite on note par

- $\lambda_{(i,j)_k}$ la longueur de la route $(i,j)_k$ et
- Children(i) un opérateur de réseau qui donne l'ensemble des sommets descendants du sommet i.

1.6.2 Modèle d'évolution

L'évolution de l'état est donnée par l'algorithme 1. Notons que, suivant cet algorithme, la loi a priori de la position sur l'arête est une loi "Gaussienne" tronquée. La queue gauche est tronquée par la position de la cible à l'instant k et la queue droite est tronquée par le sommet j_k et repartie sur les arêtes descendantes avec une pondération $p_{j_k}(\psi_k)$ (voir figure 12).

1.6.3 Poursuite multi-cible : MC-JPDAF

La poursuite multi-cible est particulièrement compliquée à cause de l'incertitude de l'origine des mesures qu'implique le calcul des probabilités pour l'association de données (PDA) [9]. Afin de résoudre ce problème dans l'application envisagée, nous avons utilisé le filtre **JPDAF**[4] [9] qui met à jour les distributions marginales pour chaque cible $p_t(\mathbf{x}_{t,k}|\mathbf{y}_{1:k})$ pour $t = 1 \dots M$ à travers les récusions de l'estimation séquentielle Bayesienne données par :

Prédiction : $p_t(\mathbf{x}_{t,k}|\mathbf{y}_{1:k-1}) = \int p_t(\mathbf{x}_{t,k}|\mathbf{x}_{t,k-1}) p_t(\mathbf{x}_{t,k-1}|\mathbf{y}_{1:k-1}) d\mathbf{x}_{t,k-1}$

Correction : $p_t(\mathbf{x}_{t,k}|\mathbf{y}_{1:k}) \propto p_t(\mathbf{y}_k|\mathbf{x}_{t,k}) p_t(\mathbf{x}_{t,k}|\mathbf{y}_{1:k-1})$

où le pas de *prédiction* se réalise indépendamment pour chaque cible, tandis que le pas de *correction* se réalise en prenant en compte l'incertitude d'association de données dans la vraisemblance pour la cible t, $p_t(\mathbf{y}_k|\mathbf{x}_{t,k})$.

[4] De l'anglais Joint Probability Data Association Filter.

Algorithm 1 : Évolution de l'état de la cible

Calculer :

$$d' = d_k + \underbrace{v_k T + \epsilon_k}_{\delta} \tag{6}$$

où ϵ_k est une variable aléatoire, gaussienne, centrée, de variance σ_d^2. L'état[3] à l'instant $k+1$ est obtenu de la façon suivante :

- si $\delta < 0$, on réitère (6),
- si $\delta \geq 0$
  - si $d' \leq \lambda_{(i,j)_k}$, alors

$$\mathbf{x}_{k+1} = \begin{bmatrix} (i,j)_k \\ d' \\ v_k + \chi_k \end{bmatrix}$$

  - si $d' > \lambda_{(i,j)_k}$, alors

$$\mathbf{x}_{k+1} = \begin{bmatrix} (j,\psi_k)_k \\ d' - \lambda_{(i,j)_k} \\ v_k + \chi_k \end{bmatrix}$$

  où T est la période d'échantillonnage, ψ_k est une suite de v.a. indépendantes à valeurs dans Children(j_k) suivant une loi $p_{j_k}(\psi_k)$ donnée de trafic. Les lois $p_{j_k}(\psi_k)$ pour l'ensemble des sommets sont supposées être connues. χ_k est une v.a. Gaussienne, centrée, de variance σ_v^2.

On suppose que les suites aléatoires ϵ_k, χ_k, ψ_k sont conjointement indépendantes.

Le JPDAF a été développé dans un cadre du filtrage de Kalman. Cependant, dans le cas envisagé, son implementation n'est pas facile à cause de la loi d'évolution des cibles qui est non-Gaussiene. C'est pourquoi l'implementation de ce filtre dans le cadre particulaire a été préférée. Nous avons donc utilisé le Monte Carlo JPDAF (**MC-JPDAF**) proposé par [87].

1.6.4 Simulations et résultats

Le scénario de simulation consiste en trois cibles et deux intercepteurs mobiles mouvant dans un réseau routier à une vitesse de 64, 72 et 79 km/h pour les cibles et de 46 et 68 km/h pour les intercepteurs. Les mesures d'angle sont obtenues chaque $T = 2$s avec une précision de $\sigma_{\theta_1} = 2\,\text{deg}$ pour l'intercepteur 1 et $\sigma_{\theta_2} = 3\,\text{deg}$ pour l'intercepteur 2. Le

nombre de trajets en NLOS a été modélisé comme une variable aléatoire poissonnienne de paramètre λ_c. La probabilité de détection de la cible est P_D.

Nous avons testé l'algorithme pour trois cas que nous avons classifié comme facile, moyen et difficile (voir table 2).

	Easy	Medium	Hard
P_D	0.99	0.8	0.6
λ_c	2	3	5

TAB. 2 – Valeurs de la probabilité de détection de la cible P_D et du taux de trajets en NLOS λ_c pour trois types de conditions différentes.

Les résultats de 100 simulations Monte Carlo sont donnés par la figure 13.

1.7 Conclusions

Cette thèse propose deux outils permettant de résoudre des problèmes de localisation et poursuite de cibles non-coopératives. Le premier outil est une méthodologie pour la localisation d'une cible fixe ou mobile (BS ou MS) d'un réseau GSM à partir de mesures de TOA, TDOA, AOA, RSS, etc. D'autre part, la méthodologie prend en compte des mesures corrompues par bruit additif, offsets systématiques, quantification, propagation à trajets multiples et propagation en NLOS. Deux applications de la méthodologie proposée pour la localisation d'une station de base et une station mobile ont donné respectivement les algorithmes TABLA et ADABLA. Les performances de ces algorithmes ont été testées sur des données synthétiques et dans le cas de TABLA sur des données réelles.

Le deuxième outil consiste en deux méthodes pour exploiter l'information d'une carte du réseau routier lorsque l'on effectue la poursuite de cibles mouvant sur un tel réseau. Basés sur ces méthodes, nous avons proposé respectivement deux algorithmes pour la poursuite mono-cible et multi-cible par mesure d'angle seul.

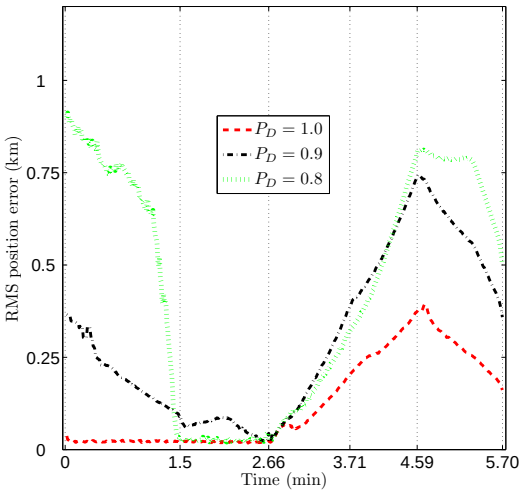

a)

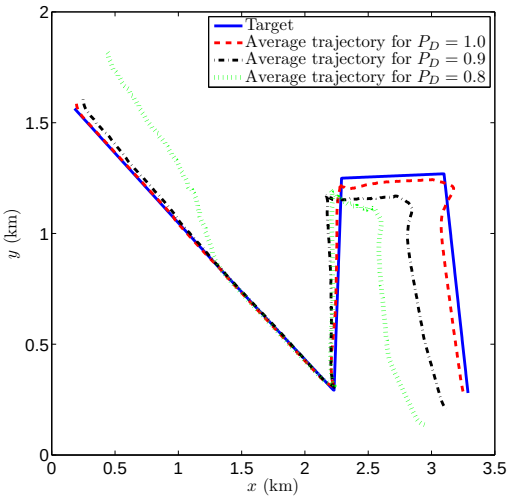

b)

FIG. 10 – Résultats de 100 simulations Monte Carlo avec un filtre particulaire standard. **a)** RMSE (km) de la position en fonction du temps (minutes). **b)** Vraie trajectoire (bleue) et trajectoires estimées. Paramètres de simulation : Probabilité de perte du LOS = 1-P_D ; Nombre d'angles observés = 3 ; Vitesse de la cible $\approx$ $54m/s$; Vitesse de l'intercepteur $\approx$ $60m/s$; $T = 0.5s$; Nombre de particules = 1000 ; $\sigma = 0.5$ deg.

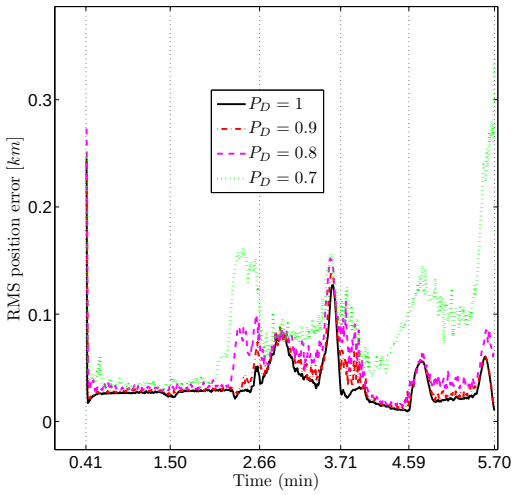

a)

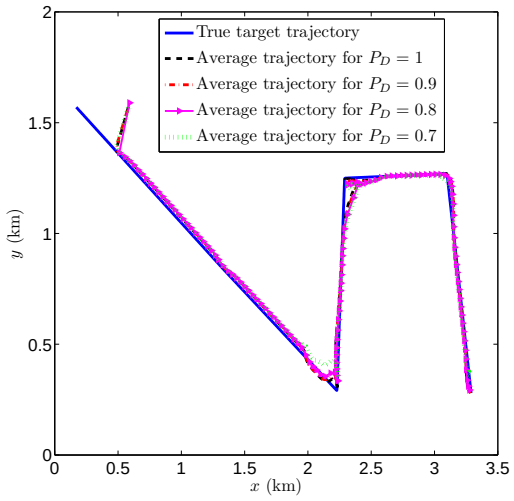

b)

FIG. 11 – Résultats de 100 simulations Monte Carlo avec un filtre particulaire régularisé. **a)** RMSE (km) de la position en fonction du temps (minutes). **b)** Vraie trajectoire (bleue) et trajectoires estimées. Paramètres de simulation : Probabilité de perte du LOS = 1-P_D ; Nombre d'angles observés = 3 ; Vitesse de la cible $\approx$ $54m/s$; Vitesse de l'intercepteur $\approx$ $60m/s$; $T = 0.5s$; Nombre de particules = 1000 ; $\sigma = 0.5$ deg.

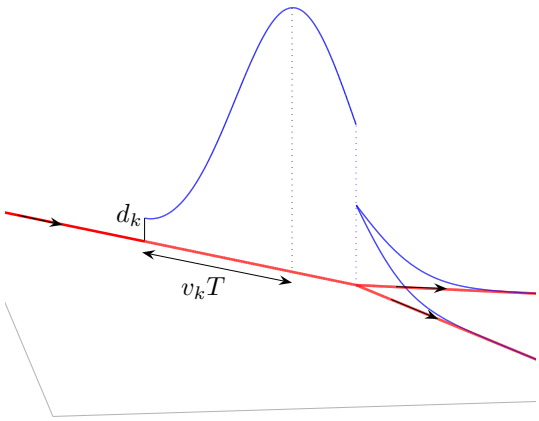

FIG. 12 – Loi a priori $p(x_{k+1}|x_k)$ lors d'une bifurcation.

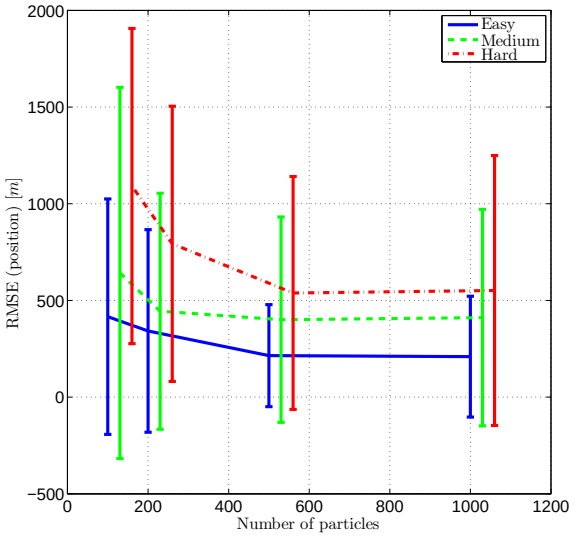

a)

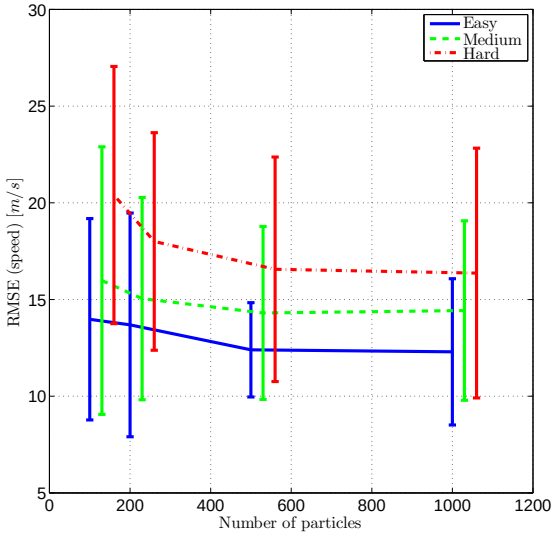

b)

FIG. 13 – Résultats de 100 simulations Monte Carlo. **a)** RMSE (m) de la position en fonction du nombre de particules du filtre particulaire. RMSE (m/s) du module de la vitesse en fonction du nombre de particules du filtre particulaire.

Geo-localization and tracking in mobile networks

by

Nadir Castañeda Palomino

Submitted to the department of Signal and Image Processing
in partial fulfillment of the requirements for the degree of

Doctor of philosophy in telecomunications

at the

École Nationale Supérieure des Télécommunications

July 4th, 2008

General introduction

Localization and tracking of emitting targets are two appealing topics from a data processing point of view because of their many civilian and military applications. Abundant examples for such applications range from safety location services for mobile users and vehicle navigation to localizing furtive networks and surveillance of threat moving targets. Localization is the process of determining the position of a target in space from measurements relating the positions of the target and the sensors employed to obtain such measurements [13]. Tracking is the processing of measurements obtained from a moving target in order to maintain an estimate of its kinematic parameters (position, velocity, acceleration, and so forth) [9,65]. In some cases, the problem of tracking may be reduced to a series of localization problems. However, localizing a stationary target often differers from tracking a moving target because the latter exhibits a dynamic behavior usually taken into account. A variety of solutions exist for the localization and tracking problem distinguished by the characteristics of the target (i.e. fixed, walking, wheeled or flaying targets), the environment (indoors or outdoors), and the available technology (i.e. the type of sensors used to obtain measurements).

This thesis focuses on the localization and tracking of non-cooperative emitting targets in outdoor environments. These non-cooperative localization and tracking problems arise whenever one is attempting to locate or track an emitting target without its active participation in the process. In the following we detail the objectives for each problem.

Localization problem

We concern about the problem of localizing a target in a wireless communication system such as the Global System for Mobile communications (GSM) and the Universal Mobile Telecommunications System (UMTS). Under this context, the target represents a network element (mobile station or base station) of the communication system. The objective is to provide a methodology to localize network elements using the most common radio measurements, i.e. time of arrival (TOA), time difference of arrival (TDOA), angle

of arrival (AOA) and received signal strength (RSS) [36, 38, 68]. We look for a robust methodology against impairments in the radio measurements introduced by the propagation environment such as multipath and non line of sight (NLOS) propagation [13, 72]. Furthermore, the methodology must also consider impairments due to network elements' calibration and today's wireless communication systems limitations (i.e. limited bandwidths), which may give rise to measurement noise [84], systematic offsets [31, 68] and quantized measurements [51, 54].

To solve the localization problem the maximum-likelihood (ML) method is adopted. The ML method finds the estimate of a parameter that maximizes the probability of observing the data (i.e. collected measurements) given a specific model for the data. As it will be shown the probabilistic model, issuing from the mathematical model proposal for the data, belongs to a mixture family. It is well-known that in presence of mixture models the expectation-maximization (EM) algorithm [26] provides a simple means to compute the maximum-likelihood estimates of parameters in the probabilistic model.

Tracking problem

Tracking ground moving targets is an interesting issue with many practical applications such as surveillance of convoys in military operations [44] and airport surface traffic management [30, 39]. Ground target tracking is challenging because measurements obtained from sensors usually contain a high number of undesirable returns (clutter) from extraneous objects in the environment [23]. However, since ground targets move on earth's surface it may exist some prior non-standard terrain information such as speed constraints, road network, and so forth, which may be used in the tracker to produce better (sequential) estimates of the target state [65]. Specifically, we are interested in tracking targets moving along road networks. Therefore, the prior information to be considered is a digitalized representation of the road network. The ultimate objective we are pursuing is to propose methods able to exploit road map information to yield accurate target state estimates and which may also help to reject clutter.

Since the incorporation of road network information usually leads to highly non-Gaussian posterior densities that are difficult to represent accurately using conventional filtering techniques [65], i.e. Kalman filtering, we use particle filtering methods [7] to solve the tracking problem.

Thesis outline

This document is organized into two main parts, whose description is in order:

The part I : is devoted to the localization problem in wireless communication systems. We introduce this part presenting the importance of localizing wireless network elements and giving the prior work done in this area. In chapter 1 we propose a methodology to localize network elements using the most common radio measurements. The methodology accounts for impairments on the radio measurements due to additive noise, systematic offsets, quantization, multipath and NLOS propagation. In chapters 2 and 3 we present, respectively, two applications using the proposed methodology to localize a base station (BS) from quantized TOA and a mobile station (MS) from joint AOA and TOA measurements. The resulting algorithms are tested under challenging simulation scenarios, and the algorithm presented in chapter 2 is tested using real field measurements.

The part II : is devoted to the ground target tracking problem using road map information. We start this part by talking about the importance of using terrain information for ground target tracking and we give the prior work done in this area. Then, in chapter 4 we formalize the problem of terrain-aided target tracking and we provide the most used methods to exploit road map information. We also introduce the concept of data association problem and we recall the theory of particle filters. Based on this study, chapter 5 proposes a combination of the classical methods to exploit road map information to yield better state estimates in the classical problem of bearings-only tracking. Chapter 6 presents a new method to incorporate road network information accounting for road direction and traffic flow information. The method is tested under a challenging multiple-observer multiple-target tracking scenario. Proposed approaches are tested under realistic simulation scenarios.

Some of the work presented in this thesis has been published during the course of this research. The applications presented in chapters 2 and 3 appear respectively in [18] and [20], and that one presented in chapter 5 appears in [21] and [19].

Contributions

This dissertation consist of statistical model definition, algorithms developing, theoretical analysis, computer simulations and real field test for some algorithms. Its main contributions are:

Part I

1. A methodology to estimate the position of a wireless network element using radio measurements (TOA, AOA, TDOA and RSS) corrupted by measurement noise, systematic offsets, quantization, multipath and NLOS propagation.
2. A Timing Advance-Based Localization Algorithm (TABLA) to localize a BS using quantized measurements of the time of arrivals.
3. Two Angle and Delay of Arrival-Based Localization Algorithms (ADABLA) to localize an MS using joint angle and time of arrival measurements.

Part II

1. Two methods for exploiting road map information.
2. A batch-recursive algorithm to track a ground moving target constrained to roads using bearings-only measurements in clutter.
3. An algorithm to track multiple targets moving along a road network using bearings-only measurements performed by multiple observers.

Part I

Localization in radiocommunication systems

Introduction to part I

The problem of geographic localization (geolocalisation) of a radio source, operating in a geographical area, is to gather information related to the position of the source and processing that information to form a location estimate. In the context of wireless communications systems (such as GSM and UMTS) the geolocalisation of wireless network elements (mobile station or base station) has received considerable attention over the last few years [13]. This is due to the vast number of applications which can be classified into two main categories

Civil: which are those user-oriented applications proposed by mobile network operators to create new value added services such as location information for wireless E-911 calls, location-sensitive billing, fraud detection, fleet management, intelligent transportation systems, etc.

Network operator and military: which are those network operator and military oriented applications used to design and monitor the wireless network systems such as cellular system design and resource management, surveillance, furtive networks localization, etc.

Several approaches for performing geolocalisation of wireless networks elements have been proposed in the literature (good tutorials can be found in [36, 38, 68]). For civil applications the use of a GPS receiver at the mobile hand-set or techniques based on "fingerprint" and radiolocation are the most common ones [36, 38]. However, for network operator and military applications the geolocalisation has often to be performed passively (the element to geolocalise does not cooperate in the localisation process) and thus the use of radiolocation techniques seem to be the most adequate. Radiolocation techniques consist in measuring the radio signals exchanged between the network elements during a call. The most common signal measurements are the Angle-Of-Arrival (AOA), Time-Of-Arrival (TOA), Time-Difference-Of-Arrival (TDOA) and Received Signal Strength (RSS) measurements [13, 38]. Based on the mathematical approach used to process collected measurements, location algorithms can be classified as deterministic and probabilistic. In

the former the problem of geolocalising a network element is usually modeled as the intersection of a set of loci, each of which is defined by a given measurement [36]. In the event of having a number of measurements that overdetermines the equations system it is common to combine all available measurements using the lest-squares method to obtain a position estimate [68]. On the other hand, algorithms based on probabilistic models assume some knowledge about the distribution of the radio measurements and compute the position estimate using, for example, the maximum-likelihood (ML) method or a Bayesian technique [68].

Deterministic versus probabilistic location algorithms

One of the major problems in most wireless signal propagation environments is the loss of the line-of-sight path between the network element and the sensor stations, a condition which has become known as non-line of sight (NLOS) propagation. The NLOS propagation is one of the most important sources of error affecting radio measurements. Therefore, the ability of the location algorithms to deal with measurements corrupted by an NLOS propagation determines its effectiveness. In order to deal with NLOS measurements deterministic algorithms incorporates some additional constraints based on the geometry of the network element and interceptors positions to rule out or weight NLOS measurements (see as examples [14, 85, 86]). In general, the accuracy of these algorithms to determine the network element's position depends on three factors; a high number of sensor stations, the LOS condition for the majority of sensor stations and high SNRs. Unfortunately, all these conditions are rarely fulfilled in real environments, where the number of sensor stations is limited because of logistic reasons [27] and not all of them are in an LOS regime with respect to the network element to locate. Furthermore, high SNRs cannot always be assured for all participating sensor stations because of power control issues [6]. On the other hand, probabilistic algorithms take into account the random nature of radio measurements using robust error distributions (see [18, 38] as examples) or through the use of scattering models for NLOS radio measurements, i.e. the ring or the disk of scatterers models [6]. The use of such algorithms not only help to mitigate the effect of an NLOS propagation, but also can incorporated NLOS radio measurements to perform localization even in a complete NLOS regime.

The accuracy to estimate the position of a network element using a probabilistic location algorithm depends on the ability of the statistical model used to describe the random behavior of radio measurements. Robust statistical models must account for NLOS measurements, as well as some other sources of error related to the propagation environment and today's wireless com-

munication systems limitations. The most important sources of error are the presence of measurement noise [84], systematic offsets [31, 68, 93], and multipath propagation [13, 81] which may produce the observation of multiple radio measurements (one for each propagating path) at a given time. The main limitation in any wireless communication system is a reduced bandwidth, which may give rise to a measurement representation with a finite precision, i.e. quantizing measurements [51, 54, 74, 75]. Therefore, finding reliable statistical models able to take into account multipath propagation, NLOS propagation, measurement noise, systematic offsets and quantization is a key problem in this area.

Prior work

Probabilistic algorithms may be classified into parametric or nonparametric algorithms according to whether they are based on parametric or nonparametric estimation techniques. Non-parametric (or distribution-free) techniques are mathematical procedures for statistical hypothesis testing which, unlike parametric techniques, make no assumptions about the probability distributions of the variables being assessed [34].

This dissertation part focusses on the localization of wireless network elements (MSs or BSs) using parametric estimation techniques. The objective is to provide a robust methodology to localize network elements using the most common radio measurements (TOA, TDOA, AOA and RSS) corrupted by measurement noise, systematic offsets, quantization, multipath and NLOS propagation. Nonparametric-based estimation techniques are not exploited because they require the use of survey data, which may not be available for the applications faced in this dissertation. However, the reader is refereed to [52–54, 89] for some recent contributions using such techniques. A brief survey of other work that has been done in the area of network elements' position estimation using parametric estimation techniques is in order.

Several algorithms to perform geolocalisation in wireless networks have been proposed in the literature (see [1, 4, 6, 28, 62, 64, 75, 90, 94] as examples and the references there in). However, such algorithms only combat the sources of error described in the previous section partially[5]. Reference [90] proposes a method to locate an MS in IS-95 CDMA networks. The method attempts to reconstruct LOS TOA or AOA measurements from a series of both LOS and NLOS TOA or AOA measurements made over time and assumes knowledge of the NLOS standard deviation for identifying NLOS BSs. References [28, 62, 75] performs MS location estimation and tracking using

[5]Up to the knowledge of the author.

quantized measurements of TOA. Only the approach presented in [28] deals with the presence of NLOS measurements. In this case, when an NLOS measurement is detected (according to a threshold) the measurement noise variance is increased, producing a decrease in the Kalman filter gain and alleviating the effect of the error over the position estimate. Al-Jazzar and Caffery in [4, 6] consider scattering models for the TOA in NLOS environments in order to obtain an improved TOA estimate from a set of TOA measurements corrupted by multipath errors. The algorithms show a good performance even in scenarios where the minimum of three BSs are in a completely NLOS regime and there is presence of multiple TOA measurements at each scan due to multipath propagation. Finally, Riba and Urruela in [64] propose an algorithm to detect the NLOS-BSs using the redundant information present in the TOA measurements when more than the minimum number of BSs are present. In such a situation, several hypothesis of the set of BSs under NLOS scenarios are formulated and, on the basis of the ML-detection principle, the most suitable hypothesis can be selected.

Most of the proposed algorithms only cope partially with the sources of error previously discussed. Furthermore, many of these algorithms do not provide a general methodology to treat different kind of measurements. In this dissertation we seek to overcome the mentioned sources of error and to provide a general methodology able to exploit any king of radio measurements to accurately localize wireless network elements.

Overview of this part

This work addresses the localization of wireless network elements (BSs and MSs) from measurements of the radio signals exchanged between the BS(s) and the MS during a call. It is considered that the radio measurements may be corrupted by additive noise, systematic offsets and quantization. Furthermore, we considered that due to multipath propagation the observations may consist in multiple radio measurements associated to each propagation path and that in the case of an NLOS propagation regime all observations correspond to NLOS measurements. Some major assumptions we make are:

1. Each sensor station measures signals generated from the network element to geolocalise.

2. The network element to geolocalise is considered to stay at a given position in space during the whole location procedure.

The rest of this part is organized as follows. In chapter 1 we provide some general concepts on wireless network geolocalisation, as well as the principal

sources of error affecting radio measurements present in today's wireless communication systems. Based on this study we propose the statistical model and we present the theory of the expectation-maximization algorithm which has been selected as the algorithm for parameter estimation. In chapter 2 we apply the proposed methodology to localize a BS from quantized TOA measurements. The resulting algorithm is tested using simulated data and real field measurements. Chapter 3 presents an algorithm, based on the proposed methodology, to locate an MS using joint AOA and TOA measurements of the multipath signals impinging on a antenna array situated at the participating BSs. The resulting algorithm is tested using simulated data. Appendices A and B provide some material support for chapter 2, and appendices C and D for chapter 3.

Some of the work presented in this part has been published during the course of this research. The applications presented in chapters 2 and 3 appear respectively in [18] and [20].

Contributions

This part consist of statistical model definition, algorithms developing, theoretical analysis, computer simulations and real field test for some algorithms. Its main contributions to the field of wireless network geolocalisation are:

1. A methodology to estimate the position of a wireless network element using radio measurements (TOA, AOA, TDOA and RSS) corrupted by measurement noise, systematic offsets, quantization, multipath and NLOS propagation.

2. A Timing Advance-Based Localization Algorithm (TABLA) to localize a BS using quantized measurements of the time of arrivals.

3. Two Angle and Delay of Arrival-Based Localization Algorithms (ADABLA) to localize an MS using joint angle and time of arrival measurements.

Chapter 1

Measurement model

This chapter introduces a statistical model for radio measurements in wireless communication systems, which accounts for impairments due to multipath and NLOS propagation, measurement noise, systematic offsets and quantization. It also provides the theory of the expectation-maximization (EM) algorithm to estimate the parameters of interest. Because of the flexibility of the proposed approach different types of signal measurements fit in the same framework i.e. time of arrival (TOA), angle of arrival (AOA), time differences of arrival (TDOA), received signal strength (RSS), etc. The organization of this chapter is as follows. In section 1.1 we present a localization system classification, then in section 1.2 we review the most used radio measurements and the associated localization techniques. Section 1.3 discusses the most common sources of error affecting the radio measurements. The statical model accounting for the aforementioned impairments is described in section 1.4. Section 1.5 outlines the expectation-maximization algorithm to obtain the maximum likelihood estimate. Finally, we present the conclusions in section 1.6.

1.1 Localization system classification

According to where the radio measurements are made and where the position information is used, the localization systems fall into two main categories: self-localization and remote localization. In order to keep a general framework in the following discussion we mean by:

- **Target**: the network element to be localized (BS or MS), and by
- **Observer**: the fixed (or moving) sensor platform able to perform measurements from the target emissions.

1.1.1 Self-localization

In a self-localization system the target makes the appropriate signal measurements from geographically distributed transmitters and uses these measurements to determine its position. Therefore, the target becomes also the observer. For instance, a well-known form of self-localization in wireless communication systems is given by a mobile station (MS) determining its position from signals received from some base stations (BSs) or from the global positioning system (GPS).

1.1.2 Remote localization

In a remote localization system, observers at one or more locations measure a signal originating from, or reflecting off, the target to be localized. These measurements are communicated to a central site where they are combined to give an estimate of the position of the target. In wireless communication systems it is usually used to determine the position of an MS by measuring its signal parameters when received at the network BSs. In this type of localization, the BSs measure the signals transmitted from an MS and relay them to a central site for further processing and data fusion to provide an estimate of the MS location.

1.2 Measurements and localization techniques

No matter which localization system is used, the treatment of the radio measurements to estimate the position of a target is the same. There are a variety of ways in which position can be derived from the measurement of radio signals, and these can be applied to any cellular system, including GSM. The most important measurements are propagation time or time of arrival (TOA), time difference of arrival (TDOA), angle of arrival (AOA), and received signal strength (RSS). The use of a particular type of measurement defines a technique. However, all these techniques coincide in that, in general, each measurement defines a locus on which the target must lie. The point at which the loci from multiple measurements intersect defines the position of the target.

For simplicity in the following discussion on localization techniques, it is assumed that the observer(s) and target lie in the same plane. Meaning that the loci will be curves in two-dimensional space rather than surfaces in three-dimensional space. Thus, let denote the two-dimensional (2-D) target

position by

$$p = (x, y)^T$$

and the known observer position by

$$p_i = (x_i, y_i)^T$$

where $i = 1 \dots I$. Here I may have two meanings depending on whether we are using several fixed observers or a single moving observer. Therefore, for the former case I is the number of fixed observers at different positions. And for the latter case, I is the number of different positions where the same observer perform radio measurements. In both cases, the target is considered to remain at a fixed position.

The generic measurement z_i relative to the i-th observer position is a function $h_{\text{type}}(p, p_i)$ of both target position and observer position.

1.2.1 Time based techniques

In the sequel all measured times are multiplied by the speed of light to get a measure in meters rather than in nanoseconds.

Time of arrival (TOA)

The signal's travel time between the target and observer can be expressed in a completely synchronized network as follows

$$z_i = ||p - p_i|| = h_{TOA}(p, p_i)$$

The distance between the target and observer, computed from the measured propagation time, provides a circle, centered at the observer's position, on which the target must lie. Placing the observers at three different locations, the target's position is given by the intersection of its corresponding circles [40], [27] (see figure 1.1.a). This requires that the observers know the exact time at which the target will transmit, and that the observers have a very stable and accurate clock. Usually, the target clock is not synchronized, so its clock bias must be treated as a nuisance parameter.

Time difference of arrival (TDOA)

Taking time differences of TOA measurements eliminates the clock bias nuisance parameter. It is a practical target measurement related to relative distance, which can be expressed as

$$z_{i,j} = ||p - p_i|| - ||p - p_j|| = h_{\text{TDOA}}(p, p_i, p_j)$$

The time difference is converted to a constant distance difference to two observers to define a hyperbolic curve, with foci at the observers positions. The intersection of two hyperbolas determines the position of the target. Therefore, it is necessary to place three observers (2D case shown in figure 1.1.b) at different positions for localization. As for TOA, the synchronization accuracy determines the performance but also the observer locations.

Round trip time (RTT)

This approach involves the measurement of the round-trip time of a signal transmitted from an observer to a target and then echoed back to the observer, giving a result twice that of the TOA.

$$z_i = 2h_{TOA}(p, p_i)$$

As in the TOA localization technique, the target position will be given by the intersection of three circles centered at the observers positions. This method does not rely on the synchronization between the target and the observer, and is the more common means of measuring propagation time.

1.2.2 Angle-Of arrival (AOA)

The AOA may be measured either with a mechanically steered narrow beamwidth antenna or with a fixed array of antennas. The AOA measurement expressed as

$$z_i = h_{\text{AOA}}(p, p_i)$$

defines a line of bearing formed by a radial from an observer to the target. The intersection of two directional lines of bearing defines a unique position of the target (see figure 1.1.c). This technique requires a minimum of two observers to determine a position and does not require the synchronization between target and observer.

1.2.3 Received signal strength (RSS)

The transmitted and received signal power are known to the location system, so the signal attenuation (which increases with distance) can be computed.

The attenuation is averaged over fast fading and depends on the traveled distance and slow fading. The RSS measurement which can be expressed as

$$z_i = h_{\text{RSS}}(||p - p_i||)$$

provides a distance estimate between the target and observer. As in TOA case, such a distance defines a circle centered at the observer's position on which the target must lie. By collecting multiple RSS measurements at different positions, the location of the target can be determined by the intersection of at least three circles [40].

1.2.4 Hybrid techniques

A hybrid technique, i.e. mixing TDOA-RSS, AOA-TOA, etc. may be used to obtain more accurate target position estimates [79, 83] and to reduce the number of observers used in the location process [27]. For example, a location system combining a TOA measurement with an AOA measurement can estimate the target position with a single fixed observer, see figure 1.1.d.

1.3 Sources of error

The positioning techniques described above perform well in situations where the measurements are free of errors. However, radio signal propagation is a complex phenomenon subject to random errors, which may produce inaccuracies on the measurement process of the received signals. Understanding the sources of error present in radio location systems is crucial to the development of good observation models for accurate radio source location. Some of the most important sources of error are presented below.

1.3.1 Noise measurement

When the measurements are made on signals propagating via direct or line of sight (LOS) paths, then it is commonly assumed that the estimation errors are small and primarily due to equipment measurement errors or background noise. The background noise e_t is commonly assumed to be a white random process. Hence

$$\begin{aligned} \mathbb{E}(e_t) &= 0, \\ \mathbb{E}(e_t e_{t'}) &= \sigma^2 \delta(t - t') \end{aligned}$$

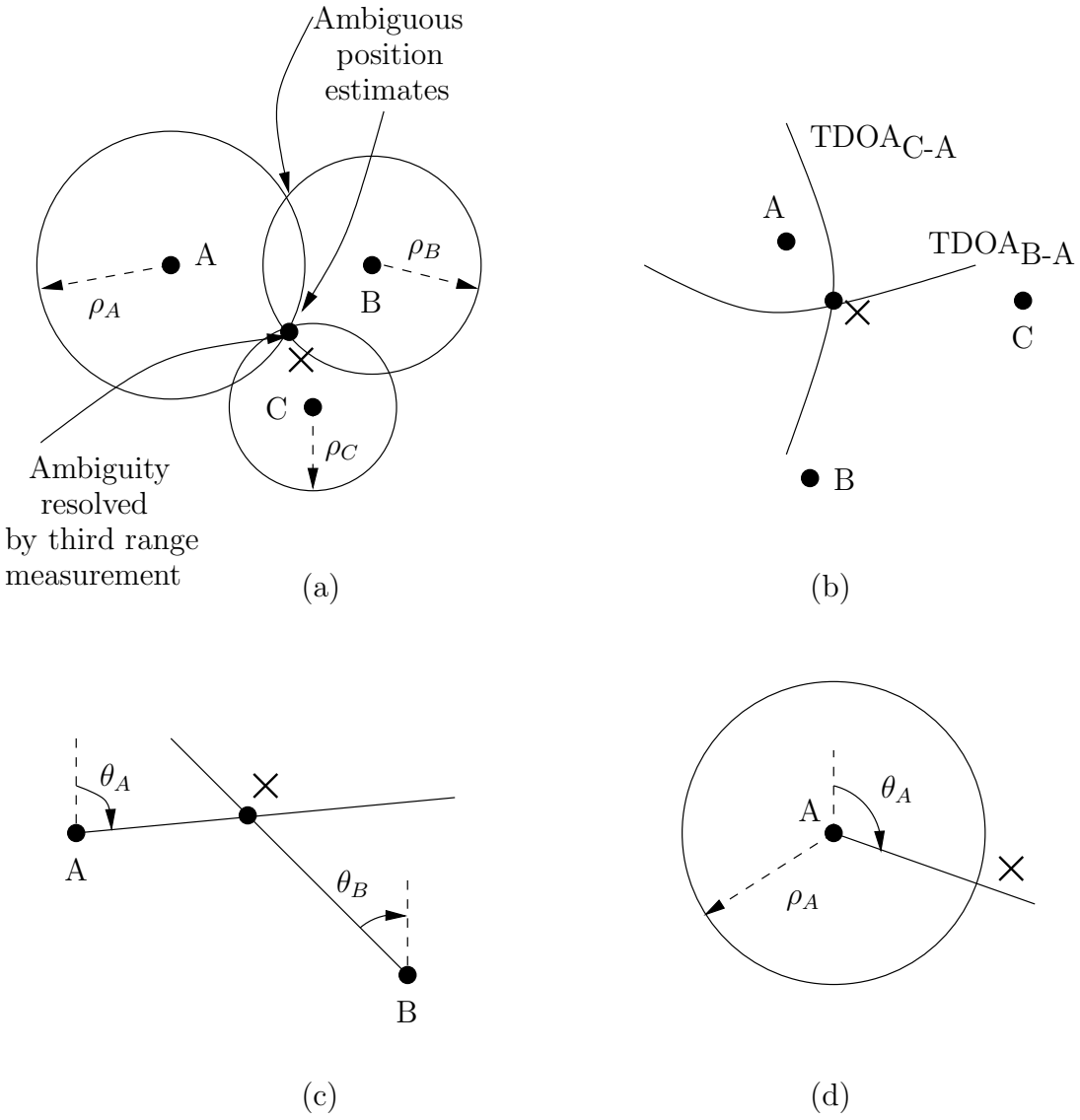

Figure 1.1: Examples of generic localization techniques: a) propagation time measurements and received signal strength (range); b) TDOA measurements; c) angle of arrival measurements; d) combination of range and angle measurements. A, B, and C represents the fixed observers. The target is positioned at the intersection of the loci and X stands for the true target position.

where $t \in \mathbb{R}$ and σ^2 is the noise variance. Motivated by asymptotic arguments or the central limit theorem, the random behavior of background noise is modeled as Gaussian distributed [84]. Therefore,

$$p_E(e_t) = \mathcal{N}(0, \sigma^2)$$

where $\mathcal{N}(0, \sigma^2)$ is short-hand notation for the Gaussian probability density function (pdf)

$$p_E(e_t) = (2\pi\sigma^2)^{-1/2} \exp(-e_t^2/2\sigma^2)$$

If this is not the case, the Gaussian distribution is the least informative distribution for a given variance, so the lower bounds to be computed still hold for estimation and filtering algorithms based on the Gaussian assumption [38]. Thus, the generic measurement accounting for noise and corresponding to the LOS path at i-th observer can be written as

$$z_i = h(p, p_i) + e_i.$$

1.3.2 Multipath

The multipath phenomenon is caused by objects (scatterers) lying in the environment a radio signal is propagating in. Multipath causes the spread of signals in time and space (and also in frequency if the target is moving), i.e. the received signal consists of multiple time-delayed replicas of the transmitted signal, arriving from various directions. The cause lies in the four basic mechanisms that govern wave propagation: reflection, refraction, diffraction and scattering, see figure 1.2. According to [81] the noiseless received signal at time t, with $t \in \mathbb{R}$, for a specular multipath environment may be written as

$$\mathbf{r}_t = \sum_{j=1}^{M_i} \mathbf{a}(\theta_j) b_j(t) s(t - \tau_j) \tag{1.1}$$

where

- M_i is the number of propagating paths at the i-th observer position,
- $\mathbf{a}(\theta_j)$ is the antenna response for a signal with an AOA of θ_j (more of this in chapter 3),
- $b_j(t)$ is the complex path attenuation (fading), and
- $s(t - \tau_j)$ is the narrowband transmitted signal with time delay τ_j.

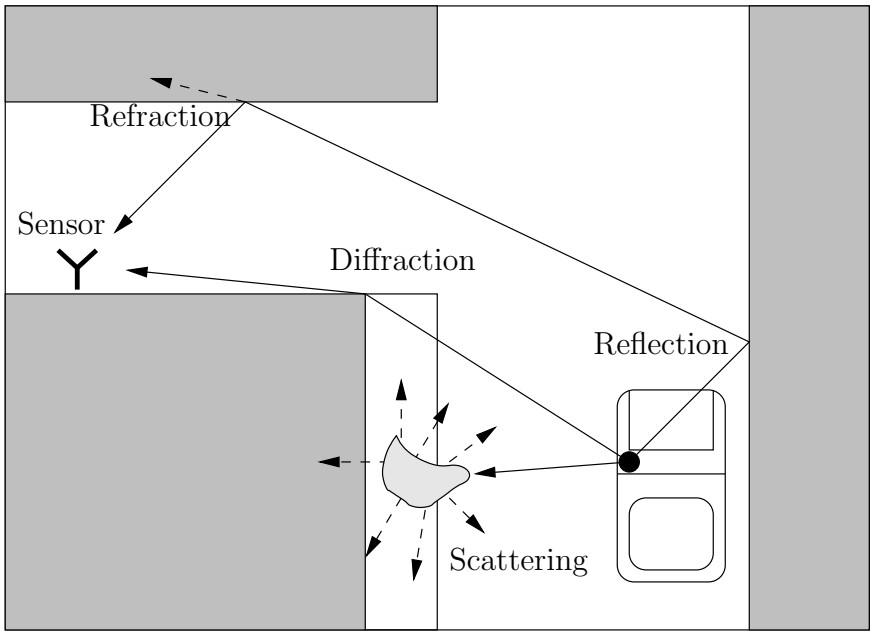

Figure 1.2: Propagation mechanisms.

As it can be inferred direct estimation of the LOS parameters (AOA, TOA, RSS, etc.) from the received signal $\mathbf{r}_t$, may present large errors due to the presence of secondary paths [13]. Therefore, the accuracy of the location method would be reduced. One way to overcome this is to detect all the multipath components and to chose that one associated to the LOS path for location purposes. For instance, in wireless communication systems high-resolution techniques, such as MUSIC and ESPRIT have been employed to estimate the multipath parameters. Therefore, detecting the multipath components at the i-th observer position, the generic measurement is not longer a scalar but a vector that can be written as

$$Y_i = \left[\begin{array}{cccc} y_i^1 & y_i^2 & \cdots & y_i^{M_i} \end{array} \right]^T$$

where y_i^j is the generic measurement corresponding to the j-th path at observer i. It should be noticed that elements in vector Y_i may be composed by an LOS (if present) and $M_i - 1$ NLOS measurements.

1.3.3 Non-line-of-sight propagation

An important source of error in the measurements is due to the presence of objects obstructing the line of sight between observer and target. In such a situation the emitted signal is reflected or diffracted and takes a longer

path than the LOS one. In time-based location systems, the non line of sight (NLOS) propagation introduces a positive error in the time measurements. This error can average 400-700m in the GSM [72]. Hence, NLOS propagation will severely bias the TOA or TDOA measurements even when high-resolution timing techniques are employed and there is no multipath interference. On the other hand, the error in AOA due to NLOS propagation can be either positive or negative [84]. Further, the magnitude of AOA error depends on the location of the scatterer or obstacle that is closest to the observer along the direction of the incoming signal. Scatterers close to the observer can result in the range $[0, 2\pi]$ and consequently the measured AOAs may be too unreliable for localization purposes [24, 84].

Since, in general, the random behavior of NLOS measurements is very dependent on the environment, as well as on the position of the scatterers with respect to the target and observer's positions, then it is often convenient to treat NLOS measurements as "outliers" [38]. Because outliers do not provide any information about the target position, then they should be ruled-out from the localization process in order to produce accurate target position estimations. Therefore, in order to deal with NLOS measurements in a statistical manner, one may assume a flat prior of such measurements over the measurement space $\mathcal{E}$. This is

$$p(y^{\text{NLOS}}) = \mathcal{U}(\mathcal{E})$$

where $\mathcal{U}(\mathcal{E})$ is short-hand notation for the uniform distribution over the space $\mathcal{E}$. Of curse, it is possible to consider a more informative pdf for the NLOS measurements (if available). For instance, in the presence of scatterers around the target well-known statistical models of an NLOS propagation are given by the *ring of scatterers* or *disk of scatterers* models [5]. This is not consider in this dissertation part. However, the methodology proposed in this chapter can be easely extended to such a situation considering a different pdf for the NLOS measurements.

1.3.4 Systematic offsets

As it was seen the TOA based location technique requires accurate synchronization between the sensor and source clocks so that the measurements are adequate approximations for the actual distances. Many of the current wireless system standards only mandate tight timing synchronization among base stations. However, some of them as the IS-95A (CDMA) standard, published by the Telecommunications Industry Association (TIA) of Arlington, Va., allows up to a 10 microsecond uncertainty in the time of transmission from the

base stations to the mobile stations [31]. Because the wireless signal propagates at the speed of light, approximately 3×10^8m/s, a 10 microsecond offset in transmission time, translates to 3 kilometers in ranging error. On the other hand, the source clock itself might have a drift that can reach a few microseconds [68]. This drift directly generates an error in the location estimate of the TOA and RTT method. For example, in the GSM standard the mobile station timing offsets are detected and reported with an accuracy of ± 1 symbol period [29]. Angle of arrival based location systems may also present some systematic offsets due to flaws in the antenna placement [94]. Typically, these errors tend to be mitigated with expensive periodical calibration and maintenance of the antenna systems. However, calibration as a means to reduce bias error will not work for existing systems designed without incorporating that approach ab initio [25].

Hence, in order to accurately obtain position estimates it is necessary to take into account such systematic offsets. Thus, the LOS measurement is

$$z_i = h(p, p_i) + \mu_i + e_i$$

where μ^i stands for a constant offset at observer i.

1.3.5 Quantization

In remote localization systems, if the communication link between observers and central site is stringent, it may be required the quantization of the measurements before its transmission. Quantized measurements may be also originated by the finite-precision hardware used to measure radio signals. For instance, in [51,54] the localization of a MS is achieved processing quantized measurements of the TDOA and/or RSS, performed by the MS. Another example is given by the localization of a BS or an MS in a TDMA based communication systems using quantized measurements of the TOA [18, 75]. In TDMA based communication systems, such as GSM, the base station (BS) send, for synchronization purposes, to each mobile station (MS) a timing advance (TA) which represents the perceived amount of round-trip propagation delay BS-MS-BS. In the GSM standard, the TA is quantized to with a quantization step of 553m. As it can be inferred, in situations where the quantization error is significant, it must be taken into account in order to obtain accurate target position estimations. Thus, to account for quantization let denote the generic measurement as

$$y^{\mathrm{LOS}} = Q(z_i)$$

where y^{LOS} now belongs to an N-element finite set $\mathcal{S}_N$, and Q stands for the quantizer.

1.4 Measurement model proposal

Let denote $h(p, p_i)$ the generic relationship between the target and the observer positions, located respectively in p and p_i, where $i = 1 \dots n$. To sum up the effects of additive noise, the presence of multiple simultaneous measurements due to multipath, outliers, systematic offsets and quantization, on the measurement process of $h(p, p_i)$, we propose the following observation model

$$Y_i = \begin{bmatrix} y_i^1 & y_i^2 & \cdots & y_i^{M_i} \end{bmatrix} \tag{1.2}$$

where

$$y_i^j = \begin{cases} Q(z_i), & \text{if} \quad \psi_i = j \\ u_i, & \text{if} \quad \psi_i \neq j \quad \text{or} \quad \psi_i = 0 \end{cases} \tag{1.3}$$

with

$$z_i = h(p, p_i) + \mu_i + e_i \tag{1.4}$$

where we made the following assumptions:

- $\{Y_i\}_{i=1:n}$ is a sequence of independent random vectors, where each M_i-dimensional vector Y_i represents the available measurement vector at position i.
- y_i^j is the j-th element in the observation vector Y_i, with $j \in \{1, 2, \dots, M_i\}$, whose discrete random values (if quantization is performed) belong to the N-element finite set $\mathcal{S}_N$.
- $\{u^i\}_{i=1:n}$ is a sequence of i.i.d. random variables representing the outlying observations, whose discrete random values (if quantization is performed) belong to the N-element finite set $\mathcal{S}_N$.
- $Q(\cdot)$ denotes the quantization function, which approximates continuous entries with a finite (preferably small) set of values taken from $\mathcal{S}_N$. It should be noticed that if quantization is not performed, i.e. $Q(z) = z$, then y_i^j and u_i, for all j and all i, are continuous random variables over the measurement space.
- $\{e_i\}_{i=1:n}$ is a sequence of independent random variables distributed as a Gaussian with zero-mean and variance σ^2.
- $\{\psi_i\}_{i=1:n}$ is a sequence of i.i.d. hidden random variables, taking its values in the set $\{0, 1, \dots, M_i\}$, with probability

$$p(\psi_i = k) = \begin{cases} 1 - P_D & \text{if} \quad k = 0 \\ P_D / M_i & \text{if} \quad k \neq 0 \end{cases} \tag{1.5}$$

where $P_D \in [0,1]$ is the prior probability of target detection. It should be noticed that $\psi_i \neq 0$ denotes the index of the LOS measurement in vector Y_i, and $\psi_i = 0$ represents the absence of LOS measurement in Y_i.

1.5 Parameter estimation via the EM algorithm

Let Y be a random vector distributed under $p(y;\theta)$, where $\{p(y;\theta), \theta \in \Theta\}$ denotes a parametric family of probability density functions indexed by a parameter $\theta \in \Theta$, where Θ is a subset of $\mathbb{R}^{d_\theta}$ (for some integer d_θ). Parameter estimation consist in estimating the parameter θ of the pdf $p(y;\theta)$ using a set of realizations of Y [43], i.e. using the set $Y_{1:n} = (Y_1, \ldots, Y_n)$. A common method for performing parameter estimation via measured data is the maximum-likelihood method [43]. Using this approach, the parameter θ may be estimated according to

$$\hat{\theta} = \underset{\theta \in \Theta}{\operatorname{argmax}} \log p(Y_{1:n};\theta)$$

where $\log p(Y_{1:n};\theta) = \sum_{i=1}^{n} \log p(Y_i;\theta)$ is known as the log-likelihood function and $p(y;\theta)$ is the pdf induced from the data model.

When the above maximization is analytically complicated, an alternative method for optimizing the log-likelihood function is through the use of the expectation-maximization (EM) algorithm introduced, in its full generality, by Dempster *et al.* (1977) in their landmark paper [26]. The common strand to problems where this approach is applicable is a notion of *incomplete data*, which includes de conventional sense of *missing data* but is much broader than that. The EM algorithm demonstrates its strength in situations where some hypothetical experiments yields *complete data* that are related to the parameters more conveniently than the measurements are. Given the literature available on the topic, the objective in this presentation is not to provide a comprehensive review of all the results related to the EM algorithm, but rather to outline the algorithm and to highlight some of its key features.

1.5.1 Expectation-Maximization algorithm outline

Using the terminology introduced by Dempster *et al.*, let denote $X_{1:n} = (X_1, \ldots, X_n)$ the set of *complete data*, where X_i, for $i = 1, \ldots, n$, are realizations of a random vector X distributed under $p(x;\theta)$. Let also rename $Y_{1:n}$ as the *incomplete data* set, which according to some statistical model it

may be viewed as a deterministic function of $X_{1:n}$. Under such a considerations, the EM algorithm consists in iteratively building a sequence $\{\theta_k\}_{k\geq 1}$ of parameter estimates given an initial guess θ_0. Each iteration is classically broken into two steps as follows:

1. **E-step**: consists in evaluating the conditional expectation
$$Q(\theta, \theta_k) = \sum_{i=1}^{n} \mathbb{E}_{\theta_k}[\log p(X_i; \theta)|Y_i] \tag{1.6}$$
where θ_k is the current estimate of θ, after k iterations of the algorithm.

2. **M-step**: maximizes expression (1.6) with respect to θ to obtain θ_{k+1}, this is
$$\theta_{k+1} = \underset{\theta\in\Theta}{\operatorname{argmax}}\, Q(\theta, \theta_k) \tag{1.7}$$

The essence of the EM algorithm is that increasing $Q(\theta, \theta_k)$ forces an increase of the log-likelihood $\log p(Y_{1:n}; \theta)$ [26], see figure 1.3 for a graphical interpretation. Hence the EM is a monotone optimization algorithm. Furthermore, if the iterations ever stop at a point $\theta^\star$, then $Q(\theta; \theta^\star)$ has to be maximal at $\theta^\star$ (otherwise it would still be possible to improve over $\theta^\star$), and hence $\theta^\star$ is such that $\nabla_\theta p(Y_{1:n}; \theta^\star) = 0$, that is, this is a *stationary point of the likelihood*. Stronger conditions are required to ensure that the sequence of parameter estimates produced by EM from any starting point indeed converges to a limit $\theta^\star \in \Theta$ [16]. However, it is actually true that when convergence to a point takes place, the limit has to be a stationary point of the likelihood. The reader is referred to [91] and [55] for the convergence properties of the EM algorithm.

Generalized EM algorithm

In the formulation of the EM algorithm described above, θ_{k+1} is chosen as the value of θ for which $Q(\theta, \theta_k)$ was maximized. While this ensures the greatest increase in $\log p(Y_{1:n}; \theta)$, it is however possible to relax the requirement of maximization to one of simply increasing $Q(\theta, \theta_k)$ so that $Q(\theta_{k+1}|\theta_k) \geq Q(\theta_k|\theta_k)$. This approach, to simply increase and not necessarily maximize $Q(\theta_{k+1}|\theta_k)$ is known as the Generalized Expectation Maximization (GEM) algorithm and is often useful in cases where the M-step is difficult.

1.6 Conclusions

In this chapter we first presented the most used positioning techniques in wireless communications systems. We also review some sources of error

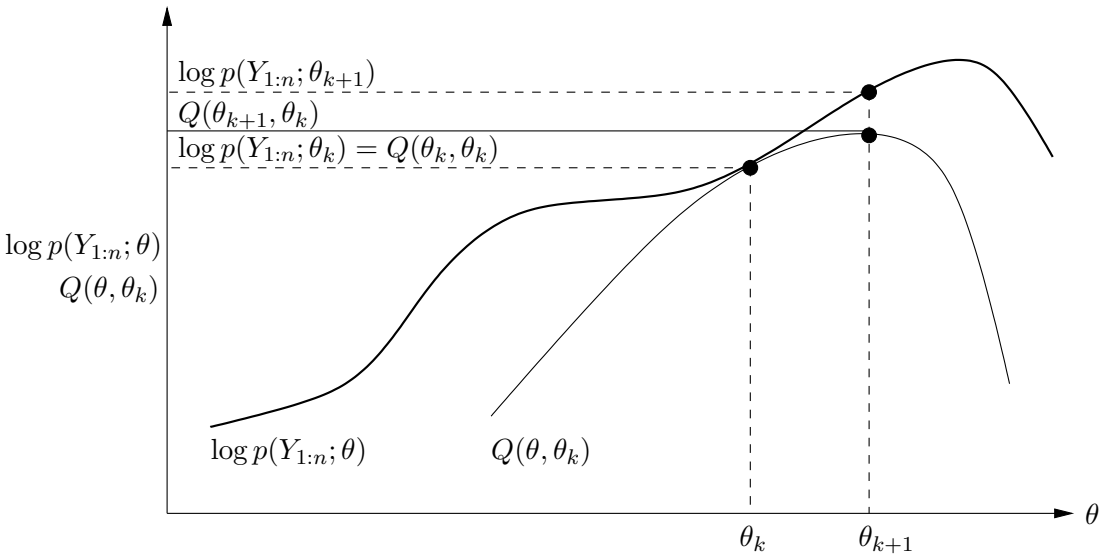

Figure 1.3: Graphical interpretation of a single iteration of the EM algorithm: The function $Q(\theta|\theta_k)$ is upper-bounded by the likelihood function $\log p(Y_{1:n};\theta)$. The functions are equal at $\theta = \theta_k$. The EM algorithm chooses θ_{k+1} as the value of θ for which $Q(\theta|\theta_k)$ is a maximum. Since $\log p(Y_{1:n};\theta) \geq Q(\theta|\theta_k)$ increasing $Q(\theta|\theta_k)$ ensures that the value of the likelihood function $\log p(Y_{1:n};\theta)$ is increased at each step.

present in the positioning measurements, which in turn lead to inaccuracies on the source position estimation in any positioning technique. Afterwards, we proposed an statical model accounting for these impairments. Finally, we presented the EM algorithm as a means to explore maxima of the likelihood of a set of available observations.

In the following chapters we employ the proposed measurement model and the EM algorithm to localize network elements of a wireless communication system.

Chapter 2

TABLA: Timing Advance-Based Localization Algorithm[1]

In this chapter we propose an algorithm to localize a BS of a GSM communications system. The BS position estimation is performed using a collection of severely quantized TOA measurements. The TOAs also present errors due systematic offsets, NLOS propagation and additive noise. Hence, the statistical model presented in chapter 1 is used to model the random behavior of the measurements. The resulting timing advance-based localization algorithm (TABLA) is tested using real field measurements collected in different environments (rural, semi-urban and urban). Test results shows the efficiency of TABLA to localize a BS with an accuracy lower than the quantization step.

The remainder of this chapter is organized as follows: section 2.1 states the requirements to perform BS localization. In section 2.2 a preliminary study is presented to get an understanding on the type of measurements, as well as the location technique to be used. Section 2.3 presents the development of the proposed algorithm, which is tested using syntectic data in section 2.4. In section 2.5 the algorithm is tested employing real field measurements. Finally, in section 2.6 we give the conclusions.

2.1 Problem statement

The objective is to propose an approach able to accurately estimate the position of a BS in the GSM communication system. The approach must

[1]Part of this material appears in [18].

fulfill the following requirements:

- the BS to be localized is a non cooperative element,
- the communication protocols must not be modified, and
- the observations consist of timing advance measurements available at the MS.

Thus, under the approach presented in the previous chapter, the target is considered to be the BS and the observer an MS.

2.2 Preliminary study

In this section we present some basic concepts concerning the radio link in the GSM communication system. Paying special attention to the timing advance measurement which can be used for localization purposes. Such a concepts will be useful in the understanding of the proposed approach to estimate the position of a BS, which is detailed in the following sections.

2.2.1 Radio link

GSM is a cellular network, which means that mobile phones connect to it by searching for cells in the immediate vicinity. GSM networks operate in four different frequency ranges. Most GSM networks operate in the 900 MHz or 1800 MHz bands. Some countries in the Americas (including Canada and the United States) use the 850 MHz and 1900 MHz bands because the 900 and 1800 MHz frequency bands were already allocated.

Since radio spectrum is a limited resource shared by all users, a method must be devised to divide up the bandwidth among as many users as possible. The method chosen by GSM is a combination of Time and Frequency Division Multiple Access (TDMA/FDMA). In the 900 MHz band the uplink (MS to BS) frequency band is $890-915$ MHz, and the downlink (BS to MS) frequency band is $935-960$ MHz. This 25 MHz bandwidth is subdivided into 125 carrier frequency channels, each spaced 200 kHz apart. The frequencies are allocated in pair, so that each uplink/downlink pair is separated with exactly 45 MHz, see figure 2.1 for a graphical explanation.

Time division multiplexing is used to divide each of the carrier frequencies into eight full-rate or sixteen half-rate logical channels. There are eight radio times-slots (giving eight burst periods) grouped into what is called a TDMA frame and lasts 4.615 ms, see figure 2.2. Half rate channels use alternate frames in the same times-lot. The duration of a burst is 577 μs. The total

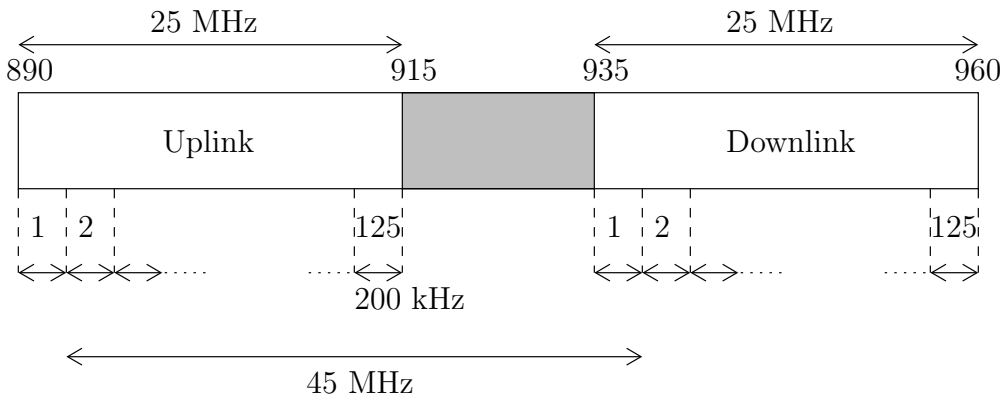

Figure 2.1: GSM frequency multiplexing

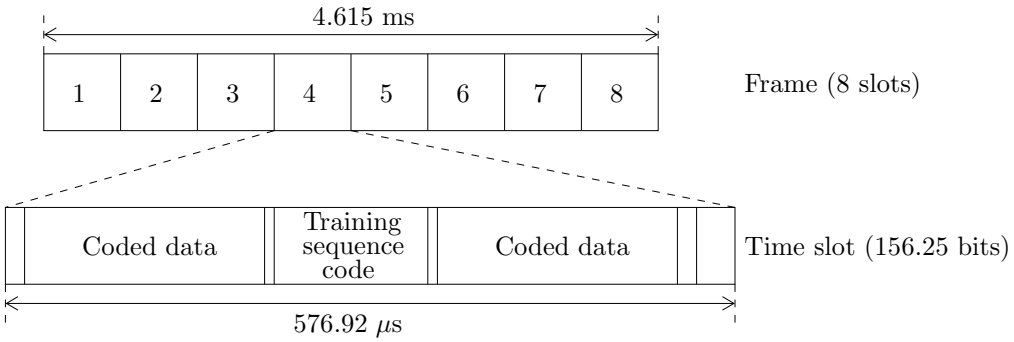

Figure 2.2: GSM time multiplexing

bit rate for all 8 channels is 270.833 kbit/s, whereas the bit rate for each channel is 22.8 kbit/s.

2.2.2 Timing Advance

In order to get TDMA scheme to work, the bursts from each MS, sharing the same frame, must fit correctly into the assigned time slot when received by the BS. Otherwise, the bursts from the MSs using adjacent time slots could overlap, resulting in a poor transmission or even in a loss of communication. Unfortunately, the MSs within the same cell are at different distances from its serving BS, and therefore their transmissions undergo different propagation delays. Thus, in order to ensure the MS' burst period is received at the BS within its respective time-slot, it is used the concept of Timing Advance (TA). This consists in indicating to each MS the time it must advance its transmission in order to not overlap its burst with others in the same frame, please see figure 2.3 for a graphical explanation.

The serving BS measures the TA by assessing the round trip time of signals exchanged between the MS and BS. Afterwards, the BS issues the TA to the MS in a 6-bit coded number, representing the number of bit periods the MS must advance its transmission time. The TA value can be mapped to distance based on the transmission rate of the radio. In GSM the duration of a bit is approximately $T_b = 1/R_b = 3.70$ μs. Therefore an advance of one bit interval will account for a round-trip delay of approximately 1,108 meters, or a one-way distance of $q = 554$ m. Since the TA is rounded to the nearest bit-period during calculation, the actual BS-MS distance, d, is:

$$\max\left\{0, \left(TA - \frac{1}{2}\right) q\right\} \leq d < \left(TA + \frac{1}{2}\right) q \tag{2.1}$$

where TA is an integer number between 0 and 63, which in turn 0 indicates no timing advance and 63 indicates the maximum timing advance corresponding to a propagation delay of 233 μs.

In the GSM standard, the TA value is computed from the first arrived propagation path which has a significant reception power level. It is available only in a connected mode (i.e. during the life time of a communication) and it is refreshed at the MS side every 480 ms [75].

2.2.3 Localization based on timing advance measurements

Consider a 2D localization and assume the absence of any kind of impairments in the measurement process of the TA. Under such a conditions, by retrieving a TA value from the MS, the BS must lie in a ring centered at the MS position and with inner and outer radii equal to $R_1 = \max\{0, (TA - 1/2)q\}$ and $R_2 = (TA + 1/2)q$, respectively. Consequently, the use of at least three TA values at different MS positions will permit to localize the BS within a region delimited by the intersection of the three rings corresponding to the each TA value, see figure 2.4. It should be notice that the size of the intersection region may be too large, for accurate positioning purposes, because of its strongly dependence on the quantization step, which is already fixed in the GSM standard and equals to $q = 554$ m. In spite of this, by collecting multiple TA measurements from closely MS positions along any direction, it is possible to detect a variation in the TA value. The detection of such a variation between two consecutive MS positions will reveal the quantization bound between the MSs, and thus the radium of the circle on which the BS lies. By repeating the procedure three times the BS position can be estimated with an accuracy that no longer depends on the quantization step,

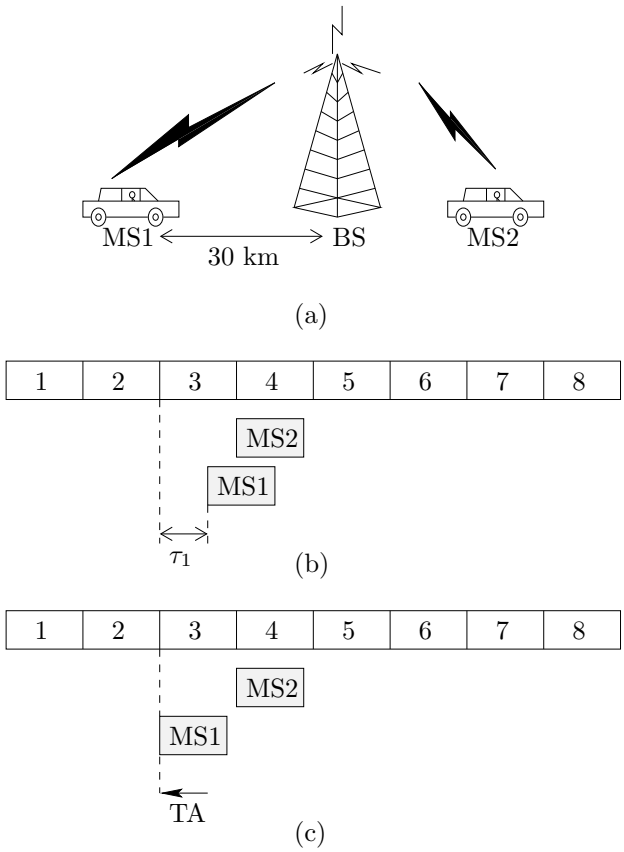

Figure 2.3: The timing advance concept: (a) two MSs at different distances from the BS. (b) The bursts of two contiguous MSs overlap because of the different propagation times. (c) Timing advance is used to avoid overlapping bursts.

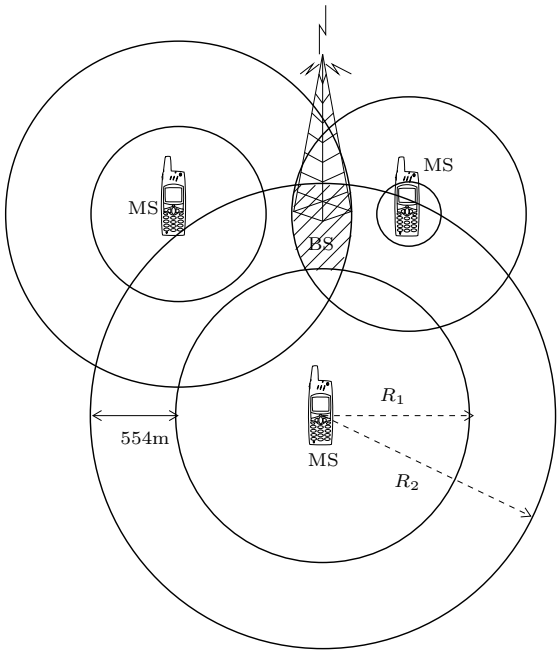

Figure 2.4: In the absence any kind of impairments, three TA values at different positions will confine the BS position to a region whose size depend on the quantization step $q = 554$ m.

but on the distance between the MS positions.

In practice, even using the technique described above, it is difficult to accurately estimate the position of the BS. This is because the absolute distances BS-MS obtained from TA measurements (i.e. using equation (2.1)) are subject to measurement errors. Three main elements contribute to this error. The first one is the systematic offsets inherent to a BS and/or MS transmission drift, which may reach up to 10 μs [31, 68]. The second one is the propagation channel which is characterized by multipath and often by a condition of NLOS between MS and BS. In such a situation, it may happened that the measured TA may be significantly different from its real value, constituting what we refer from now on an *outlying observation*. Finally, the third source of error is the finite TA resolution that allows to represent absolute distances with a resolution of $q = 554$ m.

The combined effect of these sources of error can be seen from experimental data. As an example, figure 2.5 reports the histogram of the TA measurement error computed from real field measurements performed in an urban area: the propagation channel and the systematic offsets mostly introduce outlying observations and bias the TA measurement error (the mean error μ_{TA} is positive) and the finite TA resolution introduces a minimum

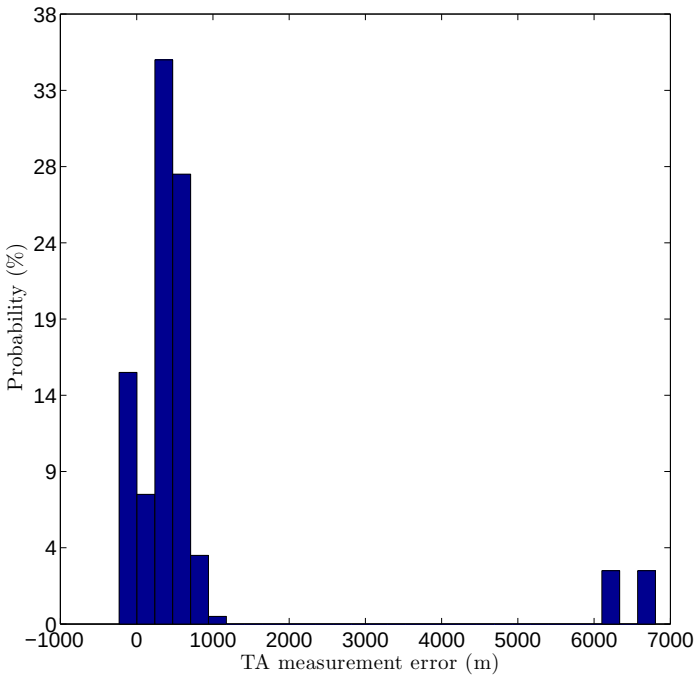

Figure 2.5: Distribution of the TA measurement error

negative measurement error [74].

2.3 Proposed approach

In order to increase the accuracy on the BS position estimation, it is necessary to account for the impairments affecting the absolute distances between BS and MS. A way to do this, is by using the statistical approach presented in chapter 1. In the this section we provide the details of such a procedure for this specific problem.

2.3.1 Observation model

Let us denote by $\chi_i(x_s)$ the absolute distance between the BS and MS, located respectively at x_s and x_i. Since only one TA measurement per refresh time is available at the MS side, only one element is present in the observation vector Y_i in expression (1.2), thus Y_i is a scalar and $\psi_i \in \{0, 1\}$, which enable

us to write

$$Y_i = Q(Z_i) \cdot \psi_i + U_i \cdot (1 - \psi_i) \tag{2.2}$$

where

- $\{Y_i\}_{i=1:n}$ is a sequence of random variables, representing the TA value at the i-th MS position, whose discrete random values belong to the 64-element finite set $\mathcal{S}_{64} = \{0, 1, \dots 63\}$,
- $Q(\cdot)$ is the quantizer defined according to (2.1) as

$$Q(z) = \begin{cases} 0 & \text{if} \quad 0 \leq z < \frac{1}{2}\, q \\ y & \text{if} \quad (y - \frac{1}{2})q \leq z < (y + \frac{1}{2})q \end{cases} \tag{2.3}$$

  where z denotes the distance between the BS and MS, $y \in \{1, \dots, 63\}$ and where $q = 554$m is the quantization step.

- $\{Z_i\}_{i=1:n}$ is the sequence of LOS distance measurements BS-MS, considered to be independent hidden random variables distributed as a Gaussian with mean $\chi_i(x_s) + \mu$ and variance σ^2. Where μ stands for a systematic drift and σ^2 for the variance of the measurement noise.
- $\{\psi_i\}_{i=1:n}$ is a sequence of i.i.d. hidden random variables, taking their values from the set $\{0, 1\}$, where $\psi_i = 1$ stands for an LOS observation and $\psi_i = 0$ for an outlier at the i-th MS position. We denote $P_D = \mathbb{P}(\psi_i = 1)$.
- $\{U_i\}_{i=1:n}$ is a sequence of i.i.d. hidden random variables representing the outlying observations. For simplicity, we assume that for an outlying observation all values in the set $\mathcal{S}_{64}$ are equally likely. Meaning that U_i is distributed as a discrete uniform random variable over the set $\mathcal{S}_{64}$, with probability $\mathbb{P}(U_i = u_i) = 1/64$, and
- triplets $\{(U_i, \psi_i, Z_i)\}_{i=1:n}$ are independent.

2.3.2 Likelihood of the observations

Let denote the joint probability distribution of (Y_i, Z_i, ψ_i) as $p(y_i, z_i, \psi_i)$. Thus, according to the above assumptions and with some abuse in the mathematical notation we write

$$p(y_i, z_i, \psi_i) = \mathbb{P}(y_i|z_i, \psi_i)p(z_i)\mathbb{P}(\psi_i) \tag{2.4}$$

To find an expression of $\mathbb{P}(y_i|z_i, \psi_i)$, notice that the relation $Y_i = Q(Z_i)$ is deterministic and that if $Z_i = z_i$ and $\psi_i = 1$, then $\mathbb{P}(y_i|z_i, \psi_i) = \mathbb{1}\{y_i = Q(z_i)\}$. On the other hand, if $\psi_i = 0$, then $\mathbb{P}(y_i|z_i, \psi_i) = 1/N$, where $N = 64$. Hence, these allow us to write

$$\mathbb{P}(y_i|z_i, \psi_i) = \mathbb{1}\{y_i = Q(z_i)\}\mathbb{1}\{\psi_i = 1\} + \frac{1}{N}\mathbb{1}\{\psi_i = 0\} \tag{2.5}$$

and in a similar manner it can be deduced that

$$\mathbb{P}(\psi_i) = P_D\mathbb{1}\{\psi_i = 1\} + (1 - P_D)\mathbb{1}\{\psi_i = 0\} \tag{2.6}$$

Now, substituting (2.5) and (2.6) into (2.4) it can be shown

$$p(y_i, z_i, \psi_i) = \left(P_D\mathbb{1}\{y_i = Q(z_i)\}\mathbb{1}\{\psi_i = 1\} + \frac{1 - P_D}{N}\mathbb{1}\{\psi_i = 0\}\right)p(z_i) \tag{2.7}$$

with

$$p(z_i) = \phi(z_i; \chi_i(x_s) + \mu, \sigma^2) \tag{2.8}$$

where $\phi(z; \mu, \sigma^2)$ stands for the pdf a Gaussian random variable z with mean μ and variance σ^2.

Marginalizing (2.7) over z_i and ψ_i we obtain the probability law of the random variable Y_i

$$\mathbb{P}(Y_i = y_i; \theta) = P_D \int_{\mathcal{I}(y_i)} (2\pi)^{-1/2} e^{-\frac{t^2}{2}} dt + \frac{1 - P_D}{N} \tag{2.9}$$

where $\theta = \{x_s, \mu, \sigma^2, P_D\}$ stands for the full parameters vector and where

$$\mathcal{I}(y_i) = \{t : y_i = Q(t)\} = \{t : a_i \leq t < b_i\} \tag{2.10}$$

represents the integration interval with lower and upper bounds given respectively by

$$a_i = \frac{\max\{0, (y_i - 1/2)q\} - \chi_i(x_s) - \mu}{\sigma} \tag{2.11}$$

$$b_i = \begin{cases} \frac{(y_i+1/2)q - \chi_i(x_s) - \mu}{\sigma} & \text{if} \quad y_i < 63 \\ +\infty & \text{if} \quad y_i = 63 \end{cases} \tag{2.12}$$

Finally, it can be shown that the likelihood of the observations $y_{1:n} = \{y_1, ...y_n\}$ may be written as

$$L(y_{1:n};\theta) = \prod_{i=1}^{n} \mathbb{P}(Y_i = y_i;\theta) \tag{2.13}$$

where $\mathbb{P}(Y_i = y_i;\theta)$ is given by (2.9).

The maximum-likelihood estimate of θ is given by the maximization of the likelihood function (eq. (2.13)) w.r.t. θ. Unfortunately, such a maximization untractable. However, a simpler procedure to obtain an ML estimate is given by expectation maximization algorithm outlined in chapter 1.

2.3.3 Identifiability

The identifiability of a statistical model is an important requirement in any estimation problem. A statistical model $\{p(\theta) : \theta \in \Theta \subset \mathbb{R}^{d_\theta}\}$ is said to be identifiable if and only if

$$p(\theta) = p(\theta') \Leftrightarrow \theta = \theta', \quad \forall\ \theta, \theta'.$$

where Θ denotes the set of all possible parameter values. Therefore, for the model under consideration (eq. (2.13)) we can state what follows:

Theorem 1 (non-identifiability) *Let $\theta = \{\mu, \sigma, \gamma, x_s\}$ be the full parameter vector and $L(y_{1:n};\theta)$ the likelihood function associated to the incomplete data $y_{1:n} = \{y_1, \cdots, y_n\}$. Then we have $L(y_{1:n};\theta') = L(y_{1:n};\theta)$, for all n and for all $y_{1:n}$, if and only if $P'_D = P_D$, $\sigma' = \sigma$ and*

$$\chi_i(x'_s) + \mu' = \chi_i(x_s) + \mu \quad \forall\ i = 1, \cdots, n. \tag{2.14}$$

Rewriting the latter equation as

$$\chi_i(x'_s) - \chi_i(x_s) = C \quad \forall\ i = 1, \cdots, n.$$

where $C = \mu - \mu'$ is a constant, it can be straightforwardly inferred that there is no identifiability between x_s and x'_s if the MS displacement is along a hyperbola (or any degenerate case of a hyperbolic curve) with one of its foci situated at x_s. *Hence, as a rule-of-thumb, the MS displacement strategy must avoid hyperbolic trajectories.*

2.3.4 3D BS position estimation issue

The BS and MS are located on the earth's surface. Thus, the distance between the MS in position x_i and the BS in position x_s, for the i-th measurement, can be written as

$$\chi_i(x_s) = \sqrt{(x_{i,1} - x_{s,1})^2 + (x_{i,2} - x_{s,2})^2 + (x_{i,3} - x_{s,3})^2} \tag{2.15}$$

where the indexes 1, 2 and 3 make reference to the three spacial coordinates within a 3D orthogonal coordinate system.

In the application under consideration, the MS moves on the earth's surface within a radium of some kilometers around the BS, thus with a few variation in altitude. Therefore, approximatively this corresponds to a quasi-planar movement in a 2D map. On the other hand, the height of the BS antenna h with respect to the ground is on the order of some tens of meters. It follows that

$$\chi_i(x_s) = \sqrt{\chi_{i,2D}^2(x_s) + h^2} \approx \chi_{i,2D}(x_s) + \frac{h^2}{2\chi_{i,2D}(x_s)}$$

where $\chi_{i,2D}(x_s)$ is the distance between the MS and the orthogonal projection of the x_s onto the 2D map. In practice the term $h^2/2\chi_{i,2D}(x_s)$, which is on the order of some units of meters, is difficult to estimate. This is because it is not distinguishable from the systematic offset μ present on the measurement process of the absolute distance BS-MS. In order to correctly estimate the value of h it is necessary to move the MS with great variations in its altitude. However, in the situation under consideration such an MS movement is not possible. Therefore, we concentrate on a 2D BS position estimation. Thus, the absolute distance to be considered is

$$\chi_i(x_s) = \sqrt{(x_{i,1} - x_{s,1})^2 + (x_{i,2} - x_{s,2})^2} \tag{2.16}$$

where the indexes 1 and 2 stand for the 2-D coordinates within the 2-D reference coordinate system.

2.3.5 Timing Advance-Based Localization Algorithm (TABLA) derivation

As it was seen in section 2.3.2 the direct maximization of the likelihood function (eq. (2.13)) to obtain an estimate of the BS position is cumbersome. However, we can use the expectation-maximization algorithm presented in chapter 1 to obtain the maximum likelihood estimate iteratively. In the following we provide the details in the derivation of such an iterative procedure.

Let $\{Y_i\}_{i=1:n}$ denote incomplete data consisting of TA values, and $\{Z_i, \psi_i\}_{i=1:n}$ the missing data. Together $\{Y_i, Z_i, \psi_i\}_{i=1:n}$ form the complete data, whose associated likelihood function is

$$L(y_{1:n}, z_{1:n}, \psi_{1:n}; \theta) = \prod_{i=1}^{n} p(y_i, z_i, \psi_i) \tag{2.17}$$

where $p(y_i, z_i, \psi_i)$ is given by (2.7).

Refereing to 1 each iteration of the EM algorithm may be formally decomposed into two steps: an E-step and an M-step.

E-step computation

The E-step consists in evaluating the conditional expectation of the likelihood of the complete data, eq. (2.17), which can be expressed as

$$Q(\theta, \tilde{\theta}) = \sum_{i=1}^{n} \mathbb{E}\left\{\log(p(\psi_i, Z_i, Y_i; \theta))|Y_i, \tilde{\theta}\right\} \tag{2.18}$$

It should be noticed that the expectation is taken w.r.t. the missing data given the incomplete data and the parameters vector $\tilde{\theta}$. Hence, it is necessary to know $p(z_i, \psi_i|y_i, \tilde{\theta})$. Using (2.7) and Bayes' rule, it is straightforward to prove that

$$p(z_i, \psi_i|y_i, \tilde{\theta}) = \frac{\left(\tilde{P_D}\mathbb{1}\{y_i = Q(z_i)\}\mathbb{1}\{\psi_i = 1\} + \frac{1-\tilde{P_D}}{N}\mathbb{1}\{\psi_i = 0\}\right)\tilde{p}(z_i)}{\mathbb{P}(Y_i = y_i; \tilde{\theta})} \tag{2.19}$$

where

$$\tilde{p}(z_i) = \phi(z; \chi_i(\tilde{x}_s) + \tilde{\mu}, \tilde{\sigma}^2)$$

Solving the expectation in (2.18), exploiting expressions (2.7) and (2.19), we obtain

$$\begin{aligned} Q(\theta, \tilde{\theta}) = \sum_{i=1}^{n} \Bigg[& \log(P_D) F_{\tilde{\theta}}(y_i) + \log\left(\frac{1-P_D}{N}\right)(1 - F_{\tilde{\theta}}(y_i)) \cdots \\ & + \frac{\tilde{\sigma}^2}{2\sigma^2}\left(F_{\tilde{\theta}}(y_i) - 2G_{\tilde{\theta}}(y_i)\delta_i(x_s) - H_{\tilde{\theta}}(y_i) - \delta_i^2(x_s) - 1\right) \cdots \\ & - \frac{1}{2}\log(2\pi\sigma^2)\Bigg] \end{aligned} \tag{2.20}$$

where

$$\delta_i(x_s) = \tilde{\sigma}^{-1}(\chi_i(\tilde{x}_s) - \chi_i(x_s) + \tilde{\mu} - \mu) \tag{2.21}$$

and

$$F_{\tilde{\theta}}(y_i) = \frac{\tilde{P}_D}{p(y_i;\tilde{\theta})}\int_{\tilde{a}_i}^{\tilde{b}_i}(2\pi)^{-\frac{1}{2}}e^{-\frac{t^2}{2}}dt, \tag{2.22}$$

$$G_{\tilde{\theta}}(y_i) = \frac{\tilde{P}_D}{p(y_i;\tilde{\theta})}\int_{\tilde{a}_i}^{\tilde{b}_i}(2\pi)^{-\frac{1}{2}}te^{-\frac{t^2}{2}}dt, \tag{2.23}$$

$$H_{\tilde{\theta}}(y_i) = \frac{\tilde{P}_D}{p(y_i;\tilde{\theta})}\int_{\tilde{a}_i}^{\tilde{b}_i}(2\pi)^{-\frac{1}{2}}t^2e^{-\frac{t^2}{2}}dt. \tag{2.24}$$

where $\tilde{a}_i$ and $\tilde{b}_i$ are respectively given by (2.11) and (2.12) with parameters $\tilde{x}_s$, $\tilde{\mu}$ and $\tilde{\sigma}$.

M-step computation

In the M-step, a new parameters estimate θ is obtained maximizing $Q(\theta,\tilde{\theta})$ w.r.t. θ. However, direct maximization of (2.20) is very difficult because of its high nonlinearity. Nevertheless, in the *generalized M-step*, we compute a new θ which is chosen in such a way that $Q(\theta,\tilde{\theta}) > Q(\tilde{\theta},\tilde{\theta})$. The essence of this is that any increase of $Q(\theta,\tilde{\theta})$ forces an increase of the likelihood of the incomplete data given by (2.9).

To implement the generalized M-step, we first maximize (2.20) w.r.t. P_D, μ and σ^2 keeping $x_s = \tilde{x}_s$ to then optimize (2.20) w.r.t. x_s regarding all others parameters as constants. Thus, keeping $x_s = \tilde{x}_s$ and canceling the first derivative w.r.t. P_D, μ and σ^2 yields

$$P_D = \frac{1}{n}\sum_{i=1}^{n}F_{\tilde{\theta}}(y_i), \tag{2.25}$$

$$\mu = \tilde{\mu} + \frac{\tilde{\sigma}}{n}\sum_{i=1}^{n}G_{\tilde{\theta}}(y_i) \tag{2.26}$$

$$\sigma^2 = \frac{\tilde{\sigma}^2}{n}\sum_{i=1}^{n}(H_{\tilde{\theta}}(y_i) - F_{\tilde{\theta}}(y_i) + 1) - (\tilde{\mu}-\mu)^2 \tag{2.27}$$

Now, to maximize (2.20) w.r.t. x_s, consider the above as constants in expression (2.20), and let drop out uninteresting terms, which allows to write

$$J(x_s) = -\frac{\tilde{\sigma}^2}{\sigma^2}\sum_{i=1}^{n}\delta_i(x_s)G_{\tilde{\theta}}(y_i) + \frac{\delta_i^2(x_s)}{2}$$

Then take its gradient w.r.t. x_s gives

$$\nabla J(x_s) = \frac{\tilde{\sigma}}{\sigma^2} \sum_{i=1}^{n} I_i(x_s) \nabla \chi_i(x_s) \tag{2.28}$$

where

$$I_i(x_s) = G_{\tilde{\theta}}(y_i) + \delta_i(x_s) \tag{2.29}$$

and

$$\nabla \chi_i(x_s) = \frac{x_s - x_i}{\chi_i(x_s)} \tag{2.30}$$

denotes the gradient of $\chi_i(x_s)$ w.r.t. x_s. Notice that finding a closed-form expression for the value of x_s that cancels $\nabla J(x_s)$ is very difficult. However, we can use the Newton-Raphson method to find out an x_s value which maximizes $J(x_s)$. This method is characterized by the extensive use of the gradient, as well as the Hessian matrix associated to the function to be maximized, in this case $J(x_s)$. The gradient is given by (2.28) and the Hessian can be readily computed as

$$\mathcal{H}_{x_s}(J(x_s)) = \frac{\tilde{\sigma}}{\sigma^2} \sum_{i=1}^{n} \left(I_i(x_s) \mathcal{H}_{x_s}(\chi_i(x_s)) - \frac{1}{\tilde{\sigma}} \nabla \chi_i(x_s) \nabla^T \chi_i(x_s) \right) \tag{2.31}$$

where

$$\mathcal{H}_{x_s^k}(\chi_i(x_s^k)) = \frac{1}{\chi_i^2(x_s^k)} \left[I_2 - \chi_i(x_s^k) \nabla \chi_i(x_s^k) \nabla \chi_i(x_s^k)^T \right] \tag{2.32}$$

is the Hessian matrix of $\chi_i(x_s)$ w.r.t x_s, and I_2 stands for the 2x2 identity matrix. Thus, according to [49] we can obtain a value of x_s, for which $J(x_s) = 0$, starting with $x_s^0 = \tilde{x}_s$ and iterating for $k = 0, \ldots, K$ the following expression

$$x_s^{k+1} = x_s^k + \lambda_k \mathcal{H}_{x_s}^{-1}(J(x_s^k)) \nabla J(x_s^k) \tag{2.33}$$

where $\lambda_k \in (0, 1]$ is a stepsize in the direction $\mathcal{H}^{-1}(J(x_s^k)) \nabla J(x_s(k))$ which assures $J(x_s^{k+1}) > J(x_s^k)$. The stepsize λ_k can be determined by a backtracking line search method [59], i.e. step halving, random, golden section search, polynomial fit, etc. [49, 88]. Using the step halving backtracking method, we first try the full Newton stepsize $\lambda_k = 1$, if it does not verify $J(x_s^{k+1}) > J(x_s^k)$, then try $\lambda_k = 1/2$, if it fails then try $\lambda_k = 1/4$ and so forth, until a predefined lower limit for the value of λ_k is reached.

It should be noticed that the use of the Newton-Raphson method implies iterate within the GEM algorithm, which is, in turn, an iterative procedure

too. This fact which may appear cumbersome and/or slow can be avoided by noticing that 1) at each iteration of the Newton-Raphson method an increase of $J(x_s)$ is assured by the backtracking line search method, and that 2) any increase of $J(x_s)$ function leads to a direct increase of the likelihood of the incomplete data. Therefore, a single iteration ($K = 0$) in the Newton-Raphson method at each iteration of the GEM algorithm would be enough in the research of a maximum likelihood estimate. Table 2.1 shows the proposed algorithm.

2.3.6 Initialization

It is well known that for multimodal distributions the EM algorithm will converge to a local maximum (or saddle point) of the observed data likelihood function, depending on the starting value. This means that there is no guarantee that the EM algorithm converges to the maximum likelihood estimate. Therefore, to avoid keeping local solutions the best approach is to use several different initial values for the parameters vector and to run the algorithm for each initial value. Finally, to choose as the maximum likelihood estimate the estimated parameters vector with the highest likelihood value.

In this application four parameters must be initialized: the prior probability of having an LOS measurement P_D, the value of the systematic offset μ, the standard deviation of the measurement noise σ, and the BS position x_s. Taking several different initial values for each parameter may be cumbersome. Instead we propose to use a priori information for the initialization of some of the parameters and for the rest to use different initial values. Hence, we initialize

- $\tilde{P}_D = 0.5$, which represents the maximum uncertainty for deciding whether an observation is LOS or not,
- $\tilde{\mu}$=550 m, according to the observed offset on the collected data obtained in real field measurements,
- $\tilde{\sigma} \geq q/2$ (277 m), as stated in the GSM standard [96], and for
- $\tilde{x}_s$, we take several departing points from a predefined grid of uniformly separated points over the the area of interest, see figure 2.6. The area of interest is defined as the physical area where the BS is expected to be found. Thus, denoting by $\mathcal{A}$ the area of interest, we will take BS position initializations from

$$\mathcal{A} = \{(x_1, x_2) : x_1 \in [x_{1,\min}, x_{1,\max}], x_2 \in [x_{2,\min}, x_{2,\max}]\}$$

Timing Advance-Based Localization Algorithm (TABLA)	
Computed parameters at p iteration $\tilde{x}_s, \tilde{\sigma}, \tilde{\mu}, \tilde{P}_D$	
GEM	Eqs.
$\mathcal{I}_i = \{z : \max\{0, (y_i - 1/2)q\} \leq z < (y_i + 1/2)q\}$	2.10
$F_{\tilde{\theta}}(y_i) = \frac{\tilde{P}_D}{p(y_i;\tilde{\theta})} \int_{z\in\mathcal{I}_i} \phi(z; \chi_i(\tilde{x}_s) + \tilde{\mu}, \tilde{\sigma}^2) dz$	2.22
$G_{\tilde{\theta}}(y_i) = \frac{\tilde{P}_D}{p(y_i;\tilde{\theta})} \int_{z\in\mathcal{I}_i} \phi(z; \chi_i(\tilde{x}_s) + \tilde{\mu}, \tilde{\sigma}^2) z' dz$	2.23
$H_{\tilde{\theta}}(y_i) = \frac{\tilde{P}_D}{p(y_i;\tilde{\theta})} \int_{z\in\mathcal{I}_i} \phi(z; \chi_i(\tilde{x}_s) + \tilde{\mu}, \tilde{\sigma}^2) (z')^2 dz$	2.24
$P_D = \frac{1}{n} \sum_{i=1}^{n} F_{\tilde{\theta}}(y_i)$	2.25
$\mu = \tilde{\mu} + \frac{\tilde{\sigma}}{n} \sum_{i=1}^{n} G_{\tilde{\theta}}(y_i)$	2.26
$\sigma^2 = \frac{\tilde{\sigma}^2}{n} \sum_{i=1}^{n} \left(H_{\tilde{\theta}}(y_i) - F_{\tilde{\theta}}(y_i) + 1\right) - (\tilde{\mu} - \mu)^2$	2.27
Newton-Raphson method	Eqs.
$x_s^0 = \tilde{x}_s$	
for $k = 0 : K$	
$\chi_i(x_s^k) = \sqrt{(x_{i,1} - x_{s,1}^k)^2 + (x_{i,2} - x_{s,2}^k)^2}$	2.16
$\delta_i(x_s^k) = \tilde{\sigma}^{-1}(\chi_i(\tilde{x}_s) - \chi_i(x_s^k) + \tilde{\mu} - \mu)$	2.21
$I_i(x_s^k) = G_{\tilde{\theta}}(y_i) + \delta_i(x_s^k)$	2.29
$\nabla\chi_i(x_s^k) = \frac{x_s^k - x_i}{\chi_i(x_s^k)}$	2.30
$\nabla J(x_s^k) = \frac{\tilde{\sigma}}{\sigma^2} \sum_{i=1}^{n} I_i(x_s^k) \nabla\chi_i(x_s^k)$	2.28
$\mathcal{H}_{x_s^k}(\chi_i(x_s^k)) = \frac{1}{\chi_i^2(x_s^k)} \left[I_2 - \chi_i(x_s^k) \nabla\chi_i(x_s^k) \nabla\chi_i(x_s^k)^T\right]$	2.32
$\mathcal{H}_{x_s^k}(J(x_s^k)) = \frac{\tilde{\sigma}}{\sigma^2} \sum_{i=1}^{n} \left(I_i(x_s^k) \mathcal{H}_{x_s^k}(\chi_i(x_s^k)) - \frac{1}{\tilde{\sigma}} \nabla\chi_i(x_s^k) \nabla^T\chi_i(x_s^k)\right)$	2.31
Determine λ_k by backtracking	
$x_s^{k+1} = x_s^k + \lambda_k \mathcal{H}_{x_s}^{-1}(J(x_s^k)) \nabla J(x_s^k)$	2.33
$x_s = x_s^K$	
Computed parameters x_s, μ, σ and P_D	

Table 2.1: Timing Advance-Based Localization Algorithm (**TABLA**): one EM algorithm's iteration.

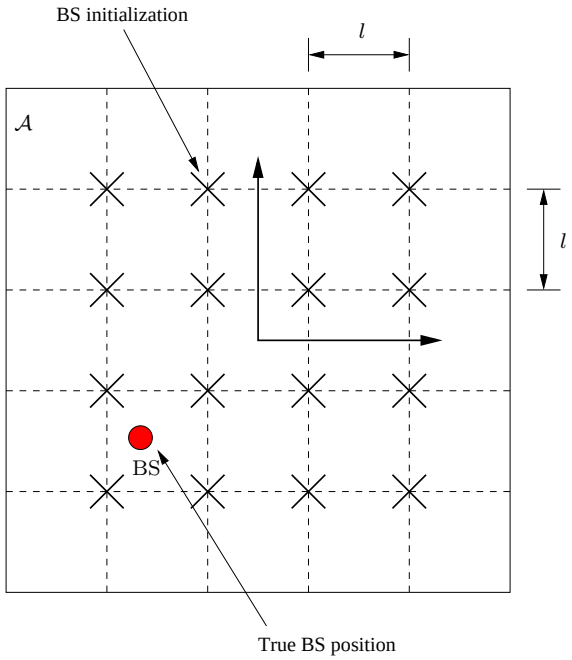

Figure 2.6: Initialization grid: TABLA is initialized for each BS position (thick crosses) taken from the grid.

where $(x_{1,\min}, x_{2,\min})$ and $(x_{1,\max}, x_{2,\max})$ are respectively the lower left and upper right coordinates of the vertices of the area of interest.

Figure 2.7 depicts the convergence of the EM algorithm for different position initializations taken from a predefined grid. Two different approaches were used to update the BS position (eq. (2.33)): **a**) the Newton-Raphson method using halving step backtracking line search method to set the stepsize, and **b**) the classical Newton-Raphson method with fixed stepsize $\lambda_k = 1$, which is an alternative version of the EM gradient algorithm presented in [48]. Two aspects should be noticed: 1) the use of different initializations permit to discard local maxima by keeping the estimated parameters vector which gives the highest value of the likelihood function, and 2) the use of a backtracking line search method ensures an increase of the likelihood at each time step.

2.3.7 Cramer-Rao bound (CRB)

An important question in estimation theory is whether an estimator $\hat{\theta}$ has certain desired properties, in particular, if it converges to the unknown parameter θ it is supposed to estimate. One typical property we want for an

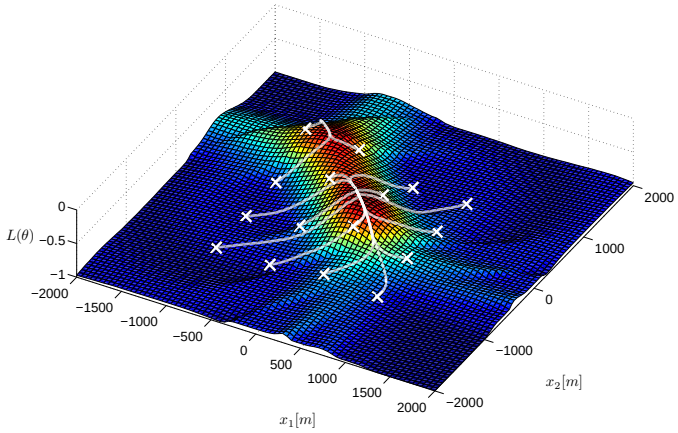

a)

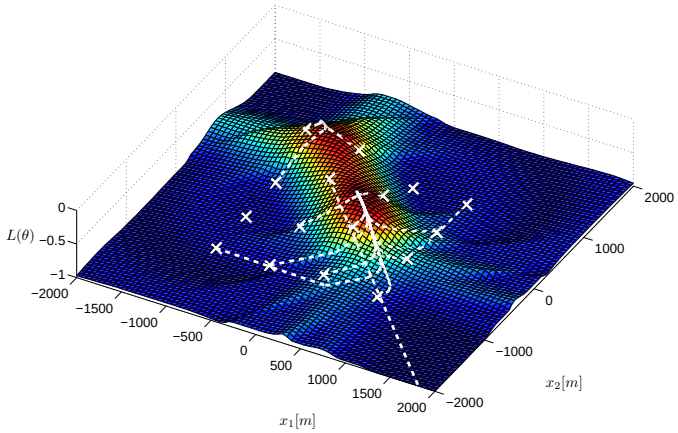

b)

Figure 2.7: Log-likelihood profile as a function of the source position and increase of the likelihood function for two different implementations: **a**) the Newton-Raphson method using halving step backtracking line search method to set the stepsize, and **b**) the classical Newton-Raphson method with fixed stepsize $\lambda_k = 1$. White crosses represent the grid of initial guesses for the source position. White dotted lines represent the path of the GEM position estimations for each initial guess.

estimator is unbiasedness, meaning that on the average, the estimator hits its target: $\mathbb{E}(\hat{\theta}) = \theta$. If we restrict ourselves to unbiased estimation then the natural question is whether the estimator shares some optimality properties in terms of its sampling variance. Since we focus on unbiasedness, we look for an estimator with the smallest possible variance.

In this context, the Cramer-Rao lower bound will give the minimal achievable variance for any unbiased estimator $\hat{\theta}(Y_{1:n})$ of θ, where $Y_{1:n} = \{Y_1, \ldots, Y_n\}$ is the set of observed data. This result is valid under very general regularity conditions. Thus, according to [69]

$$\mathbb{E}\left\{(\hat{\theta}(Y_{1:n}) - \theta)(\hat{\theta}(Y_{1:n}) - \theta)^T\right\} \geq \left(\mathcal{F}^{(n)}(\theta)\right)^{-1} \tag{2.34}$$

where

$$\mathcal{F}^{(n)}(\theta) = -\mathbb{E}\left\{\frac{\partial^2 \log p(Y_{1:n};\theta)}{\partial\theta\partial\theta^T}\right\} \tag{2.35}$$

is the Fisher information matrix (FIM) associated to the parameter vector θ.

One of the most important applications of the Cramer-Rao lower bound is that it provides the asymptotic optimality property of maximum likelihood estimators. For i.i.d. sequences $Y_{1:n}$, (2.35) may be written as

$$\mathcal{F}^{(n)}(\theta) = n\mathcal{F}_1(\theta) \tag{2.36}$$

where $F_1(\theta)$ is the FIM associated to the parameter vector θ induced from $p(Y_1;\theta)$. Following the central limit theorem (CLT) the ML estimates are asymptotically distributed according to

$$\left(\mathcal{F}^{(n)}(\theta)\right)^{\frac{1}{2}}\left(\hat{\theta}(Y_{1:n}) - \theta\right) \longrightarrow \mathcal{N}_k(0, \mathbf{I}) \tag{2.37}$$

where $\mathbf{I}$ stands for the identity matrix and $\mathcal{N}_k(m, \Sigma)$ for a k-dimensional Gaussian distribution with mean vector m and covariance matrix Σ.

In our case, for an independent (non-identically distributed) sequence $Y_{1:n}$, (2.35) may be written as

$$\mathcal{F}^{(n)}(\theta) = \sum_{i=1}^{n} \mathcal{F}_i(\theta) \tag{2.38}$$

where

$$\mathcal{F}_i(\theta) = -\mathbb{E}\left\{\frac{\partial^2 \log p_i(Y_i;\theta)}{\partial\theta\partial\theta^T}\right\}$$

and $p_i(Y_i;\theta)$ is given by (2.9). For this case we have not proved that the asymptotical behavior of $\hat{\theta}(Y_{1:n})$ verify (2.37). However we show latter, via

Monte Carlo simulations, that, for large values of n, TABLA estimates are asymptotically distributed, following (2.37), as

$$\sqrt{n}\Gamma^{-\frac{1}{2}}(\theta)\left(\hat{\theta}(Y_{1:n})-\theta\right)\longrightarrow\mathcal{N}_k(0,\mathbf{I}) \tag{2.39}$$

where

$$\Gamma(\theta)=\left(\frac{1}{n}\sum_{i=1}^{n}\mathcal{F}_i(\theta)\right)^{-1} \tag{2.40}$$

Confidence region

Instead of estimating the BS position x_s by a single value, a region of likely estimates can be provided exploiting the Cramer-Rao lower bound. How likely the estimates are, is determined by the confidence coefficient $\gamma\in[0,1]$. The more likely it is for the region to contain the parameter, the wider the region will be. Hence, according to [69] the confidence region (CR) can be defined as

$$\mathcal{C}_R=\left\{x\in\mathbb{R}^2:(x-x_s)\Gamma_{x_s}^{-1}(\theta)(x-x_s)^T\leq C\right\} \tag{2.41}$$

where $C^2=-2\ln(1-\gamma)$, x_s is the true BS position and $\Gamma_{x_s}(\theta)$ is the submatrix of the asymptotic covariance matrix $\Gamma(\theta)$ corresponding to the covariance of x_s, which depends on the true parameters vector θ. In practice, the true parameters vector is unknown, however, by replacing θ by a consistent estimate $\hat{\theta}$, i.e. the ML estimate, we can obtain an estimate of the confidence region.

2.4 Simulations results

In this section we study the performance of the proposed approach to estimate the position of a BS under a controlled, but realistic GSM simulated scenario. In the first part of our study, we show using Monte-Carlo simulations the validity of the asymptotic CRB. The second part uses the CRB to show the effects on the BS position estimation caused by the variation of the different nuisance parameters. Finally, in the third part we present the BS position estimation dependence on the MS trajectory.

In the first two parts the simulated scenario considers that the MS is moving along the non-straight-line trajectory defined by the coordinate pair $(x_{i,1},x_{i,2})$, where the abscissas $x_{i,1}$ are uniformly distributed values in the interval $(4500,4850)$ with respective ordinates given by $x_{i,2}=0.04\,(x_{i,1}-4500)^2+500$, for $i=1,2\ldots n$. The value of n is specified for each simulation. Without loss of generality the BS is considered to be located at the origin of the Cartesian coordinate system.

2.4.1 Asymptotic confidence region

In order to verify the asymptotic convergence of the BS position estimates obtained with the proposed approach we carried out 1000 independent Monte-Carlo runs with the following simulation parameters: number of observations $n = 700$, offset $\mu = 300$ m, standard deviation of the additive noise $\sigma = 100$ m, probability of LOS measurement $P_D = 0.7$.

The initialization of the algorithm was performed according to the procedure described in section 2.3.6. For the initialization grid it was considered a regular spacing of $l = 500$ m in each coordinate of the BS initial points.

The BS position estimations obtained from the 1000 independent Monte-Carlo runs, are depicted in figure 2.8: the actual BS position is represented by a filled circle at (0,0). The ellipse surrounding the BS represents the bound for the confidence region with confidence level $\gamma = 0.95$. From the 1000 BS position estimates 947 fell within the confidence region, which approximatively represents the 95% of the BS position estimates that should be fell within the ellipse, according to γ. This result shows, on the one hand, that for the considered scenario the asymptotical distribution of the BS position estimates are in good agreement with the CRB. On the other hand it shows that, despite the fact that the likelihood surface has several local maxima, the use of the initialization grid permits the algorithm to convergence almost always to the global maximum of the likelihood function.

It is worthwhile to note that the precision of the estimator is much lower than the TA quantization interval $q = 554$ m, which may appear as a surprise. As a matter of fact, the quantification does not limit the accuracy on the BS position estimation, as long as the distance between the positions where TA were collected is small as possible and produces changes in the TA values.

2.4.2 Effects of μ, σ, P_D on the BS position estimation

In order to quantify the effects of the different nuisance parameters on the BS position estimation, we provide the BS position estimation accuracy in terms of its standard deviation (std) computed according to

$$\sigma_d = \sqrt{f_{1,1}^{-1} + f_{2,2}^{-1}}$$

where $f_{i,j}^{-1}$ denotes the (i,j)-element of the inverse of the Fisher information matrix $\mathcal{F}^{(n)}$, for the matrix configuration proposed in appendix A. The FIM was computed using the actual values of the parameters vector.

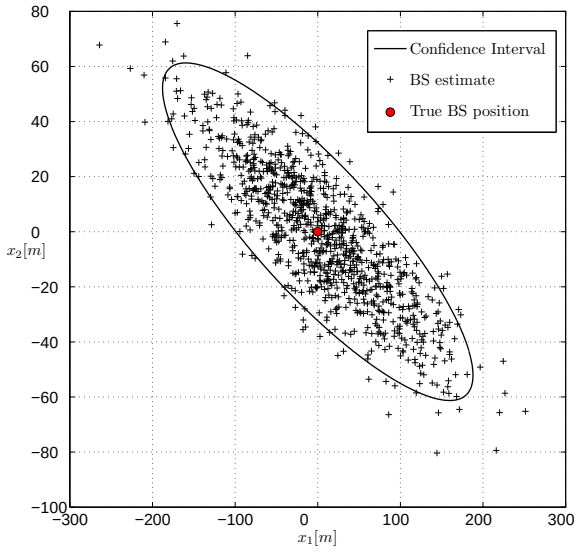

Figure 2.8: *1000 Monte-Carlo runs with* $\mu = 300$*,* $\sigma = 100$*,* $P_D = 0.7$ *and* $n = 700$ *observations with the 95% confidence ellipse, obtained from the CRB.*

Effects due to σ and P_D

In order to show the effects of the additive noise on the BS position estimation, we traced in figure 2.9 the std on the BS position estimation as a function of the additive noise's std, for a) three different number of TA observations and b) for three different values of P_D. To carried out this simulation we considered $\mu = 300$. From figure 2.9 we can deduced that:

- $\sqrt{n}\sigma_d$ is almost independent on n as it is expected from (2.39),
- for large values of σ, σ_d is almost proportional to σ [3], and
- as it may be expected $\sqrt{n}\sigma_d$ is a decreasing function of P_D.

Effects due to μ

Figure 2.10 we show σ_d as a function of μ for three values of σ and $n = 700$. The curves show that σ_d is periodic in μ with period q, that is quit logical if we consider that a shift of q on the measured MS-BS distance leads to the same observation distribution except for the two ended quantization intervals,

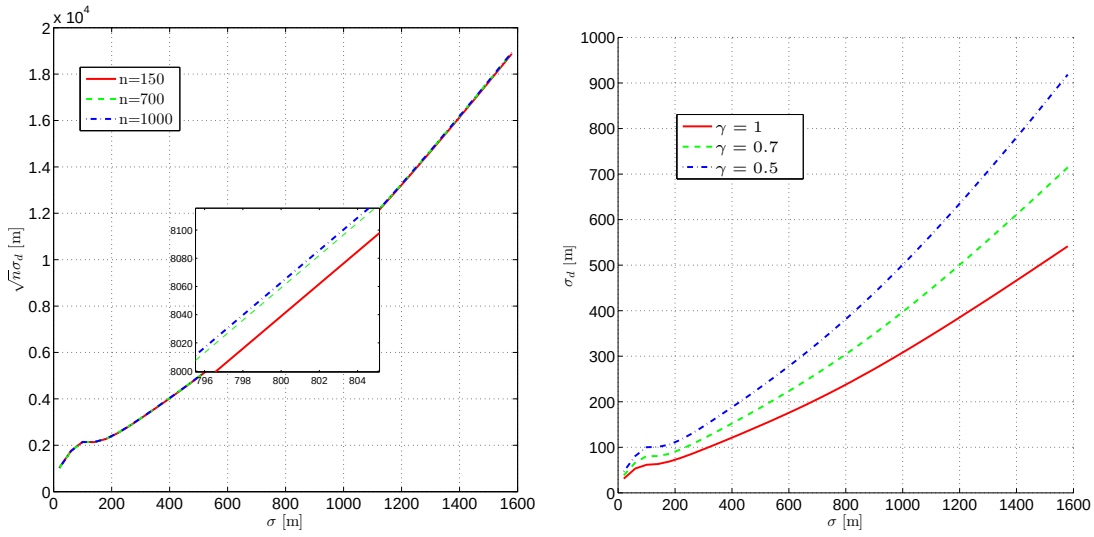

a) *b)*

Figure 2.9: a) $\sqrt{n}\sigma_d$ as function of σ with $\mu = 300$, $P_D = 0.7$, and for $n \in \{150\ 700\ 1000\}$. b) σ_d as a function of σ with $\mu = 300$, $n = 700$ and for $P_D \in \{1.0\ 0.7\ 0.5\}$.

which may also possess another certain unique problems [96], [97]. Also curves show for large values of σ, σ_d depends slightly on μ.

2.4.3 Dependence on the MS trajectory

To understand the BS position estimation's dependence on the MS trajectory, let consider the following scenario: the MS collects $n = 100$ TA measurements as it moves along a straight line. The measurements present a systematic offset of $\mu = 300$ m, and the additive noise has a standard deviation of $\sigma = 100$ m. The probability of having collected an LOS measurement is $P_D = 0.7$. Under these considerations, figures in 2.11 show the 95% confidence ellipses for the position estimation of a BS situated at (0,0), for four different configurations of the straight line trajectory. As it can be inferred from figures a), b) and c) for an MS straight line of 3Km, the MS displacement along a particular direction produce a better accuracy in such a direction. Moreover, from figures a) and c) we can deduce that a better accuracy is achieved if the MS trajectory crosses several quantization bounds at the both sides of the BS position. This is due to the fact that the rings obtained from the TA measurements will intersect in both sides of the BS, given as a result an intersection region well delimited. This is highlighted in figure d) where

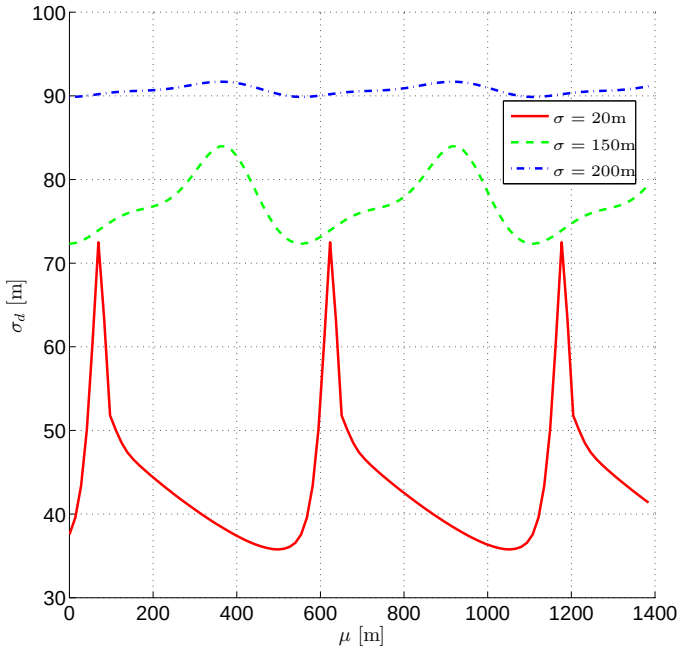

Figure 2.10: σ_d as function of μ for different values of σ and for $n = 700$.

the same number $n = 100$ TA observations were collected over a straight line trajectory of 20 Km. In such a situation the collected TA measurements vary over a large range of values, producing a great variety of rings sizes that intersect at the BS position, delimiting the intersection region in almost all directions and producing a smaller confidence region.

In general, to sharpen the BS position estimation along a specific direction, it is necessary to move the MS (to collect TA measurements) along such a direction. As seen in section 2.3.4, this also explains the difficulty to estimate the third coordinate (height) of the BS using TA measurements collected by an MS moving in a plane.

Two examples of MS displacement

To get a better understanding of the MS trajectory effects, we have displayed in figures 2.12 and 2.13 the 95% confidence ellipses for several BS positions and for two different MS trajectories of 6 km each: a straight-line segment and a circle. The BS positions are taken from an uniform grid with a grid step of 700 m. In both cases the MS moves and collects $n = 700$ TA measurements, at equally spaced positions on the trajectory. The rest of the parameters are set as in above. As we can see the major axis of the 95% confidence ellipses

are very close to the normal of the MS trajectory, except for the BSs situated near the end-points (i.e. those ones situated at $(\pm 3500, x_2)$) of the straight-line trajectory. As explained before, this is due to the fact that the MS only explores one side of the BS position, i.e. compare the confidence ellipses of the two BSs situated respectively in $BS_1 = (0, 700)$ m and $BS_2 = (3500, 700)$ m. For the BSs laying along the straight line there exist a big uncertainty and thus the confidence ellipses are not depicted in the figure. As explained in section 2.3.3, this is because the unknown offset μ produces an infinity of possible BS positions when the actual BS position belongs to the straight line MS trajectory.

It should be noticed in figure 2.13 that for the BS situated at (0,0) we get a small confidence ellipse even when the MS trajectory does not crosses any quantization bound. This is easily explained if we consider that the rings obtained from the TA measurements delimit the intersection region in all directions, thanks to the circular MS displacement, please see figure 2.14 for a graphical explanation.

MS hyperbolic displacement (examples of non-identifiability)

As stated in section 2.3.3, if the MS is moving along a hyperbolic curve with one of its two foci situated at the BS position, the likelihood function may present several maxima equally likely. The convergence to an one of those maxima will depend on the initial parameter value provided to TABLA. Two examples of MS hyperbolic movement are depicted in figures 2.15 and 2.16, respectively. Figure 2.15 shows the convergence of TABLA to the two possible solutions, for an MS moving along a hyperbolic branch with one of its two foci situated at the actual BS position. The first maximum is located at the actual BS position and the second one at the position of the second focus. Figure 2.16 depicts the worst case of a hyperbolic movement, which corresponds to a straight line containing the BS position. In such a situation, an infinity number of possible solutions are contained in the second branch of the hyperbolic curve (dashed line).

In practical applications a small deviation from a hyperbolic MS trajectory will render one of the foci more likely. Hence, using the initialization grid, explained in section 2.3.6, for the BS position initialization we avoid keeping the wrong BS position estimate.

2.5 Real experiments

In this section we test the efficiency of TABLA through real experiments carried out in a GSM network. The experiments cover three typical GSM areas: urban, semi-urban and rural. In the following we present the measurement system used to obtain TA measurements and the test results.

2.5.1 Measurement system description

To get TA measurements from the BS to localize we employ the following equipment

- a mobile test tool (MTT) to acquire the TA measurements delivered by the BS to be localized. This MTT works as a traditional mobile station with the additional characteristics that 1) it is able to force the selection of the serving BS, and 2) it reports network data related to the radio environment, particulary measurements of the received signals, coming from the serving BS, as well as the neighborhood BSs,
- a commercial GPS, to obtain the geographical position where the TA were received, and
- a laptop loaded with a specific software able to recover and to stock synchronously the network information delivered by MTT and the geographical position obtained by the GPS.

Figure 2.17 shows the configuration of the measurement system.

As it was shown in the previous section, one way to get accurate BS position estimations is by collecting TA measurements at different positions with large distances between them. This means to collect TA measurements in different quantization regions. Hence, to obtain several TA measurements at different locations we mounted the measurement system in a car. The car was driven over roads and highways in order to cover long distances.

2.5.2 Tests

We perform six field measurements in three different environments: one in rural, three in semi-urban and two in urban. Collected data consists in: TA measurements, the position coordinates where TAs were obtained, and for comparison purposes, the actual BS position x_{BS}. The position coordinates obtained from the GPS are in the geographic coordinate system (latitude, longitude and altitude). However, since the reference coordinate system to

work with is the Universal Transverse Mercator (UTM), the position coordinates obtained with the GPS were converted into UTM position coordinates using the transformation equations presented in appendix B. Once this coordinate system conversion (CSC) is achieved, data is feeded to TABLA, as well as the initial parameter values obtained from the initialization procedure described in section 2.3.6. Finally, the BS position estimation is compared with the actual BS position using the euclidian norm between the respective position vectors, figure 2.18 depicts the conceptual diagram.

Collected data analysis

Figures 2.19 to 2.24 show a) the collected TA measurements as a function of the actual BS-MS distance (see equation (2.1)) for each BS to be localized. At a first glance, figures a) show that :

- there are outlying observations in the data collected for BS4 and BS6,
- in all cases, there exist TA measurements in two or more levels for a single quantization interval (i.e. $[q/2, 3q/2]$), which may suggest the presence of a substantial amount of noise, and
- there is clearly a timing offset for each experiment, note for example that a TA measurement in the $[0, q/2]$ BS-MS distance range, theoretically corresponds to a TA = 0, however, in most of the cases TA measurements are concentred in TA = 1 for the same range, which suggests a systematic offset of at least $q/2$.

Figures 2.19 to 2.24 side b) depicts the trajectories followed by the MTT, while it was collecting the TA measurements. Notice that the trajectories cross several quantization bounds, in order to get different TA values.

Results

Table 2.2 summarizes the results obtained for the six experiments. The table provides: the BS identifier (ID), the number of collected TA measurements n, the distance between the estimated BS position and its actual position d_e, the estimated percentage of outliers $1 - \hat{P}_D$, the systematic offset $\hat{\mu}$ and the noise variance $\hat{\sigma}$, finally the last column indicates the type of environment where localization was performed. It should be noticed that

- in all cases the distance between the estimated BS position and its actual position d_e is smaller than the TA resolution $q = 544$ m,

- outlying observations were detected in the data used to localize BS3, BS4, and BS6, which agrees with what we observe in figures 2.21, 2.22, and 2.24, respectively.
- except for the localization of BS1, the rest of the estimated systematic offsets are on the order of $q/2 = 277$ m. This may be due to different offsets in transmission time at different BSs. Finally,
- an important presence of additive noise ($\hat{\sigma} > 100$ m) was estimated, which may explain the different TA values in a single quantization interval.

Figures 2.19 to 2.24 side b) also show the convergence of TABLA estimates for the position only. From these figures it is worthwhile to note that in most of the cases TABLA converges in a few iterations, despite the coarse grid used to cover the area of interest. It should be stressed that, in these scenarios, TABLA iterates converged fast toward the region of interest.

ID	n	d_e [m]	$1 - \hat{P}_D$ [%]	$\hat{\mu}$ [m]	$\hat{\sigma}$ [m]	Terrain
BS1	1148	93	0	443	261	rural
BS2	745	173	0	283	185	semi-urban
BS3	244	237	1	297	129	semi-urban
BS4	340	163	14	260	125	semi-urban
BS5	252	84	0	290	213	urban
BS6	207	378	7	241	226	urban

Table 2.2: Experimental results for three typical terrains: The third column gives the distance between the true position of the BS and the estimated position using TABLA.

2.6 Conclusions

In this chapter we applied the proposed approach presented in the previous chapter to the BS position estimation in a GSM communication system. The proposed Timing Advance-Based Localization Algorithm (TABLA) provides BS location estimates, with good accuracy, by processing severe quantized TOA measurements affected by systematic offsets, additive noise and outliers. The accuracy achieved in real field tests was under the TA resolution $q = 554$ m. Now a days TABLA is an operating algorithm being used in the industry.

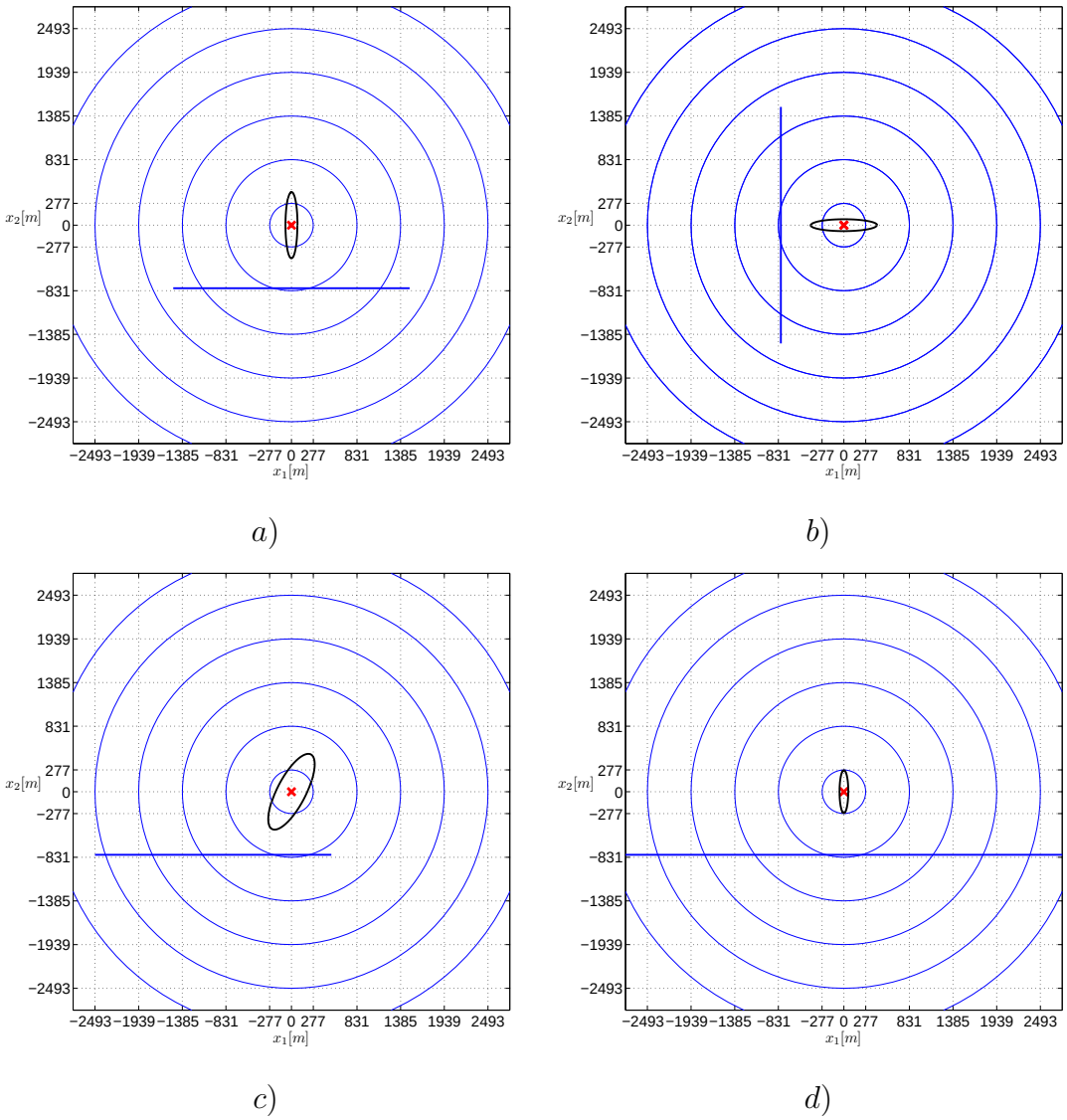

Figure 2.11: 95% confidence ellipses for a straight line trajectory of 3 Km in a), b), and c), and for 20 Km in d). $n = 100$ observations, $\mu = 300$ m, $\sigma = 100$ m and $P_D = 0.7$. Cross indicates the actual BS position. Circles represent the bounds of quantization rings (see equation (2.3)).

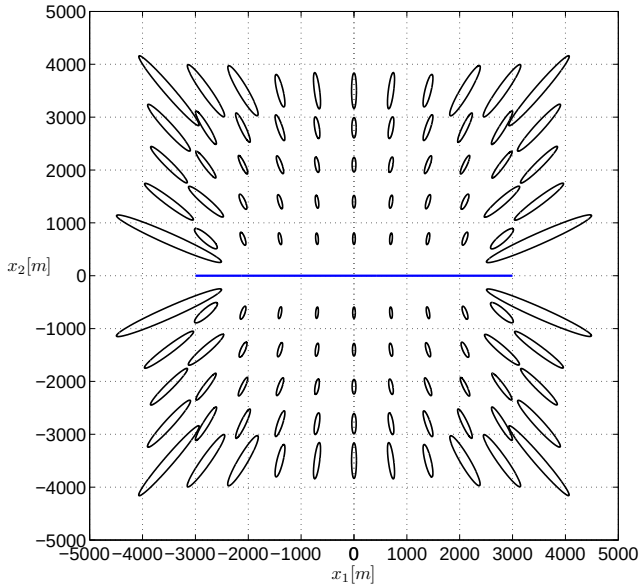

Figure 2.12: Linear MS trajectory: 95% confidence ellipses for different BS locations. $n = 700$ observations, $\mu = 300$ m, $\sigma = 100$ m and $P_D = 0.7$.

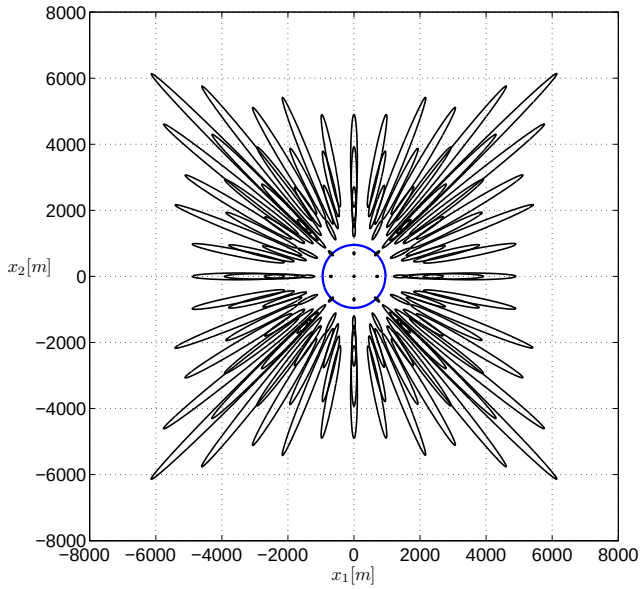

Figure 2.13: Circular MS trajectory: 95% confidence ellipses for different BS locations. $n = 700$ observations, $\mu = 300$ m, $\sigma = 100$ m and $P_D = 0.7$.

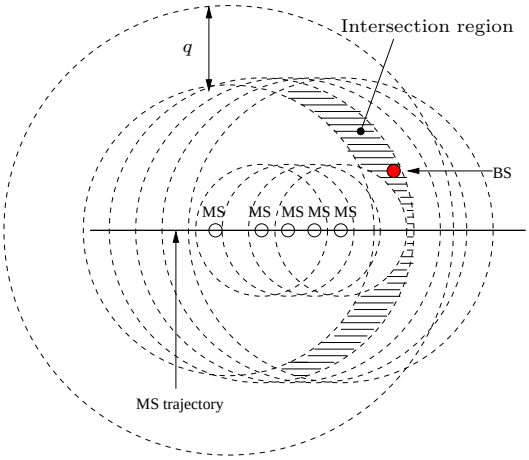

a)

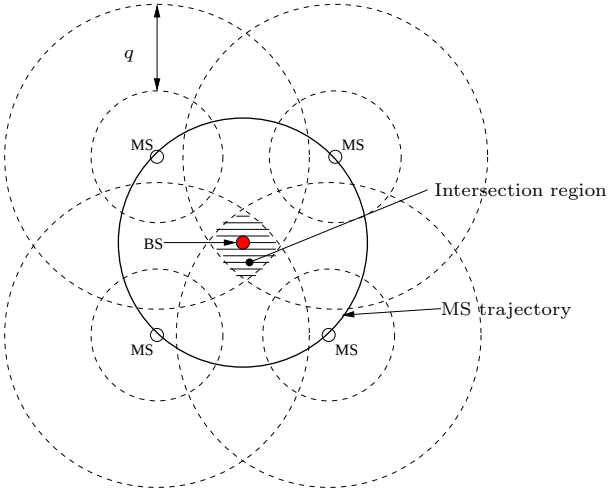

b)

Figure 2.14: Intersection region delimitation using TA measurements for different MS displacements.

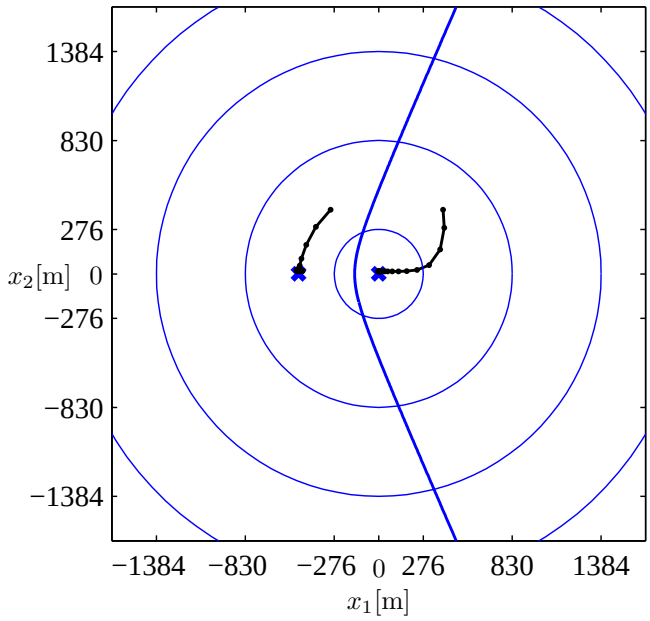

Figure 2.15: Hyperbolic MS trajectory (typical case). $n = 700$, $\mu = 300$, $\sigma = 100$ m and $P_D = 0.7$. Crosses indicate the two non identifiable BS positions. Circles represent borders of quantization rings (see equation (2.3) with $q = 553.8$ m).

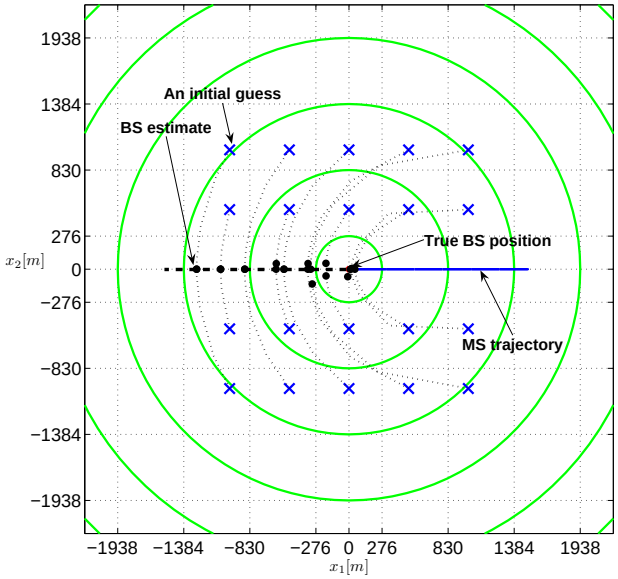

Figure 2.16: Hyperbolic MS trajectory (degenerate case). $n = 700$, $\mu = 300$, $\sigma = 100$ m and $P_D = 0.7$. Crosses indicate the initial guesses provided to TABLA and dots the BS position estimations. Circles represent borders of quantization rings (see equation (2.3) with $q = 553.8$ m).

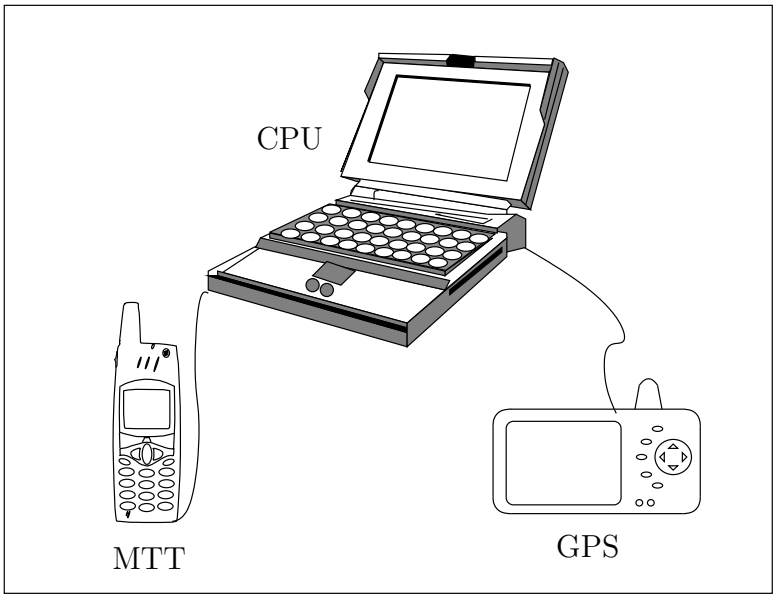

Figure 2.17: Measurement system configuration.

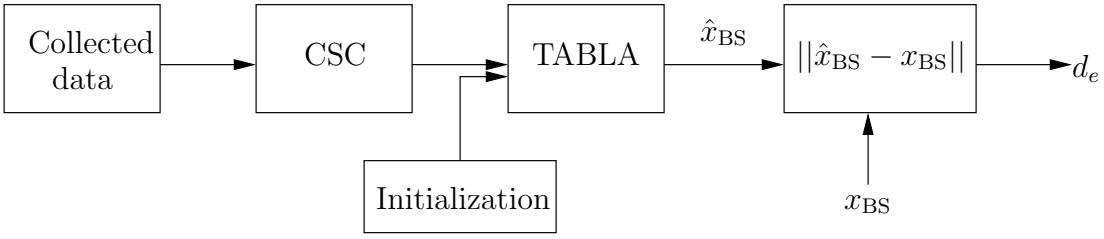

Figure 2.18: Conceptual diagram of the test

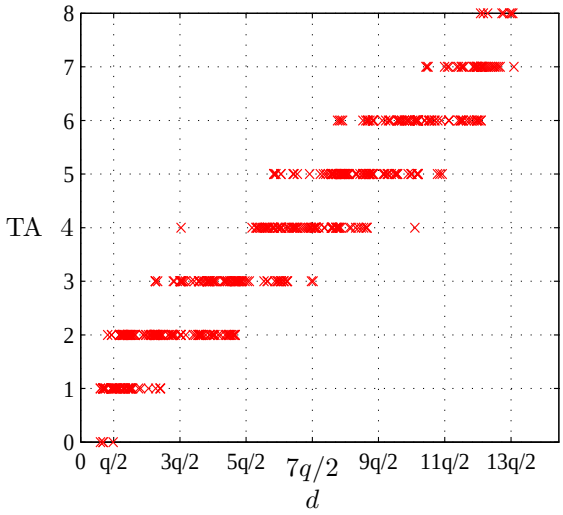

a)

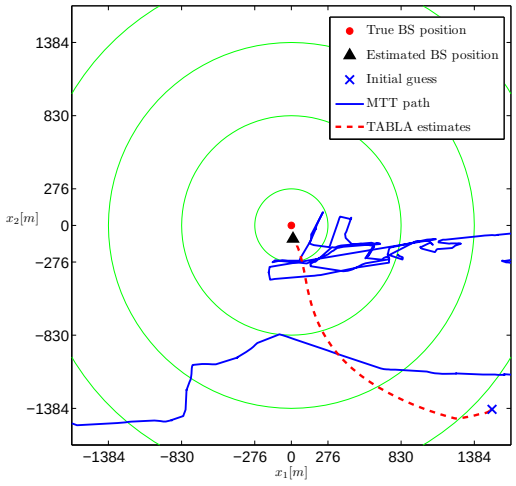

b)

Figure 2.19: BS1: **a)** TA measures as a function of BS-MS distance, **b)** EM convergence; central dot represents the true BS position. The rings around the BS represents the area where the theoretical TA is constant. The triangle and the cross markers represent, respectively, the initial and the final position of the algorithm. The thick curve is the MS trajectory.

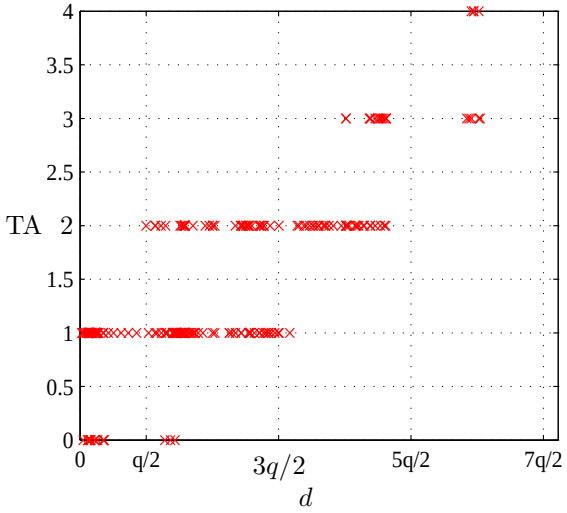

a)

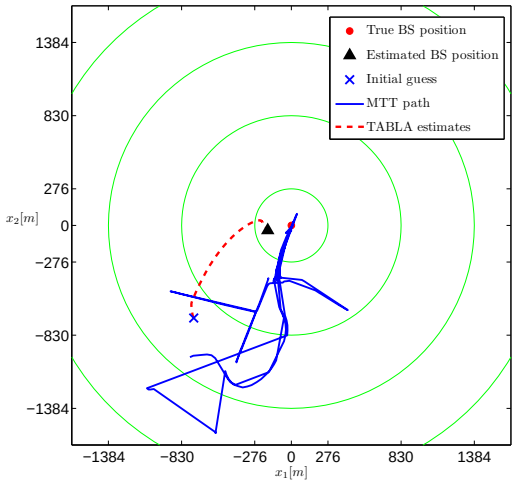

b)

Figure 2.20: BS2: **a)** TA measures as a function of BS-MS distance, **b)** EM convergence; central dot represents the true BS position. The rings around the BS represents the area where the theoretical TA is constant. The triangle and the cross markers represent, respectively, the initial and the final position of the algorithm. The thick curve is the MS trajectory.

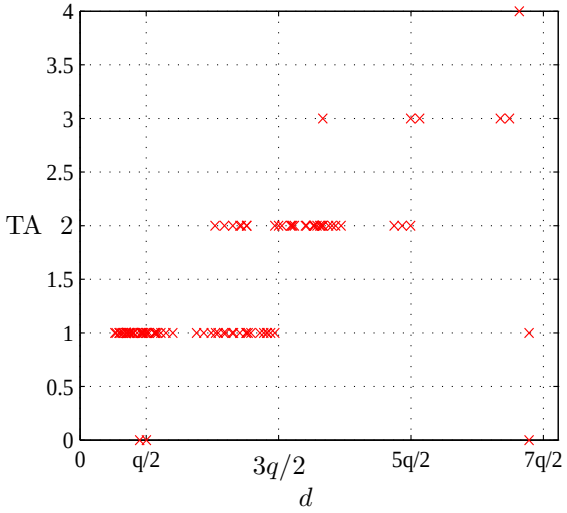

a)

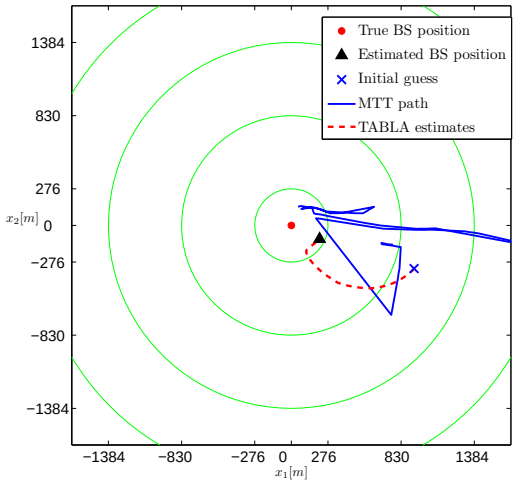

b)

Figure 2.21: BS3: **a)** TA measures as a function of BS-MS distance, **b)** EM convergence; central dot represents the true BS position. The rings around the BS represents the area where the theoretical TA is constant. The triangle and the cross markers represent, respectively, the initial and the final position of the algorithm. The thick curve is the MS trajectory.

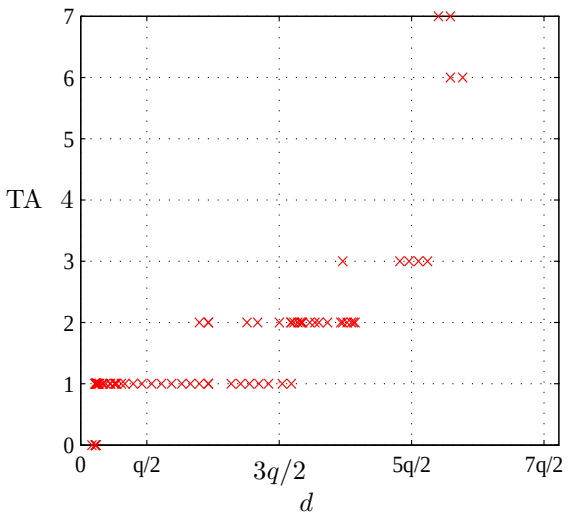

a)

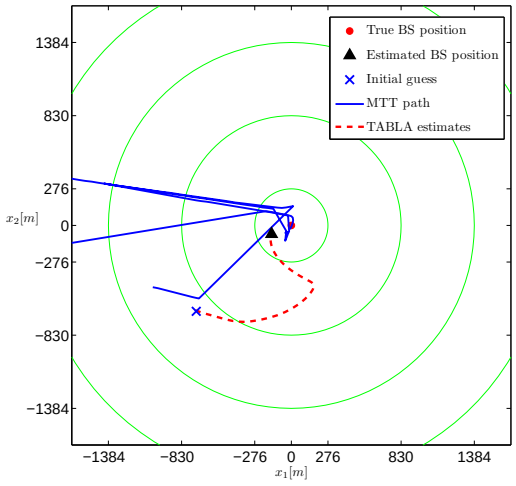

b)

Figure 2.22: BS4: **a)** TA measures as a function of BS-MS distance, **b)** EM convergence; central dot represents the true BS position. The rings around the BS represents the area where the theoretical TA is constant. The triangle and the cross markers represent, respectively, the initial and the final position of the algorithm. The thick curve is the MS trajectory.

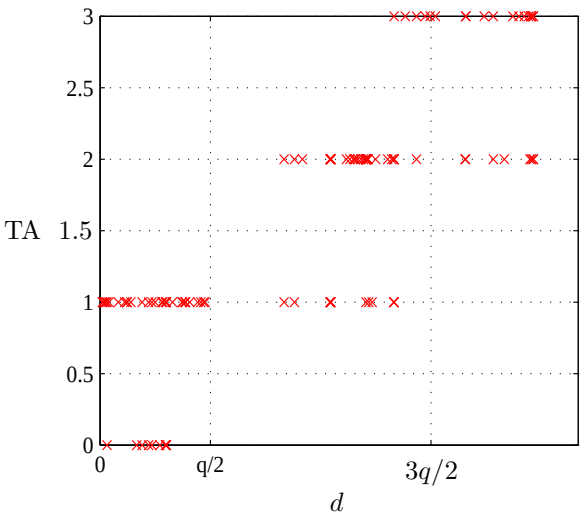

a)

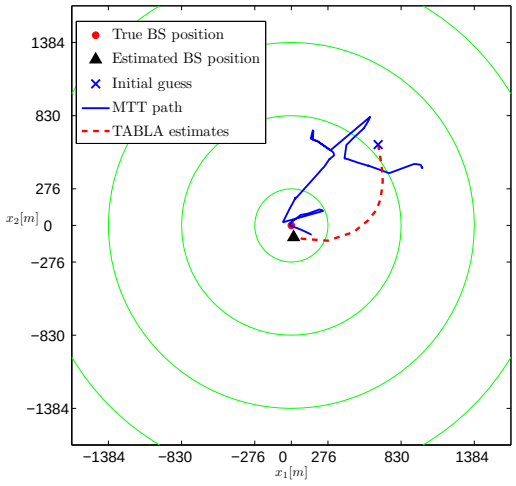

b)

Figure 2.23: BS5: **a)** TA measures as a function of BS-MS distance, **b)** EM convergence; central dot represents the true BS position. The rings around the BS represents the area where the theoretical TA is constant. The triangle and the cross markers represent, respectively, the initial and the final position of the algorithm. The thick curve is the MS trajectory.

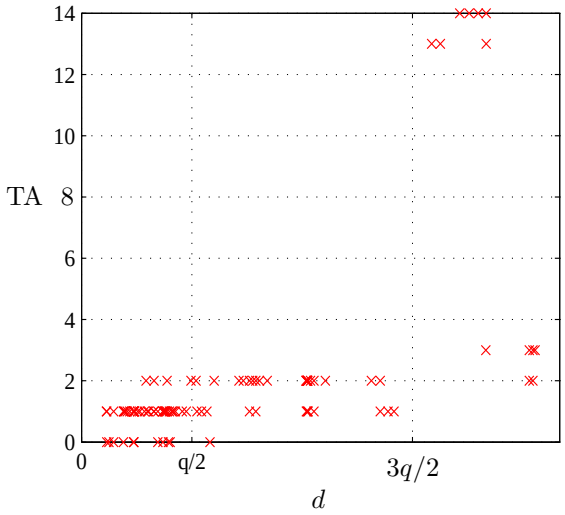

a)

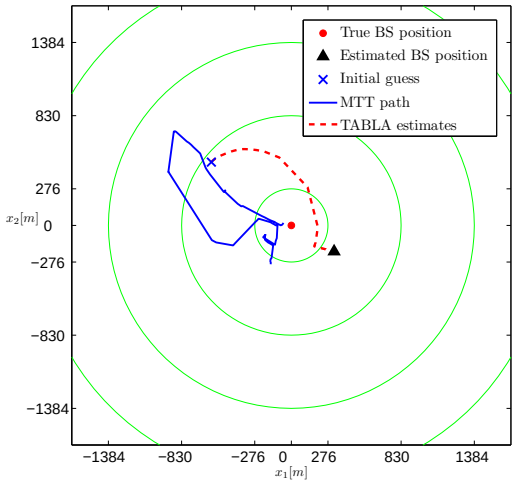

b)

Figure 2.24: BS6: **a)** TA measures as a function of BS-MS distance, **b)** EM convergence; central dot represents the true BS position. The rings around the BS represents the area where the theoretical TA is constant. The triangle and the cross markers represent, respectively, the initial and the final position of the algorithm. The thick curve is the MS trajectory.

Chapter 3

ADABLA: Angle and Delay of Arrival-Based Localization Algorithm[1]

In this chapter we present two algorithms to estimate the position of target in time division multiple access (TDMA) based communication systems. The algorithms use joint angle and delay measurements of the signals emitted by the target and received by a number of observers. The measurements not only present errors due to additive noise, but also to multipath and NLOS propagation. The statistical model presented in chapter 1 is employed in order to model the random behavior of the measurements, and the asymptotic distribution of the AOA and TOA estimators is exploited in order to reduce the number of parameters to be computed via the EM algorithm. The algorithms are applied to the problem of MS localization using a set of BSs equipped with antenna arrays.

The remainder of this chapter is organized as follows: section 3.1 presents the requirements to perform MS localization. In section 3.2 we review the theory of joint angle and delay estimation (JADE). Section 3.3 provides the development of the proposed algorithm, which is tested using syntectic data in section 3.4. Finally, in section 3.5 we give the conclusions.

3.1 Problem statement

The objective is to estimate the position of a target in a TDMA based communication system according to the following requirements:

[1]Part of this material appears in [20].

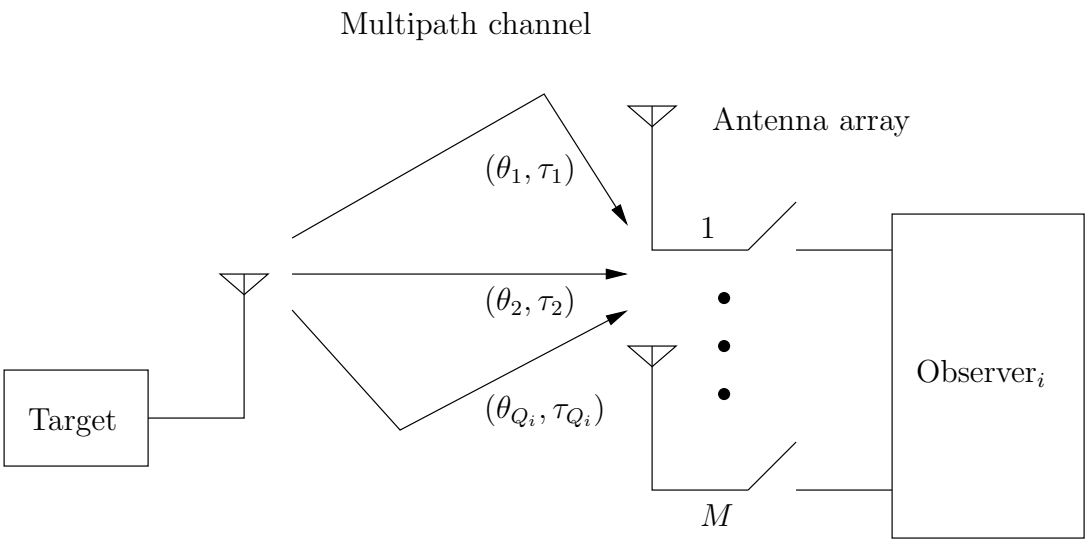

Figure 3.1: A multipath channel

- the observations consist in joint AOA and TOA measurements, which characterize the multipath propagation between target and observer(s), and
- observers are equipped with antenna arrays and complete demodulation systems.

3.2 Preliminary study

The localization of a target from its radio emissions impinging on antenna arrays, situated at the observer side, is a typical problem of radio source localization [38,68,81]. The use of antenna arrays permit to compute the space-time channel response, over which the emitted radio signals propagate [80,81]. Due to obstacles in the transmission medium signals may propagate via multiple paths. In such a situation, the space-time channel response may be a function of the propagation paths characterizing the multipath propagation between the target and the observer. Furthermore, each propagation path may be characterized by a number of parameters, such as the AOA, TOA, path loss, etc. Therefore, the estimation of such quantities may be exploited to deduce the position of the target. Unfortunately, as seen in chapter 1, the use of these measurements for localization purposes is complex because of the presence of several sources of errors affecting the radio measurements, as well as the presence of multiple paths which may generate ambiguities.

The joint angle and delay estimation (JADE) method [82] is a useful tool that employs antenna arrays to estimate the AOAs and TOAs of the multiple propagating paths. According to JADE the joint estimation of the AOA and TOA for a multipath propagation channel consists into two steps:

1. estimating the global channel response using learning sequences and observed data, and

2. exploiting the expression of the channel response as a function of AOAs and TOAs to get an estimate of these parameters.

Once the multipath parameters obtained, the selection of those ones corresponding to the LOS one is an important issue. Since some of the participating observers may be in an NLOS regime, we cannot simply chose the first arrival (smallest TOA) or the strongest path as the LOS one. Instead a more robust method must be conceived in order to process LOS and NLOS measurements for estimating the target's position. Before presenting such a method and for clarity in its explanation the remainder of this section provides *i)* the essential theory of joint angle and delay estimation (JADE) [81, 82], which has been selected as the parametric method for channel estimation, and *ii)* the asymptotic behavior of JADE-MUSIC and JADE-ML [76, 81] estimates. However, other parametric channel models and algorithms of multipath parameter estimation can be used (see [63, 80, 98] as alternatives and the references therein) by the proposed method.

3.2.1 Discrete Channel Model

For a single user transmitting a modulated digital signal in a specular multipath environment with a known number Q of multipaths (see figure 3.1), the discrete channel model can be written as [82]

$$\mathbf{H} = [\mathbf{a}(\theta_1) \dots \mathbf{a}(\theta_Q)] \begin{bmatrix} b_1 & & 0 \\ & \ddots & \\ 0 & & b_Q \end{bmatrix} \begin{bmatrix} \mathbf{g}^T(\tau_1) \\ \vdots \\ \mathbf{g}^T(\tau_Q) \end{bmatrix} = \mathbf{A}(\boldsymbol{\theta}) \mathrm{diag}[\mathbf{b}] \mathbf{G}^T(\boldsymbol{\tau}) \tag{3.1}$$

where

- $\boldsymbol{\theta} = [\theta_1 \dots \theta_Q]$, $\boldsymbol{\tau} = [\tau_1 \dots \tau_Q]$, $\mathbf{b} = [b_1 \dots b_Q]$ are respectively the vectors containing the Q AOAs, TOAs and path fadings for each propagating path,

- $\mathbf{a}(\theta)$ is the antenna-array response for signals arriving in the direction θ. In the particular case of an uniform linear antenna array (ULA)

with M isotropic sensors equally spaced by a distance d, the expression of the antenna response is given by

$$\mathbf{a}(\theta) = \begin{bmatrix} 1 \\ e^{-j2\pi d \sin\theta/\lambda} \\ \vdots \\ e^{-j2\pi(M-1)d\sin\theta/\lambda} \end{bmatrix} \tag{3.2}$$

with λ denoting the wave-length, and

- $\mathbf{g}(\tau)$ is an LP-dimensional vector defined as

$$\mathbf{g}^T(\tau) = \begin{bmatrix} g(-\tau) & g(\frac{T}{P} - \tau) & ... & g(T(L - \frac{1}{P}) - \tau) \end{bmatrix}$$

which contains the delayed samples of the known modulation pulse $g(t)$, where L stands for the (integer) channel length[1], P for the oversampling factor and T for the symbol rate. Often the modulation pulse is bandlimited and thus has infinite support in time domain, but being constructed to decay, it can be truncated to a certain finite length without incurring serious accuracy problems, i.e. it may be nonzero for $t \in [0, L_g T)$, where L_g stands for the maximum number of lobes considered. Some commonly used modulation pulse functions are the family of raised cosine pulses, given by

$$g(t) = \left(\frac{\sin(\pi t/T)}{\pi t/T}\right)\left(\frac{\cos(\alpha\pi t/T)}{1 - (2\alpha\pi t/T)^2}\right) \tag{3.3}$$

where α is the excess bandwidth beyond the minimum bandwidth π/T required to transmit without inter-symbol-interference (ISI).

3.2.2 JADE Method

In mobile communications, the AOAs and TOAs may be assumed stationary for fixed targets. For moving targets they may still be assumed stationary if the target is quite a distance from the observer and if the observation time is short enough. In contrast, the complex path attenuation (fading), is highly non-stationary. The variability of the path fading is related to the speed of the target. The fadings also change with the environment, such that even if the target is at a fixed location, other vehicles going by, people moving, etc. all cause signal fluctuations. However, the major fluctuations are caused by the mobility of the target. More precisely, the coherence time (i.e., the time

[1]The length of $g(\cdot)$ plus the maximum channel delay.

when the envelope of the fading remains highly correlated) of the fadings is roughly the inverse of the Doppler shift, or given by

$$t_{\text{coh}} \approx \frac{c}{v f_c},$$

where c is the speed of light, v the speed of the target, and f_c the carrier frequency. At 900 MHz and a target speed of 1 m/s (walking speed), the coherence time is 330 ms, at 30 m/s (100 km/h), this is 11 ms. A typical TDMA system such as GSM, PHS, DECT or DCS1800 has a time slot length of order 0.6 ms and a spacing between slots belonging to the same target (frame period) in the order of 5 ms. An example of TDMA frame structure is shown in figure 2.2. Thus the fading within a single time slot is stationary; at 30m/s it is also uncorrelated among slots, while at 1m/s it is uncorrelated every 60 slots. We also note the stationarity of the angles and delays of arrival paths, even for fast-moving targets. Over 40 slots, a target moving at 30 m/s changes angular position only by 0.1° as seen from an observer 3 km away.

The strength of the JADE method is that of exploiting the stationarity of the AOAs and TOAs over a successive number S of channel estimations of the form

$$\mathbf{H}_{est}^{(s)} = \mathbf{H}^{(s)} + \mathbf{V}_{est}^{(s)}$$

where $\mathbf{V}_{est}^{(s)}$ is the zero-mean complex Gaussian estimation noise matrix at time slot s. It should be noticed that channel estimates may be obtained via least-squares using the N_b training bits embedded in each data burst [81].

Using (3.1) and applying the *vect* operator[2] to the above yields

$$\mathbf{y}^{(s)} = \text{vect}(\mathbf{H}_{est}^{(s)}) = \mathbf{U}(\boldsymbol{\theta}, \boldsymbol{\tau})\mathbf{b}^{(s)} + \mathbf{v}^{(s)}, \text{ with } s = 1, \ldots, S \tag{3.4}$$

where

$$\mathbf{U}(\boldsymbol{\theta}, \boldsymbol{\tau}) = \mathbf{G}(\boldsymbol{\tau}) \circ \mathbf{A}(\boldsymbol{\theta}) = \left[\begin{array}{ccc} \mathbf{u}(\theta_1, \tau_1) & \ldots & \mathbf{u}(\theta_Q, \tau_Q) \end{array} \right]$$

is the $MPL \times Q$ space-time response matrix,

$$\mathbf{u}(\theta_q, \tau_q) = \mathbf{g}(\tau_q) \otimes \mathbf{a}(\theta_q)$$

is the $MPL \times 1$ space time manifold, $\mathbf{b}^{(s)}$ is a vector containing the Q fading coefficients for the s-th channel estimation and $\mathbf{v}^{(s)} = \text{vect}(\mathbf{V}_{est}^{(s)})$. In the above, symbols $\circ$ and $\otimes$ stand respectively for the well-known Khatri-Rao and Kronecker products. In a matrix form equation (3.4) is

$$\mathbf{Y} = [\mathbf{y}^{(1)} \cdots \mathbf{y}^{(S)}] = \mathbf{U}(\boldsymbol{\theta}, \boldsymbol{\tau})\mathbf{B} + \mathbf{V} \tag{3.5}$$

[2] $\text{vect}(\mathbf{A}\text{diag}[\mathbf{b}]\mathbf{C}) = (\mathbf{C}^T \circ \mathbf{A})\mathbf{b}$.

where $\mathbf{B} = [\mathbf{b}^{(1)} \cdots \mathbf{b}^{(S)}]$, and similarly for $\mathbf{V}$.

The joint angle and delay estimation (JADE) problem is, for given channel estimates $\{\mathbf{y}^{(1)}, \ldots, \mathbf{y}^{(S)}\}$, to find the angles $\boldsymbol{\theta}$ and delays $\boldsymbol{\tau}$ using the model (3.5). Many of well known methods such as maximum likelihood and MUSIC, among others, provide the means to achieve such an estimation.

3.2.3 Algorithms for Parameter Estimation and asymptotical behavior of the estimators

Among the great variety of algorithms we can find in the literature to obtain the multipath parameters $\{\boldsymbol{\theta}, \boldsymbol{\tau}\}$ from equation (3.4), we will focus on ML and MUSIC [81]. Here, we are also interested in the asymptotical distribution of their estimates $\{\hat{\boldsymbol{\theta}}, \hat{\boldsymbol{\tau}}\}$. To simplify mathematical notations, we drop the dependence of $\mathbf{U}$ on the parameters $\boldsymbol{\theta}$ and $\boldsymbol{\tau}$.

JADE-ML Estimates

To use the maximum likelihood approach we assume that the estimation noise $\mathbf{v}^{(s)}$ and path fadings $\mathbf{b}^{(s)}$ are stationary Gaussian random processes with zero-mean and respective covariance matrices $\mathbb{E}\left\{\mathbf{v}\mathbf{v}^H\right\} = \sigma_e^2\mathbf{I}$ and $\mathbb{E}\left\{\mathbf{b}\mathbf{b}^H\right\} = \mathbf{R_b}$. Moreover, it is considered that the path fadings $\mathbf{b}$ are uncorrelated between time slots. Therefore, the channel estimates $\mathbf{y}^{(s)}$ are complex Gaussian random vectors with zero-mean and covariance matrix $\mathbf{R} = \mathbb{E}\left\{\mathbf{Y}\mathbf{Y}^H\right\} = \mathbf{U}\mathbf{R_b}\mathbf{U}^H + \sigma_e^2\mathbf{I}$. Thus, employing stochastic maximum likelihood techniques, it is well know (see appendix C) that this is a separable optimization problem that reduces to

$$(\hat{\boldsymbol{\theta}}, \hat{\boldsymbol{\tau}}) = \max_{(\boldsymbol{\theta},\boldsymbol{\tau})} \left\{ -\log \mid \boldsymbol{\Phi}\hat{\mathbf{R}}\boldsymbol{\Phi} + \frac{1}{MPL - Q}\mathrm{Tr}(\boldsymbol{\Phi}^{\perp}\hat{\mathbf{R}})\boldsymbol{\Phi}^{\perp} \mid \right\} \tag{3.6}$$

where $\hat{\mathbf{R}} = S^{-1}\sum_{s=1}^{S}\mathbf{y}^{(s)}\mathbf{y}^{(s)H}$ is the estimated covariance matrix, $\boldsymbol{\Phi} = \mathbf{U}(\mathbf{U}^H\mathbf{U})^{-1}\mathbf{U}^H$ is the orthogonal projector which projects any vector onto the space spanned by columns of $\mathbf{U}$, $\boldsymbol{\Phi}^{\perp} = \mathbf{I} - \boldsymbol{\Phi}$ is the orthogonal complement projector. It should be noticed that, solving (3.6) is not simple since it requires a $2Q$-dimensional search. Newton-type techniques are possible, with excellent statistical accuracy when the global maximum is attained, but they require very good initial parameter estimates.

Once the AOAs and TOAs computed the nuisance parameters can be obtained according to

$$\hat{\sigma}_e^2 = \frac{\mathrm{Tr}(\boldsymbol{\Phi}^{\perp})\hat{\mathbf{R}}}{MPL - Q} \tag{3.7}$$

and

$$\hat{\mathbf{R}}_\beta = \mathbf{U}^\dagger(\hat{\mathbf{R}} - \hat{\sigma}_e^2 I)(\mathbf{U}^\dagger)^H \tag{3.8}$$

where $\mathbf{U}^\dagger = (\mathbf{U}^H\mathbf{U})^{-1}\mathbf{U}^H$ is the pseudo-inverse of $\mathbf{U}$.

Applying classical limit theory it may be proved that, as S goes to infinity, $\sqrt{S}(\hat{\mathbf{\Psi}} - \mathbf{\Psi})$, where $\mathbf{\Psi} = [\boldsymbol{\theta}, \boldsymbol{\tau}, \sigma_e^2, \mathrm{diag}(\mathbf{R_b})]$, is asymptotically a zero-mean Gaussian random vector, with covariance matrix given by the inverse of the Fisher Information Matrix (FIM). FIM's elements can be determined using the following formula[3] [76]

$$f_{i,j} = S \ \mathrm{Tr}\left(\mathbf{R}^{-1}\frac{\partial \mathbf{R}}{\partial \psi_j}\mathbf{R}^{-1}\frac{\partial \mathbf{R}}{\partial \psi_i}\right) \tag{3.9}$$

where ψ_l is the l-th component of $\mathbf{\Psi}$.

JADE-MUSIC Estimates

Using (3.5) and MUSIC approach, $(\hat{\boldsymbol{\theta}}, \hat{\boldsymbol{\tau}})$ are given by the Q minima of the function

$$J(\boldsymbol{\eta}) = \mathbf{u}^H(\boldsymbol{\eta})\hat{\mathbf{\Pi}}\mathbf{u}(\boldsymbol{\eta}) \tag{3.10}$$

where $\boldsymbol{\eta} = [\eta^1 \ \ \eta^2]^T = [\theta \ \ \tau]^T$ and $\hat{\mathbf{\Pi}}$ is the estimated orthogonal projector onto the noise subspace obtained from the eigen-decomposition of $\hat{\mathbf{R}}$. It should be noticed that, unlike the ML method, this method involves only 2-dimensional search.

Applying the same principle as in the JADE-ML case, it can be shown that, when S goes to infinity, $\sqrt{S}(\hat{\boldsymbol{\eta}} - \boldsymbol{\eta})$ is asymptotically a zero-mean Gaussian random vector with a (2×2) covariance matrix $\mathbf{\Gamma}_{\theta,\tau}$ whose entries are given by[4]

$$\gamma_{vw} = \sum_{j,j'=1}^{2} C_{vj}^{(-1)} C_{wj'}^{(-1)} \sum_{l,p,l',p'=1}^{MPL} \frac{\partial K^j}{\partial \mathbf{\Pi}_{lp}} \frac{\partial K^{j'}}{\partial \mathbf{\Pi}_{l'p'}} \mathrm{cov}(\mathbf{\Pi}_{lp}, \mathbf{\Pi}_{l'p'}) \tag{3.11}$$

where $v, w \in \{1, 2\}$, $C_{ii'}^{(-1)}$ denotes the four entries of the inverse matrix of

$$\mathbf{C}(\boldsymbol{\eta}) \ = \ \begin{bmatrix} \dfrac{\partial K^1}{\partial \eta^1} & \dfrac{\partial K^1}{\partial \eta^2} \\ \dfrac{\partial K^2}{\partial \eta^1} & \dfrac{\partial K^2}{\partial \eta^2} \end{bmatrix} \tag{3.12}$$

[3] Details on the computation of the FIM's elements are relegated to appendix C.

[4] See appendix D.

with

$$K^i \triangleq \frac{\partial J(\boldsymbol{\eta})}{\partial \eta^i} \tag{3.13}$$

and where the covariance between the elements of $\boldsymbol{\Pi}$ is given by

$$\begin{aligned} \mathrm{cov}(\boldsymbol{\Pi}_{ij}, \boldsymbol{\Pi}_{kl}) = \; & S^{-1} \left[(\boldsymbol{\Pi}\mathbf{R}\boldsymbol{\Pi})_{il} (\mathbf{R}\mathbf{s}^{-1}\mathbf{R}\mathbf{R}\mathbf{s}^{-1})_{kj} \right. \\ & \left. + (\mathbf{R}\mathbf{s}^{-1}\mathbf{R}\mathbf{R}\mathbf{s}^{-1})_{il} (\boldsymbol{\Pi}\mathbf{R}\boldsymbol{\Pi})_{kj} \right] \end{aligned} \tag{3.14}$$

where $\mathbf{R}\mathbf{s} = \mathbf{U}\mathbf{R}_\mathbf{b}\mathbf{U}^H$.

3.2.4 Conditions for identifiability

According to [81] to identify $\boldsymbol{\theta}$, $\boldsymbol{\tau}$ using (3.5) we need to fulfill the following conditions:

1. $\mathbf{U}(\boldsymbol{\theta}, \boldsymbol{\tau})$ be strictly tall and full rank. Thus it is necessary that $Q < MLP$. This means that, in general, JADE does not require more antennas than paths present.

2. $\mathbf{B}$ be wide and full row rank. This implies $S \geq Q$, i.e. we need to collect at least as many channel estimates as the number of multipaths.

3.3 Proposed approach

JADE-ML or JADE-MUSIC provides for the means to jointly estimate the AOAs and (relative) TOAs of multipath propagation signals emanating from a target and received by an observer equipped with an antenna array. In order to deduce the position of the target from such multipath estimates (AOAs and TOAs), collected by an observer at different positions (or similarly using several observers at different positions), we present in this section two new algorithms. The new feature present in these algorithms is the use of the asymptotical distribution of JADE-ML or JADE-MUSIC estimators, which yields to statistical models with a few number of parameters to estimate, i.e. typically the target position and the target detection probability. The methodology proposed in chapter 1 is used to derive the algorithms. In what follows we detail such a derivation.

LOS measurements

Let I be the number of fixed observers at different positions (or similarly a single moving observer at I different positions) participating in the localization process of a target. Let assume that at observer i we jointly estimate the

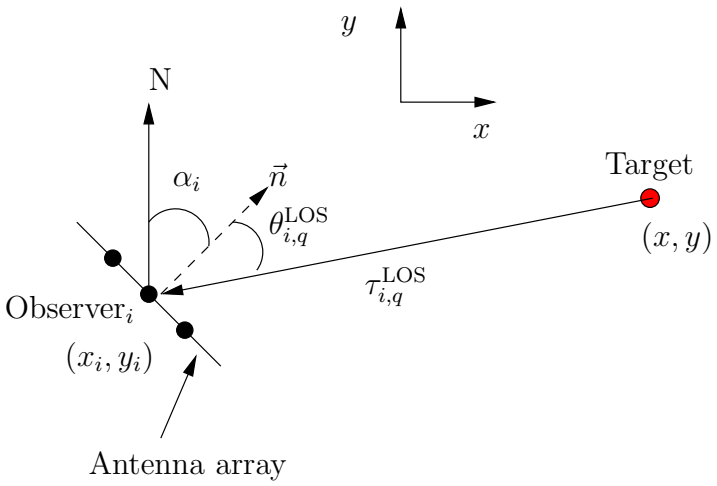

Figure 3.2: LOS measurements

AOAs $\{\theta_{i,1}, \ldots, \theta_{i,Q_i}\}$ and TOAs $\{\tau_{i,1}, \ldots, \tau_{i,Q_i}\}$ characterizing the Q_i multipaths arriving at observer i (see figure 3.1). Thus, according to (3.9) and (3.11) we further assume that the distribution of the LOS measurements, as S goes to infinity, is given by

$$\sqrt{S}(\hat{\boldsymbol{\eta}}_{i,q}^{\mathrm{LOS}} - \boldsymbol{\eta}_{i,q}) \longrightarrow \mathcal{N}(0, \boldsymbol{\Gamma}_{\theta,\tau}^{(i,q)}) \tag{3.15}$$

with mean located at the "true" value of the parameters vector $\boldsymbol{\eta}_{i,q} = [\theta_{i,q} \quad \tau_{i,q}]^T$ and covariance matrix given by $\boldsymbol{\Gamma}_{\theta,\tau}^{(i,q)}$, where i and q denote respectively the indexes of the q-th path at the i-th BS, for $i \in \{1, 2, \ldots, I\}$ and $q \in \{1, 2, \ldots, Q_i\}$. Notice that the limit covariance matrix $\boldsymbol{\Gamma}_{\theta,\tau}^{(i,q)}$ depends on the unknown true parameter values, $\boldsymbol{\theta}$, $\boldsymbol{\tau}$, $\mathrm{diag}(\mathbf{R_b})$ and σ_e^2. Nevertheless, in practical situations, these values may be replaced by consistent estimates. Hence, the use of such estimates will provide $\hat{\boldsymbol{\Gamma}}_{\theta,\tau}^{(i,q)}$ instead of $\boldsymbol{\Gamma}_{\theta,\tau}^{(i,q)}$.

Cartesian coordinate representation

The AOA and TOA measurements characterizing an LOS path are directly related to the (unknown) cartesian coordinates (x, y) of the target and the (known) cartesian coordinates (x_i, y_i) of the i-th observer by the following expressions

$$\begin{cases} \tan(\theta_{i,q} + \alpha_i) = \dfrac{x - x_i}{y - y_i}\,, & \theta_{i,q} \in [0, \pi] \\ \tau_{i,q} = c^{-1}\sqrt{(x - x_i)^2 + (y - y_i)^2}, & \tau_{i,q} \in \mathbb{R}^+ \end{cases} \tag{3.16}$$

where α_i denotes the angle between the normal's array $\vec{n}$ at i-th observer and the geographic north of the cartesian system, see figure 3.2. c denotes the speed of light. It is assumed here that α_i is known without error.

According to the *delta method* [17], the asymptotical distribution of the target position measurements $\hat{X}^{\text{LOS}}$, obtained from the transformation (3.16), is given by

$$\sqrt{S}(\hat{X}_{i,q}^{\text{LOS}} - X) \longrightarrow \mathcal{N}(0, \hat{\mathbf{\Gamma}}_{i,q}) \tag{3.17}$$

with

$$\hat{\mathbf{\Gamma}}_{i,q} = \nabla_\eta J(X) \hat{\mathbf{\Gamma}}_{\theta,\tau}^{(i,q)} \nabla_\eta J(X)^H \tag{3.18}$$

where $X = [x \quad y]^T$ is the "true" target position vector and $\nabla_\eta J(X)$ is the jacobian of the transformation

$$\boldsymbol{\eta} = \begin{bmatrix} \theta \\ \tau \end{bmatrix} \longmapsto X = \begin{bmatrix} x \\ y \end{bmatrix} \tag{3.19}$$

defined by (3.16).

NLOS measurements

As stated in chapter 1, NLOS measurements depend on the density and placement of the scatterers in a particular propagation medium. In general, the pdf of the NLOS measurements is a function of the target position, the observer position, as well as a set of parameters related to the scattering model used to describe the scattering in a particular medium. However, when no information about the distribution of the NLOS measurements is available or when the information contained by such measurements is too unreliable for localization purposes, then it is often to consider NLOS measurements as outliers [18, 38]. Adopting the latter approach, we can further assume that for these measurements all values within a delimited region $\mathcal{R}$ are equally likely. This means that the target position observations $\hat{X}_{i,q}^{\text{NLOS}}$ obtained from $\hat{\boldsymbol{\eta}}_{i,q}^{\text{NLOS}}$ using (3.16) are distributed according to

$$\hat{X}_{i,q}^{\text{NLOS}} \sim \mathcal{U}_2(\mathcal{R}) \tag{3.20}$$

where $\mathcal{U}_2(\mathcal{R})$ stands for the 2D uniform distribution in the region $\mathcal{R}$. In practice this region may be delimited by the area where the target is expected to be found. If by convenience we take a rectangular region with its sides parallel to the cartesian axis, then $\mathcal{R}$ can be defined as

$$\mathcal{R} = \{(x, y) | x \in [x_{\min}, x_{\max}], y \in [y_{\min}, y_{\max}]\} \tag{3.21}$$

where $(x_{\min}, y_{\min})$ and $(x_{\max}, y_{\max})$ are respectively the minimum and maximum values for the abscissas and ordinates.

3.3.1 Observation model

Given all considerations so far, we assume that the Q_i target position estimations $\{X_{i,1}, \ldots, X_{i,Q_i}\}$ at i-th observer, for $i = 1, \ldots, I$, are available through the following observation matrix

$$\mathbf{X}_i = \begin{bmatrix} X_{i,1} & X_{i,2} & \ldots & X_{i,Q_i} \end{bmatrix} \tag{3.22}$$

whose entries are given by

$$X_{i,q} = \begin{cases} X_{i,q}^{\text{LOS}} & \text{if} \quad \psi_i = q \\ \\ X_{i,q}^{\text{NLOS}} & \text{if} \quad \psi_i \neq q \quad \text{or} \quad \psi_i = 0 \end{cases} \tag{3.23}$$

with $q = 1, \ldots, Q_i$, and where we make the following assumptions:

- $\{\mathbf{X}_i\}_{i=1:I}$ is a sequence of $2 \times Q_i$ random matrices,
- $\{X_{i,q}^{\text{LOS}}\}_{i=1:I}^{q=1:Q_i}$ is a sequence of 2D independent random vectors. They represent the target position estimations obtained from the joint measurement of the AOA and TOA of the q-th path, supposed to be the LOS path, at the i-th observer. According to (3.17), and with some abuse of mathematical notation, the pdf of an LOS measurement is given by,

$$\phi_2(X_{i,q}; X, \mathbf{\Gamma}_{i,q}) = \frac{1}{2\pi|\mathbf{\Gamma}_{i,q}|^{1/2}} \exp\left[-\frac{1}{2}(X_{i,q} - X)^T \mathbf{\Gamma}_{i,q}^{-1}(X_{i,q} - X)\right] \tag{3.24}$$

- $\{X_{i,q}^{\text{NLOS}}\}_{i=1:I}^{q=1:Q_i}$ is a sequence of 2D independent random vectors. They represent the target position estimations obtained from the joint measurement of the AOA and TOA of the q-th path, supposed to be an NLOS path, at the i-th observer. According to (3.20) and (3.21), the pdf of an NLOS measurement is given by

$$\upsilon(X_{i,q}) = \begin{cases} \frac{1}{(x_{\max} - x_{\min})(y_{\max} - y_{\min})}, & \text{if} \quad x \in [x_{\min}, x_{\max}], y \in [y_{\min}, y_{\max}] \\ 0, & \text{otherwise} \end{cases} \tag{3.25}$$

- $\{\psi_i\}_{i=1:I}$ is a sequence of i.i.d. hidden random variables, taking its values in the set $\{0, 1, \ldots, Q_i\}$, with probability

$$\mathbb{P}(\psi_i = k) = \begin{cases} P_D/Q_i & \text{if} \quad k \neq 0 \\ \\ 1 - P_D & \text{if} \quad k = 0 \end{cases} \tag{3.26}$$

  where $P_D \in [0, 1]$ is the probability of target detection.

3.3.2 Likelihood of the observations

Let denote, with some abuse of mathematical notation, the joint probability distribution of $(\mathbf{X}_i, \psi_i)$ as $p(\mathbf{X}_i, \psi_i)$. Hence, according to the above assumptions we may write

$$p(\mathbf{X}_i, \psi_i) = p(\mathbf{X}_i|\psi_i; X)\mathbb{P}(\psi_i) \tag{3.27}$$

where $p(\mathbf{X}_i|\psi_i; X)$, using (3.23), (3.24) and (3.25), can be expressed as

$$p(\mathbf{X}_i|\psi_i; X) = \sum_{k=0}^{Q_i} p(\mathbf{X}_i|\psi_i = k; X)\mathbb{1}\{\psi_i = k\} \tag{3.28}$$

with

$$p(\mathbf{X}_i|\psi_i = k; X) = \prod_{l=1}^{Q_i} \upsilon(X_{i,l})\mathbb{1}\{\psi_i = 0\} + \phi_2(X_{i,k}; X, \mathbf{\Gamma}_{i,k}) \prod_{l=1, l\neq k}^{Q_i} \upsilon(X_{i,l})\mathbb{1}\{\psi_i \neq 0\} \tag{3.29}$$

In a similar fashion and employing (3.26) we can write

$$\mathbb{P}(\psi_i) = \frac{P_D}{Q_i}\mathbb{1}\{\psi_i \neq 0\} + (1 - P_D)\mathbb{1}\{\psi_i = 0\} \tag{3.30}$$

Substituting (3.28) and (3.30) into (3.27) we obtain

$$p(\mathbf{X}_i, \psi_i) = (1-P_D)p(\mathbf{X}_i|\psi_i = 0; X)\mathbb{1}\{\psi_i = 0\} + \frac{P_D}{Q_i}\sum_{k=1}^{Q_i} p(\mathbf{X}_i|\psi_i = k; X)\mathbb{1}\{\psi_i = k\} \tag{3.31}$$

The pdf of the observation matrix $\mathbf{X}_i$ at observer i, denoted as $p(\mathbf{X}_i)$, is readily obtained marginalizing the above expression w.r.t. ψ_i, performing such a marginalization yields

$$p(\mathbf{X}_i) = (1 - P_D)p(\mathbf{X}_i|\psi_i = 0; X) + \frac{P_D}{Q_i}\sum_{k=1}^{Q_i} p(\mathbf{X}_i|\psi_i = k; X) \tag{3.32}$$

It should be noticed that (3.32) is a mixture of Gaussian distributions for the LOS observations and uniform distributions for the NLOS observations at observer i.

The likelihood of the observations $\mathbf{X}_{1:I} = \{\mathbf{X}_i\}_{i=1:I}$ is given by

$$L(\mathbf{X}_{1:I}; \Theta) = \prod_{i=1}^{I} p(\mathbf{X}_i) \tag{3.33}$$

where $\Theta = \{X, P_D\}$. Using the maximum likelihood approach we can obtain an estimate of Θ. Unfortunately, this represents a multidimensional maximization, which is not easy to perform. Nevertheless, the use of the EM algorithm not only provides a means to explore maxima of (3.33), but also it is well-adapted to work with mixture models. The next section is devoted to the derivation of an iterative procedure based on the EM approach.

3.3.3 Algorithm derivation

Let $\{\mathbf{X}_i\}_{i=1:I}$ denote incomplete data consisting in target position estimations, and $\{\psi_i\}_{i=1:I}$ the missing data. Together $\{\mathbf{X}_i, \psi_i\}_{i=1:I}$ form the complete data, whose associated likelihood function is

$$L(\mathbf{X}_{1:I}, \psi_{1:I}; \Theta) = \prod_{i=1}^{I} p(\mathbf{X}_i, \psi_i) \tag{3.34}$$

where $p(\mathbf{X}_i, \psi_i)$ is given by 3.31.

Refereing to 1 each iteration of the EM algorithm may be formally decomposed into two steps: an E-step and an M-step.

E-step computation

The E-step consists in evaluating the conditional expectation of the likelihood of the complete data, eq. (3.34), which can be expressed as

$$Q(\Theta, \tilde{\Theta}) = \sum_{i=1}^{I} \mathbb{E}\left\{\log(p(\mathbf{X}_i, \psi_i; \Theta))|\mathbf{X}_i, \tilde{\Theta}\right\} \tag{3.35}$$

As it can be seen the expectation is taken w.r.t. the missing data given the incomplete data and the parameters vector $\tilde{\Theta}$, then it is necessary to know $p(\psi_i|\mathbf{X}_i, \tilde{\Theta})$. Using the Bayes' rule, we can express

$$p(\psi_i|\mathbf{X}_i, \tilde{\Theta}) = \frac{p(\mathbf{X}_i, \psi_i; \tilde{\Theta})}{p(\mathbf{X}_i; \tilde{\Theta})} \tag{3.36}$$

where $p(\mathbf{X}_i, \psi_i; \tilde{\Theta})$ and $p(\mathbf{X}_i; \tilde{\Theta})$ are respectively given by (3.34) and (3.32) with parameters vector $\tilde{\Theta} = \{\tilde{X}, \tilde{P}_D\}$.

Solving the expectation in (3.35), exploiting expressions (3.31) and (3.36),

it is straightforward to show that

$$Q(\Theta,\tilde{\Theta}) = \sum_{i=1}^{I}\Big\{\log\left((1-P_D)p(\mathbf{X}_i|\psi_i=0,X)\right)p(\psi_i=0|\mathbf{X}_i,\tilde{\Theta})+\cdots \sum_{k=1}^{Q_i}\left[\log\left(\frac{P_D}{Q_i}p(\mathbf{X}_i|\psi_i=k,X)\right)p(\psi_i=k|\mathbf{X}_i,\tilde{\Theta})\right]\Big\} \quad (3.37)$$

M-step computation

In the maximization step, a new parameters estimate Θ is obtained maximizing $Q(\Theta,\tilde{\Theta})$ w.r.t. Θ. Thus, taking the derivative of (3.37) w.r.t P_D we obtain

$$\frac{\partial Q(\Theta,\tilde{\Theta})}{\partial P_D} = \sum_{i=1}^{I}\left\{\frac{1}{P_D-1}p(\psi_i=0|\mathbf{X}_i,\tilde{\Theta})+\frac{1}{P_D}\sum_{k=1}^{Q_i}p(\psi_i=k|\mathbf{X}_i,\tilde{\Theta})\right\}$$

As it can be seen, this derivative does not depend on X. Thus, canceling the above expression and making some algebraic manipulations we can express

$$P_D = \frac{1}{I}\sum_{i=1}^{I}\sum_{k=1}^{Q_i}p(\psi_i=k|\mathbf{X}_i,\tilde{\Theta}) \quad (3.38)$$

Now, taking the first derivative of (3.37) w.r.t. X gives

$$\frac{\partial Q(\Theta,\tilde{\Theta})}{\partial X} = \sum_{i=1}^{I}\sum_{k=1}^{Q_i}\frac{p(\psi_i=k|\mathbf{X}_i,\tilde{\Theta})}{p(\mathbf{X}_i|\psi_i=k,X)}\frac{\partial p(\mathbf{X}_i|\psi_i=k,X)}{\partial X} \quad (3.39)$$

where $\partial p(\mathbf{X}_i|\psi_i=k,X)/\partial X$ for $k\neq 0$ can be shown to be

$$\frac{\partial p(\mathbf{X}_i|\psi_i=k,X)}{\partial X} = p(\mathbf{X}_i|\psi_i=k,X)\mathbf{\Gamma}_{i,k}^{-1}(X_{i,k}-X) \quad (3.40)$$

It should be noticed that (3.39) does not depend on P_D. Thus, canceling (3.39) we can obtain

$$X = \left(\sum_{i=1}^{I}\sum_{k=1}^{Q_i}\mathbf{\Lambda}_{i,k}\right)^{-1}\left(\sum_{i=1}^{I}\sum_{k=1}^{Q_i}\mathbf{\Lambda}_{i,k}X_{i,k}\right) \quad (3.41)$$

where

$$\mathbf{\Lambda}_{i,k} = p(\psi_i=k|\mathbf{X}_i,\tilde{\Theta})\mathbf{\Gamma}_{i,k}^{-1} \quad (3.42)$$

and where $\mathbf{\Gamma}_{i,k}$ is computed from (3.18). It should be notice that target position estimates at each iteration of the EM algorithm are obtained using the closed-form expression (3.41), which gives a relative easy-to-implement algorithm summarized in table 3.2.

3.3.4 Initialization

Two parameters must be initialized: the target detection probability P_D, and the target position X. Hence, we initialize

- $\tilde{P}_D = 0.5$, which represents the maximum uncertainty for deciding whether an observation is LOS or not, and for
- $\tilde{X}$, we take several departing points from a predefined grid of uniformly separated points over the the area of interest, see figure 3.3. The area of interest is defined as the physical area where the target is expected to be found. Thus, we will take target position initializations from the area

$$\mathcal{A} = \{(x, y) : x \in [x_{\min}, x_{\max}], y \in [y_{\min}, y_{\max}]\}$$

where $(x_{\min}, y_{\min})$ and $(x_{\max}, y_{\max})$ are respectively the lower left and upper right coordinates of the vertices of the area of interest.

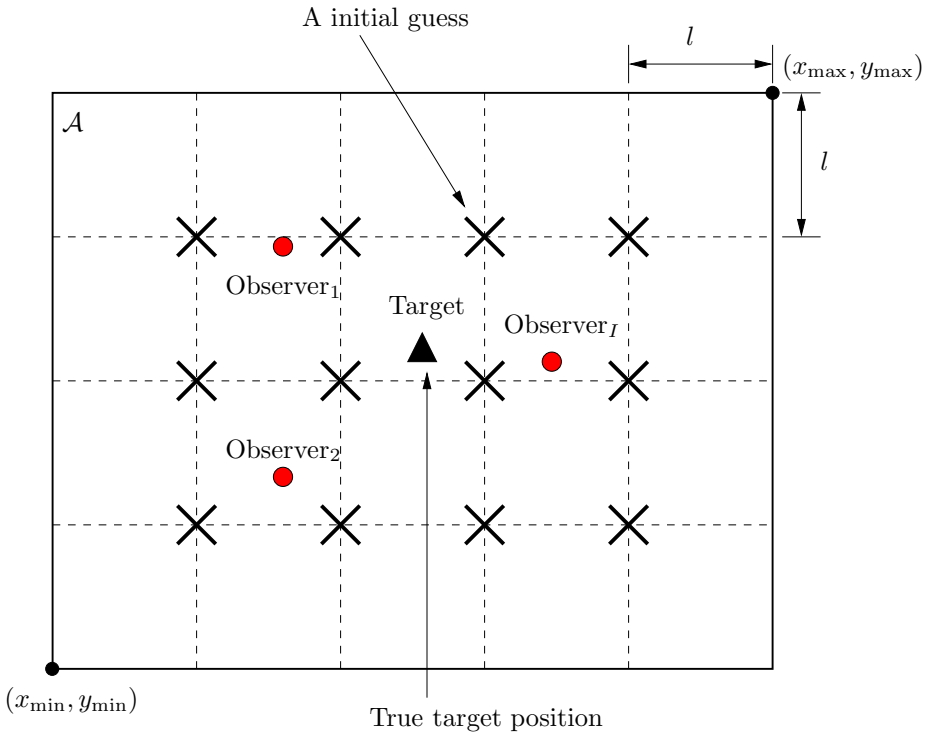

Figure 3.3: Initialization grid: ADABLA is initialized for each initial guess (thick crosses) taken form the grid.

3.4 Simulations results

This section presents some simulation results concerning the performance of ADABLA. We apply ADABLA to the problem of MS localization, within a TDMA-based communication system, using a set of BSs (as the observers) equipped with antenna arrays. For clarity in the presentation of the simulation results we organize this section as follows:

Section 3.4.1: presents an analysis of the asymptotic behavior of the position estimates using lonely JADE-ML and JADE-MUSIC methods. This means that we do not use ADABLA to estimate the position of the MS, instead we suppose as known which path is the LOS one and we analyze the MS position estimates obtained via JADE-ML and JADE-MUSIC methods for different parameter values, such as the number of elements in the antenna array, the signal-to-noise ratio, the number of multipaths, etc. The objective of these simulations is to describe the asymptotical behavior of the MS position estimates computed from JADE-ML and JADE-MUSIC methods, which will be helpful in the understanding of MS position estimation using ADABLA.

Section 3.4.2: presents the asymptotical behavior of ADABLA estimates under a controlled simulation scenario, where the LOS MS position observations are generated according to (3.17) and the NLOS observations according to (3.20). The objective is to compare ADABLA using the asymptotic covariance matrix given by JADE-ML method against that one that uses JADE-MUSIC's asymptotic covariance matrix. To differentiate both approaches we will respectively named them from now on as ADABLA-ML or ADABLA-MUSIC.

Section 3.4.3: shows ADABLA capability to localize an MS under a realistic simulation scenario, where the complete localization process is simulated. That is, we simulate the process, since the MS transmits modulated data, passing through the BSs process to compute estimates of the multipath parameters (AOAs and TOAs), until we provide the information needed for ADABLA to compute a position estimate. The objective is to compare ADABLA-ML against ADABLA-MUSIC under a realistic simulation scenario.

In all our simulations we consider parameter values which approximate those ones employed by GSM. Table 3.1 shows the considered values. Other parameters such as the number of elements in the antenna array M and the number of paths Q, etc. are specified for each simulation. The signal-to-noise

Parameter	Value	Meaning
T	3.7μs	Symbol period
N_b	26	Number of training bits
β	0.35	Roll-off factor
L_g	6	Length of $g(t)$
L	8	Channel length
P	2	Oversampling factor
S	26	Number of time slots

Table 3.1: Parameter values

ratio (SNR) is taken as the ratio of the power of the strongest path $|b_{\max}|^2$ to the variance of the noise σ^2 [81]:

$$\text{SNR} = \frac{|b_{\max}|^2}{\sigma^2} \tag{3.43}$$

3.4.1 Asymptotic behavior of JADE-ML and JADE-MUSIC estimates

To understand the asymptotic behavior of the MS position estimates obtained from JADE-ML and JADE-MUSIC methods we consider the following scenario: an MS communicates with a single BS equipped with an uniform linear array antenna with M sensors. The antenna array is oriented to the north ($\alpha = 0$) and without loss of generality is placed at the origin $(0, 0)$ of the cartesian coordinate system. The transmitted signals MS-BS propagates over a multipath channel composed of Q dominant paths, from which one is assumed to be the LOS one.

For the NLOS paths we consider a single reflection approach, where the reflected signals becomes from dominant reflectors within the propagation medium, see figure 3.4. In such a situation the reflected signal arrives to the BS with an AOA θ^{NLOS} which depends on the position of the reflector and on the BS. On the other hand, the associated TOA $\tau^{\text{NLOS}} = \tau_1 + \tau_2$ is composed by the time it takes to the signal to travel from the MS to the obstacle τ_1 and from the obstacle to the BS τ_2.

Simulation results are present in terms of the standard deviation (std) of the position estimation defined as

$$\sigma_d = \sqrt{\text{Tr}(\mathbf{\Gamma}^{\text{LOS}})}$$

where $\mathbf{\Gamma}^{\text{LOS}}$ is the 2×2 covariance matrix associated to the LOS path, computed according to (3.9) for the JADE-ML and to (3.11) for JADE-MUSIC

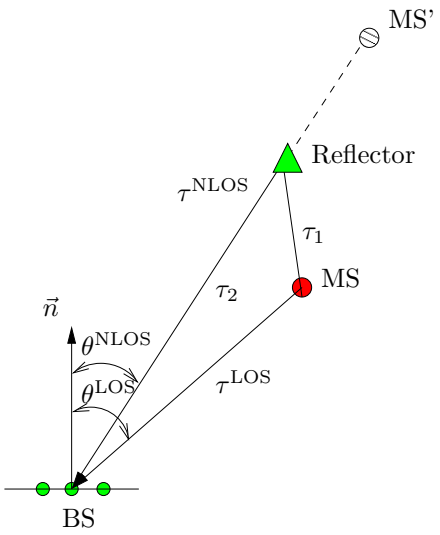

Figure 3.4: Single reflection scheme.

methods and using (3.18) to obtain σ_d in meters. In both cases, JADE-ML and JADE-MUSIC, the asymptotic covariance matrices are computed using the true values of the parameters vector.

Dependence on the TOA and AOA

In order to appreciate the dependence of the MS position estimates on the TOA and AOA, we consider a single path channel $Q = 1$, corresponding to the LOS path between MS-BS. To compute the asymptotic covariance matrices an antenna array with two elements $M = 2$ is considered and an unitary mean power of the LOS path is set $|\mathbf{b}|^2 = 1$.

Figure 3.5 a) shows the std of the position estimation for several MS locations situated over a circumference with center at the BS position and with a radium of 3km (the TOA is constant). As it can be observed, as the AOA approaches 90 degrees the std increases. This is due to fact that an ULA has no response for signals arriving at 90 degrees. In contrast, signals arriving with an AOA of 0 degrees will provide more accurate position estimations. Alternatively, the same behavior can be observed in figures 3.6 a) and b) where we show the 95% confidence ellipses for several MS positions taken from a grid with width 500m. As it can be seen, for an MS situated around ± 90 degrees w.r.t. to the normal's array direction $\vec{n}$ the confidence ellipses are bigger than those ones situated around the normal's array direction.

Figure 3.5 b) shows the std of the MS position estimates for several MS locations situated along a straight line containing the BS position (thus,

keeping the AOA constant). As it can be seen, the shorter is the distance MS-BS the lower is the std. This is mainly due to the uncertainty on the measurement of the AOA, i.e. 1 degree of uncertainty at 500 m from the BS may represent an error on the position estimation of 17m, while at a 5km, from the same BS, the error goes up to 170m. It should be noticed that increasing the SNR the std of the MS position estimation is reduced, but the form of curves is similar.

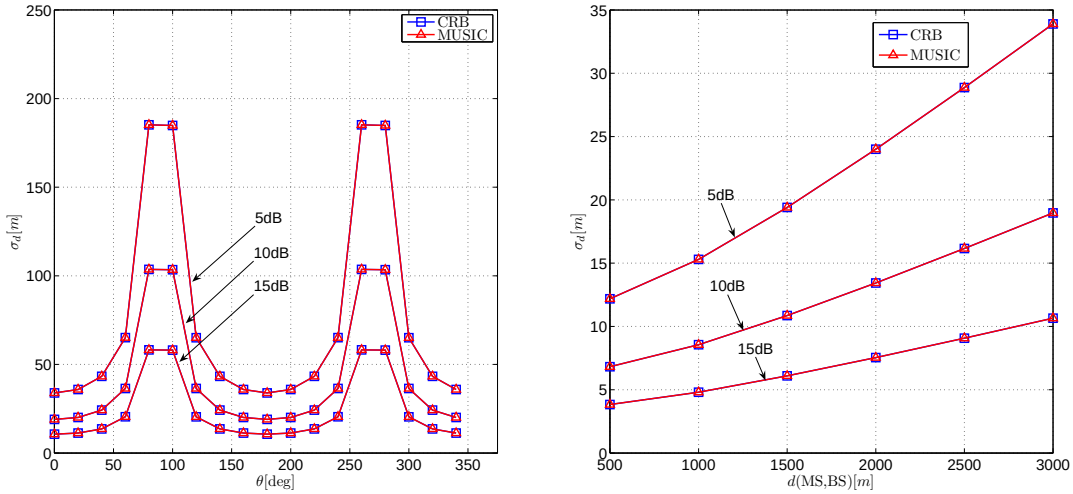

a) b)

Figure 3.5: Standard deviation of the MS position estimates as a function of a) the AOA and b) the distance MS-BS for three different SNR values.

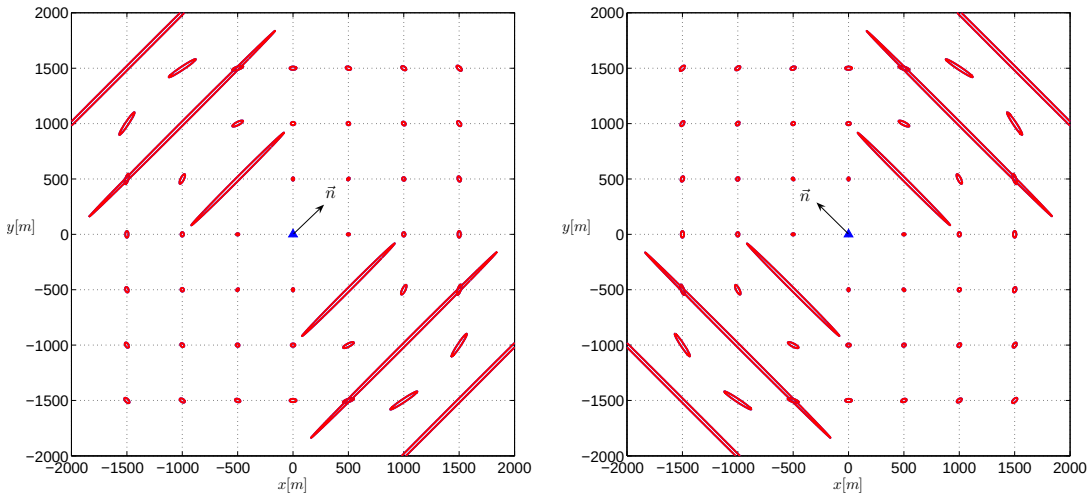

a) b)

Figure 3.6: 95% confidences ellipses for several MS positions situated over a grid with grid step of 500m. a) the ULA is oriented 45[deg] and b) −45[deg] w.r.t the north.

Dependence on the SNR

Figure 3.7 depicts the standard deviation of the position estimates as a function of the SNR for three different numbers of the elements in the antenna array. As expected, as the SNR increases the standard deviation decreases. On the other hand increasing the number of elements in the antenna array lead to a better performance in the MS position estimation and improves position estimation for an MS situated around 90 degrees of the normal's array antenna.

Multipath propagation case

It should be noticed that in the previous simulations JADE-MUSIC estimates reached the CRB for a channel propagating only one path. As we will see the difference between the two asymptotic forms becomes important as the number of secondary paths increases. In order to show this difference we consider the scenario depicted in figure 3.8. The scenario consists in a BS located at the origin of the cartesian coordinate system (big triangle) oriented at 0deg w.r.t. north, five dominant reflectors (small triangles) used to simulate secondary paths, placed respectively at a distance from the BS of 3025m, 3050m, 3100m, 2600m, and 3500m, and with respective AOA of 45deg, 50deg, 40deg, 54deg, and 37deg. Several MS positions (dots) are con-

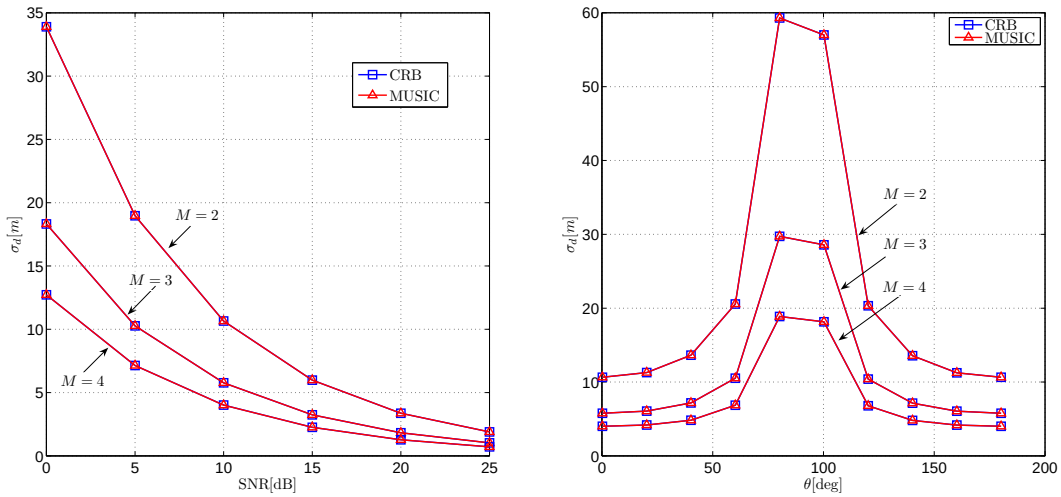

a) b)

Figure 3.7: Standard deviation of the MS position estimates as a function of a) the SNR and b) the AOA for three different number of elements in the antenna array.

sidered, taken from the perimeter of a circular sector with center at the BS position and radium of 3km.

Three simulations were performed corresponding to different multipath scenarios. The first one supposes three secondary paths generated by reflectors 1, 2 and 3, the second one uses reflectors 1, 2, 3 and 4 to simulate four secondary paths and the last simulation uses the five reflectors in figure 3.8.

Simulation results are presented in figures 3.9 to 3.11 side a) in terms of the std of the position estimates computed for each MS position and presented as a function of its AOA for a fixed SNR of 10dB. Vertical dash-doted lines correspond to the AOA of the secondary paths. Side b) shows the std as a function of the SNR for a single MS position. It should be noticed that as the number of secondary paths grows up the general performance of both approaches gets worst, however JADE-ML estimates exhibit in all cases a better performance than JADE-MUSIC estimates. To have a precise description of the dependence of JADE-ML and JADE-MUSIC based MS position estimates w.r.t. the number of secondary paths is very complex, because it not only depends on the position of the dominant reflectors and the position of the MS, but also on the other parameters such as the normal's array orientation, the attenuation, the number of elements in the antenna array, etc.

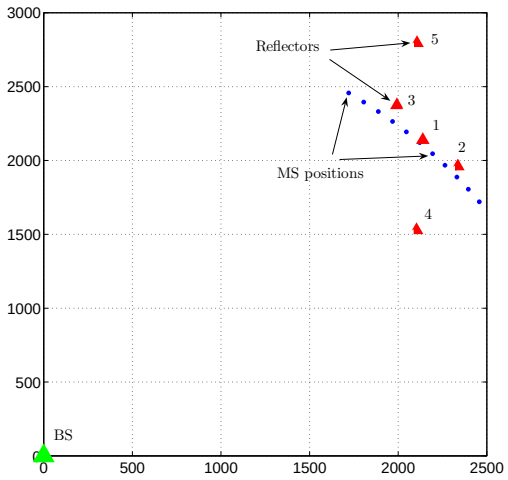

Figure 3.8: Placement of the dominant reflectors used to simulate secondary paths.

3.4.2 ADABLA in a controlled simulation scenario

As seen in the previous section JADE-ML and JADE-MUSIC based MS position estimations become inaccurate as the number of propagating paths in the transmission medium increases. However, using the approach proposed in section 3.3.3 we can obtain accurate MS position estimations by measuring the AOAs and TOAs of the multipath signals arriving at several BS participating in the localization process. In order to test the proposed approach we consider a simulation scenario were there are four BSs participating in the localization process of an MS placed at the origin of the cartesian coordinate system. The BSs are placed at the four vertices of a square of 6×6Km with center at the MS position, see figure 3.12. BSs are considered to be equipped with an ULA with $M = 2$ antennas. The normal's array at each BS is pointing to the MS position, this means that the respective angles w.r.t the north are 45, -45, 135, -135deg. We consider that the multipath channel for each of the participating BSs propagates respectively 3, 4, 4, and 3 NLOS paths plus the LOS one (if present at a particular BS). LOS MS position observations are generated according to (3.17) and the NLOS observations according to (3.20), where $\mathcal{R} = \{x, y | x \in [-1000, 1000], y \in [-1000, 1000]\}$. The initialization of the algorithm is achieved using the procedure described in section 3.3.4, where the area of interest coincide with $\mathcal{R}$ and $l = 200m$.

Experiments are run with ADABLA-ML and ADABLA-MUSIC algorithms for various signal-to-noise ratios. The experimental standard devia-

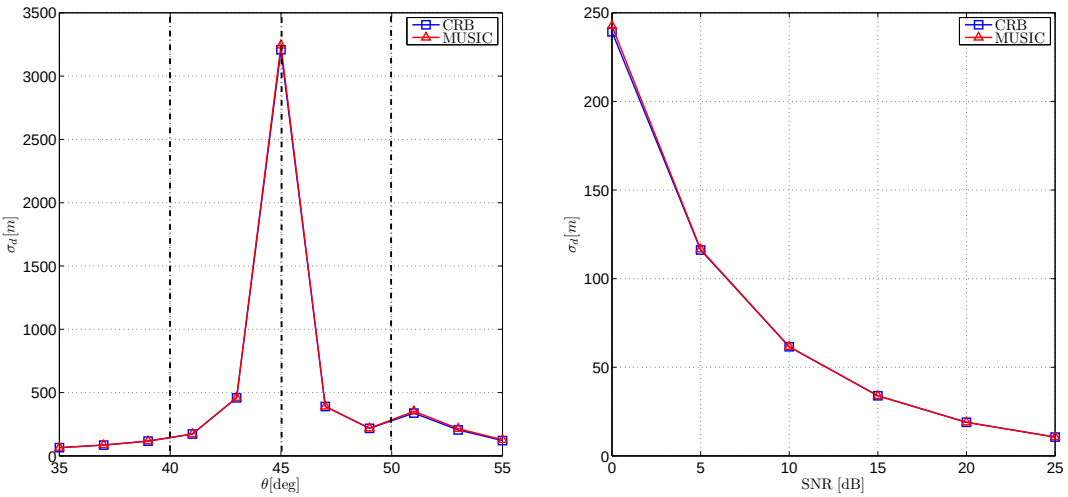

a) b)

Figure 3.9: Standard deviation of the position estimates as a function of a) the AOA of arrival of the LOS path and b) the signal to noise ratio for a multipath channel with three paths.

tion or Root Mean Square Error (RMSE), as well as the experimental bias of the position and detection probability estimates are computed from $K = 500$ Monte-Carlo runs:

$$\text{RMSE}(X) = \left(\frac{1}{K} \sum_{t=1}^{K} ||\hat{X}_t - X||^2 \right)^{\frac{1}{2}}, \quad \text{BIAS}(X) = \frac{1}{K} \sum_{t=1}^{K} (\hat{X}_t - X) \quad (3.44)$$

and similarly for the probability of MS detection P_D.

All BSs see the LOS path

The RMSE and bias of the position and detection probability estimates for four BSs seeing the LOS path, among the multiple observed ones, are plotted in figure 3.13. It should be noticed that, in spite of the multiple paths observed at each BS the difference between ADABLA-ML and ADABLA-MUSIC estimates is not significant for this simulation scenario. This is because ADABLA treats the observations from each BS jointly improving the accuracy of the position estimates and reducing the effect of the number of paths on the position estimation obtained from JADE-ML and JADE-MUSIC methods. On the other hand, the joint treatment of the observations permits to select the LOS paths at each BS without making assumptions such

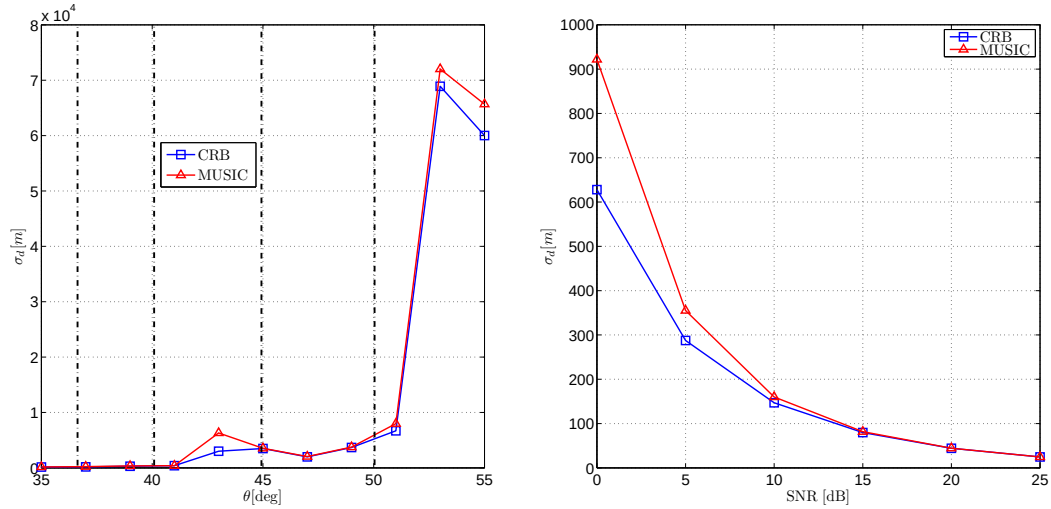

a) b)

Figure 3.10: Standard deviation of the position estimates as a function of a) the AOA of arrival of the LOS path and b) the signal to noise ratio for a multipath channel with four paths.

as the first arriving path or the path with the highest power to decide which path is the LOS one. Finally, notice that for an average error of 40% in the MS detection probability (approximately two BSs are considered in NLOS regime at 5 dB, while they are actually in an LOS one) the precision of the position estimates is quite high, this is because ADABLA needs at least two BSs in LOS regime for accurate MS position estimation.

Only two BSs see the LOS path

In this simulation we consider that only BSs 3 and 4 see the LOS path, among the multiple observed ones, and that BSs 1 and 2 are in an NLOS regime providing outlying observations only. Figure 3.14 show the simulation results for this scenario. Notice that, unlike the previous simulation, the difference between position estimates obtained from the two algorithms becomes significantly for SNRs ranging between 5 and 15 dBs. This is because the number of BSs in LOS regime is reduced and thus the joint treatment of the observations, for low SNRs, does not completely reduces the effect of the number of secondary paths on the MS position estimations obtained from JADE-ML and JADE-MUSIC methods. Notice also that, the bias of the position estimates increases for the same range. As observed in [81] in order to get accurate joint angle and delay measurements using JADE-ML

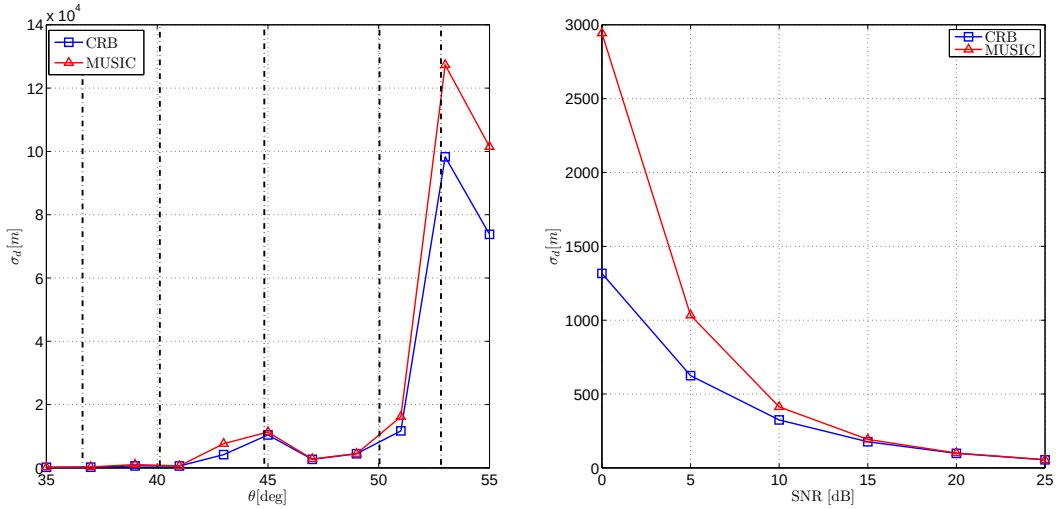

a) b)

Figure 3.11: Standard deviation of the position estimates as a function of a) the AOA of arrival of the LOS path and b) the signal to noise ratio for a multipath channel with five paths.

and JADE-MUSIC methods, and thus accurate MS position estimations in presence of multiple paths, it is needed that MPL gets large with respect to Q. One way to do this is increasing the number of antennas in the antenna array, as it can be seen in figure 3.15 where we kept the same simulation scenario, but with $M = 4$ antennas in the antenna array.

3.4.3 ADABLA in a realistic simulation scenario

We test ADABLA under a realistic simulation scenario which approximates GSM[5]. The scenario consist in three BSs, equipped with antenna arrays, participating in the localization process of an MS. It is assumed that the MS communicates with a single BS per time, and that in order to communicate with another BS a handover scheme applies. The MS transmits digital signals over a multipath channel, which propagates three dominant paths $Q = 3$ (for simplicity we consider the same number of multipaths for each BS). The symbol period is considered to be $T = 3.7\mu$s. The digital signals are modulated by a raised-cosine pulse with roll-off $\beta = 0.35$, truncated to $L_g = 6$. The noise-corrupted signals are received at the BSs using an uniform linear antenna array with five sensors $M = 5$. Then they are sampled in

[5]GSM uses a nonlinear modulation scheme, namely GSMK.

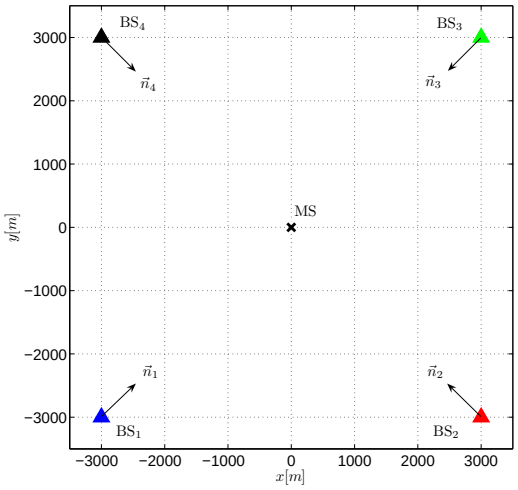

Figure 3.12: Placement of the BSs and MS to test ADABLA. $\vec{n}_i$ for $i = 1, \ldots, 4$ represent the direction of the normal vector to the antenna arrays situated at each BS.

time at a rate of twice the symbol rate, i.e. setting $P = 2$. Sampled data is used to estimate the channel at each time slot via least-squares using the $N_b = 26$ training bits. Data is collected over 30 time slots. The channel length is $L = 8$. The path gains at each BS position are $\mid \mathbf{b}_1 \mid^2 = [0.8, 1, 0.9]$, $\mid \mathbf{b}_2 \mid^2 = [0.9, 0.8, 1]$, $\mid \mathbf{b}_3 \mid^2 = [0.7, 0.8, 1]$, respectively. Path fadings are chosen to have the amplitude $|b_i|$ and a random phase. They are constant within a slot but uncorrelated from slot to slot. Channel estimates are then used to estimate the multipath parameters (AOAs and TOAs) via JADE-ML and JADE-MUSIC methods. Afterwards, the asymptotic covariance matrices computation (CMC) is performed, as well as the position estimates for each multipath, then they are transformed to its cartesian-coordinate representation. Finally, transformed data is given to ADABLA which delivers an MS position estimate based on an ML or MUSIC approach. Figure 3.16 depicts the conceptual diagram of the simulation scenario.

In order to compute the multipath parameters from channel estimates using JADE-ML or JADE-MUSIC method, it must be performed a multidimensional maximization according to (3.6) and (3.10), respectively. In both cases we employ the *fminsearch* function implemented in MATLAB® with a starting point near the actual value of the parameters vector.

Without loos of generality, the MS is considered to stay at $(0, 0)$Km of a 2-D cartesian system and the BSs at $(x_i, y_i) = \{(-1, -1.5), (2.5, -0.5), (0, 2.5)\}$Km. The angles between the normal

arrays and the geographic north are set to $\alpha = [45, -45, -179]$. We also consider that BS1 observes only NLOS paths, viewed as possible sources picked out randomly from the area $\mathcal{A} = \{(x, y) \mid x \in [-2000,\ 2000]\text{m},\ y \in [-2000,\ 2000]\text{m}\}$. To the rest of the BSs that observe the LOS path two more paths were added, randomly chosen from $\mathcal{A}$.

The performance of ADABLA-ML and ADABLA-MUSIC is presented in terms of the RMSE and bias computed from 500 Monte-Carlo runs. The RMSE and BIAS are computed according to (3.44). Figures 3.17 side a) and b) show respectively the experimental RMSE and bias on the MS position estimation using ADABLA for different SNRs. As expected, ADABLA-ML presents better performance than ADABLA-MUSIC for low SNRs. As a matter of fact, ADABLA-MUSIC does not give satisfactory results in the range of 0-8dBs, because MUSIC algorithm is not able to distinguish all the minima in its cost function. Therefore, the associated asymptotic covariance matrices are bad conditioned and no valid result is produced by the algorithm.

3.5 Conclusions

In this chapter we proposed two algorithms to locate a target from joint measurements of TOA and AOA of the emitted signals in a multipath environment. We used an antenna array at different observers to perform such measurements. Collected data were processed using the approach present in chapter 1. We did not consider the first arrival path or the path with the highest power as the LOS path. Instead the proposed statistical approach handles the presence of LOS paths and rejects the NLOS ones. The resulting algorithms are able to locate the target with at least two observser "seeing" multiple paths, comprising the LOS paths, while at the same time is able to remove information delivered by observers being in NLOS regime only.

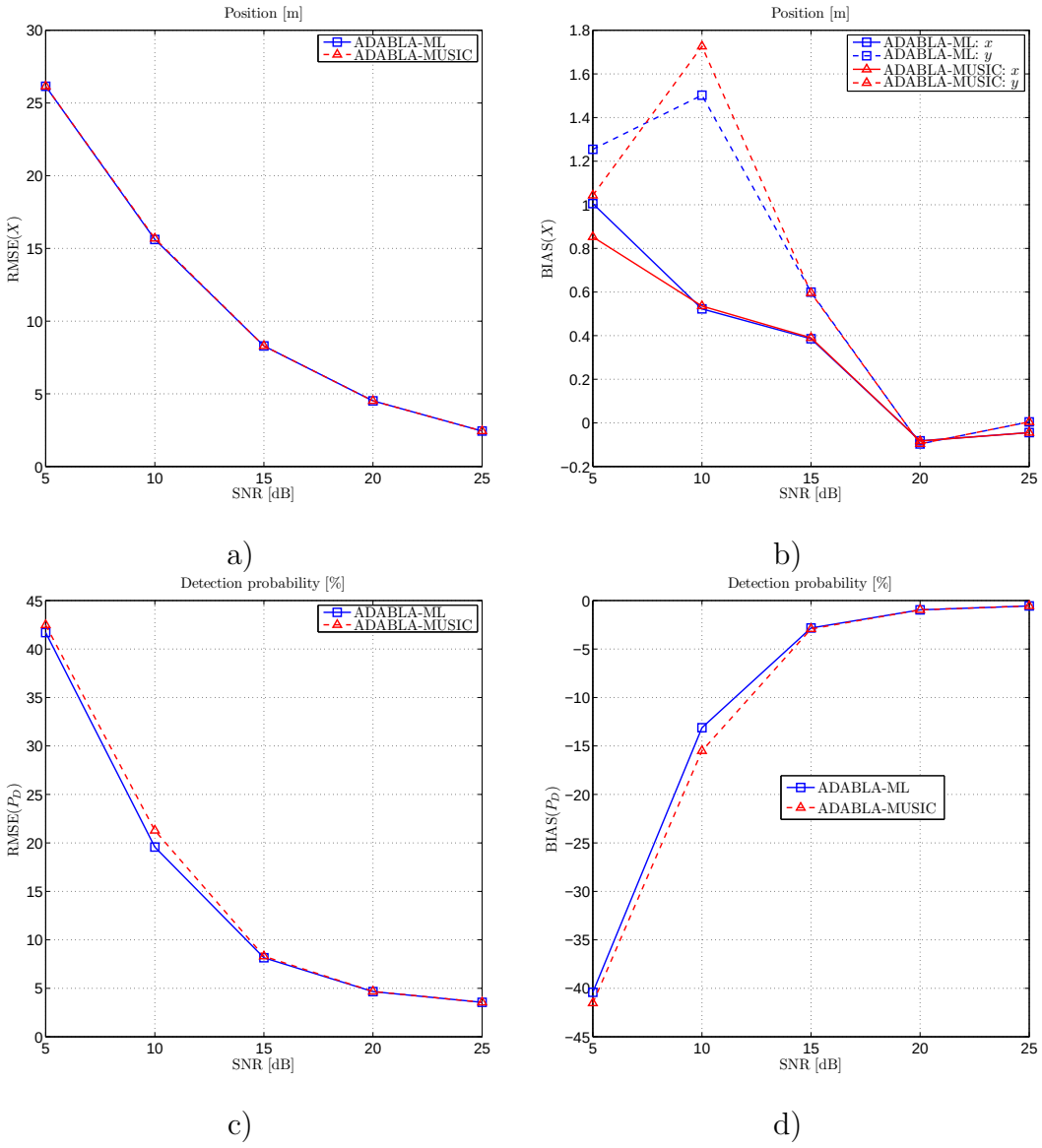

Figure 3.13: RMSE and bias for the MS position and detection probability estimates obtained from 500 Monte-Carlo run of ADABLA-ML and ADABLA-MUSIC algorithms. Four BSs with a two-element ($M = 2$) antenna array participate in the localization process of the MS. All BSs see multiple paths (including the LOS one).

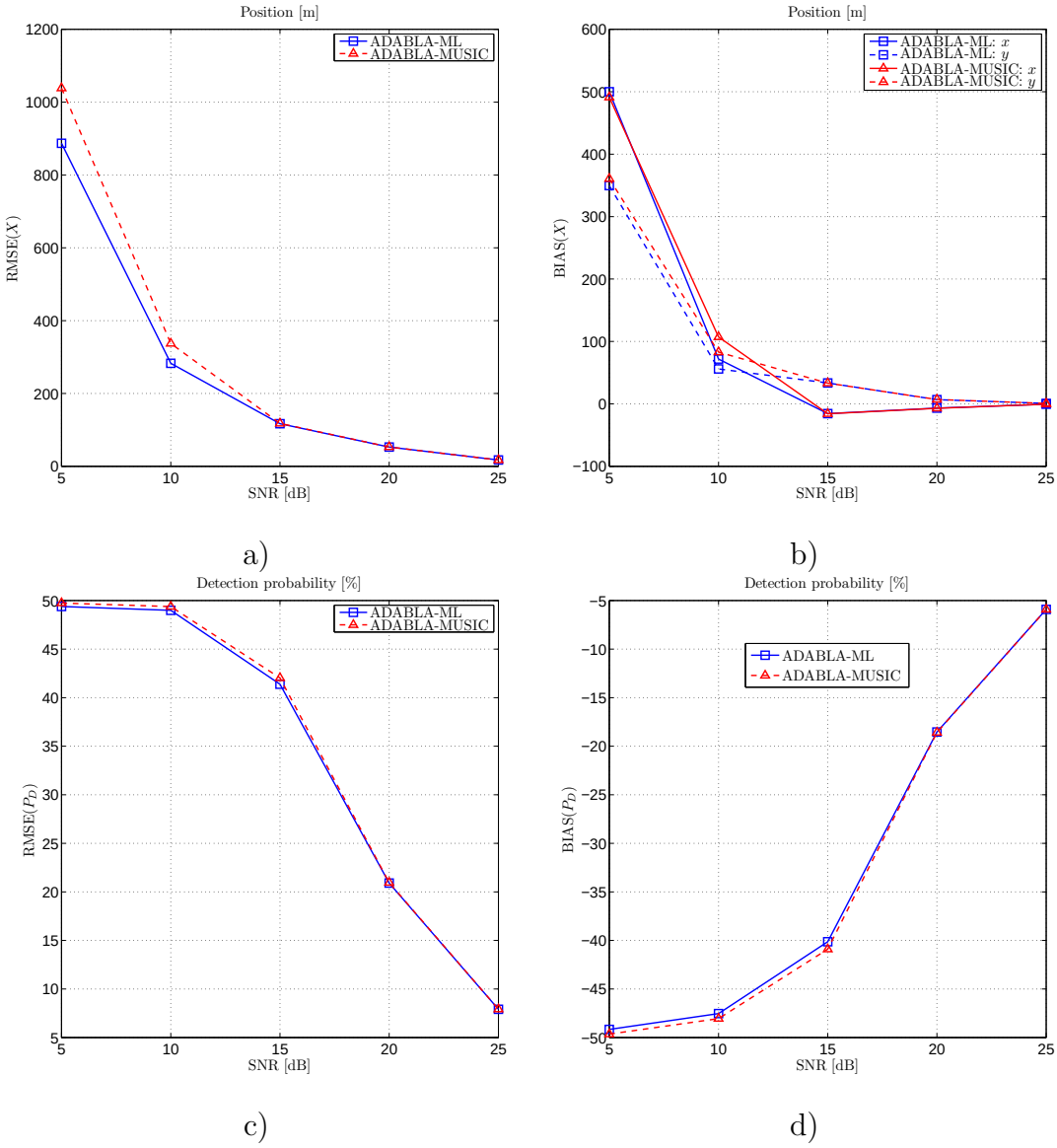

Figure 3.14: RMSE and bias for the MS position and detection probability estimates obtained from 500 Monte-Carlo run of ADABLA-ML and ADABLA-MUSIC algorithms. Four BSs with a two-element ($M = 2$) antenna array participate in the localization process of the MS. Only two BSs see the LOS path, among the multiple observed ones.

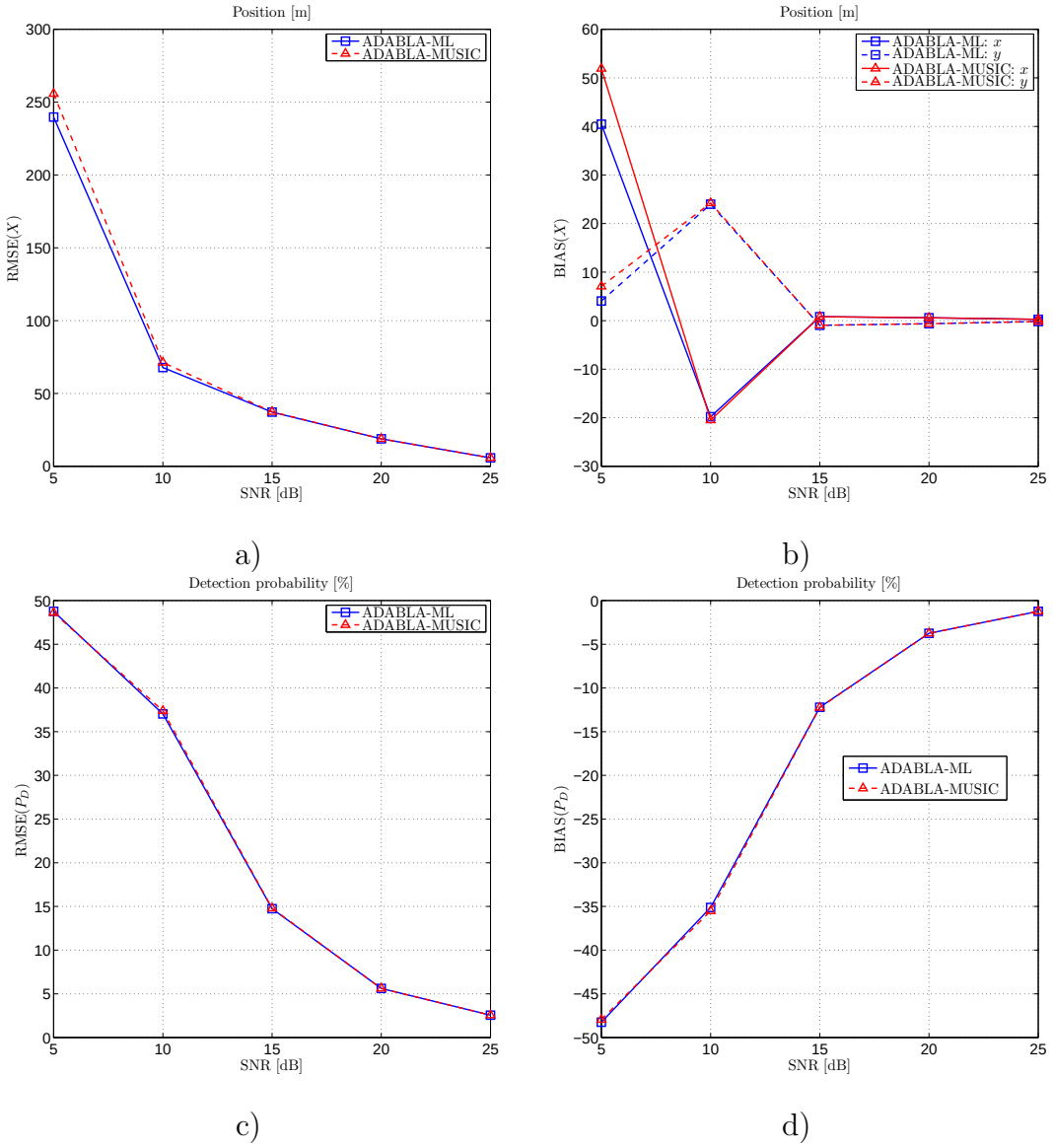

Figure 3.15: RMSE and bias for the MS position and detection probability estimates obtained from 500 Monte-Carlo run of ADABLA-ML and ADABLA-MUSIC algorithms. Four BSs with a four-element ($M = 4$) antenna array participate in the localization process of the MS. Only two BSs see the LOS path, among the multiple observed ones.

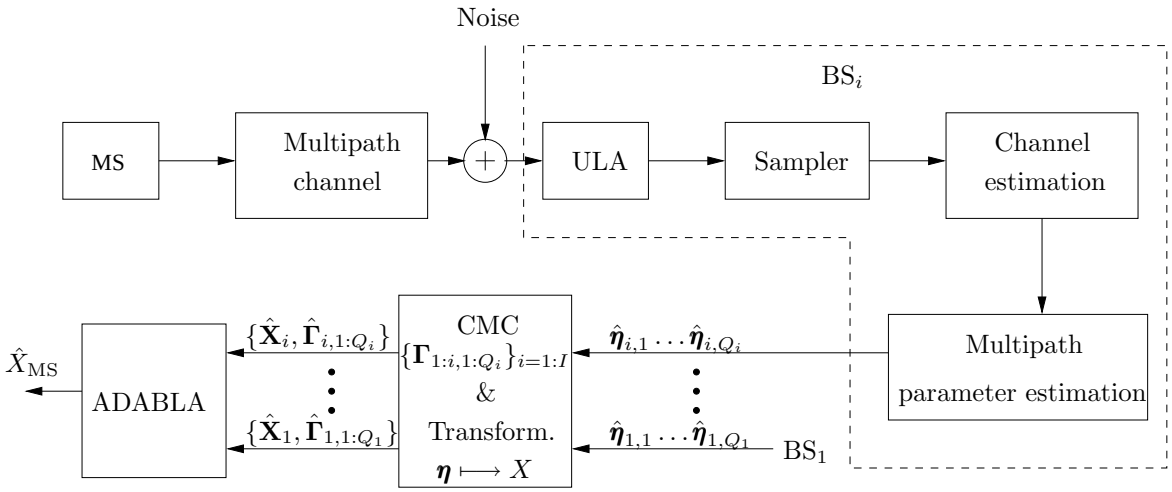

Figure 3.16: Conceptual diagram of the simulation scenario.

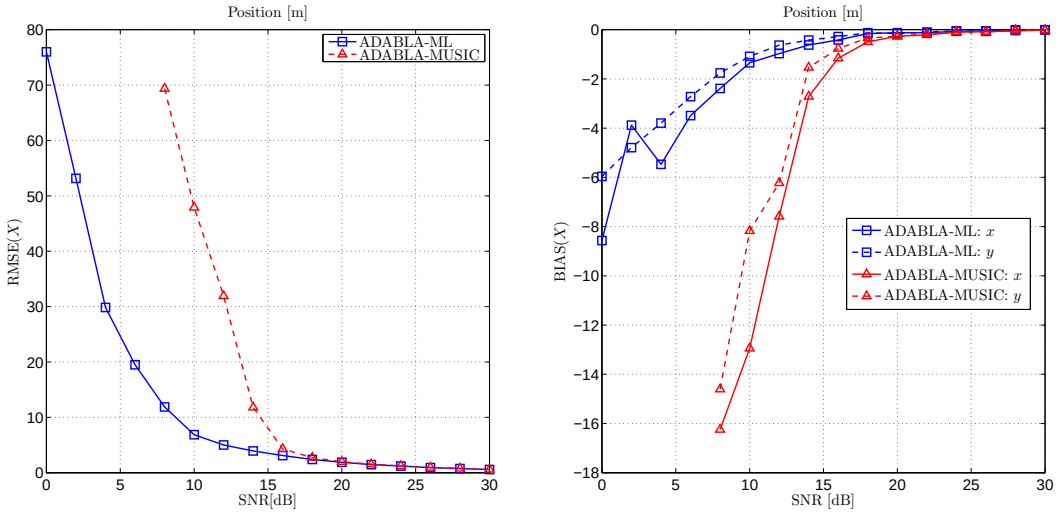

a) b)

Figure 3.17: Experimental a) RMSE and b) Bias of the MS position estimation, obtained from 500 Monte-Carlo runs. Three BSs with a five-element antenna array ($M = 5$) participate in the localization process of an MS. Only two BSs see the LOS path among the multiple detected paths.

Angle and Delay of Arrival-Based Localization Algorithm (ADABLA)

Data:

$$\mathbf{X}_i = \{X_{i,1}, \ldots, X_{i,Q_i}\} \text{ for } i = 1, \ldots, I$$
$$\mathbf{\Gamma}_{i,q} \text{ for } i = 1, \ldots, I \text{ and } q = 1, \ldots, Q_i$$

Computed parameters at p iteration:

$$\tilde{\Theta} = \{\tilde{X}, \tilde{P}_D\}$$

EM	Eqs.
FOR $i = 1 : I$	
FOR $k = 0 : Q_i$	
$p(\mathbf{X}_i \vert \psi_i = k; \tilde{X}) = \prod_{l=1}^{Q_i} \upsilon(X_{i,l}) \mathbb{1}\{\psi_i = 0\} + \cdots$ $\phi_2(X_{i,k}; \tilde{X}, \mathbf{\Gamma}_{i,k}) \prod_{l=1, l\neq k}^{Q_i} \upsilon(X_{i,l}) \mathbb{1}\{\psi_i \neq 0\}$	(3.29)
END FOR k	
$p(\mathbf{X}_i, \psi_i; \tilde{\Theta}) = (1 - \tilde{P}_D) p(\mathbf{X}_i \vert \psi_i = 0; \tilde{X}) \mathbb{1}\{\psi_i = 0\} + \cdots$ $\frac{\tilde{P}_D}{Q_i} \sum_{k=1}^{Q_i} p(\mathbf{X}_i \vert \psi_i = k; \tilde{X}) \mathbb{1}\{\psi_i = k\}$	(3.31)
$p(\mathbf{X}_i; \tilde{\Theta}) = (1 - \tilde{P}_D) p(\mathbf{X}_i \vert \psi_i = 0; \tilde{X}) + \frac{\tilde{P}_D}{Q_i} \sum_{k=1}^{Q_i} p(\mathbf{X}_i \vert \psi_i = k; \tilde{X})$	(3.32)
$p(\psi_i \vert \mathbf{X}_i, \tilde{\Theta}) = \frac{p(\mathbf{X}_i, \psi_i; \tilde{\Theta})}{p(\mathbf{X}_i; \tilde{\Theta})}$	(3.36)
END FOR i	
Parameters update	
$P_D = \frac{1}{I} \sum_{i=1}^{I} \sum_{k=1}^{Q_i} p(\psi_i = k \vert \mathbf{X}_i, \tilde{\Theta})$	(3.38)
$\mathbf{\Lambda}_{i,k} = p(\psi_i = k \vert \mathbf{X}_i, \tilde{\Theta}) \mathbf{\Gamma}_{i,k}^{-1}$	(4.26)
$X = \left(\sum_{i=1}^{I} \sum_{k=1}^{Q_i} \mathbf{\Lambda}_{i,k} \right)^{-1} \left(\sum_{i=1}^{I} \sum_{k=1}^{Q_i} \mathbf{\Lambda}_{i,k} X_{i,k} \right)$	(3.41)

Computed parameters

$$\Theta = \{X, P_D\}$$

Table 3.2: One iteration of the Angle and Delay of Arrival-Based Localization Algorithm (ADABLA).

Conclusions of part I

The problem of localizing a network element (MS or BS) of wireless communication systems was treated in this dissertation part. Unlike the classical localization problem, where a set of BSs participate in the localization process of an MS, we treat the localization problem from a more general point of view, where the element to localize can be either an MS or a BS and the observer (i.e. that one interested in knowing the position of the network element) could be the MS, the BS or an external agent equipped with the required resources to perform radio measurements or to get them from the network. This type of approach is particulary useful because it permits to localize network elements without advertising the network to do so.

The proposed methodology to achieve network element localization is based on parametric estimation techniques. The methodology consist of a statistical model proposal for the radio measurements and the use of the expectation-maximization algorithm to compute the maximum-likelihood estimate of the parameters of interest, i.e. the position of the network element. The statistical model is flexible enough to deal with the most common radio measurements in wireless communication systems, i.e. TOA, TDOA, AOA and RSS. On the other hand, it permits to consider impairments in the radio measurements introduced by the propagation environment, such as multipath and non line of sight (NLOS) propagation, and those ones introduced by a bad network element calibration and today's wireless communication systems limitations (i.e. limited bandwidths), which may give rise to measurement noise, systematic offsets and quantization.

The effectiveness of the proposed methodology was proved in two different localization problems:

BS localization : we performed the localization of a BS in the GSM communication system exploiting quantized measurements of the absolute distance (or equivalently the TOA) between the BS and the MS. Such a measurement, known as timing advance (TA), is performed by the BS and send it to the MS for synchronization purposes. Therefore, the observer in this application is considered to be the MS which receives TA

measurements each 480ms. The TA is a quantity between 0 and 63 representing BS-MS distances, where each integer represents an increment of 554m. In addition to this severely quantization it was found that distance measurements were also corrupted by additive noise, systematic offsets and NLOS propagation. Applying the proposed methodology to this problem we deduced the timing advance-based localization algorithm (TABLA). It was shown that collecting TA measurements without important variations in the MS height, the height of the BS cannot be estimated. Furthermore, a strategy for collecting TA measurements was proposed. The strategy consist in getting TA measurements from positions which do not appertain to a hyperbolic curve. This is because if the positions, where TA measurements are obtained, form a hyperbolic curve (or any degenerate form of this curve), with one of its foci situated at the BS position, then there may exist several BS position estimations equally likely. Finally, using real field measurements TABLA showed its efficacy to localize BSs in rural, semi-urban and urban environments, with a precision under the TA resolution. Nowadays TABLA is an operating algorithm being used for industrial purposes.

MS localization : we dealt with the problem of MS localization, in a TDMA-based communication system, using a set of BSs equipped with antenna arrays. Measurements for localization consisted of a sequence of channel estimates from which the multipath parameters, i.e. the TOA and the AOA of each propagating path, were estimated using the JADE-ML and JADE-MUSIC methods. A cartesian representation of the multipath parameters and of the asymptotic covariance matrices of JADE-ML or JADE-MUSIC estimates were used as inputs for the proposed methodology. The resulting angle and delay of arrival-based localization algorithm (ADABLA) is able to locate the MS with at least two BSs "seeing" multiple paths, comprising the LOS paths, while at the same time is able to remove information delivered by BSs being in NLOS regime only. Simulation results showed a superior performance of ADABLA base on ML (ADABLA-ML) over that one based on MUSIC (ADABLA-MUSIC) as the number of propagating paths becomes important.

Appendices

Appendix A

TABLA: Fisher information matrix derivation

Given the sequence of independent random variables $\{Y_i\}_{i=1:n}$ with joint pdf given by

$$p(y_{1:n};\theta) = \prod_{i=1}^{n} p(y_i;\theta)$$

where $\theta = \{x_s, \mu, \sigma^2, P_D\}$ stands for the full parameters vector and

$$p(y_i;\theta) = P_D \int_{z\in\mathcal{I}_i} \phi(z;\chi_i(x_s)+\mu,\sigma^2)dz + \frac{1-P_D}{N} \tag{A.1}$$

We look for the Fisher Information Matrix (FIM) associated to the sequence $Y_{i1=1:n}$. According to [17] FIM's elements can be computed using

$$\mathcal{F}_n(\theta) = \sum_{i=1}^{n} \mathcal{F}_i(\theta) \tag{A.2}$$

where

$$\mathcal{F}_i(\theta) = \mathbb{E}_{Y_i}\left\{ \frac{\partial \log p(Y_i;\theta)}{\partial\theta} \frac{\partial \log p(Y_i;\theta)}{\partial\theta^T} \right\} \tag{A.3}$$

In the following we provide all the elements needed for the FIM computation.

A.1 Derivatives

According to the above, we need to compute

$$\frac{\partial \log p(Y_i;\theta)}{\partial\theta} = \frac{1}{p(Y_i;\theta)} \frac{\partial p(Y_i;\theta)}{\partial\theta} \tag{A.4}$$

In the sections below we present the computation of the partial derivatives of $p(Y_i;\theta)$, w.r.t. each element of the parameters vector θ. For notational sake let define

$$F(a_i,b_i) = \int_{a_i}^{b_i}(2\pi)^{-\frac{1}{2}}e^{-\frac{t^2}{2}}dt, \tag{A.5}$$

$$G(a_i,b_i) = \int_{a_i}^{b_i}(2\pi)^{-\frac{1}{2}}te^{-\frac{t^2}{2}}dt, \tag{A.6}$$

$$H(a_i,b_i) = \int_{a_i}^{b_i}(2\pi)^{-\frac{1}{2}}t^2e^{-\frac{t^2}{2}}dt. \tag{A.7}$$

A.1.1 Derivative w.r.t x_s

$$\begin{aligned}\frac{\partial p(y_i;\theta)}{\partial x_{s,k}} &= P_D\int_{z\in\mathcal{I}_i}\frac{\partial\phi(z;\chi_i(x_s)+\mu,\sigma^2)}{\partial x_{s,k}}dz \\ &= P_D\int_{z\in\mathcal{I}_i}\phi(z;\chi_i(x_s)+\mu,\sigma^2)\left(\frac{z-\chi_i(x_s)-\mu}{\sigma^2}\right)\frac{\partial\chi_i(x_s)}{\partial x_{s,k}}dz\end{aligned}$$

making $t=\sigma^{-1}(z-\chi_i(x_s)-\mu)$ and using (A.6) gives

$$\frac{\partial p(y_i;\theta)}{\partial x_{s,k}} = \frac{P_D}{\sigma}G(a_i,b_i)\frac{\partial\chi_i(x_s)}{\partial x_{s,k}} \tag{A.8}$$

where

$$\frac{\partial\chi_i(x_s)}{\partial x_{s,k}} = \frac{x_{s,k}-x_i}{\chi_i(x_s)}$$

with $x_s=[x_{s,1}\ \ x_{s,2}]^T$.

A.1.2 Derivative w.r.t μ

$$\begin{aligned}\frac{\partial p(y_i;\theta)}{\partial \mu} &= P_D\int_{z\in\mathcal{I}_i}\frac{\partial\phi(z;\chi_i(x_s)+\mu,\sigma^2)}{\partial \mu}dz \\ &= P_D\int_{z\in\mathcal{I}_i}\phi(z;\chi_i(x_s)+\mu,\sigma^2)\left(\frac{z-\chi_i(x_s)-\mu}{\sigma^2}\right)dz\end{aligned}$$

making $t=\sigma^{-1}(z-\chi_i(x_s)-\mu)$ and using (A.6) gives

(A.9)

$$\frac{\partial p(y_i;\theta)}{\partial \mu} = \frac{P_D}{\sigma}G(a_i,b_i) \tag{A.10}$$

A.1.3 Derivative w.r.t σ

$$\begin{aligned}\frac{\partial p(y_i;\theta)}{\partial \sigma} &= P_D \int_{z\in\mathcal{I}_i} \frac{\partial \phi(z;\chi_i(x_s)+\mu,\sigma^2)}{\partial \sigma} dz \\ &= P_D \int_{z\in\mathcal{I}_i} \frac{1}{\sigma}\left(\phi(z;\chi_i(x_s)+\mu,\sigma^2)\frac{(z-\chi_i(x_s)-\mu)^2}{\sigma^2} - \phi(z;\chi_i(x_s)+\mu,\sigma^2)\right)\end{aligned}$$

making $t=\sigma^{-1}(z-\chi_i(x_s)-\mu)$ and using (A.5) and (A.7) gives

$$\frac{\partial p(y_i;\theta)}{\partial \sigma} = \frac{P_D}{\sigma}(H(a_i,b_i)-F(a_i,b_i)) \tag{A.11}$$

A.1.4 Derivative w.r.t P_D

$$\frac{\partial p(y_i;\theta)}{\partial P_D} = \int_{z\in\mathcal{I}_i} \phi(z;\chi_i(x_s)+\mu,\sigma^2)dz - \frac{1}{N}$$

making $t=\sigma^{-1}(z-\chi_i(x_s)-\mu)$ and using (A.5) gives

$$\frac{\partial p(y_i;\theta)}{\partial P_D} = F(a_i,b_i) - \frac{1}{N} \tag{A.12}$$

A.2 FIM's elements computation

Exploiting (A.3) the FIM's elements can be computed as

$$f^i_{k,j} = \mathbb{E}_{Y_i}\left\{\frac{\partial \log p(Y_i;\theta)}{\partial \theta_k}\frac{\partial \log p(Y_i;\theta)}{\partial \theta_j}\right\}$$

where $f^i_{k,j}$ denotes the (k,j) element in the FIM associated to the random variable Y_i and where $\theta_1 = x_{s,1}$, $\theta_2 = x_{s,2}$, $\theta_3 = \mu$, $\theta_4 = \sigma$ and $\theta_5 = P_D$.

As we can seen the expectation is taken w.r.t. random variable Y_i. On the other hand Y_i is a discrete random variable taking its values from the discrete set $\{0,1,\ldots,N-1\}$ and with pdf given by $p(Y_i;\theta)$. Therefore, taking the expectation in the above equation and using (A.4) the FIM's elements can be computed as

$$f^i_{k,j} = \sum_{Y_i=0}^{N-1} \frac{1}{p(Y_i;\theta)}\frac{\partial p(Y_i;\theta)}{\partial \theta_k}\frac{\partial p(Y_i;\theta)}{\partial \theta_j}$$

Using the formulae given in section A.1 and the latter equation we obtain, after some straightforward algebraic manipulations the following formulae

For $k, j \in \{1, 2\}$

$$
\begin{aligned}
f^i_{k,j} &= \frac{P_D^2}{\sigma^2} \sum_{i=1}^{n} \frac{\partial \chi_i}{\partial x_{s,k}} \frac{\partial \chi_i}{\partial x_{s,j}} \sum_{Y_i=0}^{N-1} \left\{ \frac{G(a_i, b_i)^2}{p(Y_i; \theta)} \right\} \\
f^i_{k,3} &= \frac{P_D^2}{\sigma^2} \sum_{i=1}^{n} \frac{\partial \chi_i}{\partial x_{s,k}} \sum_{Y_i=0}^{N-1} \left\{ \frac{G(a_i, b_i)^2}{p(Y_i; \theta)} \right\} \\
f^i_{k,4} &= \frac{P_D^2}{\sigma^2} \sum_{i=1}^{n} \frac{\partial \chi_i}{\partial x_{s,k}} \sum_{Y_i=0}^{N-1} \left\{ \frac{G(a_i, b_i)(H(a_i, b_i) - F(a_i, b_i))}{p(Y_i; \theta)} \right\} \\
f^i_{k,5} &= \frac{P_D}{\sigma} \sum_{i=1}^{n} \frac{\partial \chi_i}{\partial x_{s,k}} \sum_{Y_i=0}^{N-1} \left\{ \frac{G(a_i, b_i)(F(a_i, b_i) - \frac{1}{N})}{p(Y_i; \theta)} \right\}
\end{aligned}
$$

Also we have

$$
\begin{aligned}
f^i_{3,3} &= \frac{P_D^2}{\sigma^2} \sum_{i=1}^{n} \sum_{Y_i=0}^{N-1} \left\{ \frac{G(a_i, b_i)^2}{p(Y_i; \theta)} \right\} \\
f^i_{3,4} &= \frac{P_D^2}{\sigma^2} \sum_{i=1}^{n} \sum_{Y_i=0}^{N-1} \left\{ \frac{G(a_i, b_i)(H(a_i, b_i) - F(a_i, b_i))}{p(Y_i; \theta)} \right\} \\
f^i_{3,5} &= \frac{P_D}{\sigma} \sum_{i=1}^{n} \sum_{Y_i=0}^{N-1} \left\{ \frac{G(a_i, b_i)(F(a_i, b_i) - \frac{1}{N})}{p(Y_i; \theta)} \right\} \\
f^i_{4,4} &= \frac{P_D^2}{\sigma^2} \sum_{i=1}^{n} \sum_{Y_i=0}^{N-1} \left\{ \frac{(H(a_i, b_i) - F(a_i, b_i))^2}{p(Y_i; \theta)} \right\} \\
f^i_{4,5} &= \frac{P_D}{\sigma} \sum_{i=1}^{n} \sum_{Y_i=0}^{N-1} \left\{ \frac{(H(a_i, b_i) - F(a_i, b_i))(F(a_i, b_i) - \frac{1}{N})}{p(Y_i; \theta)} \right\} \\
f^i_{5,5} &= \sum_{i=1}^{n} \sum_{Y_i=0}^{N-1} \left\{ \frac{(F(a_i, b_i) - \frac{1}{N})^2}{p(Y_i; \theta)} \right\}
\end{aligned}
$$

finally the remainder FIM's elements are taken according to $f^i_{j,k} = f^i_{k,j}$.

Appendix B

UTM system and conversion formulae

The Universal Transverse Mercator (UTM) coordinate system is a grid-based method of specifying locations on the surface of the Earth. It is used to identify locations on the earth, but differs from the traditional method of latitude and longitude in several respects.

The system is based on an ellipsoidal model of the Earth. Currently, the WGS84 ellipsoid is used as the underlying model of the Earth in the UTM coordinate system.

B.1 UTM longitude zone

The UTM system divides the surface of the Earth between 80 [deg] S latitude and 84 [deg] N latitude into 60 zones, each 6 [deg] of longitude in width and centered over a meridian of longitude. Zones are numbered from 1 to 60. Zone 1 is bounded by longitude 180 [deg] to 174 [deg] W and is centered on the 177th West meridian. Zone numbering increases in an easterly direction.

Each of the 60 longitude zones in the UTM system is based on a Transverse Mercator projection, which is capable of mapping a region of large north-south extent with a low amount of distortion. By using narrow zones of 6 [deg] (to 800km resp.) in width, and reducing the scale factor along the central meridian by only 0.0004 (to 0.9996, a reduction of 1:2500) the amount of distortion is held below 1 part in 1,000 inside each zone. Distortion of scale increases to 1.0010 at the outer zone boundaries along the equator.

The secant projection in each zone creates two standard lines, or lines of true scale, located approximately 180 km on either side of, and approximately parallel to, the central meridian. The scale factor is less than 1 inside these

lines and greater than 1 outside of these lines, but the overall distortion of scale inside the entire zone is minimized.

B.2 UTM latitude zone

The UTM system segments each longitude zone into 20 latitude zones. Each latitude zone is 8 degrees high, and is lettered starting from "C" at 80 [deg] S, increasing up the English alphabet until "X", omitting the letters "I" and "O" (because of their similarity to the digits one and zero). The last latitude zone, "X", is extended an extra 4 degrees, so it ends at 84 [deg] N latitude, thus covering the northern most land on Earth. Latitude zones "A" and "B" do exist, as do zones "Y" and "Z". They cover the western and eastern sides of the Antarctic and Arctic regions respectively.

B.3 Locating a position using UTM coordinates

A position on the Earth is referenced in the UTM system by the UTM longitude zone, and the easting and northing coordinate pair. The easting is the projected distance of the position from the central meridian, while the northing is the projected distance of the point from the equator. The point of origin of each UTM zone is the intersection of the equator and the zone's central meridian. In order to avoid dealing with negative numbers, the central meridian of each zone is given a "false easting" value of 500,000 meters. Thus, anything west of the central meridian will have an easting less than 500,000 meters. In the northern hemisphere, positions are measured northward from the equator, which has an initial "northing" value of 0 meters and a maximum "northing" value of approximately 9,328,000 meters at the 84th parallel – the maximum northern extent of the UTM zones. In the southern hemisphere, northings decrease as you go southward from the equator, which is given a "false northing" of 10,000,000 meters so that no point within the zone has a negative northing value.

B.4 Latitude, longitude to UTM conversion (or vice versa)

In this section we provide formulae to transform a point from a latitude-longitude $(\text{Lat}, \text{Long})$ reference system to the easting-northing (x, y) UTM

reference system, and vice versa. Before proceeding, let set some important parameters, which are shown in table B.1.

Parameter	Value	Description
Long_0	$\frac{180}{\pi}((\text{zone} - \frac{1}{2})L - 180)$	central meridian of zone
zone	from 1 to 60	Number of an UTM earth's surface division
L	6 [deg]	Width of the zone
FE	500000 $[m]$	False Easting
FN	10000000 $[m]$	False Northing
a	6378137 [m]	Equatorial Radius
f	1/298.257223563	Flattening
k_0	0.9996	Scale factor

Table B.1: Parameters used in the transformation equations.

B.4.1 Latitude, longitude to UTM conversion formulae

The formulas to derive the projected Easting (x) and Northing (y) coordinates are:

$$x = \text{FE} + k_0\nu\left(A + (1 - T + C)\frac{A^3}{6} + \cdots (5 - 18T + T^2 + 72C - 58e'^2)\frac{A^5}{120}\right) \quad \text{(B.1)}$$

$$y = \text{FN} + k_0\left[M + \nu\tan(\text{lat})\left(\frac{A^2}{2} + (5 - T + 9C + 4C^2)\frac{A^4}{24} + \cdots (61 - 58T + T^2 + 600C - 330e'^2)\frac{A^6}{720}\right)\right] \quad \text{(B.2)}$$

where

$$
\begin{aligned}
e^2 &= 2f - f^2 \\
e'^2 &= \frac{e^2}{1-e^2} \\
\nu &= \frac{a}{(1-e^2\cos^2(\mathrm{Lat}))^{1/2}} \\
A &= (\mathrm{Long} - \mathrm{Long}_0)\cos(\mathrm{Lat}) \\
T &= \tan^2(\mathrm{Lat}) \\
C &= e'^2\cos^2(\mathrm{Lat}) \\
M &= a\left[\left(1 - \frac{e^2}{4} - \frac{3e^4}{64} - \frac{5e^6}{256}\right)\mathrm{Lat} - \left(\frac{3e^2}{8} + \frac{3e^4}{32} + \frac{45e^6}{1024}\right)\sin^2(\mathrm{Lat}) + \cdots \right. \\
&\quad \left. \left(\frac{15e^4}{256} + \frac{45e^6}{1024}\right)\sin^4(\mathrm{Lat}) - \frac{35e^6}{3072}\sin^6(\mathrm{Lat})\right]
\end{aligned}
$$

B.4.2 UTM to Latitude, longitude conversion formulae

The reverse formulas to convert Easting (x) and Northing (y) projected coordinates to latitude (Lat) and longitude (Long) are:

$$
\begin{aligned}
\mathrm{Lat} &= \phi - \frac{a\tan(\phi)}{\rho}\left(0.5D^2 - (5 + 3T_1 + 10C_1 - 4C_1^2 - 9e'^2)\frac{D^4}{24} + \cdots \right. \\
&\quad \left. (61 + 90T_1 + 298C_1 + 45T_1^2 - 252e'^2 - 3C_1^2)\frac{D^6}{720}\right) \qquad \text{(B.3)} \\
\mathrm{Long} &= \mathrm{Long}_0 + \frac{1}{\cos(\phi)}\left(D - (1 + 2T_1 + C_1)\frac{D^3}{6} + \cdots \right. \\
&\quad \left. (5 - 2C_1 + 28T_1 - 3C_1^2 + 8e'^2 + 24T_1^2)\frac{D^5}{120}\right) \qquad \text{(B.4)}
\end{aligned}
$$

where

$$
\begin{aligned}
\phi &= \mu + \left(\frac{3e_1}{2} - \frac{27e_1^3}{32}\right)\sin(2\mu) + \left(\frac{21e_1^2}{16} - \frac{55e_1^4}{32}\right)\sin(4\mu) + \cdots \\
&\quad \frac{151e_1^3}{96}\sin(6\mu) + \frac{1097e_1^4}{512}\sin(8\mu) \\
\rho &= \frac{a(1-e^2)}{(1-e^2\sin^2(\phi))^{\frac{3}{2}}} \\
\mu &= \frac{M_1}{a\left(1 - \frac{e^2}{4} - \frac{3e^4}{256} - \frac{5e^6}{256}\right)} \\
M_1 &= \frac{y'}{k_0} \\
x' &= x - \mathrm{FE} \\
y' &= y - \mathrm{FN} \\
e_1 &= \frac{1-(1-e^2)^{\frac{1}{2}}}{1+(1-e^2)^{\frac{1}{2}}} \\
T_1 &= \tan^2(\phi) \\
C_1 &= e'^2\cos^2(\phi) \\
D &= \frac{x'}{ak_0}
\end{aligned}
$$

Appendix C

Derivation of maximum likelihood for JADE

In this appendix we will derive expressions for stochastic maximum likelihood as it applies to JADE. The parameters to be estimated are $(\sigma_e^2, \boldsymbol{\eta}, \mathbf{R}_\beta)$. We show that $\hat{\boldsymbol{\eta}}$ can be obtained by maximizing a function over only the Q pairs of real angles and delays, and that $\hat{\sigma}_e^2$ and $\mathbf{R}_\beta$ are obtained by closed-form formulas. Details on the Cramer-Rao bound are also given.

C.1 Stochastic maximum likelihood: a separable solution

The stochastic maximum likelihood is based on the stochastic modeling of the path fadings. In a Rayleigh fading channel, the path fadings have a complex Gaussian distribution. Formally, $\mathbf{b}^{(s)} \sim \mathcal{N}(\mathbf{0}, \mathbf{R_b})$ and the estimation noise $\mathbf{v}^{(s)} \sim (0, \sigma_e^2\mathbf{I})$, where σ_e^2 is the variance of each entry in the estimation noise matrix. Therefore, the channel estimates $\mathbf{y}^{(s)}$ are zero-mean complex Gaussian random variables, with covariance matrix $\mathbf{R} = \mathbb{E}\{\mathbf{YY}\}$. Under such a considerations the likelihood function of the channel estimates can be written as

$$L(\mathbf{Y}; \boldsymbol{\Psi}) = \frac{1}{(\pi|\mathbf{R}|)^S} \exp\left(-S\mathrm{Tr}(\mathbf{R}^{-1}\hat{\mathbf{R}})\right) \tag{C.1}$$

and the associated negative log-likelihood function normalized by S is

$$l(\mathbf{Y}; \boldsymbol{\Psi}) = \log|\mathbf{R}| + \mathrm{Tr}(\mathbf{R}^{-1}\hat{\mathbf{R}}) \tag{C.2}$$

where

- $\mathbf{Y} = [\mathbf{y}^{(1)} \cdots \mathbf{y}^{(S)}]$, is the sequence of channel estimations,

- $\boldsymbol{\Psi} = [\boldsymbol{\eta}, \sigma_e^2, \mathbf{R}_b]$, is the full parameters vector,
- $\mathbf{R} = \mathbf{U}\mathbf{R}_\mathbf{b}\mathbf{U}^H + \sigma_e^2\mathbf{I}$, is the covariance matrix of the channel estimates,
- $\mathbf{R}_\mathbf{b} = \mathbb{E}\left\{\mathbf{B}\mathbf{B}^H\right\}$, is the covariance matrix of the fading coefficients, and
- $\hat{\mathbf{R}} = \frac{1}{S}\sum_{s=1}^{S}\mathbf{y}^{(s)}\mathbf{y}^{(s)H}$, is the estimated covariance matrix of the channel estimates.

As it its well known the maximum likelihood estimate $\hat{\boldsymbol{\Psi}}$ is given by the maximization of (C.22) w.r.t $\boldsymbol{\Psi}$. Unfortunately, this maximization is not easy, because it has to be performed over a multidimensional space, which depends on the number of multipath parameters $2Q$, the number of path fadings Q and on the variance of the additive noise. However, it is possible to alleviate this problem using the following theorem.

Theorem 2 (Separable solution) *If the estimated covariance matrix* $\hat{\mathbf{R}}$ *is positive-definite, the maximum likelihood estimates* $\hat{\boldsymbol{\eta}}$, $\hat{\sigma}_e^2$, *and* $\hat{\mathbf{R}}_\mathbf{b}$ *which maximize the log-likelihood function* (C.22) *subject to* $\mathbf{R} = \mathbf{U}\mathbf{R}_\mathbf{b}\mathbf{U}^H + \sigma_e^2\mathbf{I}$ *are given by the following:*

$$\hat{\boldsymbol{\eta}} = \max_{\boldsymbol{\eta}} \left\{ -\log \mid \boldsymbol{\Phi}(\boldsymbol{\eta})\hat{\mathbf{R}}\boldsymbol{\Phi}(\boldsymbol{\eta}) + \frac{1}{MPL - Q}\mathrm{Tr}(\boldsymbol{\Phi}(\boldsymbol{\eta})^{\perp}\hat{\mathbf{R}})\boldsymbol{\Phi}(\boldsymbol{\eta})^{\perp} \mid \right\} \tag{C.3}$$

$$\hat{\sigma}_e^2(\hat{\boldsymbol{\eta}}) = \frac{\mathrm{Tr}(\boldsymbol{\Phi}(\hat{\boldsymbol{\eta}})^{\perp}\hat{\mathbf{R}})}{MPL - Q} \tag{C.4}$$

and

$$\hat{\mathbf{R}}_\mathbf{b}(\hat{\boldsymbol{\eta}}) = \mathbf{U}(\hat{\boldsymbol{\eta}})^{\dagger}(\hat{\mathbf{R}} - \hat{\sigma}_e^2 I)(\mathbf{U}(\hat{\boldsymbol{\eta}})^{\dagger})^H \tag{C.5}$$

with $\boldsymbol{\Phi}(\boldsymbol{\eta}) = \mathbf{U}(\boldsymbol{\eta})(\mathbf{U}(\boldsymbol{\eta})^H\mathbf{U}(\boldsymbol{\eta}))^{-1}\mathbf{U}(\boldsymbol{\eta})^H$ and $\boldsymbol{\Phi}(\boldsymbol{\eta})^{\perp} = \mathbf{I} - \boldsymbol{\Phi}(\boldsymbol{\eta})$.

C.1.1 Proof

Maximization of (C.22) w.r.t. $\boldsymbol{\eta}$, σ_e^2 and $\mathbf{R}_\mathbf{b}$ is equivalent to the following two-step procedure. We first maximize the function w.r.t. to $\mathbf{R}_\mathbf{b}$ and σ_e^2 for a fixed $\boldsymbol{\eta}$ and substitute for the resulting $\hat{\mathbf{R}}_\mathbf{b}$ and $\hat{\sigma}_e^2$ as a function of $\boldsymbol{\eta}$ and $\hat{\mathbf{R}}$ back into the log-likelihood function, resulting in a function to be maximized over only the $\boldsymbol{\eta}$ parameters.

In the following proof we drop any dependence on $\boldsymbol{\eta}$ in order to alleviate mathematical notation.

Maximum likelihood estimate of $\mathbf{R_b}$

Let express $\mathbf{R}$ as

$$\mathbf{R} = \sum_{i=1}^{Q}\sum_{j=1}^{Q} b_{ij}\mathbf{u}_i\mathbf{u}_j^H + \sigma_e^2\mathbf{I} \tag{C.6}$$

where b_{ij} stands for the (i,j) element in $\mathbf{R_b}$ matrix.

Proceeding as explained above, we take the first derivative of (C.22) w.r.t b_{ij} and employing equation (C.6), we observe that two terms need to be computed

$$\begin{aligned}\frac{\partial \log \mid \mathbf{R} \mid}{\partial b_{ij}} &= \mathrm{Tr}(\mathbf{R}^{-1}\mathbf{u}_i\mathbf{u}_j^H) \\ &= \mathbf{u}_j^H\mathbf{R}^{-1}\mathbf{u}_i\end{aligned}$$

and

$$\begin{aligned}\frac{\partial \mathrm{Tr}(\mathbf{R}^{-1}\hat{\mathbf{R}})}{\partial b_{ij}} &= -\mathrm{Tr}(\mathbf{R}^{-1}\hat{\mathbf{R}}\mathbf{R}^{-1}\mathbf{u}_i\mathbf{u}_j^H) \\ &= -\mathbf{u}_j^H\mathbf{R}^{-1}\hat{\mathbf{R}}\mathbf{R}^{-1}\mathbf{u}_i\end{aligned}$$

Hence

$$\frac{\partial l(\mathbf{Y};\mathbf{\Psi})}{\partial b_{ij}} = \mathbf{u}_j^H\mathbf{R}^{-1}\mathbf{u}_i - \mathbf{u}_j^H\mathbf{R}^{-1}\hat{\mathbf{R}}\mathbf{R}^{-1}\mathbf{u}_i$$

Expressing the above in its matrix form and equating to zero we have

$$\mathbf{U}^H(\mathbf{R}^{-1}\hat{\mathbf{R}}\mathbf{R}^{-1} - \mathbf{R}^{-1})\mathbf{U} = \mathbf{0} \tag{C.7}$$

Application of one forme of the inversion matrix lema to $\mathbf{R} = \mathbf{U}\mathbf{R_b}\mathbf{U}^H + \sigma_e^2\mathbf{I}$ yields

$$\mathbf{R}^{-1} = \frac{1}{\sigma_e^2}\left[\mathbf{I} - \mathbf{U}\left(\mathbf{R_b}\mathbf{U}^H\mathbf{U} + \sigma_e^2\mathbf{I}\right)^{-1}\mathbf{R_b}\mathbf{U}^H\right] \tag{C.8}$$

which can be written as

$$\mathbf{R}^{-1}\mathbf{U} = \mathbf{U}\left(\mathbf{R_b}\mathbf{U}^H\mathbf{U} + \sigma_e^2\mathbf{I}\right)^{-1} \tag{C.9}$$

Substitution of (C.9) in (C.7) gives

$$\left(\mathbf{R_b}\mathbf{U}^H\mathbf{U} + \sigma_e^2\mathbf{I}\right)^{-1}\mathbf{U}^H[\hat{\mathbf{R}} - \mathbf{R}]\mathbf{U}\left(\mathbf{R_b}\mathbf{U}^H\mathbf{U} + \sigma_e^2\mathbf{I}\right)^{-1} = \mathbf{0}$$

which implies that

$$\mathbf{U}^H[\hat{\mathbf{R}} - \mathbf{R}]\mathbf{U} = \mathbf{0}$$

Using $\mathbf{R} = \mathbf{U}\mathbf{R_b}\mathbf{U}^H + \sigma_e^2\mathbf{I}$ in the above we get

$$\mathbf{U}^H\hat{\mathbf{R}}\mathbf{U} = \mathbf{U}^H\mathbf{U}\mathbf{R_b}\mathbf{U}^H\mathbf{U} + \sigma_e^2\mathbf{U}^H\mathbf{U}$$

and denoting by $\hat{\mathbf{R}}_\mathbf{b}$ the resulting value of $\mathbf{R_b}$ that satisfies the last equation, we obtain

$$\hat{\mathbf{R}}_\mathbf{b} = \mathbf{U}^\dagger(\hat{\mathbf{R}} - \sigma_e^2\mathbf{I})\mathbf{U}^{\dagger H} \tag{C.10}$$

where $\mathbf{U}^\dagger = (\mathbf{U}^H\mathbf{U})^{-1}\mathbf{U}^H$.

Finally, letting

$$\mathbf{R}_{\text{op}} = \mathbf{U}\hat{\mathbf{R}}_\mathbf{b}\mathbf{U}^H + \sigma_e^2\mathbf{I}$$

and substituting (C.10) into the above equation we can express $\mathbf{R}_{\text{op}}$ as

$$\mathbf{R}_{\text{op}} = \mathbf{\Phi}\hat{\mathbf{R}}\mathbf{\Phi} + \sigma_e^2\mathbf{\Phi}^\perp \tag{C.11}$$

where $\mathbf{\Phi} = \mathbf{U}(\mathbf{U}^H\mathbf{U})^{-1}\mathbf{U}^H$ and $\mathbf{\Phi}^\perp = \mathbf{I} - \mathbf{\Phi}$.

Maximum likelihood estimate of σ^2

Taking the partial derivative of (C.22) respect to σ^2 we obtain

$$\begin{aligned}
\frac{\partial l(\mathbf{Y};\mathbf{\Psi})}{\sigma_e} &= \frac{\partial \log|\mathbf{R}|}{\partial\sigma_e} + \frac{\partial \text{Tr}(\mathbf{R}^{-1}\hat{\mathbf{R}})}{\partial\sigma_e} \\
&= \text{Tr}(2\sigma_e\mathbf{R}^{-1}) + \text{Tr}(-2\sigma_e\mathbf{R}^{-1}\hat{\mathbf{R}}\mathbf{R}^{-1}) \\
&= \text{Tr}(\mathbf{R}^{-1}) - \text{Tr}(\mathbf{R}^{-1}\hat{\mathbf{R}}\mathbf{R}^{-1})
\end{aligned} \tag{C.12}$$

Equating (C.12) to zero, it constitutes a non linear equation in σ_e^2 for which no closed-form solution is known. However, one can make use of a Taylor series expansion of the two terms in (C.12), giving as result [11]:

$$\text{Tr}(\mathbf{R}^{-1}) \simeq \sigma_e^{-2}\left[MPL - \frac{1}{\sigma_e^2}\mathbf{Tr}(\mathbf{R}_s)\right] \tag{C.13}$$

and

$$\text{Tr}(\mathbf{R}^{-1}\hat{\mathbf{R}}\mathbf{R}^{-1}) \simeq \sigma_e^{-4}\left[\text{Tr}(\hat{\mathbf{R}}) - 2\text{Tr}(\mathbf{R}_s)\right] \tag{C.14}$$

where $\mathbf{R}_s = \mathbf{U}\mathbf{R_b}\mathbf{U}^H$ and thus

$$\mathbf{R} = \mathbf{R}_s + \sigma_e^2\mathbf{I} \tag{C.15}$$

Substituting (C.13) and (C.14), with $\mathbf{R}_s = \mathbf{R} - \sigma_e^2\mathbf{I}$, into (C.12) and equating to zero, we get

$$\mathrm{Tr}(\mathbf{R}) - \mathrm{Tr}(\hat{\mathbf{R}}) = 0$$

Finally, making $\mathbf{R} = \mathbf{R}_{\mathrm{op}}$, and substituting (C.11) into the above equation we obtain the following expression

$$\hat{\sigma}_e^2 = \frac{\mathrm{Tr}(\mathbf{\Phi}^{\perp}\hat{\mathbf{R}})}{MPL - Q} \tag{C.16}$$

Maximum likelihood estimate of $\boldsymbol{\eta}$

Let

$$\mathbf{R}_{\mathrm{op}} = \mathbf{U}\hat{\mathbf{R}}_{\mathbf{b}}\mathbf{U}^H + \sigma_e^2\mathbf{I} \tag{C.17}$$

Substituting the above in (C.22) we have

$$l(\mathbf{Y};\mathbf{\Psi}) = \log|\mathbf{R}_{\mathrm{op}}| + \mathrm{Tr}(\mathbf{R}_{\mathrm{op}}^{-1}\hat{\mathbf{R}}) \tag{C.18}$$

From (C.8) we can write

$$\mathbf{R}_{\mathrm{op}}^{-1}\hat{\mathbf{R}} = \frac{1}{\sigma_e^2}\hat{\mathbf{R}} - \frac{1}{\sigma_e^2}\mathbf{U}\left(\hat{\mathbf{R}}_{\mathbf{b}}\mathbf{U}^H\mathbf{U} + \sigma_e^2\mathbf{I}\right)^{-1}\hat{\mathbf{R}}_{\mathbf{b}}\mathbf{U}^H\hat{\mathbf{R}} \tag{C.19}$$

but

$$\left(\hat{\mathbf{R}}_{\mathbf{b}}\mathbf{U}^H\mathbf{U} + \sigma_e^2\mathbf{I}\right) = (\mathbf{U}^H\hat{\mathbf{R}}\mathbf{U})^{-1}\mathbf{U}^H\mathbf{U}$$

Now, using the latter expression into (C.19) and taking its trace we obtain

$$\mathrm{Tr}(\mathbf{R}_{\mathrm{op}}^{-1}\hat{\mathbf{R}}) = \frac{\mathrm{Tr}(\hat{\mathbf{R}})}{\sigma_e^2} - \frac{1}{\sigma_e^2}\mathrm{Tr}(\hat{\mathbf{R}}_{\mathbf{b}}\mathbf{U}^H\mathbf{U})$$

Employing the relation $\hat{\mathbf{R}}_{\mathbf{b}}\mathbf{U}^H\mathbf{U} = (\mathbf{U}^H\mathbf{U})^{-1}\mathbf{U}^H\hat{\mathbf{R}}\mathbf{U} - \sigma_e^2\mathbf{I}$ in the above equation, it is straightforward to show

$$\mathrm{Tr}(\mathbf{R}_{\mathrm{op}}^{-1}\hat{\mathbf{R}}) = \frac{1}{\sigma_e^2}\mathrm{Tr}\left(\mathbf{\Phi}^{\perp}\hat{\mathbf{R}}\right) + Q \tag{C.20}$$

Finally, substituting (C.11) and (C.20) into (C.18) and neglecting uninteresting terms, it is easy to show that the maximum likelihood estimate of $\boldsymbol{\eta}$ is given by

$$\hat{\boldsymbol{\eta}} = \max_{\boldsymbol{\eta}}\left\{-\log\mid \mathbf{\Phi}\hat{\mathbf{R}}\mathbf{\Phi} + \frac{1}{MPL - Q}\mathrm{Tr}(\mathbf{\Phi}^{\perp}\hat{\mathbf{R}})\mathbf{\Phi}^{\perp}\mid\right\} \tag{C.21}$$

which together with (C.10) and (C.16) completes the proof.

C.2 Fisher information matrix computation

Given (C.1) the log-likelihood function may be expressed as

$$l(\mathbf{Y};\mathbf{\Psi}) = -S(\log|\mathbf{R}| + \mathrm{Tr}(\mathbf{R}^{-1}\hat{\mathbf{R}})) \tag{C.22}$$

where $\mathbf{\Psi} = [\boldsymbol{\eta}, \sigma_e^2, \mathbf{R}_b]$.

Following [76] FIM's elements can be computed according to

$$f_{i,j} = S\mathrm{Tr}\left(\mathbf{R}^{-1}\frac{\partial \mathbf{R}}{\partial \psi_j}\mathbf{R}^{-1}\frac{\partial \mathbf{R}}{\partial \psi_i}\right) \tag{C.23}$$

where ψ_i stands for the i-th element in $\mathbf{\Psi}$. Thus according to the above we need to compute the first derivatives of $\mathbf{R}$ w.r.t each the element of $\mathbf{\Psi}$. Below, we provide the expressions obtained in the derivation process.

C.2.1 Derivatives

In order to compute the derivatives in (C.23), let us consider the summation-form of $\mathbf{R}$ given by (C.6)

$$\mathbf{R} = \sum_{i=1}^{Q}\sum_{j=1}^{Q} b_{ij}\mathbf{u}_i\mathbf{u}_j^H + \sigma_e^2\mathbf{I}$$

with $\mathbf{u}_i = \mathbf{a}(\theta_i) \otimes \mathbf{g}(\tau_i)$.

Derivatives w.r.t $\boldsymbol{\eta}$

Taking the first derivative of (C.6) w.r.t. the each element of $\boldsymbol{\eta}$ we obtain

$$\frac{\partial \mathbf{R}}{\partial \theta_l} = b_{l,l}\left(\frac{\partial \mathbf{a}(\theta_l)}{\partial \theta_l}\mathbf{a}^H(\theta_l) \otimes \mathbf{g}(\tau_l)\mathbf{g}^H(\tau_l) + \mathbf{a}(\theta_l)\frac{\partial \mathbf{a}^H(\theta_l)}{\partial \theta_l} \otimes \mathbf{g}(\tau_l)\mathbf{g}^H(\tau_l)\right) \tag{C.24}$$

$$\frac{\partial \mathbf{R}}{\partial \tau_l} = b_{l,l}\left(\mathbf{a}(\theta_l)\mathbf{a}^H(\theta_l) \otimes \frac{\partial \mathbf{g}(\tau_l)}{\partial \tau_l}\mathbf{g}^H(\tau_l) + \mathbf{a}(\theta_l)\mathbf{a}^H(\theta_l) \otimes \mathbf{g}(\tau_l)\frac{\partial \mathbf{g}(\tau_l)}{\partial \tau_l}\right) \tag{C.25}$$

Derivatives w.r.t $\mathbf{R_b}$

Taking the first derivative of (C.6) w.r.t. the elements in matrix $\mathbf{R_b}$ we get

$$\frac{\partial \mathbf{R}}{\partial b_{k,l}} = \mathbf{u}_k\mathbf{u}_l^H \tag{C.26}$$

Derivative w.r.t σ_e

Finally, the first derivative of (C.6) w.r.t. to σ_e gives

$$\frac{\partial \mathbf{R}}{\sigma_e} = 2\sigma_e \mathbf{I} \tag{C.27}$$

Appendix D

Asymptotical behavior of JADE-MUSIC estimator

In this appendix we are interested in finding an expression to compute the covariance matrix of the angle and delay estimators based on the JADE-MUSIC method.

D.1 JADE-MUSIC estimates

Given the channel estimates

$$\mathbf{Y} = [\mathbf{y}^{(1)} \cdots \mathbf{y}^{(S)}] = \mathbf{U}(\boldsymbol{\theta}, \boldsymbol{\tau})\mathbf{B} + \mathbf{V}$$

we look for the joint estimation of the angles $\boldsymbol{\theta} = [\theta_1 \dots \theta_Q]^T$ and times $\boldsymbol{\tau} = [\tau_1 \dots \tau_Q]^T$ of arrival of the multipath signals propagating in a multipath channel with Q propagating paths.

Using the MUSIC approach, $\hat{\boldsymbol{\theta}}$ and $\hat{\boldsymbol{\tau}}$ are given by the Q minima of the cost function

$$J(\boldsymbol{\eta}) = \mathbf{u}^H(\boldsymbol{\eta})\hat{\mathbf{\Pi}}\mathbf{u}(\boldsymbol{\eta}) \tag{D.1}$$

where $\boldsymbol{\eta} = [\theta \quad \tau]^T$, and $\hat{\mathbf{\Pi}}$ is the estimated orthogonal projector onto the noise subspace obtained from the eigen-decomposition of $\hat{\mathbf{R}}$.

3.2 JADE-MUSIC covariance matrix deduction

Let define

$$\begin{aligned} K^i(\boldsymbol{\eta}) &= \frac{\partial J(\boldsymbol{\eta})}{\partial \eta^i} \\ &= 2\Re\left\{\frac{\partial \mathbf{u}^H}{\partial \eta^i}\boldsymbol{\Pi}\mathbf{u}\right\} \end{aligned} \tag{3.2}$$

Now, lets take the first derivatives of (3.2) w.r.t η^j and $\mathbf{Pi}_{l,p}$, which gives

$$\frac{\partial K^i(\boldsymbol{\eta})}{\partial \eta^j} = 2\Re\left\{\frac{\partial \mathbf{u}^H}{\partial \eta^j \partial \eta^i}\boldsymbol{\Pi}\mathbf{u} + \frac{\partial \mathbf{u}^H}{\partial \eta^i}\boldsymbol{\Pi}\frac{\partial \mathbf{u}}{\partial \eta^j}\right\} \tag{3.3}$$

and

$$\frac{\partial K^i(\boldsymbol{\eta})}{\partial \boldsymbol{\Pi}_{lp}} = \frac{\partial \mathbf{u}_l^H}{\partial \eta^i}\mathbf{u}_p + \mathbf{u}_l^H\frac{\partial \mathbf{u}_p}{\partial \eta^i} \tag{3.4}$$

The exact differential of $K^i(\boldsymbol{\eta})$ is given by

$$dK^i(\boldsymbol{\eta}) = \sum_{j=1}^{2}\frac{\partial K^i(\boldsymbol{\eta})}{\partial \eta^j}d\eta^j + \sum_{l=1}^{MPL}\sum_{p=1}^{MPL}\frac{\partial K^i(\boldsymbol{\eta})}{\partial \boldsymbol{\Pi}_{lp}}d\boldsymbol{\Pi}_{lp} \tag{3.5}$$

Since we are interested in the Q minima of $J(\boldsymbol{\eta})$, we consider $K^i(\boldsymbol{\eta}) = 0$, which also implies $dK^i(\boldsymbol{\eta}) = 0$, and thus we can express the above equation as

$$d\eta^j = \sum_{i=1}^{2} C_{ji}^{(-1)} \sum_{l=1}^{MPL}\sum_{p=1}^{MPL}\frac{\partial K^i(\boldsymbol{\eta})}{\partial \boldsymbol{\Pi}_{lp}}d\boldsymbol{\Pi}_{lp} \tag{3.6}$$

where $C_{ji}^{(-1)}$ denotes the (j,i) element of the inverse matrix of

$$\mathbf{C}(\boldsymbol{\eta}) = \begin{bmatrix} \dfrac{\partial K^1}{\partial \eta^1} & \dfrac{\partial K^1}{\partial \eta^2} \\ \dfrac{\partial K^2}{\partial \eta^1} & \dfrac{\partial K^2}{\partial \eta^2} \end{bmatrix} \tag{3.7}$$

Therefore, exploiting (3.6), it can be show that the elements of the covariance matrix of $\boldsymbol{\eta}$ is given by

$$\operatorname{cov}(\eta^u, \eta^v) = \frac{1}{S}\mathbb{E}\left\{d\eta^u d\eta^u\right\} \tag{3.8}$$

Substitution of (3.6) into the above gives

$$\operatorname{cov}(\eta^u, \eta^v) = \frac{1}{S}\sum_{j=1}^{2}\sum_{j'=1}^{2} C_{uj}^{(-1)} C_{vj'}^{(-1)} \sum_{l=1}^{MPL}\sum_{p=1}^{MPL}\sum_{l'=1}^{MPL}\sum_{p'=1}^{MPL} \frac{\partial K^j(\boldsymbol{\eta})}{\partial \boldsymbol{\Pi}_{lp}} \frac{\partial K^{j'}(\boldsymbol{\eta})}{\partial \boldsymbol{\Pi}_{l'p'}} \operatorname{cov}(\boldsymbol{\Pi}_{lp}, \boldsymbol{\Pi}_{l'p'})$$

where $\operatorname{cov}(\boldsymbol{\Pi}_{lp}, \boldsymbol{\Pi}_{l'p'})$ is given by (3.14), deducted in the following section.

3.2.1 $\operatorname{cov}(\boldsymbol{\Pi}_{lp}, \boldsymbol{\Pi}_{l'p'})$ deduction

Given the projector's definition

$$\boldsymbol{\Pi} = \frac{1}{2j\pi}\int_{\gamma} (\lambda \mathbf{I} - \mathbf{R})^{-1} d\lambda \tag{3.9}$$

where γ is a contour containing the eigenvalues associated to $\boldsymbol{\Pi}$. It is straight forward to show that

$$\delta\boldsymbol{\Pi} = -(\boldsymbol{\Pi}\delta\mathbf{R}\mathbf{R}\mathbf{s}^{\dagger} + \mathbf{R}\mathbf{s}^{\dagger}\delta\mathbf{R}\boldsymbol{\Pi}) \tag{3.10}$$

from which we can express

$$\delta\boldsymbol{\Pi}_{ij} = -\left(\sum_{m}^{MPL}\sum_{n}^{MPL} \boldsymbol{\Pi}_{im}\delta\mathbf{R}_{mn}\mathbf{R}\mathbf{s}^{\dagger}_{nj} + \sum_{m'}^{MPL}\sum_{n'}^{MPL} \mathbf{R}\mathbf{s}^{\dagger}_{im'}\delta\mathbf{R}_{m'n'}\boldsymbol{\Pi}_{n'j}\right) \tag{3.11}$$

where

$$\delta\mathbf{R}_{ij} = \hat{\mathbf{R}}_{ij} - \mathbf{R}_{ij} \tag{3.12}$$

with

$$\mathbb{E}\left\{\delta\mathbf{R}_{ij}\delta\mathbf{R}_{kl}\right\} = \mathbf{R}_{il}\mathbf{R}_{kj} \tag{3.13}$$

Now, we want to compute

$$\operatorname{cov}(\boldsymbol{\Pi}_{ij}, \boldsymbol{\Pi}_{kl}) = \mathbb{E}\left\{\delta\boldsymbol{\Pi}_{ij}\delta\boldsymbol{\Pi}_{kl}\right\}$$

Hence, substituting (3.11) in to the above expression and taking into account (3.13) it is straightforward to show that

$$\operatorname{cov}(\boldsymbol{\Pi}_{ij}, \boldsymbol{\Pi}_{kl}) = (\boldsymbol{\Pi}\mathbf{R}\boldsymbol{\Pi})_{il}(\mathbf{R}\mathbf{s}^{\dagger}\mathbf{R}\mathbf{R}\mathbf{s}^{\dagger})_{kj} + (\mathbf{R}\mathbf{s}^{\dagger}\mathbf{R}\mathbf{R}\mathbf{s}^{\dagger})_{il}(\boldsymbol{\Pi}\mathbf{R}\boldsymbol{\Pi})_{kj} \tag{3.14}$$

Part II

Terrain-aided target tracking

Introduction to part II

Over the past four decades, target tracking has developed into a fairly mature technology with applications in diverse areas such as air traffic control, air and missile defense, avionics, ocean surveillance, port monitoring, etc. [23]. In this standard tracking problems, the only inputs available to the tracker are sensor measurements obtained from one or more sensors. In certain applications, however, there may be some additional prior information available, which could be exploited in the Bayesian estimation framework. For instance, we may have some knowledge of the environment in which the target is being tracked or some limitations in the dynamic motion of the target (such speed or acceleration constraints). In the context of ground-moving target tracking, one may have some prior information of the terrain and road maps over which ground targets evolve. Some interesting examples we can find in the literature are ground target surveillance for military purposes using the ground moving target indicator (GMTI) radar employed in the Gulf War in 1991 [10, 42, 44, 61]. Another example is given in the context of airport surface traffic management, where the objective is to ensure safe, orderly, and expeditious movement of aircraft and support vehicles (buses, cars) along the airport runway network [30, 39]. The ultimate objective in such applications was to exploit prior non-standard terrain information such as speed constraints, road networks, and so forth, in the tracker to produce better (sequential) estimates of the target state.

It turns out, however, that incorporating such nonstandard information within the conventional Kalman filtering framework is not an easy task. The reason is that in general, non standard information leads to highly non-Gaussian posterior densities that are difficult to represent accurately using conventional techniques. However, the use of particle filters represent a more suited approach since particle filtering methods have no restrictions on the type of models, including the noise distributions used. This thesis part is primarily devoted to such applications using passive measurements of the target emissions. The passive tracking problem is encountered whenever one is attempting to locate an emitting target by observing only the direction

from which the emission arrives. The name comes from the fact that this information can be obtained passively, without active emission on the sensor's part. This is clearly an advantage in a military applications, since the observer need not advertise its position. The major challenges with this approach are 1) that such observations rarely include any distance information, and 2) the observations depend nonlinearly on the target location.

Prior work

This thesis part focusses on the passive tracking of ground moving targets constrained to roads. The recursive estimation of the target state vector is performed within the Bayesian framework via particle filters. The objective of this thesis part is to propose robust algorithms able to exploit road map information to yield accurate target state estimates. A brief survey of other work that has been done in the area of ground target tracking using road map information is in order.

There has been significant work on incorporating road map information into the tracking filters, see [10, 30, 32, 37, 39, 44, 61, 77] as examples and the references there in. According to the method used to exploit road map information, these contributions fall into three main categories:

Road projection methods [32]: employing this methodology, road map information is used to "correct" measurements and/or target state estimations by projecting them onto the road network space. The main drawback is that a systematic projection of measurements and/or state estimates on wrong roads leads to a target loss.

Constraining the target state dynamics [10, 30, 39, 44]: Road map information is directly incorporated into the target dynamics via mathematical equations obtained from the modeled constraints imposed by the roads, i.e. if the road is modeled as a straight line segment, the position of the target may be contained in the line and its velocity vector should be in the road direction. The use of this method, to exploit road map information, closely models the true target motion on roads, and the resulting target state estimates are, in general, more accurate. However, special attention must be payed in order to properly handle target transitions among roads, i.e., when the target approaches a junction.

The pseudo-measurement [37, 77]: The influence of roads is incorporated as a pseudo-measurement each time the filter is measurement

updated. This is an effective but usually criticized solution since it results in an unrealistic coupling between purely motion constraints and measurement process.

Most of the contributions cited above have been tested in the context of active ground moving target tracking using GMTI radar, which provides measurements of bearing, range and range rate. This facilitates the use of state spaces that employ spatial parameters that are naturally linked with the road constraints. However, it is harder to incorporate the road information into a bearings-only tracker, since the spatial position constraints are not immediately translated into regular bearing constraints.

Overview of this part

This work addresses the passive tracking of ground targets moving on constrained paths using bearings-only measurements in clutter. Constrained paths consist in a realistic road network considered to be available to the tracker via digital maps. Therefore, we focus on methods to exploit this prior information to yield accurate target state estimates. Because the incorporation of these constraints lead to highly non-Gaussian posterior densities we adopt a particle filter approach to recursively estimate the target state vector. Some major assumptions we make are:

1. The number of targets to be tracked is fixed and known.
2. Each target can generate at most one measurement per sensor at a particular time step, but may go undetected.
3. Additional clutter measurements may result due to multipath effects, spurious objects, sensor errors, etc.

The remainder of this thesis part is organized as follows: In chapter 4 we present the problem of terrain-aided target tracking and we provide the most used methods to exploit road network information. We also introduce the concept of data association problem and we recall the theory of particle filters. Based on this study, chapter 5 proposes a combination of the classical methods to exploit road map information to yield better state estimates in the classical problem of bearings-only tracking. Chapter 6 presents a new method to incorporate road network information accounting for road direction and traffic flow information. The method is tested under a challenging multiple-observer multiple-target tracking scenario. Proposed approaches are tested under realistic simulation scenarios.

Some of the work presented in this thesis part has been published during the course of this research. The application presented in chapter 5 appears in [21] and [19].

Contributions

This thesis part consist of methods to exploit road map information, algorithms developing for a single and multiple target tracking, and computer simulations. Its main contributions to the field of ground moving target tracking are:

1. Two methods for exploiting road map information.
2. A batch-recursive algorithm to track a ground moving target constrained to roads using bearings-only measurements in clutter.
3. An algorithm to track multiple targets moving along a road network using bearings-only measurements performed by multiple observers.

Chapter 4

Terrain aided tracking

This chapter aims to provide a background of the different types of terrain information and the different techniques proposed in open literature to include such a valuable source of information in the context of ground target tracking. It also present some important issues concerning the data association problem for multiple target tracking. The concepts we review here will be extensively used in chapters 5 and 6.

This chapter is organized as follows: section 4.1 presents two types of digital maps commonly used in the context of ground target tracking. In section 4.2 we describe the problem of ground target tracking exploiting nonstandard information. The most used methods to include road network information are presented in section 4.3. Section 4.4 presents further issues on ground target tracking and the data association problem for multiple target tracking. In section 4.5 we provide a tutorial on particle filters, and finally section 4.6 we provide the conclusions.

4.1 Digital maps

There is a growing interest in ground target tracking, stimulated in large part by the success of the joint surveillance target attack radar system (JSTARS) [23, 42] and similar ground moving target indicator (GMTI) radar systems. Great efforts have been made in order to conceive accurate ground target tracking algorithms. However, ground target tracking is a more challenging problem than tracking other types of targets, such as air targets. This is because of the possibility to concentrate many targets in a reduced area and make them possible to move close to each other, which represents a heavy traffic density. Moreover, the terrain in which the targets evolve may have obstacles and obscuration zones producing a decrease in the target

	Air targets	Ground targets
Environment	3D	2D or 1D
Dynamics	Less mobile, it cannot stop	Highly mobile, it may stop
Density	Low	High
Detection probability	High	Low due to terrain obscuration
Clutter	Low	High

Table 4.1: Ground versus Air target tracking: a qualitative comparison.

detection probability and an increase in the number of false measurements. Besides, ground targets are able to perform sudden menoeuvers which requires complicated dynamic models to properly track them, see table 4.1 for a qualitative comparison between ground and air target tracking.

In contrast, since ground targets move over the earth's surface they can be considered to move in a two dimensional space. Furthermore, for targets moving on roads, the space becomes one dimensional on a road segment until it reaches an intersection, when it moves to other road segments. The region where the vehicles can move may be further constrained, i.e., rough terrain may limit accessibility. On the other hand, the actual target dynamics depend on the local condition, i.e., slope, terrain type, type of road, etc. These constraints, when available, constitute a valuable information source that can be exploited to improve tracking performance. The most common form to get terrain information is by means of digital maps. The most used digital maps for terrain-aided target tracking are: Hospitability maps [41,78] and road maps. A description of each of which is in order.

4.1.1 Hospitability maps

Since the earth's surface is rarely unvarying in a given area of large enough dimensions, it is quite logical to assume that different terrain types in the area may influence where and how the target moves given its current location. This motivates introducing the concept of the hospitability map (HMap) to constrain the area of interest into regions of higher/lower hospitability for a given class of targets. Hence, the HMap is a map providing a likelihood or a "weight" for each point on the earth's surface proportional to the ability of a target to move and maneuver at that location [41, 78]. The following factors are considered while deriving the hospitability value: slope, surface roughness, transportation, geology, landform, soil, vegetation, hydrology, urban areas, and climate. Additionally, the HMap is a function of the nature

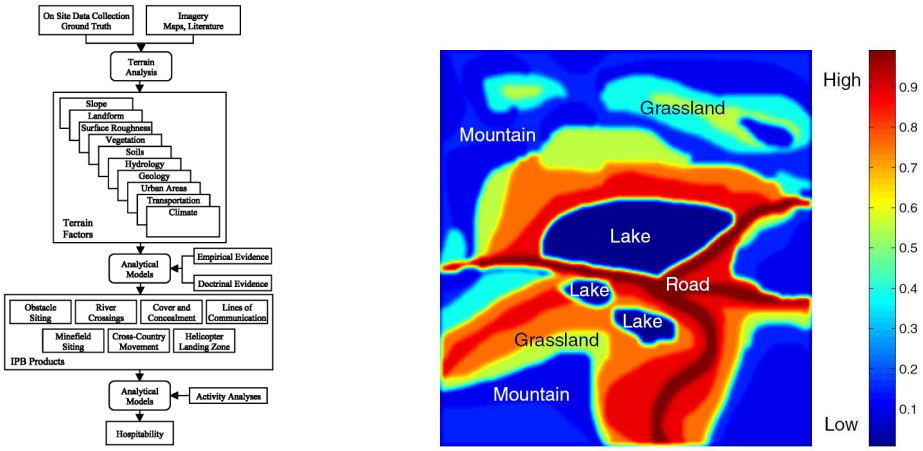

a) b)

Figure 4.1: Hospitability maps: a) Data flow in classic terrain analysis procedure and b) and example of a Hmap.

of the target itself, i.e. there exists different models for deriving the HMap for different classes of targets (eg. cars, tanks, amphibious vehicles, etc.). Figure 4.1 side a) details the data flow for terrain analysis and side b) depicts a generic HMap, where the HMap values has been normalized to lie in the interval $[0, 1]$, with 1 being the highest hospitability index.

4.1.2 Road maps

Road maps gathers information concerning the road network over which ground targets can move. Road networks are commonly modeled as a directed graph [44, 60, 67, 92]. This is, each junction and road-segment end corresponds to a node or vertex of the graph and each connecting road-segment is an edge or arc of the graph. In its simplest representation, road maps are composed of a large collection of roads, each of which consists of a number of interconnected road-segments (edges), where each road-segment is assumed to be a straight line between two referenced points (nodes). In addition, road maps may also contain some road attributes such as [77]:

1. Speed limit.
2. Size of the road.
3. Whether the road is one way or not.

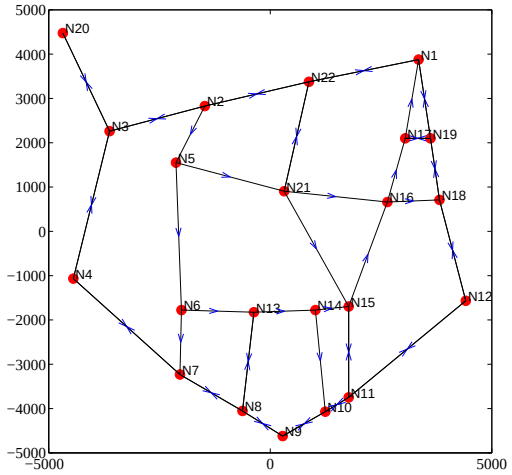

Figure 4.2: Road network example: dots represent the nodes, lines between two nodes are the roads and arrows indicate the direction of the roads.

4. Accuracy of the coordinates, etc.

An example of a road network in a typical urban area is shown in figure 4.2. As it can be inferred, the only information to be stoked in a digital road map is the position coordinates of the nodes, the relationships between them, i.e. whether two nodes are connected or not, and possibly road attributes.

4.1.3 Hospitability versus road maps for ground target tracking

In general, hospitability maps give a more complete description of the terrain constraints than road maps. This is because the information contained in hospitability maps is not only limited to roads, as the road network maps, but also it describes target motion in open fields for that specific ground target type. Unfortunately, their primary use is for military applications, which makes them less accessible. Furthermore, to emulate realistic Hmaps is not a simple task because of their complicated process of construction, see figure 4.1 side a). In contrast, road maps are pretty accessible, since they have a great variety of commercial applications, i.e. the use of a geographical information system (GIS) providing road map information for vehicle navigation. Moreover, emulating realistic road networks is not complicated, since they only consist in a large collection of roads with specific attributes. On the other hand, when tracking ground moving targets constrained to roads

(which is the application we are interested in) road maps provide harder constraints than Hmaps, which can be immediately incorporated into the target dynamics. For these reasons, the algorithms we propose in this thesis part use road maps.

4.2 Problem description and basic formulation

Some of the methods, proposed in open literature, to incorporate road map information into the tracker system, apply to the unconstrained target tracking problem. In order to review such methods, this section describes and provides the basic formulation of the unconstrained single-observer single-target tracking problem. Then, based of this formulation we outline the problem of terrain aided-tracking.

4.2.1 Unconstrained target tracking problem

State space

Consider the problem of tracking a target in the $x-y$ plane. This is, for instance, to estimate its position and velocity for each time step using line-of-sight measurements of the signals emanating from it and measured by an observer. To do so, let define the target state at time k in cartesian coordinates as follows:

$$\mathbf{x}_k^C = \begin{bmatrix} x_k & y_k & \dot{x}_k & \dot{y}_k \end{bmatrix}^T, \tag{4.1}$$

where (x_k, y_k) and $(\dot{x}_k, \dot{y}_k)$ stand respectively for the position and velocity components of the target state vector.

Dynamic model

It is supposed that a priori information about the target dynamics is available, i.e. it has linear motion in the $x-y$ coordinate system and the evolution of the true target state $\mathbf{x}_k^C$ is given by the following discrete-time stochastic model:

$$\mathbf{x}_k^C = F\mathbf{x}_{k-1}^C + G\epsilon_{k-1}, \tag{4.2}$$

where

$$F = \begin{bmatrix} 1 & 0 & T & 0 \\ 0 & 1 & 0 & T \\ 0 & 0 & 1 & 0 \\ 0 & 0 & 0 & 1 \end{bmatrix} \quad \text{and} \quad G = \begin{bmatrix} T^2/2 & 0 \\ 0 & T^2/2 \\ T & 0 \\ 0 & T \end{bmatrix} \tag{4.3}$$

Here T is the sampling time, ϵ_k is the white Gaussian process noise sequence modeling unpredictable target accelerations in x and y directions with covariance matrix $\mathbf{Q}_{xy} = \text{diag}(\sigma_x^2, \sigma_y^2)$, where σ_x^2 and σ_y^2 stand, respectively, for the noise variances in x and y directions.

It is possible, of course, to consider other kind of target behavior, for which an specific state evolution model will be given. Reference [66] provides a complete list of target evolution models. However, for the applications will face in this thesis part, a linear model may suffice, since most of the time ground targets traveling on road maintain a constant velocity [95].

Measurement model

Suppose that measurements $\mathbf{y}_k \in \mathbb{R}^{n_\mathbf{y}}$, performed by the observer, are available at time k, where $n_\mathbf{y}$ is the dimension of the measurement. The measurements are related to the target state via the measurement equation:

$$\mathbf{y}_k = \mathbf{h}_k(\mathbf{x}_k^C) + \mathbf{w}_k \tag{4.4}$$

where $\mathbf{h}_k$ is a known, possibly non linear function and $\mathbf{w}_k$ is a measurement noise sequence. The nature of the measurements and, thus, the expression of $\mathbf{h}_k$ depends on the type of sensors used to measure the signals arriving at the observer. Most common measurements for target tracking are: range and/or azimuth (bearing), time of arrival difference between two sensors, frequency of narrow-band signal emitted by the target, observed frequency difference between two sensors, signal strength, etc. [9].

4.2.2 Description of road map-aided tracking problem

Under the assumption that ground targets evolve in road networks, road map-aided tracking problem can be summarized as follows: given the noisy sensor measurements (4.4) and given the (nonstandard) road maps (described in section 4.1), the objective is to estimate sequentially the target state vector (E.1), given a priori information about the target dynamics (E.4). The key feature of this tracking problem is to exploit the nonstandard information to yield an enhanced tracker performance.

It turns out, however, that incorporating such nonstandard information leads to highly non-Gaussian posterior densities that are difficult to represent accurately using the conventional techniques [65], such as Kalman filters. Since particle filtering methods have no restrictions on the type of models, including the noise distributions used, we adopt such methods to recursively estimate the target state under road constraints. A survey on particle filters

is given in section 4.5. The next section presents methods to exploit road map information.

4.3 Methods to include road map information

In this section we present the most used methods, that we have identified in our research work, to incorporate road network information into the problem of ground target tracking. The methods are classified into three main categories, according to the stage at which the road map information is exploited, i.e., if it is used as a merely map matching procedure for existing unconstrained algorithms, if it is introduced in the target dynamics, or if it is exploited at the measurement update.

4.3.1 Projection methods

This kind of methods rely on the following assumption: since targets move along roads, then the measurements and state estimates must belong to roads too. Therefore, in order to correct non-on-road measurements and/or state estimates a projection version of these estimates is computed onto the road segment on which the target is supposed to travel. Since projection methods only attempt to correct estimates, they can be applied to conventional target tracking algorithms (i.e. those ones which do not incorporate road priors). In the following we explain the state estimate projection method, however, measurement projection method can be achieved similarly. Thus, correcting the state estimate $\hat{\mathbf{x}}_k$ can be performed according to two different approaches [32]:

1. *Deterministic approach*: the estimate state $\hat{\mathbf{x}}_k$ is orthogonally projected on a given road segment s, which is supposed to be the road segment in which the target evolves. The resulting corrected state estimate, $\hat{\mathbf{x}}_k^p$, whose position is constrained on the segment s, and whose velocity is in the direction of s, is the solution of the following equation

$$\hat{\mathbf{x}}_k^p = \arg\min_{\mathbf{x}\in s} \|\hat{\mathbf{x}}_k - \mathbf{x}\|_2.$$

2. *Probabilistic approach*: the unconstrained filtered target state $\hat{\mathbf{x}}_k$ is the mean value of the posterior state distribution $p(\mathbf{x}_k|\mathbf{y}_{1:k})$. The constrained $\hat{\mathbf{x}}_k^{pp}$, resulting from the probabilistic projection, maximizes the

probability distribution $p(\mathbf{x}_k|\mathbf{y}_{1:k})$, while also satisfying the road constraints. This is given by the minimization of the Mahalanobis distance

$$\hat{\mathbf{x}}_k^{pp} = \arg\min_{\mathbf{x}\in s} \|\mathbf{x} - \hat{\mathbf{x}}_k\|^2_{\mathrm{P}_k^{-1}}.$$

where P_k^{-1} is the covariance matrix of the unconstrained state estimate.

In both cases the corrected version of the unconstrained covariance matrix, can be achieved by computing their projected version onto the road segment s. This is not presented here, however, interested readers are referred to [32] in order to have their expressions.

Compared to the projection of the measurement, the state projection method uses the additional velocity constraint [32]. Thus, the resulting algorithms comply with the assumption that the target's velocity estimate is in the road direction, and that its position estimate belongs to the same road segment s. Unfortunately, projection methods do not model the physical reality of ground target motion and can lead to track loss by erroneous projections [32].

4.3.2 Incorporating road map information into the dynamic model

This sort of methods attempt to model the physical reality of targets evolving on roads by bringing the road constraints into the target state dynamics. Resulting algorithms using this approach are, in general, more accurate and robust.

Directional process noise

This approach models target motion along a road segment by tuning the process noise's covariance matrix, i.e. the covariance matrix of ϵ_{k-1} in equation (E.4), according to the road segment on which the target is supposed to travel [44]. The standard motion models assume that the target can move in any direction and, therefore, use equal process noise variances in both the x and y directions (i.e. $\sigma_x^2 = \sigma_y^2$). This means that for off-road targets the motion uncertainties in both directions are equal. For on-road targets, the road constraint means more uncertainty along the road than orthogonal to it [44, 65].

The variances of the process noise components along σ_a^2 and orthogonal σ_o^2 to the road in the on-road motion models verify $\sigma_a^2 >> \sigma_o^2$. Therefore, if we define α_s as the direction of the road along which the motion model is

matched, i.e. the road in which the target travels, then the covariance matrix corresponding to on-road motion is given by

$$\mathbf{Q}_s = \mathbf{R}_{\alpha_s} \begin{bmatrix} \sigma_o^2 & 0 \\ 0 & \sigma_a^2 \end{bmatrix} \mathbf{R}_{\alpha_s}$$

where

$$\mathbf{R}_{\alpha_s} = \begin{bmatrix} -\cos\alpha_s & \sin\alpha_s \\ \sin\alpha_s & \cos\alpha_s \end{bmatrix} \tag{4.5}$$

is the (anti-clockwise) rotation matrix.

The directional process noise, even when it brings the road network information into the target dynamics, it does not provide a mechanism to incorporate hard constraints on position and speed. Because of this, using the directional process noise as the single means to exploit road network information in terrain aided tracking systems, will only result in a modest improvement in accuracy over methods that do not use such nonstandard information [65].

Constraining the target dynamics: 1D approach

Since the movement of targets along roads is approximatively in one-dimension (1D), it is possible to model the target dynamics in 1D. Typically, this 1D modeling implies a target state vector composed by the position of the target, given in terms of its distance d_k from a reference point, which may be the starting point of the road segment s, in which it is supposed to travel, and its speed v_k. This is

$$\mathbf{x}_{s,k} = \begin{bmatrix} d_k & v_k \end{bmatrix}^T.$$

Using this approach the target dynamics simplify considerably, i.e., for a constant velocity target, the dynamic model may be given by

$$\mathbf{x}_{s,k} = H\mathbf{x}_{s,k-1} + \epsilon_{k-1},$$

where H is the transition matrix given by

$$H = \begin{bmatrix} 1 & T \\ 0 & 1 \end{bmatrix}$$

and ϵ_{k-1} stands for the target motion uncertainties. Special care on the modeling of ϵ_{k-1} must be payed, specially, when the target approaches a road intersection, which may conduce to a non-Gaussian noise models. This issue is treated in chapter 6.

A key merit of this 1D modeling is that it relates a tracking filter more closely to the physical reality. In addition, this modeling also provides a means to explicitly incorporate road information into the tracking filters. The only drawback is that the 1D model renders the measurement equations highly nonlinear [95].

Constraining the target dynamics: 2D approach

Taking advantage of the road network representation, i.e. straight line segments and junction points, this approach constraints the motion of the target to the linear segment in which it is supposed to travel using two-dimensional (2D) mathematical relationships [10, 60]. For instance, for a target moving along a road segment s the components of its state vector may have the following constraints

$$ax_k + by_k = c \tag{4.6}$$

$$\vec{v}_k \cdot \vec{n}_s = 0 \tag{4.7}$$

where the coefficients a, b and c are the parameters of the straight line equation associated to the road segment s, $\vec{v}_k = \begin{bmatrix} \dot{x}_k & \dot{y}_k \end{bmatrix}^T$ is the target velocity vector and $\vec{n}_s$ is an orthogonal vector to the segment s. Notice that equation (4.6) constraints the position of the target to the road segment s and that equation (4.7) assures that its velocity vector is in the direction of s.

Under such constraints the state dynamics may then be written as follows:

$$\mathbf{x}_k = \mathbf{f}_{s,k}(\mathbf{x}_{k-1}) + G\epsilon_{s,k-1}, \tag{4.8}$$

where $\mathbf{f}_{s,k}(\cdot)$ is a vector function accounting for the constraints on the target dynamics, i.e. accounting for (4.6) and/or (4.7), and where $\epsilon_{s,k-1}$ is a white Gaussian process noise with covariance matrix $\mathbf{Q}_s$, which may be constructed using the directional process noise presented above.

At this point, it is fair to ask: why we should use the 2D method to exploit road network information, if the 1D method (i.e. that one presented above) seems to be more suitable for constrained target motion? The answer is because algorithms based on the 2D method can be easily extended to the case in which targets can come off out of the road at any given time. This also applies to cases when the road map is suspected to be incomplete. In such situations, a 2D modeling of the target dynamics may benefit of the road map information without constraining the state estimates to be always on-road. This fact, together with a mechanism indicating whether the target motion is on-road or not permits to take into account the two types of target motion. In contrast, a 1D modeling of the target dynamics produces state

estimates belonging to the road network only, which makes difficult to detect whether a target has evolved to an off-road situation or not.

4.3.3 Road information as a pseudo-measurement

An alternative approach to incorporate road network information is through the use of pseudo-measurements [22] or fictitious measurements [37,77], which represent "synthetic" measurements usually created to constraint the target dynamics to the road network. Consider, for instance, the constraint on the target velocity vector, given by (4.7), but this time written as

$$\phi_k = \vec{v}_{s,k} \cdot \vec{n}_s + w_k \tag{4.9}$$

where w_k is an error term accounting for road width, uncertainty in the position, and digitalization error in the database. Under the assumption that the road segment s is a straight line, ϕ_k may be seen as a measurement of the target heading. This contrast with the method given in the previous section in that the velocity constraint is not included in the target dynamics, but is treated as an additional measurement.

Another example is given by the constraint of the target position to the road network. Consider that the target dynamic model yields state vectors $\mathbf{x}_k$ not belonging to the road network, i.e. road constraints are not directly introduced into the state dynamics. In such a situation a measurement of how far the target state is with respect to the road segment s, in which the target is supposed to travel, may be given by the minimum Euclidian distance from the target state to the road segment s [37, 77],

$$z_k = h(\mathbf{x}_k, s) + e_k \tag{4.10}$$

where $h()$ is the nonlinear function providing such a distance and e_k is the measurement noise assumed to be zero-mean white and Gaussian. Assuming that z_k always equals zero (according to the on-road condition) the target position is constrained about the actual position of the target in the road segment s.

The pseudo-measurement methods are often criticized because they are somewhat unsatisfactory from a theoretical standpoint since the road information is only incorporated at the measurement update. Which results in an unrealistic coupling between purely kinematic constraints and the measurement process. However, this methods have proved to be effective practical solutions in several tracking applications [37].

4.4 Further issues on ground target tracking

Due to the challenging environment in which ground targets evolve, sensor measurements not only consist of LOS measurements between the target(s) and sensor(s), but also measurements corresponding to extraneous sources, such as potential false alarms produced by noise and clutter. The term clutter refers to detections or "returns" from nearby objects, weather, electromagnetic interference, acoustic anomalies, etc., that are generally random in number, location, and intensity. Whatever their origin, this kind of undesired detections must be discriminated in order to produce accurate algorithms for ground target tracking.

"Gating" is a procedure to select the measurements to be incorporated into the state estimator from among several candidates[1]. This procedure consists in creating a validation region or gate for a target that is in track, i.e. its filter has at least been initialized. The gate is centered at the predicted measurement vector $\hat{\mathbf{y}}$, and the size of the gate depends on its associated covariance matrix $\Sigma_{\mathbf{y}}$, as well as the value of the probability mass to be included in the validation gate. Then, measurements that lie inside the gate are considered valid; those outside are discarded.

The crux problem is to associate each validated measurement with the appropriate target or to discard it as arising from clutter. This is known as *data association*.

4.4.1 A single target in clutter

Because of clutter, there may be (possibly) several measurements in the validation region (gate) of a single target. This set of validated measurements consist of:

- The correct measurement (if it has been detected and it fell in the gate).
- Incorrect measurements (originated from clutter).

It is assumed that the components of the measurement vector include all of the variables that could help discard undesirable measurements. Therefore, when all the available information has been used, any measurement that has been validated could have originated from the target of interest. The implication of the single-target assumption is that the undesirable measurements constitute random interference. A common mathematical model for such interference is a uniform distribution in the measurement space.

[1] A more formal explanation of the gating procedure is presented in chapter 6.

This situation is depicted in figure 4.3 where the (two-dimensional) validation region is an ellipse centered at the predicted measurement $\hat{\mathbf{y}}$. The size an shape of the ellipse are determined by the covariance matrix of the innovation $\Sigma_{\mathbf{y}}$. All the measurements in the validation region are "not too unlikely" to have originated from the target of interest, even though only one is assumed to be the true one.

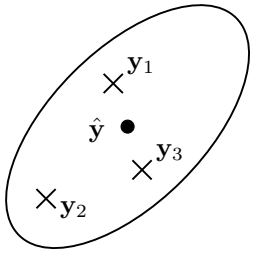

Figure 4.3: Measurements in the validation region of a target.

4.4.2 Multiple targets in clutter

The underlying assumption associated with clutter is that the false measurements are randomly distributed in space, time, and intensity; the technique presented in chapter 5 may fail when there is "persistent" or time-correlated interference. The most common source of persistent interference, of course, is the presence of another targets or extraneous objects.

Tracking several targets in the same vicinity, as well as dealing with clutter or false alarms, is significantly more complicated than the single-target-in-clutter case. For instance, consider the simplified scenario depicted in figure 4.4: the measurement $\mathbf{y}_1$ could have originated from target 1 or clutter, $\mathbf{y}_2$ from either 1 or 2 or clutter, and $\mathbf{y}_3$ and $\mathbf{y}_4$ from either 2 or clutter. Furthermore, if $\mathbf{y}_2$ originate from 2 then it is quite likely that $\mathbf{y}_1$ originated from 1. This illustrates the interdependence of measurement association when "persistent" (a neighboring target) is present in addition to the "random interference" (clutter).

The above discussion assumes that a measurement could have originated from either target 1, or target 2, or clutter. However, in view of the fact that any signal processing system has an inherent resolution threshold, an additional possibility should be considered: measurement $\mathbf{y}_2$ could be the result of the "merging" of the measurements from the two targets. This constitutes a fourth origin hypothesis for a measurement that lies in the intersection of two validation regions. This possibility, is not considered in

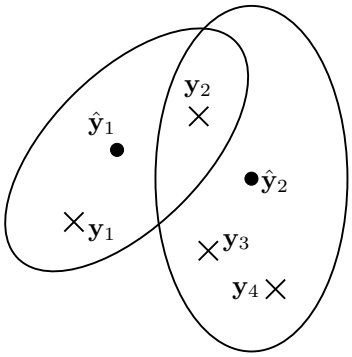

Figure 4.4: Two targets in the vicinity with a common measurement.

this document, however, the reader is referred to [47, 73] for some methods dialing with such a situation.

4.5 Bayesian estimation

As explained in section 4.2.2 the algorithms for ground target tracking presented in this dissertation part are based on particle filters. This section describes the fundamentals of filtering and how the filtering problem could be solved using a Bayesian approach. As will be shown, the implementation of Bayesian estimation needs to be based on some form of numerical approximation and this will end up in the use of Sequential Monte Carlo methods, also known as particle filters.

4.5.1 Recursive Bayesian estimation

Consider the following generic nonlinear dynamic system described in state-space form:

- system model

$$\mathbf{x}_k = f(\mathbf{x}_{k-1}, \mathbf{v}_{k-1}) \leftrightarrow \overbrace{p(\mathbf{x}_k|\mathbf{x}_{k-1})}^{\text{Transition density}} \tag{4.11}$$

- measurement model

$$\mathbf{y}_k = h(\mathbf{x}_k, \mathbf{w}_k) \leftrightarrow \overbrace{p(\mathbf{y}_k|\mathbf{x}_k)}^{\text{Observation density}} \tag{4.12}$$

where the hidden states $\mathbf{x}_k$ and data $\mathbf{y}_k$ are assumed to be generated by non-linear functions $f(\cdot)$ and $h(\cdot)$, respectively, of the state and noise disturbances $\mathbf{v}_{k-1}$ and $\mathbf{w}_k$. The precise form of the functions and the assumed probability distributions of the state $\mathbf{v}_{k-1}$ and the observation $\mathbf{w}_k$ noises imply via a change of variables the transition probability density function $p(\mathbf{x}_k|\mathbf{x}_{k-1})$ and the observation probability density function $p(\mathbf{y}_k|\mathbf{x}_k)$. We make the assumption that $\mathbf{x}_k$ is Markovian, i.e., its conditional probability density given the past states $\mathbf{x}_{0:k-1} = \{\mathbf{x}_0, \ldots, \mathbf{x}_{k-1}\}$ depends only on $\mathbf{x}_{k-1}$ through the transition density $p(\mathbf{x}_k|\mathbf{x}_{k-1})$, and that the conditional probability density of $\mathbf{y}_k$ given the states $\mathbf{x}_{0:k}$ and the past observations $\mathbf{y}_{0:k-1}$, where $\mathbf{y}_0$ is the set of no measurements, depends only upon $\mathbf{x}_k$ through the conditional likelihood $p(\mathbf{y}_k|\mathbf{x}_k)$.

According to [65] the *filtering problem* is to determine estimates of $\mathbf{x}_k$ based on the sequence of all available measurements $\mathbf{y}_{1:k}$ up to time k. From a Bayesian perspective, the problem is to recursively quantify some degree of belief in the state $\mathbf{x}_k$ at time k, taking different values, given the data $\mathbf{y}_{1:k}$ up to time k. This involves computing the *posterior distribution* of the state $\mathbf{x}_k$ conditioned on a batch of observations, $\mathbf{y}_{1:k}$, which we denote $p(\mathbf{x}_k|\mathbf{y}_{1:k})$. The posterior distribution may be obtained, recursively, in two stages: prediction and update [7, 65].

The prediction stage may be written as

$$p(\mathbf{x}_k|\mathbf{y}_{0:k-1}) = \int_{\mathbb{R}^{n_\mathbf{x}}} p(\mathbf{x}_k|\mathbf{x}_{k-1}) p(\mathbf{x}_{k-1}|\mathbf{y}_{0:k-1}) d\mathbf{x}_{k-1} \tag{4.13}$$

and the update stage as

$$p(\mathbf{x}_k|\mathbf{y}_{0:k}) = c_k^{-1} p(\mathbf{y}_k|\mathbf{x}_k) p(\mathbf{x}_k|\mathbf{y}_{0:k-1}) \tag{4.14}$$

where

$$c_k = \int_{\mathbb{R}^{n_\mathbf{x}}} p(\mathbf{y}_k|\mathbf{x}_k) p(\mathbf{x}_k|\mathbf{y}_{0:k-1}) d\mathbf{x}_k \tag{4.15}$$

The recursion has to be initialized with $p(\mathbf{x}_0|\mathbf{y}_{-1}) = p(\mathbf{x}_0)$, where $p(\mathbf{x}_0)$ is some representation of prior knowledge, for instance a uniform distribution.

Theoretically, knowing the posterior distribution an estimate of the state vector at time k can be obtained according to [65] as

$$\hat{\mathbf{x}}_k = \mathbb{E}\{\mathbf{x}_k|\mathbf{y}_{0:k}\} \tag{4.16}$$

and an estimate of its posterior covariance as

$$\mathrm{P}_k = \mathbb{E}\{(\mathbf{x}_k - \hat{\mathbf{x}}_k)(\mathbf{x}_k - \hat{\mathbf{x}}_k)^T|\mathbf{y}_{0:k}\} \tag{4.17}$$

Implementation

Despite the apparent simplicity of the recursive solution, given by (4.13) and (4.14), the posterior distribution can be computed in closed form only in very specific cases, principally; the linear Gaussian model (where the functions $f()$ and $h()$ are linear and $\mathbf{v}_k$ and $\mathbf{w}_k$ are Gaussian), for which an optimal solution is given by the Kalman filter [7], and the discrete hidden Markov model (where $\mathbf{x}_k$ takes its values in a finite alphabet). In the vast majority of cases, nonlinearity or non-Gaussianity render an analytic solution intractable [15].

The classical inference methods for nonlinear dynamic systems are the extended Kalman filter (EKF) and its variants. However, the EKF is known to fail if the system exhibits substantial nonlinearity and/or if the state and the measurement noise are significantly non-Gaussian [15]. Therefore, when implementing a solution, in general, some form of numerical approximation need to be considered. Methods of special interest are the sequential Monte Carlo methods, also known as "particle filters" and those are the ones that this dissertation part will focus on.

4.5.2 Particle filters

The basic idea behind the particle filter is to approximate $p(\mathbf{x}_k|\mathbf{y}_{1:k})$ with a set of N random samples (particles) $\{\mathbf{x}_k^i\}_{i=1}^N$, where each particle $\mathbf{x}_k^i$ is assigned a weight. The weight of each particle should in some way reflect how probable it is that the properties of this particle are the correct ones. Those particles with the highest weights are propagated in time and natural selection is performed. It should be noted that the number of particles, N, has to be chosen large enough to represent the probability density function [7]. In the following we detail the sequential approximation of the posterior distribution.

Monte Carlo integration

Suppose we want to numerically evaluate a multidimensional integral:

$$\mathcal{I} = \int g(\mathbf{x})d\mathbf{x} \tag{4.18}$$

where $\mathbf{x} \in \mathbb{R}^{n_\mathbf{x}}$. Monte Carlo (MC) methods for numerical integration factorize $\mathbf{g}(\mathbf{x}) = \mathbf{f}(\mathbf{x})\pi(\mathbf{x})$ in such a way that $\pi(\mathbf{x})$ is interpreted as a probability density satisfying $\pi(\mathbf{x}) \geq 0$ and $\int \pi(\mathbf{x})d\mathbf{x} = 1$ [65]. The assumption is that it is possible to draw $N \gg 1$ samples $\{\mathbf{x}^i\}_{i=1}^N$ distributed according to $\pi(\mathbf{x})$. The MC estimate of integral

$$\mathcal{I} = \int \mathbf{f}(\mathbf{x})\pi(\mathbf{x})d\mathbf{x} \tag{4.19}$$

is the sample mean:

$$\mathcal{I}_N = \frac{1}{N}\sum_{i=1}^{N}\mathbf{f}(\mathbf{x}^i). \tag{4.20}$$

If the samples $\mathbf{x}^i$ are independent then $\mathcal{I}_N$ is an unbiased estimate and according to the law of large numbers $\mathcal{I}_N$ will almost surely converge to $\mathcal{I}$. It is some times, however, not possible to sample directly from the distribution $\pi(\mathbf{x})$, i.e. in the Bayesian estimation context, $\pi(\mathbf{x})$ is the posterior density, which may be multivariate, nonstandard, and only known up to a proportionality constant. Therefore, a possible solution is to apply the importance sampling method.

Importance sampling

Suppose we can only generate samples from a density $q(\mathbf{x})$, which is similar to $\pi(\mathbf{x})$. Then a correct weighting of the sample set still makes the MC estimation possible. The pdf $q(\mathbf{x})$ is referred to as the *importance* or *proposal* density. Its "similarity" can be expressed by the following condition:

$$\pi(\mathbf{x}) > 0 \Rightarrow q(\mathbf{x}) > 0 \quad \text{for all } \mathbf{x} \in \mathbb{R}^{n_\mathbf{x}} \tag{4.21}$$

which means that $q(\mathbf{x})$ and $\pi(\mathbf{x})$ have the same support. Condition (4.21) is necessary for the importance sampling theory to hold and, if valid, any integral of the form (4.19) can be written as:

$$\mathcal{I} = \int \mathbf{f}(\mathbf{x})\frac{\pi(\mathbf{x})}{q(\mathbf{x})}q(\mathbf{x})d\mathbf{x} \tag{4.22}$$

provided that $\pi(\mathbf{x})/q(\mathbf{x})$ is upper bounded. A Monte Carlo estimate of $\mathcal{I}$ is computed by generating $N \gg 1$ independent samples $\{\mathbf{x}^i\}_{i=1}^N$ distributed according to $q(\mathbf{x})$ and forming the weighted sum:

$$\mathcal{I}_N = \frac{1}{N}\sum_{i=1}^{N}\mathbf{f}(\mathbf{x}^i)\tilde{\omega}(\mathbf{x}^i) \tag{4.23}$$

where

$$\tilde{\omega}(\mathbf{x}^i) = \frac{\pi(\mathbf{x}^i)}{q(\mathbf{x}^i)} \tag{4.24}$$

are the importance weights. If the normalizing factor of the desired density $\pi(\mathbf{x})$ is unknown, we need to perform normalization of the importance weights. Then we estimate $\mathcal{I}_N$ as follows:

$$\mathcal{I}_N = \sum_{i=1}^{N}\mathbf{f}(\mathbf{x}^i)\omega(\mathbf{x}^i) \tag{4.25}$$

where the normalized importance weights are given by:

$$\omega(\mathbf{x}^i) = \frac{\tilde{\omega}(\mathbf{x}^i)}{\sum_{j=1}^{N} \tilde{\omega}(\mathbf{x}^i)}. \tag{4.26}$$

Sequential Importance Sampling (SIS) algorithm

Importance sampling is a general MC integration method that we now apply to perform nonlinear filtering specified by the solution in section 4.5.1. The resulting sequential importance sampling (SIS) algorithm is a Monte Carlo method that forms the basis for most sequential MC (SMC) filters developed over the past decades.

In order to develop the details of the SIS algorithm, let $\{\mathbf{x}_{0:k}^i, \omega_k^i\}_{i=1}^N$ denote a random measure that characterizes the posterior pdf $p(\mathbf{x}_{0:k}|\mathbf{y}_{1:k})$, where $\{\mathbf{x}_{0:k}^i, i = 0, \ldots, N\}$ is a set of supporting points with associated weights $\{\omega_k^i, i = 0, \ldots, N\}$ and $\mathbf{x}_{0:k} = \{\mathbf{x}_j, j = 0, \ldots, k\}$ is the set of all states up to time k. The weights are normalized such that $\sum_i \omega_k^i = 1$. Then, the posterior density at time k can be approximated as follows

$$p(\mathbf{x}_{0:k}|\mathbf{y}_{1:k}) \approx \sum_{i=1}^{N} \omega_k^i \delta(\mathbf{x}_{0:k} - \mathbf{x}_{0:k}^i). \tag{4.27}$$

We therefore have a discrete weighted approximation to the true posterior, $p(\mathbf{x}_{0:k}|\mathbf{y}_{1:k})$. The normalized weights are chosen using the principle of importance sampling. Therefore if the particles were drawn form an importance density $q(\mathbf{x}_{0:k}|\mathbf{y}_{1:k})$, then according to (4.24)

$$\omega_k^i \propto \frac{p(\mathbf{x}_{0:k}^i|\mathbf{y}_{1:k})}{q(\mathbf{x}_{0:k}^i|\mathbf{y}_{1:k})} \tag{4.28}$$

At time $k-1$ one could have samples constituting an approximation to $p(\mathbf{x}_{0:k-1}|\mathbf{y}_{1:k-1})$ and want to approximate $p(\mathbf{x}_{0:k}|\mathbf{y}_{1:k})$ with a new set of samples. If the importance density is chosen to factorize such that

$$q(\mathbf{x}_{0:k}|\mathbf{y}_{1:k}) = q(\mathbf{x}_k|\mathbf{x}_{0:k-1}, \mathbf{y}_{1:k}) q(\mathbf{x}_{0:k-1}|\mathbf{y}_{1:k-1}) \tag{4.29}$$

then one can obtain samples $\mathbf{x}_{0:k}^i \sim q(\mathbf{x}_{0:k}|\mathbf{y}_{1:k})$ by augmenting each of the existing samples $\mathbf{x}_{0:k-1}^i \sim q(\mathbf{x}_{0:k-1}|\mathbf{y}_{1:k-1})$ with the new state $\mathbf{x}_k \sim$, $q(\mathbf{x}_k|\mathbf{x}_{0:k-1}, \mathbf{y}_{1:k})$. To derive the weight update equation, let express $p(\mathbf{x}_{0:k}|\mathbf{y}_{1:k})$, after applying Bayes's rule and making some manipulations, as

$$p(\mathbf{x}_{0:k}|\mathbf{y}_{1:k}) \;\; \propto \;\; p(\mathbf{y}_k|\mathbf{x}_k) p(\mathbf{x}_k|\mathbf{x}_{k-1}) p(\mathbf{x}_{0:k-1}|\mathbf{y}_{1:k-1})$$

By substituting (4.29) and (4.30) into (4.28) the weight update equation can be then shown to be

$$\omega_k^i \propto \frac{p(\mathbf{y}_k|\mathbf{x}_k^i)p(\mathbf{x}_k^i|\mathbf{x}_{k-1}^i)}{q(\mathbf{x}_k^i|\mathbf{x}_{0:k-1}^i,\mathbf{y}_{1:k})} \underbrace{\frac{p(\mathbf{x}_{0:k-1}^i|\mathbf{y}_{1:k-1})}{q(\mathbf{x}_{0:k-1}^i|\mathbf{y}_{1:k-1})}}_{\omega_{k-1}^i} \tag{4.30}$$

$$= \omega_{k-1}^i \frac{p(\mathbf{y}_k|\mathbf{x}_k^i)p(\mathbf{x}_k^i|\mathbf{x}_{k-1}^i)}{q(\mathbf{x}_k^i|\mathbf{x}_{0:k-1}^i,\mathbf{y}_{1:k})} \tag{4.31}$$

Furthermore, if $q(\mathbf{x}_k|\mathbf{x}_{0:k-1},\mathbf{y}_{1:k}) = q(\mathbf{x}_k|\mathbf{x}_{k-1},\mathbf{y}_k)$, then the importance density becomes only dependent on $\mathbf{x}_{k-1}$ and $\mathbf{y}_k$. This is particulary useful in the common case when only a filtered estimate of $p(\mathbf{x}_k,\mathbf{y}_{1:k})$ is required at each time step. In such scenarios, one can discard the path $\mathbf{x}_{0:k-1}^i$ and history of observations $\mathbf{y}_{1:k-1}$. The modified weight is then

$$\omega_k^i \propto \omega_{k-1}^i \frac{p(\mathbf{y}_k|\mathbf{x}_k^i)p(\mathbf{x}_k^i|\mathbf{x}_{k-1}^i)}{q(\mathbf{x}_k^i|\mathbf{x}_{k-1}^i,\mathbf{y}_k)}. \tag{4.32}$$

and the posterior filtered density $p(\mathbf{x}_k|\mathbf{y}_{1:k})$ can be approximated as

$$p(\mathbf{x}_k|\mathbf{y}_{1:k}) \approx \sum_{i=1}^{N} \omega_k^i \delta(\mathbf{x}_k - \mathbf{x}_k^i) \tag{4.33}$$

Therefore, filtering via SIS algorithm consists of recursive propagation of importance weights ω_k^i and support points $\mathbf{x}_k^i$ as each measurement is received sequentially. Table 2 summarizes this algorithm.

Finally, it should be noticed that normalizing the weights, i.e., computing

$$\bar{\omega}_k^i = \frac{\omega_k^i}{\sum_i \omega_k^i}, \quad \text{for} \quad i = 1,\ldots,N, \tag{4.34}$$

the integrals of interest, (4.16) and (4.17), can now be approximated as

$$\hat{\mathbf{x}}_k \approx \sum_{i=1}^{N} \bar{\omega}_k^i \mathbf{x}_k^i \tag{4.35}$$

$$\mathrm{P}_k \approx \sum_{i=1}^{N} \bar{\omega}_k^i (\mathbf{x}_k^i - \hat{\mathbf{x}}_k)(\mathbf{x}_k^i - \hat{\mathbf{x}}_k)^T. \tag{4.36}$$

Algorithm 2 : Sequential Importance Sampling (SIS) Algorithm

$$[\{\mathbf{x}_k^i, \bar{\omega}_k^i\}_{i=1}^N] = \text{SIS } [\{\mathbf{x}_{k-1}^i, \bar{\omega}_{k-1}^i\}_{i=1}^N, \mathbf{y}_k]$$

- For $i = 1 : N$
  - Draw: $\mathbf{x}_k^i \sim q(\mathbf{x}_k^i | \mathbf{x}_{k-1}^i, \mathbf{y}_k)$
  - Compute:
$$\omega_k^i \propto \bar{\omega}_{k-1}^i \frac{p(\mathbf{y}_k|\mathbf{x}_k^i)p(\mathbf{x}_k^i|\mathbf{x}_{k-1}^i)}{q(\mathbf{x}_k^i|\mathbf{x}_{k-1}^i, \mathbf{y}_k)}$$
- End for
- Calculate: $\kappa = \sum_{i=1}^N \omega_k^i$
- For $i = 1 : N$
  - Normalize: $\bar{\omega}_k^i = \frac{\omega_k^i}{\kappa}$
- End for

Resampling

It is well known that SIS algorithm suffers from the *degeneracy problem*: where after a while the importance weights may become very skewed, e.g. only a few particles are likely, whereas the rest have weights close to zero. A suitable measure of degeneracy of an algorithm is the effective sample size N_{eff}, defined as follows:

$$N_{\text{eff}} \approx \frac{1}{\sum_{i=1}^N (\bar{\omega}_k^i)^2}. \tag{4.37}$$

where $1 \leq N_{\text{eff}} \leq N$, with N_{eff} maximized when all weights have the same weight, that means no skewing, and minimized when only one weight is non-zero, i.e. the samples are concentrated to a single spot.

Therefore, whenever a significant degeneracy is observed, i.e. setting a threshold N_{thr}, resampling is required in the SIS algorithm. Resampling eliminates samples with low importance weights and multiplies samples with high importance weights. The resampling can be performed in a deterministic or in a stochastic way. An example of the latter is *multinomial resampling*. The method is to create an ordered set of numbers, u_i, uniformly distributed

$$u_i \in \mathcal{U}(0, 1), \quad i = 1, \ldots, N, \tag{4.38}$$

and then create the set of the cumulative sum of weights (CSW) according

to

$$\text{CSW} = \left\{ 0, c_j = \sum_{l=1}^{j} \bar{\omega}_k^l \right\}_{j=1}^{N} \tag{4.39}$$

For each i find the smallest c_j that is larger than u_i and keep the corresponding sample $\mathbf{x}_k^i$, figure 4.5 depicts the procedure and algorithm 3 shows its implementation. There exist several schemes based on clever probabilistic results that may be exploited to reduce the computational load associated with multinomial resampling, some of them can be found in [16].

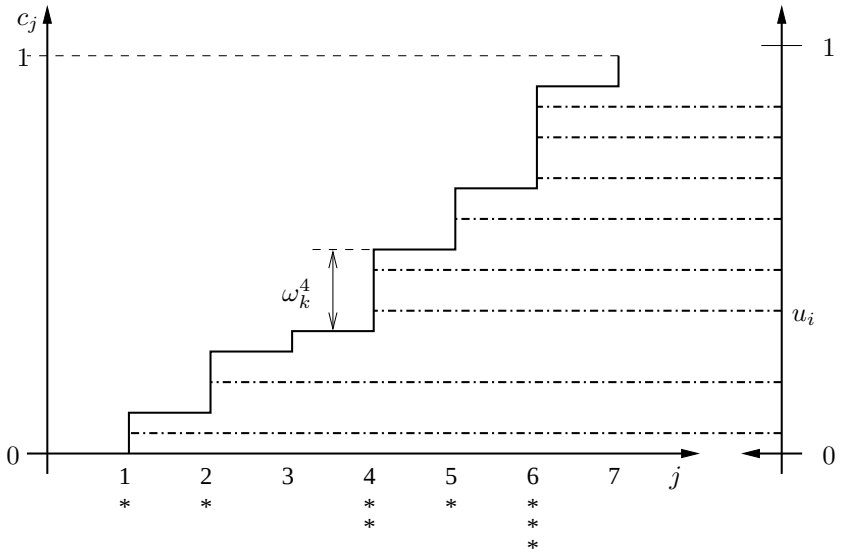

Figure 4.5: Multinomial resampling. The asterisks represent the number of samples drawn from sample i. The dash-doted lines are samples drawn from $\mathcal{U}(0,1)$.

Generic particle filter and the Bootstrap filter

Using algorithms 2 and 3 a generic particle filter can be conceived. The generic particle filter is summarized in algorithm 4. Notice, however, that a particular form of the generic particle filter can be obtained using the state transition density $p(\mathbf{x}_k|\mathbf{x}_{k-1})$ as the importance distribution, i.e. making $q(\mathbf{x}_k|\mathbf{x}_{k-1}, \mathbf{y}_k) = p(\mathbf{x}_k|\mathbf{x}_{k-1})$, which simplifies the importance weights, given by (4.32), to

$$\omega_k^i \propto \omega_{k-1}^i p(\mathbf{y}_k|\mathbf{x}_k^i) \tag{4.40}$$

This particular form of the generic particular filter is known as the *Bootstrap filter* [15]. In the original version of the Bootstrap filter [35] resampling is

Algorithm 3 : Multinomial Resampling Algorithm (MRA)

$$[\{\mathbf{x}_k^{j*}, \bar{\omega}_k^j\}_{j=1}^N] = \text{MRA } [\{\mathbf{x}_k^i, \bar{\omega}_k^i\}_{i=1}^N]$$

- Initialize: $c_1 = \bar{\omega}_k^1$
- For $i = 2 : N$
  - Construct CSW: $c_i = c_{i-1} + \omega_k^i$
- End for
- For $j = 1 : N$
  - Draw: $u_j \sim \mathcal{U}(0, 1)$
  - Set $i = 1$
  - While $u_j > c_i$
    - $i = i + 1$
  - end While
  - $\mathbf{x}_k^{j*} = \mathbf{x}_k^i$
  - $\omega_k^j = N^{-1}$
- End for

carried out at each every time step, in which case the term $\omega_{k-1}^i = N^{-1}$ is a constant, which may thus be ignored. The version we present in algorithm 4 carries out resampling when $N_{\text{eff}} < N_{\text{thr}}$ in order to reduce computation burden. A distinctive feature of the Bootstrap filter is that it is very easy to implement because it only involves simulating from the transition density $p(\mathbf{x}_k|\mathbf{x}_{k-1})$ and evaluation of the conditional likelihood $p(\mathbf{y}_k|\mathbf{x}_k)$ [16].

4.6 Conclusions

This chapter introduced the problem of ground target tracking using nonstandard information, such as digital maps containing road network information. The most used methods to track ground moving targets constrained to roads were also presented. It outlined the problem of target tracking in presence of multiple simultaneous measurements, as well as the data association problem when tracking multiple targets. Finally, as ground target tracking using road network information is usually highly a non-Gaussian problem, a tutorial on

particle filters was provided.

Algorithm 4 : Generic particle filter and Bootstrap filter

$$[\{\mathbf{x}_k^i, \bar{\omega}_k^i\}_{i=1}^N] = \text{PF } [\{\mathbf{x}_{k-1}^i, \bar{\omega}_{k-1}^i\}_{i=1}^N, \mathbf{y}_k]$$

- Filtering via SIS, algorithm 2:

$$[\{\mathbf{x}_k^i, \bar{\omega}_k^i\}_{i=1}^N] = \text{SIS } [\{\mathbf{x}_{k-1}^i, \bar{\omega}_{k-1}^i\}_{i=1}^N, \mathbf{y}_k]$$

(with $\omega_k^i \propto \omega_{k-1}^i p(\mathbf{y}_k|\mathbf{x}_k^i)$ for the Bootstrap filter.)

- Compute:

$$N_{\text{eff}} \approx \frac{1}{\sum_{i=1}^N (\bar{\omega}_k^i)^2}$$

- IF $N_{\text{eff}} < N_{\text{thr}}$
  - Resample using algorithm 3:

$$\{\mathbf{x}_k^{j*}, \bar{\omega}_k^j\}_{j=1}^N] = \text{MRA } [\{\mathbf{x}_k^i, \bar{\omega}_k^i\}_{i=1}^N]$$

- END IF

Chapter 5

Single target tracking with road constraints[1]

In this chapter we propose a batch-recursive algorithm for tracking ground moving targets constrained to roads using bearings-only measurements in clutter collected by a ground moving observer. The proposed algorithm, in its batch stage, uses a fast and low-complexity procedure based on the maximum-likelihood method to obtain an estimate of the line-of-sight bearing. Once this is achieved, such an estimate is employed at the recursive stage to initialize a *regularized particle filter*, which provides track maintenance by recursively estimating a modified polar coordinate representation of the state vector. The scenario represents a target moving along a realistic road network with junctions, roads branching or crossing, where the probability of having the line-of-sight bearing, among the multiple observed ones, is less than the unity. Realistic simulations are presented to support our findings.

The organization of this chapter is as follows: In section 5.1 we present the modified polar coordinate system used to represent the target dynamics and measurement models. Moreover, we show how to include road network information in such models. Section 5.2 describes the algorithm to track the target, and present an efficient and easy procedure for its initialization. Section 5.3 presents some realistic simulation results. And in section 5.4 we provide the conclusions.

[1]Part of this material appears in [19, 21].

5.1 Road Constrained Target Dynamics and Measurement Models

The basis of BOT problem relies on estimating the trajectory of a target, i.e. position and velocity from noise-corrupted bearing measurements, performed by a single-maneuvering observer. The vast literature of BOT problem agrees that the representation of the state vector and measurement model in the modified polar coordinate system produces more stable algorithms than those ones based on a cartesian representation [2, 12]. For this reason, we choose the MP coordinate system to work with.

Since, in this chapter, the target and the observer are supposed to evolve in a surveillance region constrained by known road networks, we consider such an information as *a prior* to be integrated in the tracker system. As seen in the previous chapter, road network information is modeled as a large collection of roads, each of which consists of a number of interconnected segments. Each segment is assumed to be a straight line between two geo-referenced nodes [77], [50]. Therefore, in order to incorporate road network information into the tracker system we propose to use such an information in three different ways:

1. constraining the direction of the velocity components, of the target state vector, to be parallel to the direction of the road segment in which the target is supposed to travel [60],

2. constraining the target's position exploiting the concept of pseudo-measurement [22, 37, 77], and

3. using the concept of *directional process noise* [44], that assumes for on-road targets more uncertainty along a road segment than orthogonal to it.

Details on how to perform this, as well as the reasons to exploit road network information according to the above points will become clear below.

5.1.1 Modified polar coordinate system

Initially the BOT problem was extensively, if not exclusively, formulated in the cartesian coordinate system, because it permits a simple linear representation of the state dynamics; all system nonlinearities are embedded in a single scalar measurement equation. However, some theoretical and experimental findings demonstrate that cartesian-based Kalman filters are unstable

for single sensor bearings-only tracking. Such unstable behavior is due to the non-observability of the target state vector, which even in the absence of noise remains non-observable if the observer does not maneuver [57].

Aidala and Hammel in [2] show that the utilization of the modified polar coordinate system to formulate the BOT problem renders Kalman filter based algorithms more stable. They prove that this coordinate system is well-suited for bearings-only tracking because it automatically decouples observable and unobservable components of the estimated state vector. Such decoupling prevents covariance matrix ill-conditioning, which is the primary cause of filter instability.

The algorithm presented in this chapter is based on particle filters, however, as pointed out by [12] the use of the modified polar coordinate system for BOT using particle filters, produces more stable algorithms. Which represents the principal motivation to keep such a coordinate system. The formulae to go from the cartesian $(x_k, y_k, \dot{x}_k, \dot{y}_k)$ to the modified polar coordinate system $(\theta_k, \dot{\theta}_k, \xi_k, r_k)$, and vice versa are given in table 5.1 [2].

MP to Cartesian	Cartesian to MP
$x_k = r_k \cos\theta_k$	$\theta_k = \arctan\left(\dfrac{y_k}{x_k}\right)$
$y_k = r_k \sin\theta_k$	$\dot{\theta}_k = \dfrac{\dot{y}_k x_k - \dot{x}_k y_k}{x_k^2 + y_k^2}$
$\dot{x}_k = \xi_k r_k \cos\theta_k - \dot{\theta}_k r_k \sin\theta_k$	$\xi_k = \dfrac{\dot{x}_k x_k + \dot{y}_k y_k}{x_k^2 + y_k^2}$
$\dot{y}_k = \xi_k r_k \sin\theta_k + \dot{\theta}_k r_k \cos\theta_k$	$r_k = \sqrt{x_k^2 + y_k^2}$

Table 5.1: Modified polar to cartesian coordinate (and vice versa) transformation equations.

5.1.2 Constrained Dynamic Model Formulation

The position and velocity of a target moving along a road are characterized by the equation of the linear segment modeling the road. The position should appertain to the linear segment and the direction of the velocity vector should be parallel to the direction of the road [60]. Furthermore, according to [44] the on-road condition implies that the estimation of the target's state vector is more uncertainty along the road segment than orthogonal to it.

In this section we show how to introduce the constraint on the target's velocity vector, as well as the directional incertitude in the estimation of the target's state vector. The constraint on the position of the target is

handled using the concept of pseudo-measurement and is presented in the next section.

Constraining the direction of the velocity vector

Knowing the event that the target is evolving on a specific road segment s, we can constraint the direction of the velocity components to be parallel to the road segment s. To perform this, we use the orthogonal condition between the velocity vector and a normal vector to the road segment s, given by equation (4.7). This condition in the cartesian coordinate system my be written as

$$\dot{y}_k - m_s \dot{x}_k = 0 \tag{5.1}$$

where m_s stands for the slope of the road segment s.

Using equation (5.1), the noiseless approximate dynamic equations [58] and the cartesian to MP coordinates (and vice versa) transformation equations (table 5.1), it can be proved that the constrained relative dynamics of a constant velocity target w.r.t. a maneuvering observer can be expressed as[1]

$$\boldsymbol{\chi}_{k+1} = \boldsymbol{f}_s(\boldsymbol{\chi}_k) - \boldsymbol{\varrho}_k + \boldsymbol{\upsilon}_k \tag{5.2}$$

where

• $\boldsymbol{\chi}_k$ is the relative discrete target state vector at time k in modified polar coordinates defined as

$$\boldsymbol{\chi}_k = \left[\begin{array}{cccc} \theta_k & \dot{\theta}_k & \xi_k & r_k \end{array} \right]^T \tag{5.3}$$

where θ_k and r_k stand, respectively, for the relative bearing angle and range, with first order derivatives $\dot{\theta}_k$ and $\dot{r}_k$, and where $\xi_k = \dot{r}_k / r_k$ is the normalized range rate,

• $\boldsymbol{f}_s(\boldsymbol{\chi}_k)$ is a vector function describing the noiseless relative dynamics of a target, w.r.t a non-maneuvering observer, whose velocity vector is parallel to the road segment s, and which is given by

$$\boldsymbol{f}_s(\boldsymbol{\chi}_k) = \left[\begin{array}{l} \arctan\left(A_k / B_k\right) \\ E_k(m_s B_k - A_k) \\ E_k(B_k + m_s A_k) \\ r_k C_k \end{array} \right] \tag{5.4}$$

[1] Details on the derivation of the constrained motion model are relegated to appendix E.

with

$$\begin{aligned} A_k &= \sin\theta_k + m_s T D_k \\ B_k &= \cos\theta_k + T D_k \\ C_k^2 &= A_k^2 + B_k^2 \\ D_k &= \xi_k \cos\theta_k - \dot{\theta}_k \sin\theta_k \\ E_k &= D_k / C_k^2 \end{aligned}$$

where T stands for the sampling time,

• $\boldsymbol{\varrho}_k$ is a vector function accounting for a constant observer acceleration, given by

$$\boldsymbol{\varrho}_k = \frac{T}{r_k C_k^2} \begin{bmatrix} 0 \\ \gamma_y B_k - \gamma_x A_k \\ \gamma_y A_k + \gamma_x B_k \\ 0 \end{bmatrix} \tag{5.5}$$

where (γ_x, γ_y) stand, respectively, for the known observer acceleration components in x and y directions, and

• $\boldsymbol{\upsilon}_k$ is the process noise used to model unpredictable target accelerations, assumed to be zero-mean, white and Gaussian with covariance matrix $\mathbf{Q}_k$. According to [44] road network information can be introduced in the construction of the covariance matrix $\mathbf{Q}_k$. The following procedure provides de details to construct a directional covariance matrix.

Directional process noise

Consider a target moving along a road segment s. Following [44] the unpredictable target acceleration components along and orthogonal to the road segment s, given respectively by a_o and a_a are zero-mean Gaussian random variables with respective variances σ_o^2 and σ_a^2, with $\sigma_a^2 >> \sigma_o^2$. Thus, according to this constraint the covariance matrix modeling unpredictable target accelerations in a cartesian coordinate system is given by

$$\mathbf{Q}_s^{\mathrm{CS}} = \mathbf{G}\mathbf{R}_s \begin{bmatrix} \sigma_o^2 & 0 \\ 0 & \sigma_a^2 \end{bmatrix} \mathbf{R}_s^T \mathbf{G}^T$$

where $\mathbf{G}$ is the transition matrix given by (E.5), and $\mathbf{R}_s$ is the rotation matrix associated to s given by (4.5). Now, we need the express $\mathbf{Q}_s^{\mathrm{CS}}$ in the MP coordinate system, which can be achieved using the following equation

$$\mathbf{Q}_{s,k}^{\mathrm{MP}} = \mathbf{J}_k \mathbf{Q}_s^{\mathrm{CS}} \mathbf{J}_k^T \tag{5.6}$$

where $\mathbf{J}_k$ stands for the Jacobian matrix containing the partial derivatives of $\boldsymbol{\chi}_k$ w.r.t. to the position and velocity components. The expression of $\mathbf{J}_k$ as function of the parameters of the state vector in MP coordinates is given by

$$\mathbf{J}_k = \frac{1}{r_k}\begin{bmatrix} \sin(\theta_k) & \cos(\theta_k) & 0 & 0 \\ \xi_k\sin(\theta_k) - \dot{\theta}_k\cos(\theta_k) & -\dot{\theta}_k\sin(\theta_k) - \xi_k\cos(\theta_k) & -\sin(\theta_k) & \cos(\theta_k) \\ -\dot{\theta}_k\sin(\theta_k) - \xi_k\cos(\theta_k) & \xi_k\sin(\theta_k) - \dot{\theta}_k\cos(\theta_k) & \cos(\theta_k) & \sin(\theta_k) \\ r_k\cos(\theta_k) & r_k\sin(\theta_k) & & \end{bmatrix}$$

5.1.3 Measurement Equations

Traditional BOT scheme considers a single bearing measurement at each sensor scan. However, in practical situations signals coming from the target may propagate via multiple paths due to reflection/refraction before reaching the observer. Furthermore, it may happen that in presence of obstacles between target and observer all measured bearings belong to non-line-of-sight paths only. Hence, measurement models which take into account such impairments are necessary to properly track the target.

In the following, we present the measurement model corresponding to the bearings collected by the ground moving sensor and we introduce the concept of pseudo-measurement to constraint the position of the target to the road network.

Bearing Measurements

The M_k bearing measurements available at time k, are disposed in vector $\mathbf{y}_k$, whose elements are given by

$$y_{j,k} = \begin{cases} \theta_k + w_{1,k} & \text{if } \psi_k = j, \\ u_k & \text{if } \psi_k \neq j \text{ or } \psi_k = 0 \end{cases} \tag{5.7}$$

where the following assumptions take place:

- $j \in \{1, \ldots, M_k\}$ denotes the index element in vector $\mathbf{y}_k$,
- $w_{1,k}$ is a zero-mean independent Gaussian noise with variance σ_θ^2,
- u_k is a random variable accounting for the bearings due to clutter. For simplicity, we assume that for a bearing due to clutter all values in the interval $\mathcal{I} = [0, 2\pi]$ are equally likely. Meaning that u_k is distributed as an uniform random variable in $\mathcal{I}$ [8],

• ψ_k is a $\{0, 1, \ldots, M_k\}$-valued random variable with probability

$$p(\psi_k = i) = \begin{cases} 1 - P_D & \text{si} \quad i = 0 \\ P_D/M_k & \text{si} \quad i \neq 0 \end{cases} \tag{5.8}$$

where P_D is the prior probability of target detection. It should be noticed that for $\psi_k \neq 0$, ψ_k denotes the index of the LOS bearing in vector $\mathbf{y}_k$, and for $\psi_k = 0$, it represents the absence of LOS bearing in $\mathbf{y}_k$.

Distance pseudo-measurement: constraining the position of the target

As seen in the previous chapter, an alternative approach to incorporate road network information is through the use of pseudo-measurements [22] or fictitious measurements [37, 77], which represent "synthetic" measurements usually created to constraint the target dynamics to the road network. Here we use such an approach for three purposes;

1. to define the road segment in which the target is evolving,
2. to handle target transitions between road segments (e.i. when the target approaches a node), and
3. to penalize the target evolution far away from the road network.

Notice that purpose 3. implies that we are going to permit the evolution of the target out of roads, instead of imposing hard constraints so that the target's position estimate appertains to the road segment in which it is supposed to travel.

Thus, let define a pseudo-measurement of the minimum Euclidian distance between the target's position $\mathbf{x}_k$ at time k and the road network Ω_R as

$$d_k = h(\mathbf{x}_k, \Omega_R) + w_{2,k} \tag{5.9}$$

where $\omega_{2,k}$ is the measurement noise, assumed to be zero-mean white Gaussian process with variance σ_d^2, and $h(\cdot)$ denotes the non linear function providing the distance defined as

$$h(\mathbf{x}_k, \Omega_R) = \min_{\mathbf{x} \in \Omega_R} ||\mathbf{x}_k - \mathbf{x}||_2$$

It should be notice that the above expression provides de distance between the target's position $\mathbf{x}_k$ at time k and the nearest road segment s to that position.

In order to satisfy purpose 1. we consider that the dynamics of the target state is constrained to the road segment s, if s is the nearest road segment to the current position of the target. An efficient technique to find the nearest road segment is presented in the next section. The research of the nearest road segment to the target's position satisfies purpose 2. Purpose 3. is automatically satisfied by assuming the pseudo-measurements as normally distributed with zero-mean (on-road condition).

5.2 Algorithm implementation

This section provides details on the implementation of a batch-recursive algorithm to track a ground moving target using bearings-only measurements in clutter. The target's movement is governed by the constrained dynamic model introduced in the previous section.

5.2.1 Particle filter implementation

Consider the system described by equations (5.2), (5.7) and (5.9)

$$\begin{aligned} \boldsymbol{\chi}_{k+1} &= \boldsymbol{f}_s(\boldsymbol{\chi}_k) - \boldsymbol{\varrho}_k + \boldsymbol{\upsilon}_k, \\ \mathbf{y}_k &= \begin{bmatrix} y_{1,k} & \dots & y_{M_k,k} \end{bmatrix}^T, \\ d_k &= h(\mathbf{x}_k, \Omega_R) + w_{2,k}. \end{aligned}$$

and let denote the set of available observations at time k by $\mathbf{Z}_k = \{\mathbf{z}_0, \dots, \mathbf{z}_k\}$, with $\mathbf{z}_k = [\ \mathbf{y}_k^T \quad d_k\ ]^T$. From a Bayesian perspective, the tracking problem is to recursively calculate some degree of belief in the state $\boldsymbol{\chi}_k$ at time k, taking different values, given the data $\mathbf{Z}_k$ up to time k. Hence, it is required to construct the posterior density $p(\boldsymbol{\chi}_k|\mathbf{Z}_k)$. In this procedure, it is assumed that the initial density $p(\boldsymbol{\chi}_0) = p(\boldsymbol{\chi}_0|\mathbf{Z}_0)$ is available.

One simple method to approximate the posterior density is by means of particle filters [7]. Thus, starting with a weighted set of samples (particles) $\{\boldsymbol{\chi}_{k-1}^i, \omega_{k-1}^i\}_{i=1}^N$ approximately distributed according to $p(\boldsymbol{\chi}_{k-1}|\mathbf{Z}_{k-1})$, new samples are drawn from a suitable proposal distribution, which may depend on the previous state and the new measurements, however, for simplicity it is often chosen to be the prior, i.e. $\boldsymbol{\chi}_k^i \sim p(\boldsymbol{\chi}_k|\boldsymbol{\chi}_{k-1})$. In order to maintain a consistent sample, the new importance weights are set to

$$\omega_k^i \propto \omega_{k-1}^i p(\mathbf{Z}_k|\boldsymbol{\chi}_k^i) \tag{5.10}$$

where $\sum_{i=1}^N \omega_k^i = 1$. Thus, the new particle set $\{\boldsymbol{\chi}_k^i, \omega_k^i\}_{i=1}^N$ is then approximately distributed according to $p(\boldsymbol{\chi}_k|\mathbf{Z}_k)$ and, therefore, an estimate

of the state can be obtained using, for instance, the minimum mean square (MMS) [37]. It should be noticed that in order to consider multiple bearing measurements and pseudo-measurements, the likelihood function $p(\mathbf{Z}_k|\boldsymbol{\chi}_k^i)$ may be written as

$$\begin{aligned} p(\mathbf{Z}_k|\boldsymbol{\chi}_k^i) &= p(\mathbf{y}_k, d_k^i|\boldsymbol{\chi}_k^i) \\ &= p(d_k^i|\boldsymbol{\chi}_k^i)p(\mathbf{y}_k|\boldsymbol{\chi}_k^i) \\ &= p(d_k^i|\boldsymbol{\chi}_k^i)\sum_{\psi_k=0}^{M_k} p(\mathbf{y}_k|\boldsymbol{\chi}_k^i, \psi_k)p(\psi_k) \end{aligned} \tag{5.11}$$

where d_k^i is the minimum Euclidian distance from particle i to the nearest road segment, eq. (5.9), and where $p(\mathbf{y}_k|\boldsymbol{\chi}_k^i, \psi_k)$ and $p(d_k^i|\boldsymbol{\chi}_k^i)$ according to (5.7) and (5.9) can be computed as

$$p(\mathbf{y}_k|\boldsymbol{\chi}_k^i, \psi_k) = \begin{cases} \phi(y_{j,k}; \theta_k^i, \sigma_\theta^2)(2\pi)^{1-M_k}, & \psi_k = j \\ (2\pi)^{-M_k}, & \psi_k = 0 \end{cases} \tag{5.12}$$

$$p(d_k^i|\boldsymbol{\chi}_k^i) = \phi(d_k^i; 0, \sigma_d^2) \tag{5.13}$$

To avoid the *degeneracy problem* we take N samples with replacement from the set $\{\boldsymbol{\chi}_k^i\}_{i=1}^N$ if

$$N_{\text{eff}} = \frac{1}{\sum_i (\omega_k^i)^2} < N_{\text{thr}} \tag{5.14}$$

where the probability to take sample i is ω_k^i and where N_{eff} is the effective number of samples and $N_{\text{thr}} = 2/3N$ is a threshold [37]. It should be noticed that following this procedure and in presence of small process noise, particles that have high weights are statistically selected many times giving a poor representation of the posterior density [7]. This arises due to the fact that in the resampling stage, samples are drawn from a discrete distribution rather than a continuous one. Thus, as proposed in [56] a potential solution to this problem is to draw samples from a continuous approximation of the posterior density

$$p(\boldsymbol{\chi}_k|\mathbf{Z}_k) \approx \sum_{i=1}^N \omega_k^i K_h(\boldsymbol{\chi}_k - \boldsymbol{\chi}_k^i) \tag{5.15}$$

where

$$K_h(\boldsymbol{\chi}) = \frac{1}{h^n} K(\frac{\boldsymbol{\chi}}{h})$$

is the rescaled Kernel density $K(\cdot)$, $h > 0$ is the Kernel bandwidth and n is the dimension of the state vector $\boldsymbol{\chi}$.

The kernel and bandwidth are chosen to minimize the mean integrated square error (MISE) between the true posterior density and the corresponding regularized empirical representation (5.15). In the particular case of equally weighted samples, the optimal choice of the kernel is the Epanechnikov kernel [56]

$$K_{opt}(\boldsymbol{\chi}) = \begin{cases} \frac{n+2}{2c_n}(1 - \|\boldsymbol{\chi}\|^2) & \text{if } \|\boldsymbol{\chi}\| < 1 \\ 0 & \text{otherwise} \end{cases} \tag{5.16}$$

where c_n is the volume of the unit sphere in $\mathfrak{R}^n$ (for $n = 4$, $c_4 = 4.9348$). Furthermore, when the posterior density is Gaussian with a unit covariance matrix, the optimal choice for the bandwidth is

$$h_{opt} = \left(\frac{8(n+4)(2\sqrt{\pi})^n}{c_n} \right)^{\frac{1}{n+4}} N^{-\frac{1}{n+4}} \tag{5.17}$$

Although these results are optimal only in the special case of equally weighted particles and Gaussian posterior density, it can still be applied in the general case to obtain a suboptimal filter [7].

5.2.2 ML Method for Track Initialization

The most effective and simplest way to initialize particles is spreading them over the roads contained in the surveillance region. Following this procedure, and in the case where only the LOS bearing is observed at each time step $M_k = 1$, particles laying around the LOS direction will become soon more likely than the other ones and will be concentrated in roads where the target is likely to be evolving, see figure 5.1.

In the case of having multiple spurious bearing measurements at each time step $M_k > 1$ and a probability of target detection less than the unity $P_D < 1$, the procedure described above may not always work. This is because it may occur that the first available bearing observations $\mathbf{y}_k$ do not include the LOS bearing, producing particles to concentrate on roads that may be far away from the one on which the target is actually evolving, see figure 5.2. In such a situation, it may happen that those particles be resampled, and then become very unlikely and soon die out as the new observations are available. Nevertheless, in order to render particles around the LOS direction more likely, even in presence of multiple spurious bearing measurements and for low target detection probabilities, we propose the following four-step procedure

1. Spread particles over the surveillance region,
2. estimate the LOS direction via a batch procedure,
3. use the estimated LOS bearing in the first iteration of the particle filter as if it was the only available observation, and
4. force resampling.

Following this procedure, resampled particles will be concentrated in clouds around the roads where the target is likely to be evolving. As the target evolves and new bearing measurements become available only one cloud will survive.

LOS bearing estimation

According to (5.7) the pdf of the measurement vector $\mathbf{y}_k$ at time k can be expressed as:

$$p(\mathbf{y}_k) = \prod_{j=1}^{M_k} \left(\frac{1 - P_T}{2\pi} + P_T \phi(y_{j,k}; \theta_k, \sigma^2) \right) \tag{5.18}$$

where $P_T = P_D/M_k$, and where $\phi(z; m, \sigma^2)$ stands for the pdf of a Gaussian random variable with mean m and variance σ^2. As we can see in (5.18), the LOS bearing θ_k changes as the relative position of the target w.r.t. the observer changes. However, since we are interested in a raw estimation of the LOS direction to initialize particles, we consider that the position of the target w.r.t the observer does not change significatively over a short period of time. This implies that $\theta_k = \theta_{\text{LOS}}$ remains constant for a few number of observations, let say for $k = 1 : N_m$, then the estimated LOS bearing $\hat{\theta}_{\text{LOS}}$ and its estimated variance $\hat{\sigma}_{\text{LOS}}$ are given by the maximization of the log-likelihood associated to the observations set $\{\mathbf{y}_1, \ldots, \mathbf{y}_{N_m}\}$, thus

$$(\hat{\theta}_{\text{LOS}}, \hat{\sigma}^2_{\text{LOS}}) \approx \underset{\theta_{LOS}, \sigma^2}{\text{argmax}} \left(\sum_{k=1}^{N_m} \log p(\mathbf{y}_k) \right) \tag{5.19}$$

It should be noticed that using the above approximation the LOS bearing is computed as the mean value of the LOS bearings in the observation set $\{\mathbf{y}_1, \ldots, \mathbf{y}_{N_m}\}$, and that the precision of the estimated LOS bearing depends on the relative positions of the target w.r.t the observer within the time interval $k = 1 : N_m$. For small target position changes, $\hat{\theta}_{\text{LOS}}$ will be a good approximation of the LOS bearing, and the value of $\hat{\sigma}^2_{\text{LOS}}$ will be small. In contrast, if the position of the target change a lot within the time interval

$k = 1 : N_m$, a less accurate estimate of the LOS bearing will be obtained, and the value of $\hat{\sigma}^2_{\text{LOS}}$ will be bigger. In both cases, the use of $\hat{\theta}_{\text{LOS}}$ and $\hat{\sigma}^2_{\text{LOS}}$ in the first iteration of the particle filter (evaluating weights (5.12)) will produce particles around the LOS direction become more likely than the other ones. The only difference is that using an accurate $\hat{\sigma}^2_{\text{LOS}}$ and a small value of $\hat{\sigma}^2_{\text{LOS}}$ will produce less spread of initial particles around the LOS direction. Notice also that, since we are interested in spreading particles only around the direction of the LOS bearing, approximation (5.19) not only results effective enough to do so, but also computationally inexpensive compared to the approaches where at the batch stage obtain an estimate of the full target state vector [46].

5.2.3 Finding the nearest road segment

The most straightforward way to find the closest road segment is to use brute force. This means that for each particle, all the road segments has to be iterated in order to find the closest match. This can be really cumbersome if the number of particles is large and if the map contains a lot of roads. The first thing to do in order to decrease the calculation burden is obviously to reduce the number of roads to search. Since the particles are limited in space, a bounding box can be defined that guarantees that no road that lies entirely outside it is closest to any particle.

Now consider a set of M road segments that lie within the bounding box. The segments are defined by their nodes:

$$\bar{R} = \{a_{i,x}, a_{i,y}, b_{i,x}, b_{i,y}\}_{i=1}^{M} \tag{5.20}$$

Assume that N particles are positioned according to:

$$\bar{P} = \{x_i, y_i\}_{i=1}^{N} \tag{5.21}$$

With these definitions an upper bound of the distance from particle j to the nearest road can be calculated by observing that the nearest road can lie no further away than

$$r_j \leq \min_i(\min(|x_j - a_{i,x}| + |y_j - a_{i,y}|, |x_j - b_{i,x}| + |y_j - b_{i,y}|)) \tag{5.22}$$

This is a direct result of the triangular inequality theorem where $|x + y| < |x| + |y|$ for all non-parallel vectors x and y. The upper bound calculation contains no costly operations, so it should be a quite quick operation. Once this upper bound is calculated a course lower bound can be found for each

road:

$$\begin{aligned} r_{j,i} \geq\ & \max(\min(|x_j - a_{i,x}|, |x_j - b_{i,x}|) - \frac{|a_{i,x} - b_{i,x}|}{2}, \\ & \min(|y_j - a_{i,y}|, |y_j - b_{i,y}|) - \frac{|a_{i,y} - b_{i,y}|}{2}, 0). \end{aligned} \tag{5.23}$$

So, if $r_{j,i} \leq r_j$ then the exact minimum distance from particle P_j to road segment R_i should be calculated, otherwise the road is guaranteed not to be the closest road. The exact minimum distance from particle P_j to some point on the road segment R_i is obtained as

$$r_{j,i} = |ax_j - by_j + c| \tag{5.24}$$

$$a = \frac{a_{i,y} - b_{i,y}}{d} \tag{5.25}$$

$$b = \frac{a_{i,x} - b_{i,x}}{d} \tag{5.26}$$

$$c = \frac{a_{i,x}b_{i,y} - b_{i,x}a_{i,y}}{d} \tag{5.27}$$

$$d = \sqrt{(a_{i,x} - b_{i,x})^2 + (a_{i,y} - b_{i,y})^2} \tag{5.28}$$

Once computed the minimum Euclidian distance between particle P_j and the nearest road segment R_i, pdf in (5.13) can be evaluated. Notice also that, identifying R_i a constrained dynamic model tuned to R_i can be assigned to particle P_j.

5.2.4 Drawing an Epanechnikov random variable

The acceptance-rejection method [33] is an algorithm for generating random samples from an arbitrary probability distribution, given as ingredients random samples from a related distribution and the uniform distribution. Here we use it to generate random variables distributed according to the Epanechnikov kernel. The method is outlined below.

Set-up

- Let X be a random variable with some other probability distribution that we know how to draw samples from.
- Let U be a random variable uniformly distributed on the interval $[0, 1]$.
- Let Y be the random variable that we want to be able to generate. Assume that Y has a probability distribution that is absolutely continuous to the probability distribution for X, with density ρ.

- Further assume that the density ρ is bounded above by a constant c. So $\rho(x) \leq c$ for all x in the range of X; and necessarily $c \geq 1$.

Algorithm 5 : Rejection acceptance algorithm

1. Generate a value for X.
2. Generate a value for U
3. If $U \leq \rho(X)/c$, then set $Y = X$ ("accept")
4. Otherwise, go back to step 1 ("reject"), repeating until we obtain a value of Y in step 3.

Intuitive explanation

When we generate X and U following the algorithm 5, we are in fact picking the point (X, cU) in the rectangular box, shown in figure 5.3. And the test $U \leq \rho(X)/c$ determines that point lies below the graph of ρ. It seems plausible that if we keep only the points that fall under the graph of the density ρ, and ignore the points above, then the distribution of the abscissa should have density ρ.

The acceptance-rejection method works more efficiently as the distribution of X and Y become similar enough. That is, $\rho(x)$ and its upper bound c are close to one. This makes the rejection region smaller, and so the algorithm is likely to go through fewer repetitions discarding the rejects. The reader is referred to [33] for a more formal justification of the rejection-acceptance method.

5.3 Simulation results

The scenario used to demonstrate the performance of the proposed algorithm is depicted in figure 5.4. The road network consists in twenty six roads (dashed lines) meeting at different nodes (solid triangles labeled by its node number). The target initially situated at node 16 maintains a constant velocity course, $v_T = 16$ m/s, changing its direction at nodes $\{15, 2, 3, 4, 18\}$ and describing the solid line trajectory at the bottom of figure 5.4. The observer departs from node 12 with a constant velocity of $v_o = 17$ m/s and undergoes a constant acceleration of $a_o = 0.3$ m/s^2 in the interval 0.5-1.0 minutes, after

this it maintains the initial constant velocity changing its course at nodes $\{13, 9, 10, 5\}$ and describing the doted line trajectory at the top of figure 5.4. Three bearing measurements are received at each sensor scan $T = 0.5\ s$, for an approximated observation period of 5.5 minutes. When present, the LOS bearings are measured with an accuracy of $\sigma_\theta = 0.5$ deg.

At the batch stage of the algorithm, 50 bearing measurements are processed in order to obtain an estimation of the LOS direction. For simplicity, in this process, we considered the standard deviation noise $\sigma_{\text{LOS}} = \sigma_\theta$ as a known parameter and the estimation is made for the LOS bearing θ_{LOS} only. To find the maximum of the log-likelihood function (5.19), or analogously the minimum of the negative log-likelihood the *fminsearch* function of MATLAB was employed. Since the *fminsearch* finds local minima given initial values we initialized it for different values of θ_{LOS} going from 0 to 2π rad with a step of 0.15 rad and we kept the estimated bearing $\hat{\theta}_{LOS}$ which provides the minimum value of the negative log-likelihood function.

The following nominal filter parameters were used at the recursive stage: the directional process noise standard deviations (STDs) for the acceleration components along and orthogonal to the road were respectively set to $\sigma_a = 5.5$ m^2/s and $\sigma_o = 3$ m^2/s. The pseudo-measurement STD was $\sigma_d = 5.5$ m and the regularized particle filter used $N = 1000$ particles, carrying out resampling if $N_{\text{eff}} < N_{\text{thr}}$, with $N_{\text{thr}} = 2/3N$.

The estimation performance of the proposed algorithm is provided in terms of the root-mean-square (RMS) position errors using 100MC trials. The RMS position error at time k is computed according to

$$\text{RMS}_k = \sqrt{\frac{1}{n}\sum_{i=1}^{n}(\hat{x}_k^i - x_k^i)^2 + (\hat{y}_k^i - y_k^i)^2} \tag{5.29}$$

where (x_k^i, y_k^i) and $(\hat{x}_k^i, \hat{y}_k^i)$ denote the true and estimated target positions at time k at the ith MC trial.

Figure 5.5 side a) shows the RMS error curves corresponding to four different target detection probabilities $P_D = \{1.0, 0.9, 0.8, 0.7\}$. As expected, low target detection probabilities leads to a degradation on the accuracy of the target tracking. However, in spite of the multiple spurious bearing measurements at each sensor scan, a target detection probability of less than the unity and the use of a low-complexity target motion model, the proposed algorithm exhibits a high performance with errors ranging from 0 to 300 m. Furthermore, the use of road network information does not require an observer maneuver to deal with the problem of observability of the range in the target state vector. In our approach, the initial range in the target

state vector depends on the position of the observer, as well as the position of the particles on specific roads. At the beginning of the tracking process, particles may be distributed over several roads, however, as the target passes from one road to another only on cloud of particles will survive and will give the estimate of the target state vector, without any observer maneuver.

It should be noticed that, for a fixed target detection probability, the highest RMS position errors are observed at the beginning of the target tracking process (0.41 minutes) and when the target travels through road segment $\overline{\text{N4N18}}$ (4.35-5.40 minutes), see 5.5 side a). The former case is due to the initialization process, where particles, initially lying in several roads encountered along the LOS direction produce several clouds traveling trough such roads and thus, producing an estimated target position far away from the true one. However, as the new measurements become available there is only one possible cloud that fits the constrained motion model and the target is then positioned onto one road. The latter case, is due to the relative movement between target and observer, which produces LOS bearings almost parallel to the road segment $\overline{\text{N4N7}}$, increasing uncertainty about the road in which the target is actually evolving.

Figure 5.5 side b) depicts the average over the trajectories followed by the target for 100MC trials. As we can see, even for a target detection probability of 0.7, in most of the cases the estimated trajectory is the right one. This can be deduced by noticing that the average trajectory resembles more to the true one that any other composed trajectory in the road network.

Finally, figure 5.6 presents simulation results for the same scenario but using a classical particle filter (without the regularization step) and without using the batch procedure. As we can see in figure 5.6 side a) the general accuracy on the position estimation is lower than that one obtained using the proposed approach (compare with 5.5 side a)). It should be noticed that, because of the absence of the batch procedure to initialize particles, the error obtained at the beginning of the tracking process is considerably bigger.

5.4 Conclusions

We proposed a new batch-recursive bearings-only tracking algorithm for ground moving targets constrained to roads, able to handle multiple bearing measurements in clutter. Observer maneuver may not be a requirement because the information provided by the road network improves observability of the state vector. Simulation results showed a high accuracy of target tracking using simple target motion models, even for a low target detection probabilities.

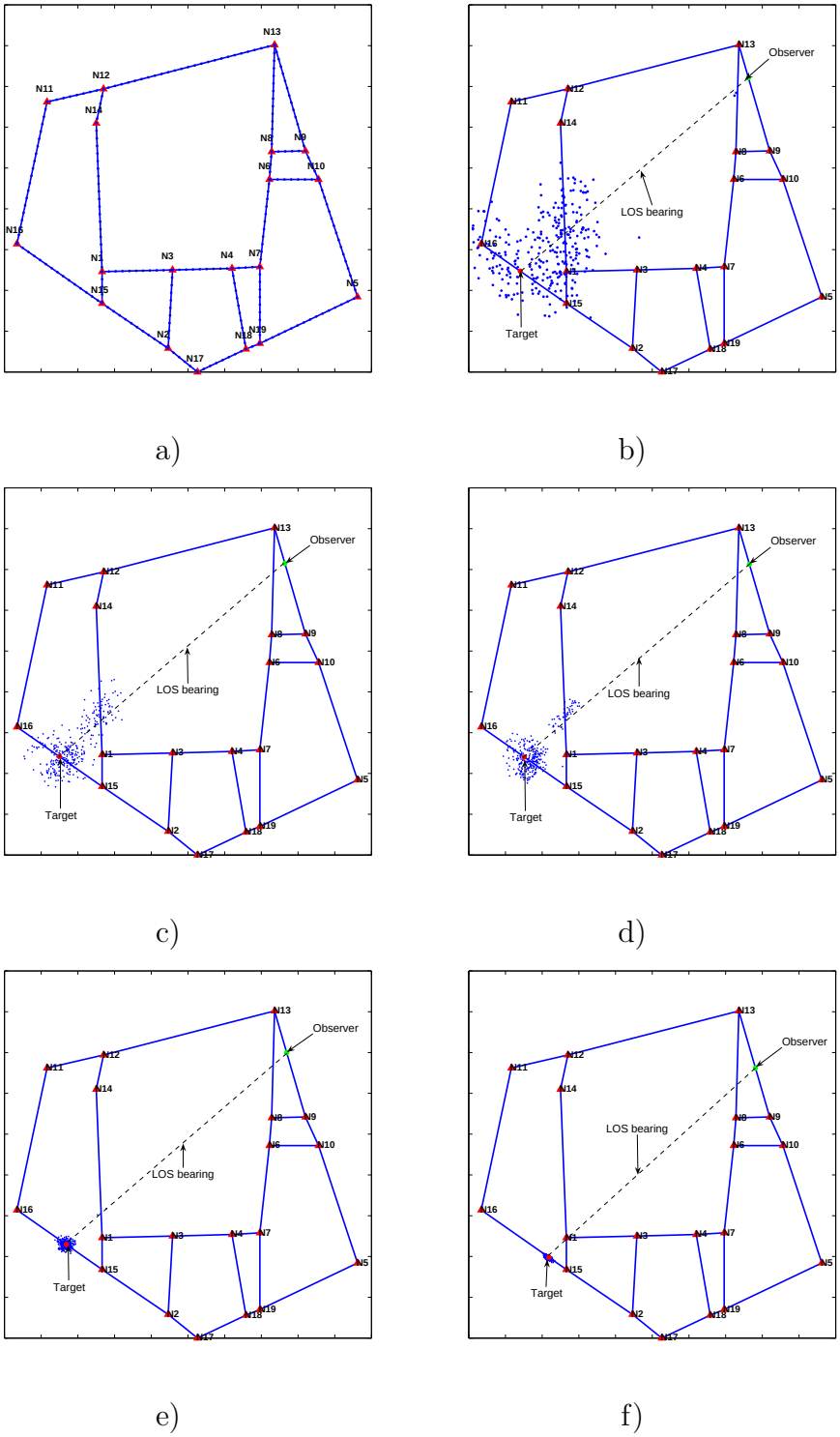

Figure 5.1: a) initial particles are distributed over the entire road network. Sequence b) to d) shows particles to concentrate in roads lying in the LOS direction. The new available measurements together with the target's velocity constraint make one of the clouds become more likely than the others e) and f).

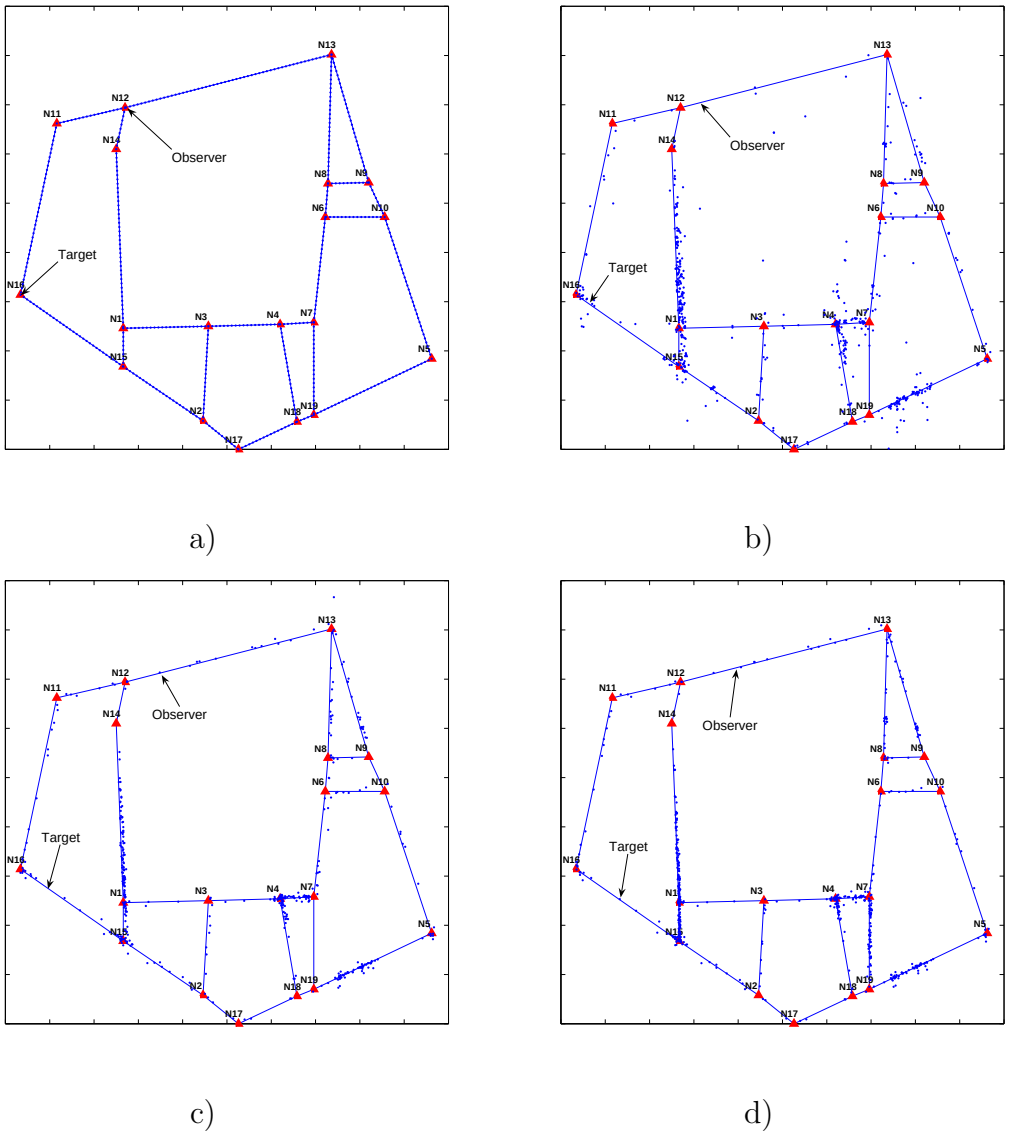

Figure 5.2: a) initial particles are distributed over the entire road network. Sequence b), c) and d) shows particles to concentrate in wrong roads because of a low probability of target detection $P_D = 0.5$ and the presence of multiple spurious bearing measurements at each time scan.

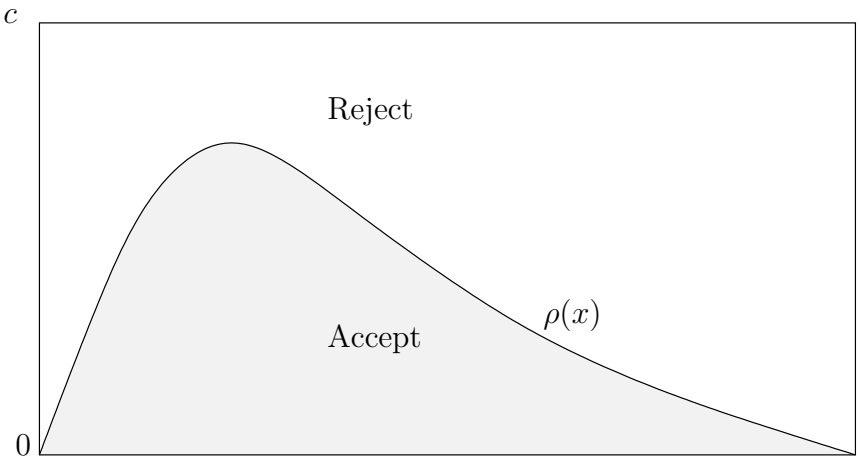

Figure 5.3: Acceptance and rejection regions for a density

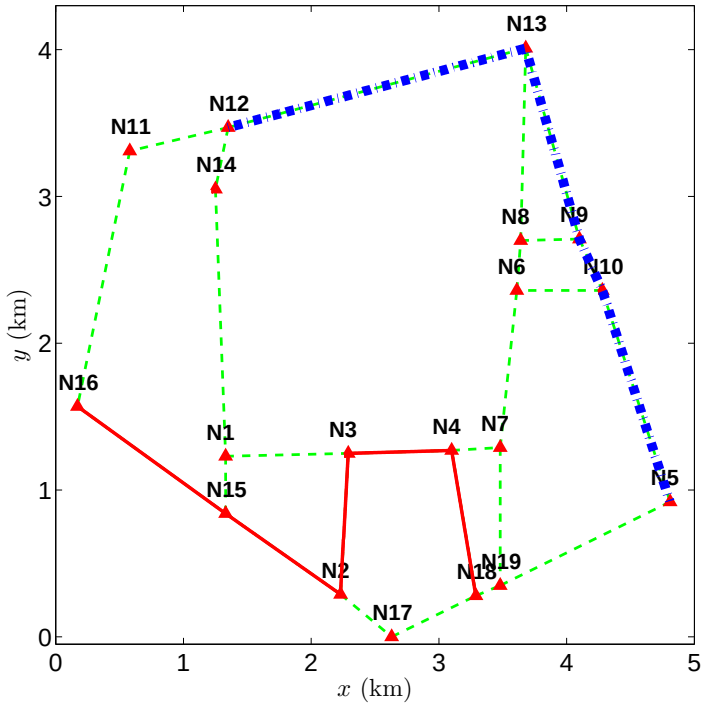

Figure 5.4: Simulation scenario: dashed lines and solid triangles represent respectively the road segments and nodes of the road network. Bottom solid trajectory represents the target path. Top doted trajectory is the observer's path.

Algorithm 6

Batch stage (ML approach):

1. Collect N_m bearing measurements and solve (5.19) to obtain $(\hat{\theta}_{\text{LOS}}, \hat{\sigma}^2_{\text{LOS}})$.
2. Propose N particles $\{\boldsymbol{\chi}^i_{N_m}\}^N_{i=1}$; with position components taken from equally spaced points distributed over the roads in the surveillance region. Set the velocity components to zero and their weights to $\{\omega^i_{N_m} = 1/N\}^N_{i=1}$.
3. Transform particles from cartesian to modified polar coordinates using (E.9).

Recursive stage (RPF):

1. Compute weights using (5.10) considering $\mathbf{y}_{N_m} = \hat{\theta}_{\text{LOS}}$ and $\sigma^2_\theta = \hat{\sigma}^2_{\text{LOS}}$.
2. Resample with replacement and set $\{\omega^i_{N_m} = 1/N\}^N_{i=1}$.
3. Set $k = N_m$
4. FOR $i = 1 : N$
   - *Draw particles*: $\boldsymbol{\chi}^i_{k+1} \sim p(\boldsymbol{\chi}_{k+1}|\boldsymbol{\chi}^i_k)$, using (5.2).
   - *Road segment assignment*: Find the nearest road segment s to particle i using the procedure described in section 5.2.3, and assign a constrained dynamic model accordingly. Keep the corresponding distances $\{d^i_k\}^N_{i=1}$.
   - *Measurement update*: Update the weights using (5.10) and normalize them.
5. END FOR
6. *Estimation:* Take $\hat{\boldsymbol{\chi}}_k \approx \sum^N_{i=1} \omega^i_k \boldsymbol{\chi}^i_k$ as an approximation to the MMS estimate.
7. *Regularization*: If $N_{\text{eff}} < N_{\text{thr}}$, eq. (6.32), reset the weights to $\omega^i_k = 1/N$, and
   - Compute the empirical covariance matrix as $\hat{\boldsymbol{\Sigma}}_k \approx \sum^N_{i=1} \omega^i_k (\boldsymbol{\chi}^i_k - \hat{\boldsymbol{\chi}}_k)(\boldsymbol{\chi}^i_k - \hat{\boldsymbol{\chi}}_k)^T$.
   - Compute $\boldsymbol{\Delta}_k$ such that $\boldsymbol{\Delta}_k \boldsymbol{\Delta}^T_k = \hat{\boldsymbol{\Sigma}}_k$.
   - Resample with replacement.
   - FOR $i = 1 : N$
   - Draw $\epsilon^i \sim K$ from the Epanechnikov kernel
   - Set $\boldsymbol{\chi}^i_k = \boldsymbol{\chi}^i_k + h\boldsymbol{\Delta}_k \epsilon^i$
   - END FOR
8. Set $k = k + 1$ and repeat from 4.

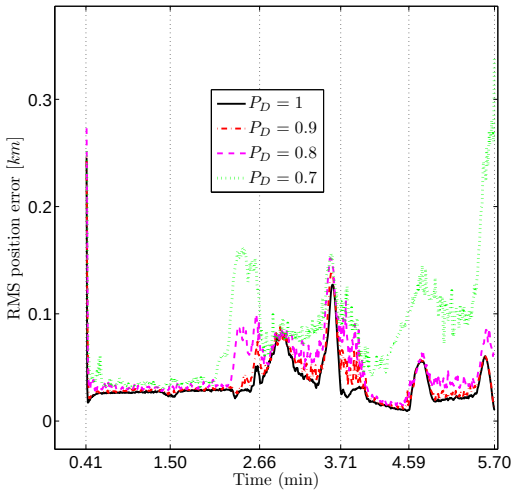

a)

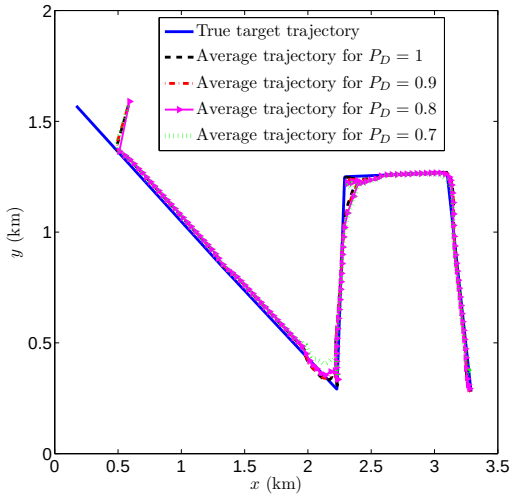

b)

Figure 5.5: Simulation results using the proposed algorithm (regularized particle filter and with the batch stage to initialize particles): a) RMS error on the position estimation versus time and b) actual and average trajectories from 100 MC runs.

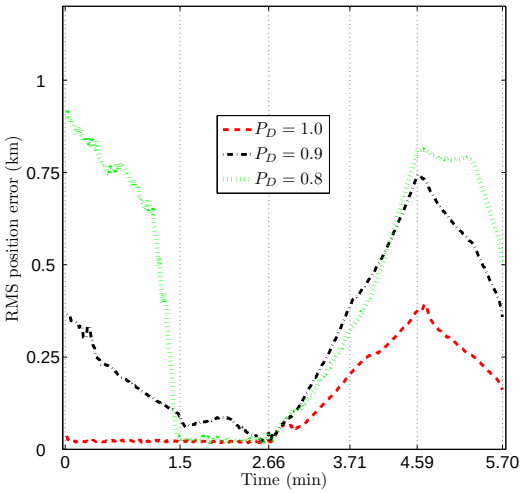

a)

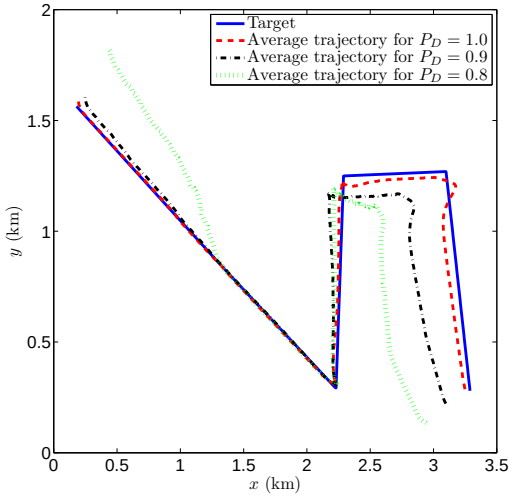

b)

Figure 5.6: Simulation results using the proposed approach (but using an standard particle filter and without the batch stage to initialize particles): a) RMS error on the position estimation versus time and b) actual and average trajectories from 100 MC runs.

Chapter 6

Multiple target tracking with road constraints

Multiple-target tracking is an essential requirement for surveillance systems employing one or more sensors, together with computer subsystems, to interpret the environment. Typical sensor systems, such as radar, infrared, and sonar, report measurements from diverse sources: targets of interest, background noise sources such as radar ground clutter, or internal error sources such as thermal noise. The multitarget tracking objective is to partition the sensor data into sets of observations, or tracks, produced by the same source. Once tracks are formed and confirmed (so the background and other false targets are reduced), the number of targets can be estimated and quantities, such as target velocity, future predicted position, and target classification characteristics can be computed for each track.

While the signal environment for ground targets is challenging, roads and terrain often provide motion constraints that are more rigid than those found, for instance, in airborne and maritime tracking applications. As it was seen in the previous chapter, these constraints constitute an additional information source that can be exploited to improve tracking performance. In this chapter we propose a novel procedure to constraint the dynamics of ground moving targets evolving on constrained paths. Specifically, we propose to include road network information by constraining the target dynamics solely. Furthermore, we exploit two more features included in digital maps: i) the sense of the road, and ii) the probability to take an specific road while crossing an intersection (traffic flow).

The proposed approach is tested under a multiple ground target tracking scenario: where a known number of targets evolving in a surveillance region, constrained by roads, are tracked from LOS measurements performed by one (or more) static (or moving) sensor(s). Track maintenance is performed

by the Monte Carlo joint probabilistic data association filter (MC-JPDAF), which approximates with particles the marginal filtering distributions for each of the targets. Therefore, avoiding the course of dimensionality as the number of target increases.

This chapter is organized as follows: In section 6.1 we explain additional characteristics included in road networks, and its importance to consider some of them to model the target state dynamics. Section 6.2 proposes a representation of the target state vector, as well as the state dynamics which includes road network information. In section 6.3 the state space and measurement equations for the problem of multiple-observer multiple-target tracking with road constraints is presented. Section 6.4 presents the MC-JPDAF and its implementation. In section 6.5 we present some simulation results. Finally, in section 6.6 we give the conclusions.

6.1 Exploiting road network information for tracking ground moving targets

One of the main objectives is to make ground target tracking algorithms more robust. One idea to achieve this is to take traffic information into account. As described in chapter 4, digital maps does not only contain coordinates of the road segments of the road network, but also a lot of additional information. Some examples of the information provided are:

1. Speed limit.
2. Size of the road.
3. Whether the road is one way or not.
4. Accuracy of the coordinates.
5. Traffic flow.

It is not surprising that including as much traffic information as possible into the tracking algorithms will enhance their accuracy and robustness for ground target tracking. However, the inclusion of each constraint may render ground target tracking algorithms difficult to implement. Therefore, in order to conceive easy-to-implement tracking algorithms able to exploit road network information, one must identify those information which will have an important impact on the target tracking accuracy. For example, at junctions, target motion uncertainty increases, because the target can move along any

of the roads meeting at the junction. Thus, the inclusion of probability factors describing the preferred direction taken in a particular junction (traffic flow) can help to reduce such an uncertainty. On the other hand, when a target is moving along a road, its motion uncertainty is expected to be in the way of the road. Thus, knowing the sense of the road the uncertainty on the target position and velocity components can be tuned accordingly. Hence, in what follows we consider the inclusion of : one-way or two-way roads and traffic flow information.

6.2 Road Constrained Target dynamics

Given a target evolving in a known road network, composed by a large collection of roads and including the traffic information discussed above. We propose to model the target state vector at time k as

$$\mathbf{x}_k = \begin{bmatrix} (i,j)_k \\ d_k \\ v_k \end{bmatrix} \tag{6.1}$$

where

- $(i,j)_k$ stands for the couple of nodes defining the road segment going from node i to node j, in which the target is evolving at time k,
- $d_k \in \mathbb{R}^+$ is the distance between node i and the current position of the target, and
- $v_k \in \mathbb{R}^+$ is the speed of the target onto the road, see figure 6.1 side a).

In the following we let

- $\lambda_{(i,j)_k}$ be the length of the road segment $(i,j)_k$, and
- Children(i) be a road network operator providing the set of nodes descendant from node i (see example in figure 6.2 side a)).

Now, assume that: *i)* a target can turn back over the same road only if it is crossing one of the two end points of such a road (and under the condition of being a two-way road), and *ii)* an uniform discretisation with a sampling period of T seconds. Therefore, under the considerations given so far, the target state evolution is given by the algorithm 7.

It should be notice that following algorithm 7, the pdf of the target's position over a given road $(i,j)_k$ is a truncated Gaussian. The left Gaussian's

Algorithm 7 : Target state evolution

Compute:

$$d' = d_k + \underbrace{v_k T + \epsilon_k}_{\delta} \tag{6.2}$$

where ϵ_k is a Gaussian random variable with zero-mean and variance σ_d^2.

- if $\delta < 0$, we reiterate equation (6.2),
- otherwise ($\delta \geq 0$)
  - if $d' \leq \lambda_{(i,j)_k}$, then

$$\mathbf{x}_{k+1} = \begin{bmatrix} (i,j)_k \\ d' \\ v_k + \chi_k \end{bmatrix}$$

  - otherwise ($d' > \lambda_{(i,j)_k}$), then

$$\mathbf{x}_{k+1} = \begin{bmatrix} (j,\psi_k)_k \\ d' - \lambda_{(i,j)_k} \\ v_k + \chi_k \end{bmatrix}$$

    where χ_k is a Gaussian random variable with zero-mean and variance σ_v^2, ψ_k is a sequence of independent discrete random variables taking its values from Children(j_k) with known pdf given by $p_{j_k}(\psi_k)$.

It is assumed that the random sequences ϵ_k, χ_k, and ψ_k are jointly independent.

tail is truncated by the position of the target at time k, and the right Gaussian's tail is truncated at node j_k and shared out among the roads connected to j_k, with a weight given by $p_{j_k}(\psi_k)$, see figure 6.1 side b).

Notice also that, exploiting uniquely the collection of nodes in the road network, a target crossing a particular node i is supposed to be able to move along any of the roads meeting at that node or similarly towards the descendant nodes of i, given by Children(i). In such a situation, the set of possible roads is given by the couple of nodes of the form (i, ψ_k), where $\psi_k \in$Children(i). Now, using the approach presented above, which exploits road sense and traffic flow some of the roads connected to i be ban for the target, and the rest of them will have an non-zero probability to be taken, see example in figure 6.2 side a) and b).

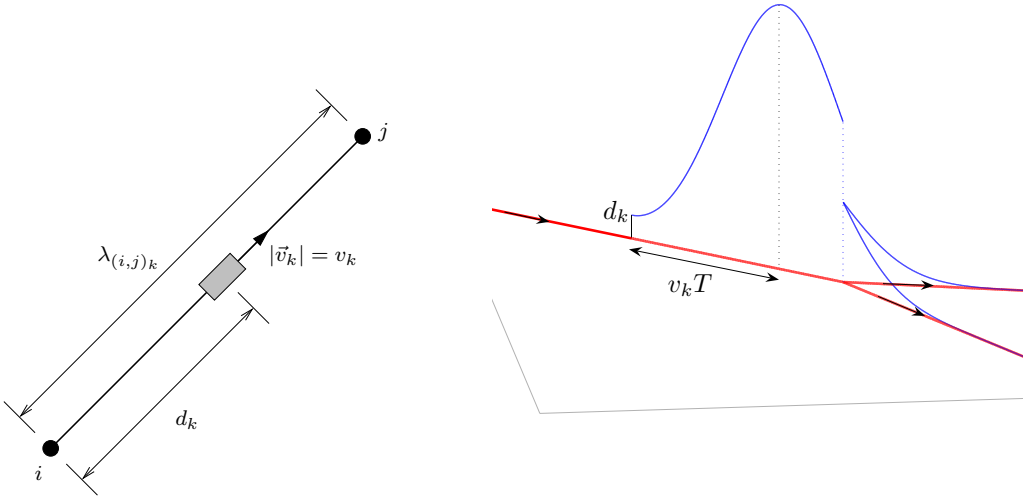

a) b)

Figure 6.1: Target on road: a) Components of the target state vector at time k, and b) Probability distribution of the target's position at time $k+1$, while approaching a junction, equal probabilities to go on a specific direction is considered.

6.3 Model description for multiple-observer multiple-target tracking with road constraints

In this section we introduce the details of modeling the multi-target state vector, as well as the measurements used to track a known number of targets evolving in a road network. We also describe the data association problem and formulate the likelihood conditional on a known association hypothesis.

6.3.1 State-space of constrained targets

Consider a known number of targets M moving along a road network, where targets are assumed to respect the motion constraints imposed by the road network, i.e. to travel a road only in the permitted direction. Under such

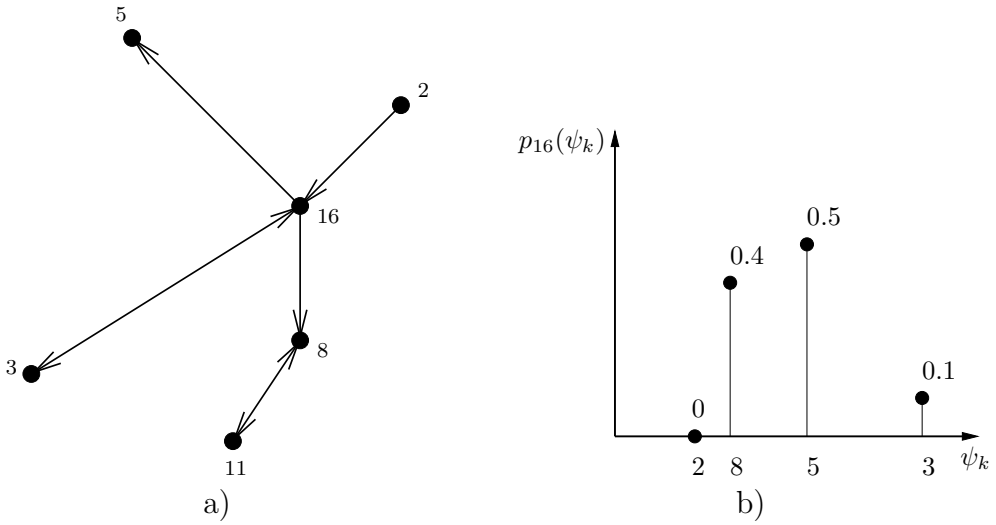

Figure 6.2: a) A target crossing a node (black-filled circles) can move towards its descendant nodes, i.e. if the target is crossing node 16 the possible nodes are Children(16)=$\{2, 3, 5, 8\}$, b) The probability to go towards a specific node is given by the traffic flow information at that particular node.

considerations, each target is parameterized by a state $\mathbf{x}_{t,k}$, $t = 1 \dots M$, whose structure is given by equation (6.1). The combined multi-target state is constructed as the concatenation of the individual target states as:

$$\mathbf{x}_k = (\mathbf{x}_{1,k} \dots \mathbf{x}_{M,k}).$$

The individual targets are assumed to evolve independently according to the Markovian dynamic process described in algorithm 7, with pdf $p_t(\mathbf{x}_{t,k}|\mathbf{x}_{t,k-1})$, $t = 1 \dots M$. This implies that the pdf for the multi-target state factorizes over the pdf of the individual targets as:

$$p(\mathbf{x}_k|\mathbf{x}_{k-1}) = \prod_{t=1}^{M} p_t(\mathbf{x}_{t,k}|\mathbf{x}_{t,k-1}).$$

Notice that $\mathbf{x}_{t,k} = \begin{bmatrix}(i,j)_k & d_k & v_k\end{bmatrix}^T$ provides the position and magnitude of the velocity vector of a target traveling along the road segment (i, j). To obtain the position and velocity components of the target into a specific reference system it must be traduced accordingly. Thus, considering the cartesian coordinate system as the position reference system, see figure 6.3, the components of the four dimensional state vector $\mathbf{x}^C_{t,k}$ corresponding to

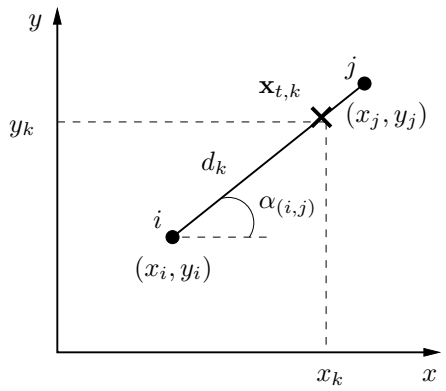

Figure 6.3: Relation between the position of a target in the road segment (i, j) and its position on the Cartesian coordinate system.

target t are given by

$$x_k^C = x_i + d_k \cos(\alpha_{(i,j)}) \tag{6.3}$$
$$y_k^C = y_i + d_k \sin(\alpha_{(i,j)}) \tag{6.4}$$
$$\dot{x}_k^C = v_k \cos(\alpha_{(i,j)}) \tag{6.5}$$
$$\dot{y}_k^C = v_k \sin(\alpha_{(i,j)}) \tag{6.6}$$

where

$$\alpha_{(i,j)} = \tan^{-1}\left(\frac{y_j - y_i}{x_j - x_i}\right) \tag{6.7}$$

is the angle between the road segment (i, j) and the direction of x-axe, and where (x_i, y_i) and (x_j, y_j) stand, respectively, for the position coordinates of the nodes i and j defining the road where the target is evolving.

In the recursive procedure we will present latter, the target state vector we estimate is $\mathbf{x}_{t,k}$, and $\mathbf{x}_{t,k}^C$ is used for plotting purposes, as well as position error computation.

6.3.2 Measurements

Measurements for multi-target tracking are assumed to be available from N_o observers. The observers are supposed to be fixed or moving and their positions at any given time are denoted by $\mathbf{p}_k^i$, $i = 1 \dots N_o$. At any given time the combined set of measurements from all the observers is denoted by

$$\mathbf{y} = (\mathbf{y}^1 \dots \mathbf{y}^{N_o}),$$

where $\mathbf{y}^i = [\mathbf{y}_1^i \dots \mathbf{y}_{M^i}^i]$ is the vector comprising the M^i measurements at the i-th observer. Note that the number of measurements at each observer

can vary with time. The nature of the individual measurements $\mathbf{y}_j^i$ will depend on the characteristics of the sensors. Typically each measurement will correspond to an estimated line of sight from the observer location to the measurement source. Measurements do not only arise from the targets to be tracked. Additional clutter measurements may result due to multipath effects, spurious objects, sensor errors, etc. It is assumed that each of the targets can generate at most one measurement per sensor at a particular time step, but may go undetected. It is further assumed that several or all measurements may be due to clutter.

Data association

Data association is the process of associating observations with targets or similarly targets to observations. In order to deal with this problem it is necessary to define a set of association variables, which we specified as target to measurement associations. Thus, a target t to measurement j association at observer i is denoted as

$$r_t^i = \begin{cases} 0 & \text{if target } t \text{ is undedected at observer } i \\ j \in \{1 \dots M^i\} & \text{if target } t \text{ generated measurement } j \text{ at observer } i. \end{cases} \tag{6.8}$$

and the set of target to measurement associations r_t^i, for $t = 1 \dots M$ are arranged into the association vector

$$\mathbf{r}^i = (r_1^i \dots r_M^i)$$

A target to measurement association hypothesis for the measurements at the i-th observer is denoted by

$$\boldsymbol{\lambda}^i = (\mathbf{r}^i, M_C^i, M_T^i),$$

where M_C^i is the number of measurements associated to clutter, and M_T^i the number of measurements associated to a target. Note that the total number of measurements at observer i for a given time can be expressed as $M^i = M_C^i + M_T^i$. Finally, a target to measurement association hypothesis accounting for the observations performed by the N_o observers is denoted by

$$\boldsymbol{\lambda} = (\boldsymbol{\lambda}^1 \dots \boldsymbol{\lambda}^{N_o}).$$

Likelihood

Conditional on the association hypothesis we assume the measurements at a particular observer to be independent of each other. Hence, the conditional pdf at observer i of a measurement given the association hypothesis is given by

$$p(\mathbf{y}^i|\mathbf{x},\boldsymbol{\lambda}^i) = \prod_{j\in\mathcal{I}_0^i} p_C^i(\mathbf{y}_j^i) \cdot \prod_{j\in\mathcal{I}^i} p_T^i(\mathbf{y}_j^i|\mathbf{x}_{t(j)}) \tag{6.9}$$

where $\mathcal{I}_0^i = \{j = 1\dots M^i : j \notin \{r_1^i \dots r_M^i\}\}$ and $\mathcal{I}^i = \{j = 1\dots M^i : j \in \{r_1^i \dots r_M^i\}\}$ are, respectively, the subsets of measurement indices at the i-th observer corresponding to clutter measurements and measurements from targets to be tracked. The function $t(j) = \{t : r_t^i = j, j \in \{1,\dots M^i\}\}$ is an index indicator function providing the target index t to which the measurement j is assigned. In the above p_C^i denotes the clutter likelihood model for the i-th observer, which is usually asumed to be uniform over the volume of the measurement space V^i. The likelihood for a measurement at the i-th observer associated with a particular target, denoted by p_T^i, depends only on the state of the target with which it is associated. Under these assumptions and considering independence between measurements performed at different observers we can write

$$p(\mathbf{y}|\mathbf{x},\boldsymbol{\lambda}) = \prod_{i=1}^{N_o} \left[(V^i)^{-M_C^i} \prod_{j\in\mathcal{I}^i} p_T^i(\mathbf{y}_j^i|\mathbf{x}_{t(j)}) \right]. \tag{6.10}$$

There is an increasingly utilization in multiple target tracking of passive sensors that produce no range measurements. In such a situation, sensors yield LOS bearing measurements of the targets relative to the observers in the xy plane, the individual measurements at the i-th observer can be written as $\mathbf{y}_j^i = \theta_j^i$, where θ_j^i is the bearing angle from the source to the observer, measured anti-clockwise from the x axis. Assuming the LOS bearings to be corrupted by independent Gaussian noise, the likelihood for the j-th measurement, under the hypothesis that it is associated with the t-th target, becomes

$$p_T^i(\mathbf{y}_j^i|\mathbf{x}_t) = \mathcal{N}(\mathbf{y}_j^i; \hat{\theta}_t^i, \sigma_{\theta^i}^2)$$

where $\sigma_{\theta^i}^2$ is the fixed noise variance, and $\hat{\theta}_t^i$ is given by

$$\hat{\theta}_t^i = \tan^{-1}\left(\frac{y_t^C - y_o^i}{x_t^C - x_o^i}\right) \tag{6.11}$$

with $\mathbf{p}_o^i = (x_o^i, y_o^i)$ the position of observer i and (x_t^C, y_t^C) the position of target t. For this measurement model the volume of the measurement space for the i-th observer is $V^i = 2\pi$.

6.3.3 Association Prior

In most situations of practical interest the association hypothesis is unknown, and thus needs to be estimated alongside the other unknowns, or marginalized from the problem. To achieve this within a Bayesian framework it is necessary to define a prior distribution over the association hypothesis. It is assumed that the prior for the association hypothesis to be independent of the state and past values of the association hypothesis. Thus, it is assumed that the prior factorizes over the observers as

$$p(\boldsymbol{\lambda}) = \prod_{i=1}^{N_o} p(\boldsymbol{\lambda}^i).$$

Note that given $\boldsymbol{\lambda}^i$, the number of clutter measurements M_C^i, as well as the number of target measurements M_T^i are completely defined. Therefore

$$p(\boldsymbol{\lambda}^i) = p(\mathbf{r}^i, M_C^i, M_T^i)$$

The above probability can be written as

$$p(\boldsymbol{\lambda}^i) = p(\mathbf{r}^i | M_C^i, M_T^i) p(M_C^i, M_T^i) \tag{6.12}$$

The first factor is obtained by observing that in event $\boldsymbol{\lambda}^i$, the set of targets assumed detected contains $M^i - M_C^i$ targets. The number of target to measurement assignment events $\boldsymbol{\lambda}^i$ in which the same set of targets is detected is given by the number of permutations of the M^i measurements taken as $M^i - M_C^i$, the number of targets assigned to a measurement under the same detection event. Therefore, assuming each such event a priori equally likely, one has

$$\begin{aligned} p(\mathbf{r}^i | M_C^i, M_T^i) &= \left(P_{M^i - M_C^i}^{M^i} \right)^{-1} \\ &= \left(\frac{M^i!}{M_C^i!} \right)^{-1} \\ &= \frac{M_C^i!}{M^i!} \end{aligned} \tag{6.13}$$

The last factor in (6.12) is

$$p(M_C^i, M_T^i) = \prod_{t=1}^{M} (P_D^{t,i})^{\delta_t} (1 - P_D^{t,i})^{1-\delta_t} \mu_F(M_C^i) \tag{6.14}$$

where $P_D^{t,i}$ is the detection probability of target t at observer i, δ_t is an indicator function which equals 1 if target t is associated to a measurement

and 0 if it is undetected in the event $\boldsymbol{\lambda}^i$ under consideration. $\mu_F(M_C^i)$ is the prior PMF of the number of clutter measurements. Two models can be used for this PMF:

1. Parametric model: a Poisson density,

$$\mu_F(M_C^i) = \frac{(\lambda_c^i)^{M_C^i}}{M_C^i!}\exp(-\lambda_c^i), \qquad M_C^i = 0, 1, 2, \ldots \tag{6.15}$$

   where λ_c^i is the expected number of clutter measurements at observer i.

2. Nonparametric model: a "diffuse prior"

$$\mu_F(M_C^i) = \frac{1}{N}, \qquad M_C^i = 0, 1, 2, \ldots, N-1 \tag{6.16}$$

   where N may be as large as is necessary.

Finally, combining (6.13) and (6.14) into (6.12) yields the prior probability of a joint association event $\boldsymbol{\lambda}^i$ as

$$p(\boldsymbol{\lambda}^i) = \frac{M_C^i!}{M^i!}\mu_F(M_C^i)\prod_{t=1}^{M}(P_D^{t,i})^{\delta_t}(1-P_D^{t,i})^{1-\delta_t} \tag{6.17}$$

6.4 Monte Carlo JPDAF

The Joint Probability Data Association Filter (JPDAF) is probably the most widely applied and successful strategy for multi-target tracking under data association uncertainty. The JPDAF compute a Bayesian estimate of the correspondence between targets to be tracked and measurements performed by sensors. Mostly, all existing approaches to tracking multiple targets apply Kalman filters to estimate the states of the individual targets. However, while Kalman filters have been shown to provide highly efficient state estimates, they are restricted to linear and Gaussian distributions of the state and measurement models.

When tracking ground moving targets using road network information, which is the application we are interested in, the incorporation of such an information generally renders the dynamic process non-linear and non-Gaussian. Therefore, a particle filter approach of the problem is more suitable. The major advantage of using particle filters is that they can represent multi-modal state densities, a property which will be very useful in

our application, because of the approach adopted to deal with target transitions between roads meeting at junctions. The Monte Carlo JPDAF (MC-JPDAF) [70, 87] is a particle filter implementation of the general JPDAF framework [9], which combines the particle filters to track the states of the targets and applies JPDAFs to assign targets to measurements. Since the MC-JPDAF has been chosen as the filter to test our approach we present in the sections below the background and implementation of such a filter adapted to our problem.

6.4.1 JPDAF framework

To keep track of multiple moving targets one generally has to estimate the joint probability distribution of the state of all targets $p(\mathbf{x}_k|\mathbf{y}_{1:k})$. This, however, is difficult in practice even for a small number of objects since the size of the state space grows exponentially in the number of targets [70]. The JPDAF effectively combats the curse of dimensionality by recursively updating the marginal filtering distributions for each of the targets $p_t(\mathbf{x}_{t,k}|\mathbf{y}_{1:k})$, $t = 1 \dots M$, through the Bayesian sequential estimation recursions

prediction step:

$$p_t(\mathbf{x}_{t,k}|\mathbf{y}_{1:k-1}) = \int p_t(\mathbf{x}_{t,k}|\mathbf{x}_{t,k-1}) p_t(\mathbf{x}_{t,k-1}|\mathbf{y}_{1:k-1}) d\mathbf{x}_{t,k-1} \tag{6.18}$$

filtering step:

$$p_t(\mathbf{x}_{t,k}|\mathbf{y}_{1:k}) \propto p_t(\mathbf{y}_k|\mathbf{x}_{t,k}) p_t(\mathbf{x}_{t,k}|\mathbf{y}_{1:k-1}) \tag{6.19}$$

Notice, however, that unlike the prediction step which proceeds independently for each target, the filtering step cannot be performed independently for the individual targets due to data association uncertainty in the likelihood for the t-th target $p_t(\mathbf{y}_k|\mathbf{x}_{t,k})$. The JPDAF gets around this difficulty by performing a soft assignment of targets to measurements according to the corresponding posterior probabilities of these marginal associations. More specifically, it achieves this by defining the likelihood for the t-th target as

$$p_t(\mathbf{y}_k|\mathbf{x}_{t,k}) = \prod_{i=1}^{N_o} \left[\beta_{0,t}^i + \sum_{j=1}^{M^i} \beta_{j,t}^i p_T^i(\mathbf{y}_{j,k}^i|\mathbf{x}_{t,k}) \right]$$

where

$$\beta_{j,t}^i = p(r_{t,k}^i = j|\mathbf{y}_{1:k}), \tag{6.20}$$

with $j = 1 \dots M^i$, is the posterior probability that the t-th target is associated with j-th measurement, with $\beta_{0,t}^i$ the posterior probability that the t-th target is undetected. The likelihood is assumed independent over the observers. The component of the likelihood for each observer is a mixture, with one mixture component for each possible target to measurement association, and the mixture weights equal to the posterior probabilities of the corresponding marginal associations. The posterior probabilities of the marginal associations $\beta_{j,t}^i$, are obtained from the joint association probabilities by summing over all the joint avens in which the marginal event of interest occurs. More formally we compute

$$\beta_{j,t}^i = \sum_{\boldsymbol{\lambda}_k^i \in \boldsymbol{\Lambda}_k^i : r_{t,k}^i = j} p(\boldsymbol{\lambda}_k^i | \mathbf{y}_{1:k}) \tag{6.21}$$

where $\boldsymbol{\Lambda}_k^i$ is the set of all valid target to measurement association hypothesis for the data at the i-th observer and where $i = 1 \dots N_o$ ranges over the observers, $j = 0 \dots M^i$ ranges over the measurements, with 0 signifying that the target in question is not associated with any of the measurements, and $t = 1 \dots M$ ranges over the targets.

The derivation of the probabilities of the joint events is done using Bayes' rule. Hence, assuming independence between the set of measurements $\{\mathbf{y}_k^1 \dots \mathbf{y}_k^{N_o}\}$ over the observers such probabilities can be computed according to

$$\begin{aligned} p(\boldsymbol{\lambda}_k^i | \mathbf{y}_{1:k}) &= p(\boldsymbol{\lambda}_k^i | \mathbf{y}_k, \mathbf{y}_{1:k-1}) \\ &= \frac{1}{c} p(\mathbf{y}_k | \boldsymbol{\lambda}_k^i, \mathbf{y}_{1:k-1}) p(\boldsymbol{\lambda}_k^i | \mathbf{y}_{1:k-1}) \\ &= \frac{1}{c'} p(\mathbf{y}_k^i | \boldsymbol{\lambda}_k^i, \mathbf{y}_{1:k-1}) p(\boldsymbol{\lambda}_k^i) \end{aligned}$$

where c and c' are normalization constants and the irrelevant prior conditioning term has been omitted in the last line of the equation. Furthermore, assuming independence between the individual measurements at each of the observers the above expression can be written as

$$p(\boldsymbol{\lambda}_k^i | \mathbf{y}_{1:k}) \propto p(\boldsymbol{\lambda}_k^i) (V^i)^{-M_C^i} \prod_{j \in \mathcal{I}^i} p_{t(j)}(\mathbf{y}_{j,k}^i | \mathbf{y}_{1:k-1}) \tag{6.22}$$

where $p(\boldsymbol{\lambda}_k^i)$ is the joint association prior given by (6.17), and $p_t(\mathbf{y}_{j,k}^i | \mathbf{y}_{1:k-1})$ is the predictive likelihood for the j-th measurement at the i-th observer using the information from the t-th target, given in the standard way by

$$p_t(\mathbf{y}_{j,k}^i | \mathbf{y}_{1:k-1}) = \int p_T^i(\mathbf{y}_{j,k}^i | \mathbf{x}_{t,k}) p_t(\mathbf{x}_{t,k} | \mathbf{y}_{1:k-1}) d\mathbf{x}_{t,k}. \tag{6.23}$$

In its original version the JPDAF [9] assumes linear and Gaussian forms for the dynamic and likelihood models, and a Gaussian approximation for the filtering distribution. Under these assumptions Kalman filter updates are obtained for the one step ahead prediction distribution in (6.18) and the predictive likelihood in (6.23). The mixture likelihood in (6.20) is collapsed into a single Gaussian, so that a Kalman filter update is also obtained for the filtering distribution in (6.19). On the other hand, in order to reduce computation burden in the computation of the marginal posterior probabilities (6.21), the JPDAF uses gating techniques to eliminate unlikely target-to-measurements pairings. Such a gating procedure is explained below.

Gating

Gating is a procedure that selects the measurements to be incorporated into the state estimator from among several candidates. This is performed by constructing for each target a validation region or gate using available information. Once the gate is constructed measurements falling within the target gate are considered as possible candidates to be associated with that particular target. Since gating applies independently to each observer, in the following discussion, we focus on a single observer, and drop the observer index i.

In order to construct the gates, consider a target t that is in track, i.e., its filter has at least been initialized. Assume that the predicted value of the true measurement, using information from target t, is $\hat{\mathbf{y}}_{t,k}$ with associated covariance matrix $\Sigma_{t,k}$. Assuming that the true measurement at time k, conditioned upon $\mathbf{y}_{1:k-1}$, is normally distributed,

$$p_t(\mathbf{y}_k|\mathbf{y}_{1:k-1}) = \mathcal{N}(\mathbf{y}_k; \hat{\mathbf{y}}_{t,k}, \Sigma_{t,k}) \tag{6.24}$$

one may define a region in the measurement space where the measurement will be found with some (high) probability:

$$\tilde{V}_{t,k}(\gamma) = \{\mathbf{y} : d^2_{t,k}(\mathbf{y}) \leq \gamma\} \tag{6.25}$$

where γ is a parameter to be explained below, and $d^2_{t,k}(\mathbf{y})$ is the squared distance based on the measurement innovations, given by

$$d^2_{t,k}(\mathbf{y}) = (\mathbf{y} - \hat{\mathbf{y}}_{t,k})^T (\Sigma_{t,k})^{-1} (\mathbf{y} - \hat{\mathbf{y}}_{t,k}) \tag{6.26}$$

The region defined by (6.25) is called the validation region or gate. It is the ellipse (or ellipsoid) of probability concentration-the region of minimum volume that contains a given probability mass under the Gaussian assumption.

γ	1	4	9	16	25
$n_{\mathbf{y}} = 1$	.683	.954	.997	.99994	1.0
$n_{\mathbf{y}} = 2$	.393	.865	.989	.9997	1.0
$n_{\mathbf{y}} = 3$	.199	.739	.971	.9989	.99998

Table 6.1: Gating thresholds and values of probability mass in the gate.

Measurements that lie inside the gate are considered valid; those outside are discarded.

The value of the parameter γ is related to the specified value of the probability mass to be included in the validation region. It can be obtained using the fact that $d^2_{t,k}(\mathbf{y})$ is approximately chi-squared distributed with number of degrees of freedom equal to the dimension of $\mathbf{y}$. Table 6.1 gives the probability mass

$$P_G = p(\mathbf{y}_k \in \tilde{V}_{t,k}(\gamma))$$

which is the probability that the (true) measurement will fall in the gate, for various values of γ and dimensions $n_{\mathbf{y}}$ of the measurement. However, this does not fully define the probability mass in the gate, because of the dependence on $n_{\mathbf{y}}$. The threshold γ is usually selected beforehand and kept constant for any given application.

It should be notice that the use of gates limits the volume of the measurement space for each target at each time step, given by $\tilde{V}_{t,k}(\gamma)$. Implying that the PDF of the clutter measurements associated to a specific target differs from the others, leading to more complex expressions for the probabilities of the events $\mathbf{\Lambda}_k$. Furthermore, it is necessary to replace the target detection probability P_D in the association prior with $P_D P_G$, and restrict the predictive likelihood in (6.22) to the validation region, i.e., normalized with P_G. However, the gating technique used here is a logic artifice to consider uniquely the joint events made up of marginal events involving validated measurements. Validation gates are thus used for the selection of "feasible joint events" but not in the evaluation of their probabilities. Therefore, the formulae presented so far remain the same. This logic, which avoids considering events whose probabilities are negligible and thus has a negligible effect on the other probabilities, is exemplified in figure 6.4.1 and explained below.

The set of valid target to measurement associations for the t-th target follows straightforwardly as

$$\mathcal{R}_t = \{j : d^2_{t,k}(\mathbf{y}_{j,k}) \leq \gamma\} \cup \{0\} \tag{6.27}$$

which allows each of the targets to be undetected to take account of the possibility that any or all of the measurements within the target validation

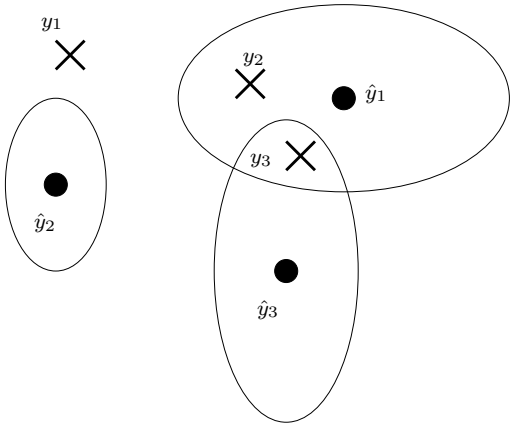

a)

Valid association hypothesis					
Without Gating			With Gating		
r_1	r_2	r_3	r_1	r_2	r_3
0	0	0	0	0	0
0	0	1	0	0	3
0	1	0	2	0	3
0	1	2	2	0	0
0	2	1	3	0	0
1	0	0			
1	0	2			
1	2	0			
⋮	⋮	⋮			

b)

Figure 6.4: Measurement gating: a) targets mapped into measurement space (circles) and their validation regions (ellipses). Only measurements (crosses) that fall inside validation region for a particular target are candidates to be associated with that target.

region may be due to clutter. In the example presented in figure 6.4.1, the valid association sets are $\mathcal{R}_1 = \{0, 2, 3\}$, $\mathcal{R}_2 = \{0\}$ and $\mathcal{R}_3 = \{0, 3\}$. The set of viable joint associations $\mathbf{\Lambda}_k$ can now be constructed by enumerating all the valid combinations of the elements in the marginal sets $\mathcal{R}_t$, $t = 1 \dots M$. The number of hypotheses obtained in this manner will typically be smaller than the number obtained by an exhaustive enumeration.

6.4.2 Implementation of the JPDAF with particles

The Monte Carlo implementation of the JPDAF presented in this section is a variant of the strategy proposed in [87] to track multiple targets constrained to roads with different target-observer pair detection probabilities, and arbitrary PMFs of clutter measurements. As in its original version it aims to represent the marginal filtering distributions for each of the targets with particles. More specifically, for the t-th target, assume that a set of samples $\{\omega_{t,k-1}^{(n)}, \mathbf{x}_{t,k-1}^{(n)}\}_{n=1}^{N}$ is available, approximately distributed according to the marginal filtering distribution at the previous time step $p_t(\mathbf{x}_{t,k-1}|\mathbf{y}_{1:k-1})$. At the current time step new samples for the target state are generated from a suitably constructed proposal distribution, which may depend on the old

state and the new measurements,

$$\mathbf{x}_{t,k}^{(n)} \sim q_t(\mathbf{x}_{t,k}|\mathbf{x}_{t,k-1}^{(n)}, \mathbf{y}_k), \qquad n = 1 \dots N.$$

Using these particles the predictive likelihoods in (6.23) can straightforwardly be approximated as

$$p_t(\mathbf{y}_{j,k}^i|\mathbf{y}_{1:t-1}) \approx \sum_{n=1}^{N} \alpha_{t,k}^{(n)} p_T^i(\mathbf{y}_{j,k}^i|\mathbf{x}_{t,k}^{(n)}) \tag{6.28}$$

where the predictive weights are given by

$$\alpha_{t,k}^{(n)} = \omega_{t,k-1}^{(n)} \frac{p_t(\mathbf{x}_{t,k}^{(n)}|\mathbf{x}_{t,k-1}^{(n)})}{q_t(\mathbf{x}_{t,k}|\mathbf{x}_{t,k-1}^{(n)}, \mathbf{y}_t)}, \qquad \text{with} \qquad \sum_{n=1}^{N} \alpha_{t,k}^{(n)} = 1.$$

The gates for each target can now be constructed by approximating the Gaussian mixture given by (6.28) into a single Gaussian, see (6.24), with mean and covariance matrix

$$\hat{\mathbf{y}}_{t,k}^i = \sum_{n=1}^{N} \alpha_{t,k}^{(n)} \hat{\mathbf{y}}_{t,k}^{i,(n)} \tag{6.29}$$

$$\Sigma_{t,k}^i = \Sigma_{\mathbf{y}}^i + \sum_{n=1}^{N} \alpha_{t,k}^{(n)} (\hat{\mathbf{y}}_{t,k}^{i,(n)} - \hat{\mathbf{y}}_{t,k}^i)(\hat{\mathbf{y}}_{t,k}^{i,(n)} - \hat{\mathbf{y}}_{t,k}^i)^T. \tag{6.30}$$

where $\hat{\mathbf{y}}_{t,k}^{i,(n)}$ is the mapping of particle $\mathbf{x}_{t,k}^{(n)}$ into the measurement space (6.11). Once the gates constructed we can define the set of viable joint associations $\mathbf{\Lambda}_k^i$ using the procedure described in the previous section. Considering the reduced set of events $\mathbf{\Lambda}_k^i$ and approximation (6.28) we can now compute the joint association posterior probabilities in (6.22), from which approximations for the marginal target to measurement association posterior probabilities can be computed according to (6.21). These approximations can, in turn, be used in (6.18) to approximate the target likelihood. Finally, setting the new importance weights to

$$\omega_{t,k}^{(n)} \propto \omega_{t,k-1}^{(n)} \frac{p_t(\mathbf{y}_k|\mathbf{x}_{t,k}^{(n)}) p_t(\mathbf{x}_{t,k}^{(n)}|\mathbf{x}_{t,k-1}^{(n)})}{q_t(\mathbf{x}_{t,k}|\mathbf{x}_{t,k-1}^{(n)}, \mathbf{y}_k)}, \qquad \text{with} \qquad \sum_{n=1}^{N} \omega_{t,k}^{(n)} = 1, \tag{6.31}$$

leads to the sample set $\{\omega_{t,k}^{(n)}, \mathbf{x}_{t,k}^{(n)}\}_{n=1}^N$ being approximately distributed according to the marginal filtering distribution at the current time step $p_t(\mathbf{x}_{t,k}|\mathbf{y}_{1:k})$.

To avoid the *degeneracy problem* we resample independently for each target taking N samples with replacement from the set $\{\mathbf{x}_{t,k}^{(n)}\}_{n=1}^{N}$ if

$$N_{\text{eff}} = \frac{1}{\sum_n (\omega_{t,k}^{(n)})^2} < N_{\text{thr}} \tag{6.32}$$

where the probability to take sample n is $\omega_{t,k}^{(n)}$ and where N_{eff} is the effective number of samples and $N_{\text{thr}} = 2/3N$ is a threshold [37]. The whole procedure is outlined in algorithm 8.

6.5 Simulations

In this section we evaluate the performance of the proposed approach to track multiple ground moving targets constrained to roads. The implemented algorithm is that one base on the parametric model of the clutter measurements, which employs the Poisson probability mass function given by (6.15) with parameter λ_c.

We are interested in tracking slowly manoeuvring targets moving along the road network depicted in figure 6.5. The road network $\Omega_R = (N, R)$ consist in a large collection of nodes N representing the intersections between roads, and a set R of oriented roads. Information such as road sense and traffic flow are also included in the road network. However, to keep a challenging scenario, in the following simulations we set the traffic flow prior to be equally likely to all roads meeting a particular junction, which represent the maximum uncertainty at the junction.

The targets depart from nodes $N9 = (280, -4600)$m, $N2 = (-1480, 3400)$m, and $N22 = (880, 3750)m$ moving along the road network with respective constant speeds of 22, 20, and 18 m/s, and describing the trajectories showed from figure 6.6 a) to c). We model each target motion with the approach presented in algorithm 7, with $\sigma_d = 1$ m and $\sigma_v = 0.5$ m/s. The discretisation time step for the evolution model is set to $T = 2$ s.

Target tracking is performed using bearings-only measurements collected by two ground moving observers with respectives constant speeds of 18 et 13 m/s. The evolution of the observers is modeled using algorithm 7, for which we admit some uncertainty in their position and velocity components given by $\sigma_d = 1$ m and $\sigma_v = 0.1$ m/s. The trajectories described by the observers are depicted in figures 6.6 c). Each observer measures bearings with a precision of $\sigma_{\theta_1} = 2$, and $\sigma_{\theta_2} = 3$, respectively.

This simulation scenario is evaluated for three sets of conditions, with increasingly level of difficulty, shown in table 6.2. For simplicity, we kept the

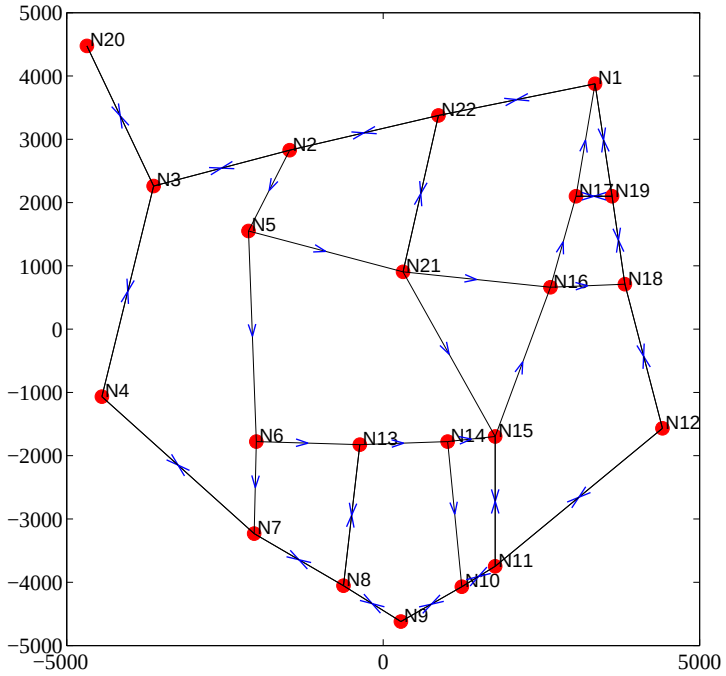

Figure 6.5: Road network example: dots represent the nodes, lines between two nodes are the roads and arrows indicate the sense of the roads.

same target detection probability P_D and the clutter rate λ_c for all targets and observers. Synthetic data is generated for $K = 150$ time steps using the target and sensor models specified above.

	Easy	Medium	Hard
P_D	0.99	0.8	0.6
λ_c	2	3	5

Table 6.2: Values of the target detection P_D and clutter rate λ_c for three different conditions.

For each setting we run the algorithm with an increasingly number of particles, $N = 100, 200, 500, 1000$, and we repeated each experiment 100 times to get a statistical reflection of the behavior of the algorithm. Gating is applied to reduce computation burden. The gate parameter γ is set to 4, for a probability mass of 0.954. Initial particles are proposed around the true initial target states according to a Gaussian distribution. For simplicity the proposal distribution is considered to be the prior distribution of the target

states. At each time step, the state estimate for each target is computed according to the minimum mean square method, given by

$$\hat{\mathbf{x}}_{t,k} = \sum_{n=1}^{N} \omega_{t,k}^{(n)} \mathbf{x}_{t,k}^{(n)}$$

The performance of the multiple ground target tracking algorithm is presented in terms of the root mean square error (RMSE) statistics, given for a single run as

$$\text{RMSE} = \sqrt{\frac{1}{K} \sum_{k=1}^{K} ||\hat{\mathbf{x}}_k^C - \tilde{\mathbf{x}}_k^C||^2}$$

where $\hat{\mathbf{x}}_k^C$ and $\tilde{\mathbf{x}}_k^C$ stand respectively for the estimated multi-target state vector and the true state at time k, given in a cartesian coordinate representation.

The root mean square error statistics are depicted in figure 6.7 for a) the position and b) the velocity components of the multi-target state vector. As expected error decreases with an increase in the number of particles and seems to converge to a fixed value for a number of particles between 600 and 1000. On the other hand, the accuracy on the target state estimates decreases with an increase in the difficulty of the simulation scenario. This is quite logic because increasing the mean number of clutter measurements and decreasing the target detection probability lead to a less informative set of measurements at each time step. However, even in the worst case (hard scenario using 100 particles per target) the mean error accounting for the three targets is about 1000 m, thus, an error per target of approximatively 330m. At a first glance, such an error may seem high, but it must be considered that we are tracking targets using bearings-only measurements in presence of dense clutter and low target detection probabilities. Furthermore, the presence of multiple crossing targets (as is the case of targets 2 and 3 for this simulation) introduces "persistent" or time-correlated interference between the measurements to be assigned to each target. This represent a more challenging aspect in this passive tracking application, because targets do not need to be physically close to each other in order to interfere. They produce false measurements in the azimuth gate, even if they are far away from the target of interest. In such a situation, road network information play a key role, because even if wrong target-to-measurement assignments are persistently done during long periods of time, the detrimental effects to the multiple target position estimation are restricted by the hard constraints imposed by the road network, i.e. by the roads in which the targets are evolving. This fact, can be observed from figures 6.8 to 6.10 where we depict the average trajectories for the three

targets, a) altogether and for each target b), c) and d), obtained from 100 Monte Carlo runs. Notice that targets 2 and 3 cross between nodes N2 and N22, however, the average trajectories corresponding to this segment are constrained to the road segment N2N22. This is, errors are only contained in the direction of the road. For the rest of the average trajectories we note that they are not contained in the road when targets are near road intersections, which is due to the manner in which the target evolution model handles road intersections, see algorithm 7.

6.6 Conclusions

In this chapter we proposed a new approach to incorporate road network information into the state dynamics of slow manoeuvering targets evolving on constrained paths. The approach not only exploits the knowledge of the road segments, but also incorporates specific characteristics usually included in road networks, such as road sense and traffic flow information. We test the proposed approach under a challenging scenario. The scenario consisted in tracking a known number of targets evolving on a road network using bearings-only measurements. The algorithm used for multiple target tracking was the MC-JPDAF, which has been further extended to include arbitrary PMFs of the clutter measurements and to consider different target detection probabilities for each target-observer pair. Simulation results showed a good performance on tracking multiple crossing targets in presence of dense clutter and low target detection probabilities.

Algorithm 8 : MC-JPDAF

1. For $t = 1 \dots M$, $n = 1 \dots N$, generate new samples for the target states

$$\mathbf{x}_{t,k}^{(n)} \sim q_t(\mathbf{x}_{t,k}|\mathbf{x}_{t,k-1}^{(n)}, \mathbf{y}_k).$$

2. For $t = 1 \dots M$, $n = 1 \dots N$, compute and normalize the predictive weights

$$\alpha_{t,k}^{(n)} = \omega_{t,k-1}^{(n)} \frac{p_t(\mathbf{x}_{t,k}^{(n)}|\mathbf{x}_{t,k-1}^{(n)})}{q_t(\mathbf{x}_{t,k}|\mathbf{x}_{t,k-1}^{(n)}, \mathbf{y}_t)}, \qquad \sum_{n=1}^{N} \alpha_{t,k}^{(n)} = 1.$$

3. For $i = 1 \dots N_o$, $t = 1 \dots M$, $j = 1 \dots M^i$, compute the Monte Carlo approximation for the predictive likelihood

$$p_t(\mathbf{y}_{j,k}^i|\mathbf{y}_{1:t-1}) \approx \sum_{n=1}^{N} \alpha_{t,k}^{(n)} p_T^i(\mathbf{y}_{j,k}^i|\mathbf{x}_{t,k}^{(n)}).$$

4. For $i = 1 \dots N_o$, $t = 1 \dots M$, compute gating parameters

$$\hat{\mathbf{y}}_{t,k}^i = \sum_{n=1}^{N} \alpha_{t,k}^{(n)} \hat{\mathbf{y}}_{t,k}^{i,(n)}, \qquad \Sigma_{t,k}^i = \Sigma_{\mathbf{y}}^i + \sum_{n=1}^{N} \alpha_{t,k}^{(n)} (\hat{\mathbf{y}}_{t,k}^{i,(n)} - \hat{\mathbf{y}}_{t,k}^i)(\hat{\mathbf{y}}_{t,k}^{i,(n)} - \hat{\mathbf{y}}_{t,k}^i)^T,$$

and define $\mathbf{\Lambda}_k^i$.

5. For $i = 1 \dots N_o$, $\boldsymbol{\lambda}_k^i \in \mathbf{\Lambda}_k^i$, compute the joint association posterior probability

$$p(\boldsymbol{\lambda}_k^i|\mathbf{y}_{1:k}) \propto p(\boldsymbol{\lambda}_k^i)(V^i)^{-M_C^i} \prod_{j \in \mathcal{I}^i} p_{t(j)}(\mathbf{y}_{j,k}^i|\mathbf{y}_{1:k-1}).$$

6. For $i = 1 \dots N_o$, $t = 1 \dots M$, $j = 0 \dots M^i$, compute the marginal association posterior probability

$$\beta_{j,t}^i = p(r_{j,k}^i = t|\mathbf{y}_{1:k}) = \sum_{\boldsymbol{\lambda}_k^i \in \mathbf{\Lambda}_k^i : r_{j,k}^i = t} p(\boldsymbol{\lambda}_k^i|\mathbf{y}_{1:k})$$

7. For $t = 1 \dots M$, $n = 1 \dots N$, compute the target likelihood

$$p_t(\mathbf{y}_k|\mathbf{x}_{t,k}) = \prod_{i=1}^{N_o} \left[\beta_{0,t}^i + \sum_{j=1}^{M^i} \beta_{j,t}^i p_T^i(y_{j,k}^i|\mathbf{x}_{t,k}) \right]$$

8. For $t = 1 \dots M$, if $N_{\text{eff}} = \frac{1}{\sum_n (\omega_{t,k}^{(n)})^2} < N_{\text{thr}}$ then resample with replacement from the set $\{\mathbf{x}_{t,k}^{(n)}\}_{n=1}^N$ using algorithm 3.

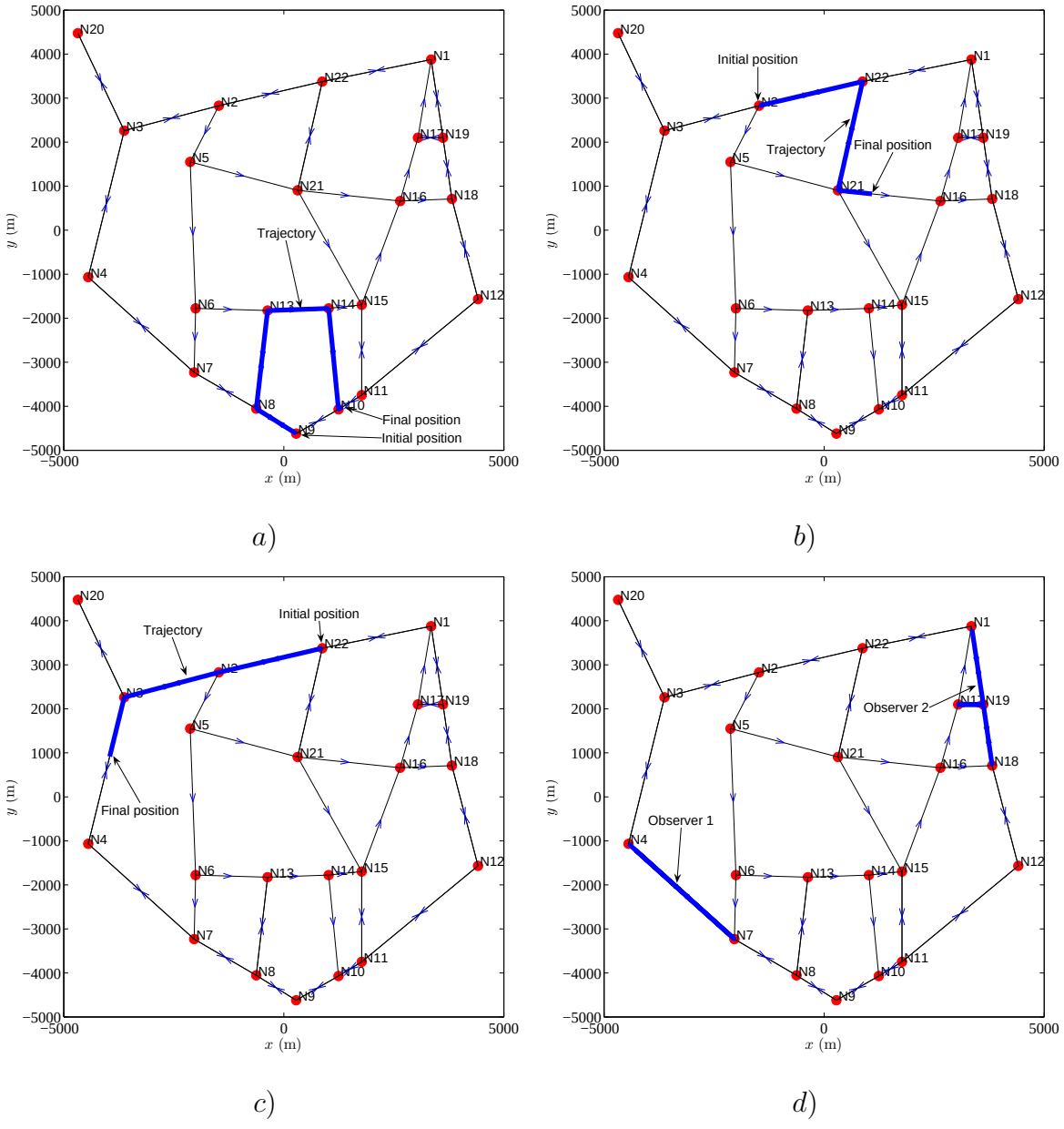

Figure 6.6: Followed trajectories by targets and observers. a) target one b) target two c) target three and d) observers.

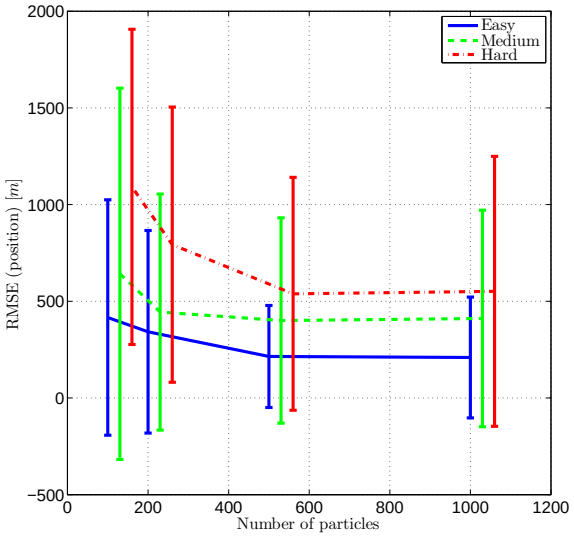

a)

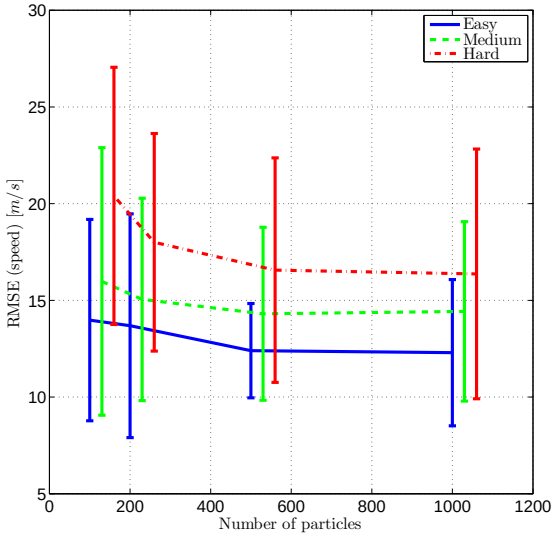

b)

Figure 6.7: RMSE statistics versus number the of particles for a) the position and b) the velocity components of the joint target state vector. Solid line is for the easy scenario ($P_D = 0.99$, $\lambda_c = 2$), dashed line is for the medium scenario ($P_D = 0.8$, $\lambda_c = 3$), and dash-doted line is for the hard scenario ($P_D = 0.6$, $\lambda_c = 5$).

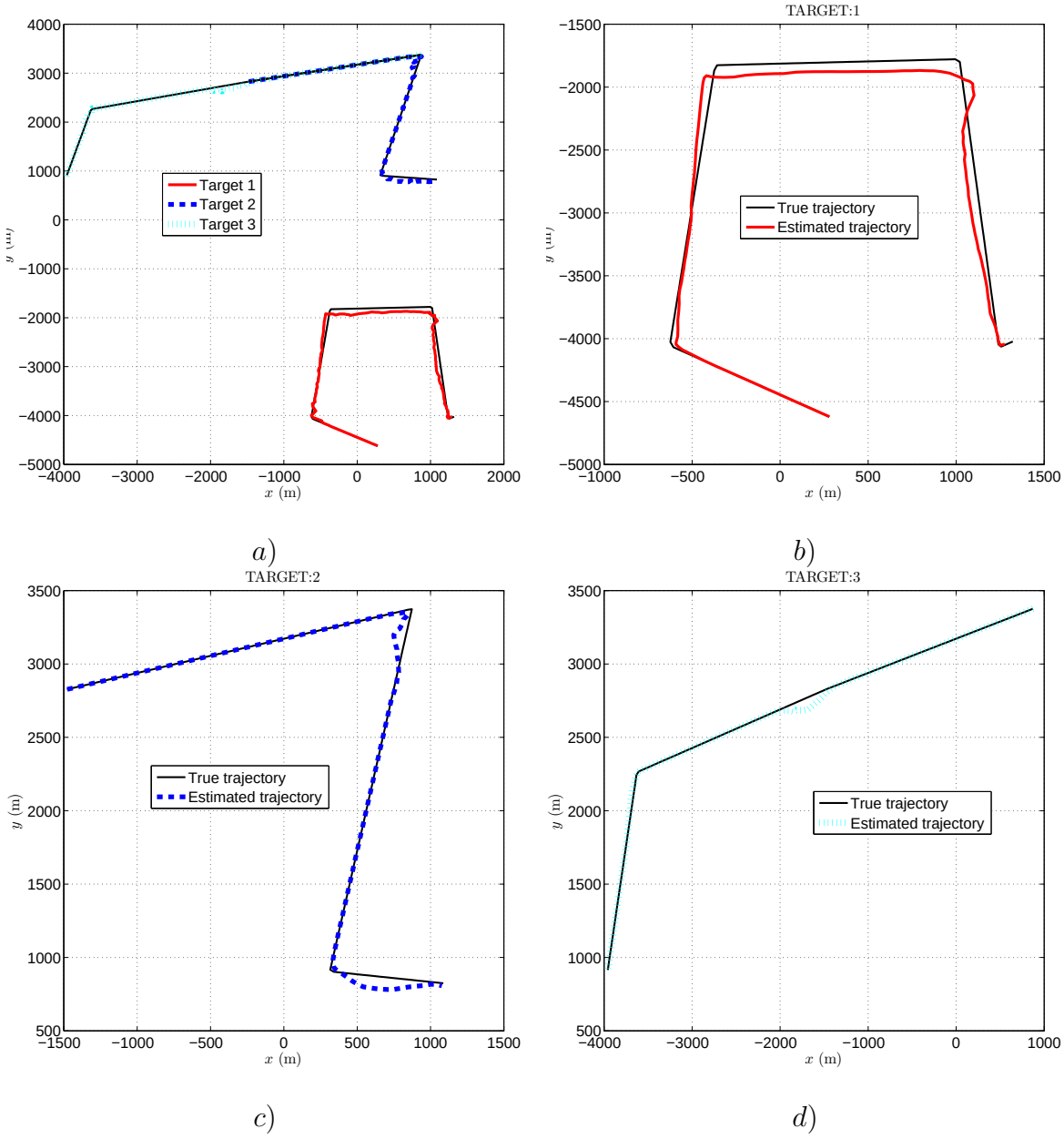

Figure 6.8: Average trajectories obtained from 100 Monte Carlo runs for the easy scenario ($P_D = 0.99$, $\lambda_c = 2$). The three average trajectories are shown altogether in a), while the individual ones for targets 1, 2 and 3 are shown respectively in b), c), and d).

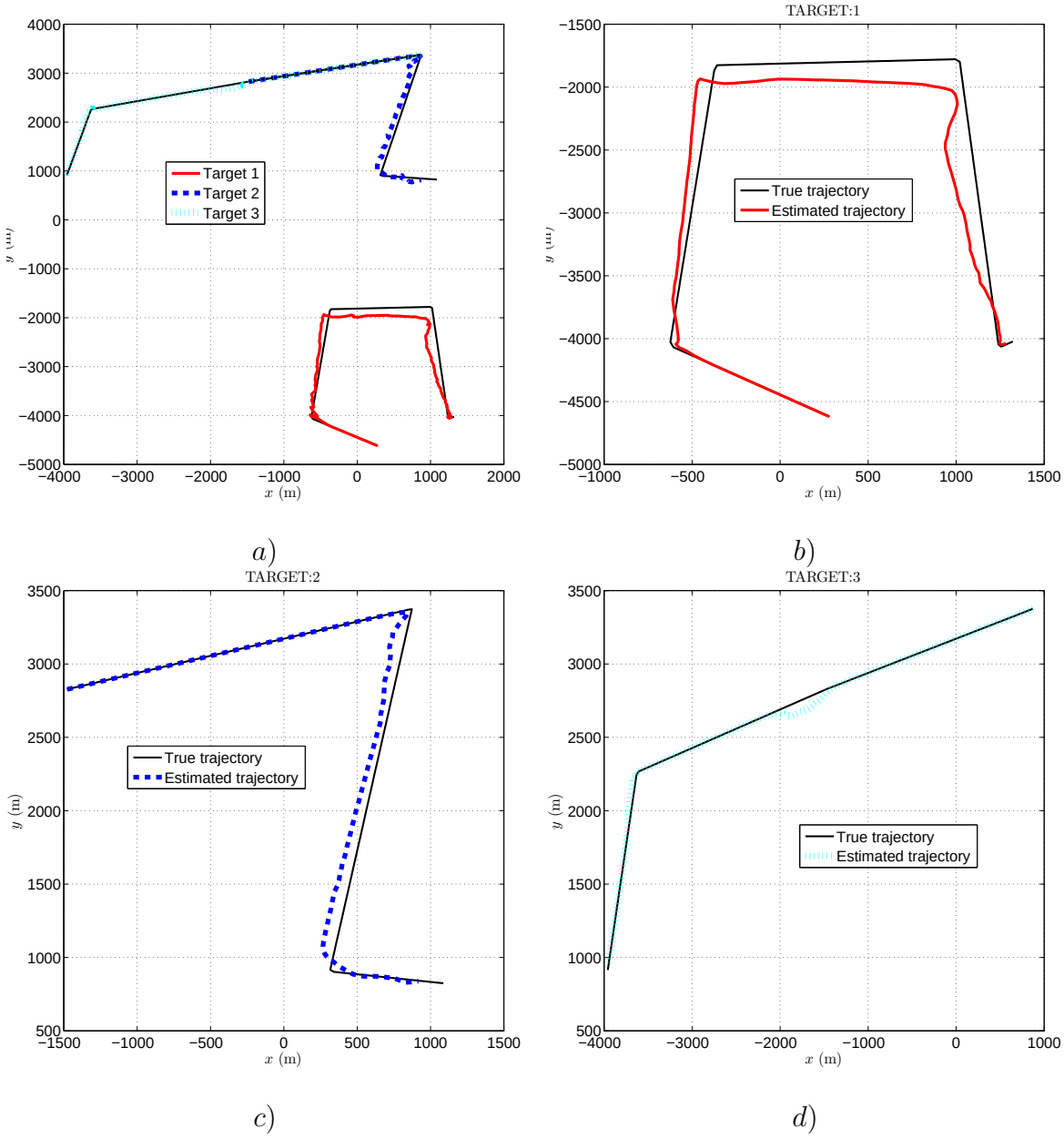

Figure 6.9: Average trajectories obtained from 100 Monte Carlo runs for the medium scenario ($P_D = 0.8$, $\lambda_c = 3$). The three average trajectories are shown altogether in a), while the individual ones for targets 1, 2 and 3 are shown respectively in b), c), and d).

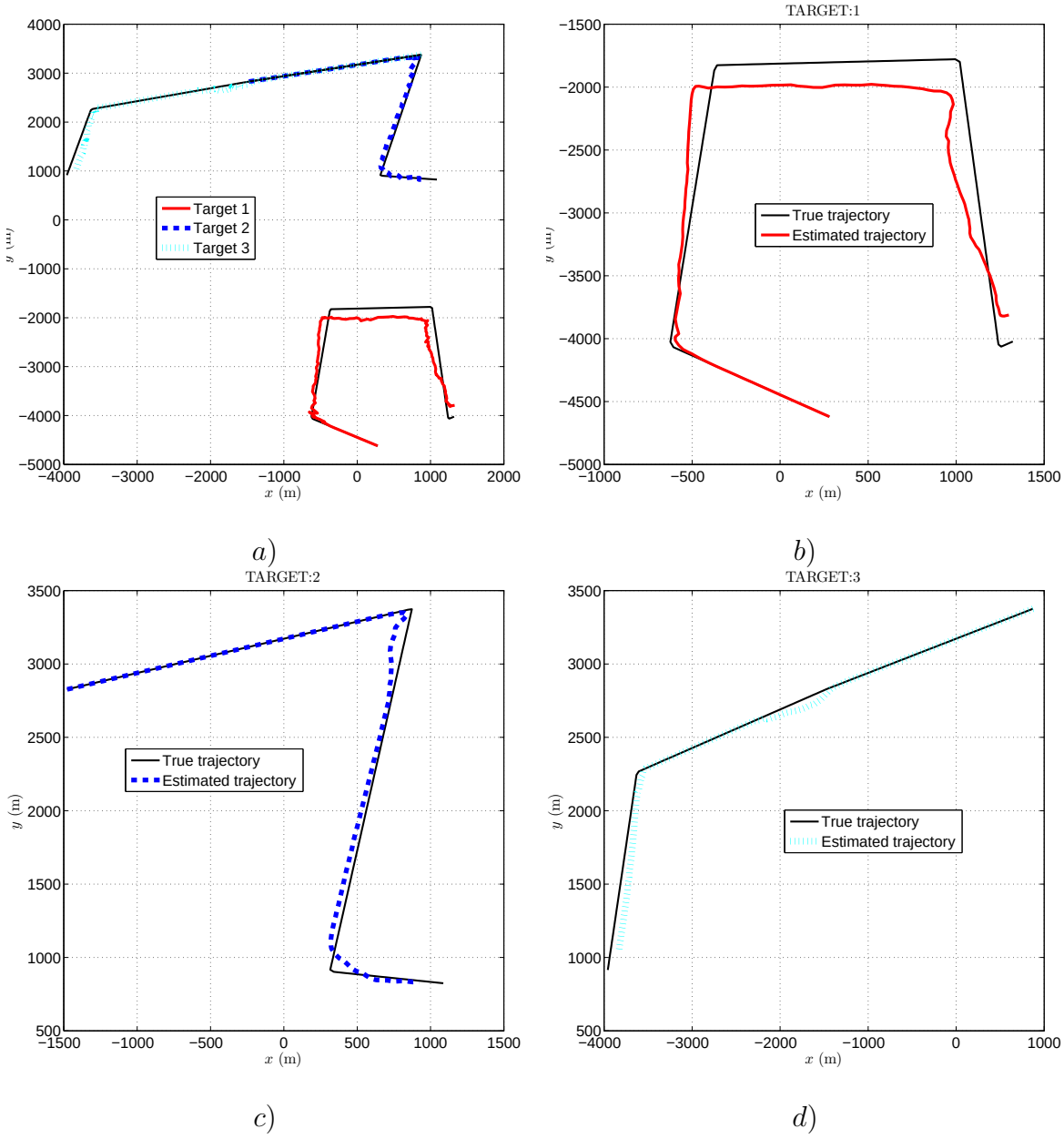

Figure 6.10: Average trajectories obtained from 100 Monte Carlo runs for the hard scenario ($P_D = 0.6$, $\lambda_c = 5$). The three average trajectories are shown altogether in a), while the individual ones for targets 1, 2 and 3 are shown respectively in b), c), and d).

Conclusions of part II

The problem of passive ground target tracking exploiting prior non-standard information, to obtain better estimates of the target state, was treated in this dissertation part. Prior non-standard information consisted in road maps containing a digitalized version of the road network where targets were supposed to be moving. Road networks were modeled as a large collection of roads, each of which may be constituted by several road segments and each road segment was modeled as a straight line between two referenced nodes. Based on this type of road network modeling we proposed two algorithms to track, respectively, a single and multiple ground moving targets using bearings-only measurements in clutter. Each algorithm exploits road maps in a different manner, but in both the recursive estimation of the target state vector is driven by particle filters. In the following we summarized both algorithms:

Single target tracking algorithm : The problem of tracking a single target moving along a road network was considered. Road map information was incorporated into the target state equations using an efficient combination of existing methods; firstly, we constraint the direction of the target velocity vector to be parallel to the direction of the road segment in which the target is supposed to travel. Secondly, the position of the target is constrained using the concept of pseudo-measurement. Finally, the target motion uncertainty was modeled using the directional process noise. Based on the new set of target state equations (those ones including constraints) we proposed a batch-recursive algorithm to track the target. In the batch stage a low complexity procedure based on the maximum-likelihood method computes a raw estimate of the LOS bearing. Such an estimate is used at the recursive stage to initialize a regularized particle filter which recursively estimates a modified polar representation of the target state vector. The proposed batch-recursive algorithm was tested under a challenging simulation scenario, where the target moves along a road network with roads branching and crossing, and the available observations consist in bearing mea-

surements in clutter. Simulation results showed that the proposed algorithm provides accurate state estimates even for low target detection probabilities. Furthermore, it was found that the non-observability issue in bearings only tracking do not represent a problem to the proposed algorithm because of the use of road map information.

Multiple target tracking algorithm : The problem of tracking multiple targets moving along a road network was treated. Road map information was exploited representing the target dynamics for a one-dimension (1D) target motion. Such a 1D modeling permitted to simplify the target kinematics considerably and to relate the tracking filter more closely to the physical reality, since a ground target has one degree of freedom when traveling along roads. Furthermore, two more features were exploited; the direction of the road and the probability to take an specific road while crossing an intersection. Based on this model of the target dynamics and considering the two additional features we track a known number of targets using bearings-only measurements in clutter. The algorithm used for multiple target tracking was the Monte Carlo joint probabilistic data association filter (MC-JPDAF), which was further extended to include arbitrary PMFs of the clutter measurements and to consider different target detection probabilities for each target-observer pair. Simulation results showed that road map information improves accuracy on the target state estimates even in presence of dense clutter and low target detection probabilities. Moreover, the incorporation of the road direction information reduces uncertainty on the measurement-to-target assignment for crossing targets.

Appendices

Appendix E

Constrained dynamic model derivation

This appendix presents the derivation of an expression in the modified polar coordinate system for the relative movement of a target (with constraints on its velocity components) with respect to a maneuvering observer.

E.1 State space, dynamic models, and velocity constraint

Let define the target state vector at time k in the cartesian coordinate system as

$$\mathbf{x}_{t,k} = \begin{bmatrix} x_{t,k} & y_{t,k} & \dot{x}_{t,k} & \dot{y}_{t,k} \end{bmatrix}^T, \tag{E.1}$$

where (x_k, y_k) and $(\dot{x}_k, \dot{y}_k)$ stand respectively for the position and velocity components of the target state vector. Similarly, the state vector of a moving observer is defined at time k as:

$$\mathbf{x}_{o,k} = \begin{bmatrix} x_{o,k} & y_{o,k} & \dot{x}_{o,k} & \dot{y}_{o,k} \end{bmatrix}^T. \tag{E.2}$$

Now, assuming the observer state vector as known it is convenient to define the target state relative to the observer, which gives

$$\mathbf{x}_k = \mathbf{x}_{t,k} - \mathbf{x}_{o,k} = \begin{bmatrix} x_k & y_k & \dot{x}_k & \dot{y}_k \end{bmatrix}^T. \tag{E.3}$$

Dynamic model

It is supposed that a priori information about the target dynamics is available, i.e. it evolves according to the following discrete-time stochastic model:

$$\mathbf{x}_{t,k} = F\mathbf{x}_{t,k-1} + G\epsilon_{k-1}, \tag{E.4}$$

where

$$F = \begin{bmatrix} 1 & 0 & T & 0 \\ 0 & 1 & 0 & T \\ 0 & 0 & 1 & 0 \\ 0 & 0 & 0 & 1 \end{bmatrix} \quad \text{and} \quad G = \begin{bmatrix} T^2/2 & 0 \\ 0 & T^2/2 \\ T & 0 \\ 0 & T \end{bmatrix} \tag{E.5}$$

Here T the sampling time, ϵ_k is the white Gaussian process noise sequence modeling unpredictable target accelerations in x and y directions with covariance matrix $\mathbf{Q}_{xy} = \text{diag}(\sigma_x^2, \sigma_y^2)$, where σ_x^2 and σ_y^2 stand respectively for the noise variances in x and y directions.

On the other hand the observer state dynamic equation is given by

$$\mathbf{x}_{o,k} = F\mathbf{x}_{o,k-1} + \mathbf{u}_{k-1}, \tag{E.6}$$

where $\mathbf{u}_k$ is a deterministic 4×1 vector accounting for the effects of observer accelerations.

Constraint of the target's velocity vector

A target evolving along a road segment s has, according to [10, 60], a constraint on their velocity components imposed by

$$\vec{v}_{t,k} \cdot \vec{n}_s = 0,$$

where $\vec{v}_{t,k} = \begin{bmatrix} \dot{x}_{t,k} & \dot{y}_{t,k} \end{bmatrix}^T$ is the target velocity vector and $\vec{n}_s$ is an orthogonal vector to the road segment s. Writing this constraint in terms of the target velocity components and the straight line parameters gives

$$\dot{y}_{t,k} = m_s \dot{x}_{t,k} \tag{E.7}$$

where m_s is the slope of the road segment s.

Considering a slow movement of the observer with respect to the target's movement, i.e., $|\vec{v}_{t,k}| \gg |\vec{v}_{o,k}|$, where $\vec{v}_{o,k} = \begin{bmatrix} \dot{x}_{o,k} & \dot{y}_{o,k} \end{bmatrix}^T$ stands for the observer velocity vector at time k, then we may write an approximated constraint for the relative velocity components of the state vector (E.3) as

$$\dot{y}_k = m_s \dot{x}_k \tag{E.8}$$

It should be noticed that (E.8) is obtained by considering that the relative velocity vector $\vec{v}_k$ issuing from $\vec{v}_{t,k} - \vec{v}_{o,k}$ has, approximatively, the same direction and magnitude of $\vec{v}_{t,k}$ when the elements of $\vec{v}_{o,k}$ are smaller than those ones of $\vec{v}_{t,k}$. Such an approximation is very helpful in order to obtain tractable relative dynamic models of the target w.r.t to the observer in the modified polar coordinate system, which is addressed in the following sections.

E.2 Relative target dynamics in MP: URM case

Using the noiseless representation of the target dynamics obtained from (E.4), considering an observer in an uniform rectilinear movement (URM), i.e., equation (E.6) with $\mathbf{u}_{k-1} = \mathbf{0}$, and introducing the velocity constraint (E.8), we may write the constrained noiseless relative dynamics of the target w.r.t the observer as follows

$$\begin{aligned} x_{k+1} &= x_k + T\dot{x}_k \\ y_{k+1} &= y_k + Tm_s\dot{x}_k \\ \dot{x}_{k+1} &= \dot{x}_k \\ \dot{y}_{k+1} &= m_s\dot{x}_k \end{aligned}$$

Now, taking the cartesian to MP transformation equations from table 5.1 at time $k+1$ and substituting the above expressions we may obtain

$$\begin{aligned} \theta_{k+1} &= \arctan\left(\frac{y_k + Tm_s\dot{x}_k}{x_k + T\dot{x}_k}\right) \\ \dot{\theta}_{k+1} &= \frac{\dot{x}_k(m_s(x_k + T\dot{x}_k) - (y_k + Tm_s\dot{x}_k))}{(x_k + T\dot{x}_k)^2 + (y_k + Tm_s\dot{x}_k)^2} \\ \xi_{k+1} &= \frac{\dot{x}_k(x_k + T\dot{x}_k + m_s(y_k + Tm_s\dot{x}_k))}{(x_k + T\dot{x}_k)^2 + (y_k + Tm_s\dot{x}_k)^2} \\ r_{k+1} &= \sqrt{(x_k + T\dot{x}_k)^2 + (y_k + Tm_s\dot{x}_k)^2} \end{aligned}$$

Finally, defining

$$\boldsymbol{\chi}_k = \begin{bmatrix} \theta_k & \dot{\theta}_k & \xi_k & r_k \end{bmatrix}^T$$

and substituting the MP to cartesian transformation equations from table 5.1 into the latter expressions we may write the relative noiseless dynamics of a constrained target w.r.t. a non-maneuvering observer as

$$\boldsymbol{\chi}_{k+1} = \boldsymbol{f}_s(\boldsymbol{\chi}_k) \tag{E.9}$$

where

$$\boldsymbol{f}_s(\boldsymbol{\chi}_k) = \begin{bmatrix} \arctan\left(A_k/B_k\right) \\ E_k(m_s B_k - A_k) \\ E_k(B_k + m_s A_k) \\ r_k C_k \end{bmatrix} \tag{E.10}$$

with

$$\begin{aligned} A_k &= \sin\theta_k + m_s T D_k \\ B_k &= \cos\theta_k + T D_k \\ C_k^2 &= A_k^2 + B_k^2 \\ D_k &= \xi_k \cos\theta_k - \dot{\theta}_k \sin\theta_k \\ E_k &= D_k / C_k^2 \end{aligned}$$

E.3 Relative target dynamics in MP: UAM case

Using the noiseless representation of the target dynamics obtained from (E.4), considering an observer in an approximative[1] uniform accelerated movement (UAM), equation (E.6), and introducing the velocity constraint (E.8), we may write the constrained noiseless relative dynamics of the target w.r.t the maneuvering observer as follows

$$\begin{aligned} x_{k+1} &= x_k + T\dot{x}_k \\ y_{k+1} &= y_k + T m_s \dot{x}_k \\ \dot{x}_{k+1} &= \dot{x}_k + T\gamma_x \\ \dot{y}_{k+1} &= m_s \dot{x}_k + T\gamma_y \end{aligned}$$

where (γ_x, γ_y) stand, respectively, for the known observer acceleration components in x and y directions.

Following a similar procedure to that one used in the previous section to obtain the relative dynamics of the target in the MP coordinate system, it can be proved that the noiseless approximative relative dynamics of a constrained target w.r.t. a maneuvering observer in the MP coordinate system may be written as

$$\boldsymbol{\chi}_{k+1} = \boldsymbol{f}_s(\boldsymbol{\chi}_k) - \boldsymbol{\varrho}_k \tag{E.11}$$

[1] In order to make it exact we must consider the appropriate displacement terms for the position resulting from an observer acceleration. However, because the time between samples is considered to be small relative to the time constants of the dynamics, these terms have been neglected as in [58].

where

$$\boldsymbol{\varrho}_k = \frac{T}{r_k C_k^2} \begin{bmatrix} 0 \\ \gamma_y B_k - \gamma_x A_k \\ \gamma_y A_k + \gamma_x B_k \\ 0 \end{bmatrix} \tag{E.12}$$

and $\boldsymbol{f}_s(\boldsymbol{\chi}_k)$ is given by (E.10).

General conclusions and future work

Review of main contributions

This dissertation proposes two tools for localizing and tracking non-cooperative targets. The first tool (part I) consist in a methodology to localize network elements (BS or MS) in wireless communication systems such as GSM and UMTS. Unlike the classical localization problem, where a set of BSs participate in the localization process of an MS, we treat the localization problem from a more general point of view, where the element to localize can be either an MS or a BS and the observer (i.e. that one interested in knowing the position of the network element) could be the MS, the BS or an external agent equipped with the required resources to perform radio measurements or to get them from the network. The proposed methodology is flexible enough to perform localization using the most common radio measurements in wireless communication systems, i.e. TOA, TDOA, AOA, RSS. On the other hand, it is able to cope with typical impairments present in radio measurements such as additive noise, systematic offsets, quantization, presence of multiple spurious measurements due to multipath propagation and NLOS propagation. Two algorithms developed under the proposed methodology support its effectiveness for localizing network elements.

The second tool (part II) consist of two methods to exploit prior road map information in the tracking process of ground targets moving along road networks. Such a terrain-aided tracking problem became important with the introduction of the GMTI radar employed in the Gulf War in 1991, as well as in the context of airport surface traffic management. In both cases, the use of prior terrain information was exploited in the tracker system to yield better target state estimates. Until now, most of the proposed methods to include road map information into the tracker system has been tested under a GMTI radar-type framework, where measurements consist of bearing, range and range rate. This has facilitated the use of state spaces that employ

spatial parameters that are naturally linked with the road constraints. The methods presented in this dissertation are tested in the context of passive tracking, where the only available observations are bearing measurements. This constituted an additional challenge because it is harder to incorporate road map information into a bearings-only tracker, since the spatial position constraints are not immediately translated into regular bearings constraints. Based on the proposed methods to exploit road map information, we proposed two algorithms to track, respectively, a single and a known number of targets using bearing measurements in clutter.

Future directions

There is an important work to do in the context of network element localization in wireless communication systems. In the applications we provided to localize network elements we used a uniform distribution over the space measurement for the NLOS measurements. In other words, we considered the NLOS measurements as outliers, which should be rule-out because it does not provide information about the position of the network element to localize. However, scatterers in a specific environment (rural, semi-urban or urban) may be distributed in a particular way, i.e. the ring of scatterers or the disk of scatterers model [6], producing a particular NLOS propagation. Therefore, NLOS measurements will no longer be uniform distributed and in the event of knowing their distribution, it could be used to exploit the information contained in NLOS measurements for localization purposes. Furthermore, it could also be possible to localize network elements using NLOS measurements only. Hence, the questions to answer are: Which type of distribution should we use to model NLOS measurements? Does the precision of the resulting algorithms will be improved significantly?

In the context of ground target tracking using prior road map information, one of the most interesting problems to be solved is to provide a general methodology to include road map information able to account for on-road and off-road target motion. The algorithms proposed in this dissertation only consider the on-road target motion. Most of the proposed algorithms in recent literature, trying to deal with both forms of target motion, propose state equations which do not fully exploit road map information, i.e. they do not produce target state estimates appertaining to the road network space. This is because, such a modeling would not permit to detect a possible off-road evolution of a target. As a result, such algorithms are able to handle the off-road target motion, but when the target is on-road, road map information is not optimally exploited. Another important issue to be treated is the use of road map information to write explicit constraints permitting to discard

clutter measurements, i.e. the use of traffic flow information imposes all targets to move in one direction, knowledge of this may help to reject clutter that would otherwise bring the target going backward.

Bibliography

[1] *Mobile Station Location Estimation Using The Maximum Likelihood Method in Sector Cell Systems*, vol. 2, Sept. 2002.

[2] V. Aidala and S. Hammel, *Utilization of modified polar coordinates for bearings-only tracking*, Automatic Control, IEEE Transactions on **28** (1983), no. 3, 283–294.

[3] T. Ajdler, I. Kozintsev, R. Lienhart, and M. Vetterli, *Acoustic Source Localization in Distributed Sensor Networks*, Asilomar Conference on Signals, Systems and Computers, Pacific Grove, CA **2** (2004), 1328–1332.

[4] S. Al-Jazzar and Jr. Caffery, J., *Ml and bayesian toa location estimators for nlos environments*, Vehicular Technology Conference, 2002. Proceedings. VTC 2002-Fall. 2002 IEEE 56th, vol. 2, 24-28 Sept. 2002, pp. 1178–1181vol.2.

[5] S. Al-Jazzar, Jr. Caffery, J., and H.-R. You, *A scattering model based approach to nlos mitigation in toa location systems*, Vehicular Technology Conference, 2002. VTC Spring 2002. IEEE 55th, vol. 2, 6-9 May 2002, pp. 861–865vol.2.

[6] Saleh Al-Jazzar, James Caffery, and Heung-Ryeol You, *Scattering-model-based methods for toa location in nlos environments*, IEEE TRANSACTIONS ON VEHICULAR TECHNOLOGY, **26** (2007), 583–593.

[7] M.S. Arulampalam, S. Maskell, N. Gordon, and T. Clapp, *A tutorial on particle filters for online nonlinear/non-gaussian bayesian tracking*, Signal Processing, IEEE Transactions on [see also Acoustics, Speech, and Signal Processing, IEEE Transactions on] **50** (2002), no. 2, 174–188.

[8] Y. Bar-Shalom, T. Kirubarajan, and X. Lin, *Probabilistic data association techniques for target tracking with applications to sonar, radar and eo sensors*, Aerospace and Electronic Systems Magazine, IEEE **20** (2005), no. 8, 37–56.

[9] Yaakov Bar-Shalom and Thomas E. Fortmann, *Tracking and data association*, vol. 179, 1988.

[10] K. Benameur, B. Pannetier, and V. Nimier, *A comparative study on the use of road network information in gmti tracking*, Information Fusion, 2005 8th International Conference on, vol. 1, 25-28 July 2005, p. 8pp.

[11] O. Besson, F. Vincent, P. Stoica, and A.B. Gershman, *Approximate maximum likelihood doa estimation in multiplicative noise environments*, Sensor Array and Multichannel Signal Processing Workshop. 2000. Proceedings of the 2000 IEEE, 16-17 March 2000, pp. 332–336.

[12] Thomas Bréhard, *Estimation séquentielle et analyse de performances pour un problème de filtrage non linéaire partiellement observé. Application à la trajectographie par mesure d'angles*, Ph.D. thesis, Université de Rennes I, 2005.

[13] J.J. Caffery and G.L. Stuber, *Overview of radiolocation in CDMA cellular systems*, IEEE Communications Magazine **36** (1998), 38 – 45.

[14] J.J. Caffery and G.L. Stuber, *Subscriber location in cdma cellular networks*, IEEE Trans. on Vehicular technology **47** (1998), 406–416.

[15] Olivier Cappé, Simon J. Godsill, and E. Moulines, *An Overview of Existing Methods and Recent Advances in Sequential Monte Carlo*, Proceedings of the IEEE **95** (2007), 899 – 924.

[16] Olivier Cappé, Eric Moulines, and Tobias Rydén, *Inference in Hidden Markov Models*, Springer Series in Statistics, 2005.

[17] G. Casella and R. L. Berger, *Statistical inference*, 2ed ed., Duxbury Advanced Series, 2nd ed., 2002.

[18] Nadir Castañeda, Maurice Charbit, and Eric Moulines, *Source localization from quantized time of arrival measurements*, International Conference on Acoustics, Speech and Signal Processing, 2006. **4** (2006), IV933–IV936.

[19] N. Castaneda, M. Charbit, and E. Moulines, *A batch-recursive algorithm for passive ground target tracking*, GRETSI (Troyes, France), Sep. 2007.

[20] ———, *A new approach for mobile localization in multipath scenarios*, Communications, 2007. ICC '07. IEEE International Conference on, 24-28 June 2007, pp. 4680–4685.

[21] ———, *A New Bearings-Only Tracking Algorithm for Ground Moving Targets Constrained to Roads*, IEEE Workshop on Signal Processing Advances in Wireless Communications (Helsinki, Finland), Jun. 2007.

[22] V. Cevher, R. Velmurugan, and J.H. McClellan, *Multi target direction-of-arrival tracking using road priors*, Aerospace Conference, 2006 IEEE, 04-11 March 2006, pp. 1–9.

[23] Chee-Yee Chong, D. Garren, and T.P. Grayson, *Ground target tracking-a historical perspective*, Aerospace Conference Proceedings, 2000 IEEE, vol. 3, 18-25 March 2000, pp. 433–448vol.3.

[24] Li Cong and Weihua Zhuang, *Hybrid tdoa/aoa mobile user location for wideband cdma cellular systems*, IEEE Transactions on Wireless Communications **1** (2002), 439 – 447.

[25] M. Rose Conrad and M. Dangle Kurt, *Precise bearings only geolocation in systems with large measurements bias errors*, US Patent, No. 383669, June 1996.

[26] A. P. Dempster, N. M. Laird, and D. B. Rubin, *Maximum Likelihood from Incomplete Data via the EM Algorithm*, Journal of Royal Statistical Society : series B **no. 39** (1977), 1–38.

[27] C. Drane, M. Macnaughtan, and C. Scott, *Positioning gsm telephones.*, IEEE Commun. Mag. **36** (1998), 46–54.

[28] V. Enescu and Sahli H., *Recursive filtering approach to ms locating using quantized toa measurements*, 3G Mobile Communication Technologies, 2001 (2001), no. 477, 206–210.

[29] ETSI., *Digital cellular telecommunications system (phase 2); radio subsystem synchronization (ets 300 579).*, ETSI, Sophia Antipolis - France.

[30] A. Farina, L. Ferranti, and G. Golino, *Constrained tracking filters for A-SMGCS*, Proceedings of the Sixth International Conference of Information Fusion., vol. 1, 2003, pp. 414 – 421.

[31] Peter Gaal and Samir Soliman, *Base station time calibration using position measurement data sent by mobile stations during regular position location sessions*, US Patent, No. 10034941, February 2006.

[32] S. Gattein, B. Pannetier, and P. Vannoorenberghe, *Analysis and integration of road projection methods for multiple ground target tracking*, Information Fusion, 2005 8th International Conference on, vol. 1, 25-28 July 2005, p. 8pp.

[33] J. E. Gentle, *Random number generation and monte carlo methods*, second edition ed., Springer, 2003.

[34] Jean Dickinson Gibbons and Subhabrata Chakraborti, *Nonparametric statistical inference*, 4 ed., CRC; 4 edition, May 2003.

[35] N.J. Gordon, D.J. Salmond, and A.F.M. Smith, *Novel approach to nonlinear/non-Gaussian Bayesian state estimation*, IEE Proceedings F Radar and Signal Processing **140** (1993), 107 – 113.

[36] Sun Guolin, Chen Jie, and and Liu-K.J.R. Wei, Guo, *Signal processing techniques in network-aided positioning: a survey of state-of-the-art positioning designs*, IEEE Signal Processing Magazine **22** (2005), 12 – 23.

[37] F. Gustafsson, F. Gunnarsson, N. Bergman, U. Forssell, J. Jansson, R. Karlsson, and P.-J. Nordlund, *Particle filters for positioning, navigation, and tracking*, IEEE Transactions on Signal Processing **50** (2002), 425 – 437.

[38] Fredrik Gustafsson and Fredrik Gunnarsson, *Mobile Positioning Using Wireless Networks; possibilities and fundamental limitations based on available wireless network measurements*, IEEE Signal Processing Magazine (2005), 41–53.

[39] J.G. Herrero, J.A. Besada Portas, and J.R. Casar Corredera, *Use of map information for tracking targets on airport surface*, IEEE Transactions on Aerospace and Electronic Systems **39** (2003), 675 – 693.

[40] J. James, Jr. Caffery, and L. Stuber Gordon, *Overview of Radiolocation in CDMA Cellular Systems*, IEEE Communications Magazine **36** (1998), 38 – 45.

[41] Z.M. Kassas, U. Ozguner, and J. Layne, *Out-of-surveillance target state estimation: a combined hospitability and synthetic inclination approach*, Decision and Control, 2004. CDC. 43rd IEEE Conference on, vol. 1, 14-17 Dec. 2004, pp. 710–715Vol.1.

[42] K. Kastella and C. Kreucher, *Multiple model nonlinear filtering for low signal ground target applications*, Aerospace and Electronic Systems, IEEE Transactions on **41** (2005), no. 2, 549–564.

[43] Steven M. Kay, *Fundamentals of Statistical Signal Processing: Estimation Theory*, Prentice Hall, 1993.

[44] T. Kirubarajan, Y. Bar-Shalom, K.R. Pattipati, and I. Kadar, *Ground target tracking with variable structure imm estimator*, Aerospace and Electronic Systems, IEEE Transactions on **36** (2000), no. 1, 26–46.

[45] T. Kirubarajan, Y. Bar-Shalom, K.R. Pattipati, I. Kadar, B. Abrams, and E. Eadan, *Tracking ground targets with road constraints using an imm estimator*, Aerospace Conference, 1998. Proceedings., IEEE, vol. 5, 21-28 March 1998, pp. 5–12vol.5.

[46] T. Kirubarajan, Y. Bar-Sralom, and D. Lerro, *Bearings-only tracking of maneuvering targets using a batch-recursive estimator*, Aerospace and Electronic Systems, IEEE Transactions on **37** (2001), no. 3, 770–780.

[47] Chang Kuo-Chu and Y. Bar-Shalom, *Joint probabilistic data association for multitarget tracking with possibly unresolved measurements and maneuvers*, IEEE Transactions on Automatic Control **9** (1984), 585 – 594.

[48] K. Lange, *A Gradient Algorithm Locally Equivalent to the EM Algorithm*, Journal of Royal Statistical Society : series B **no. 2** (1995), 425–437.

[49] Kenneth Lange, *Optimization*, Springer-Verlag, 2004.

[50] K.W. Lee, W.S. Wijesoma, and J. Ibanez-Guzman, *Map aided slam in neighbourhood environments*, Intelligent Vehicles Symposium, 2004 IEEE, 14-17 June 2004, pp. 836–841.

[51] M. McGuire, *Location of mobile terminals with quantized measurements*, Personal, Indoor and Mobile Radio Communications, 2005. PIMRC 2005. IEEE 16th International Symposium on, vol. 3, 11-14 Sept. 2005, pp. 2045–2049Vol.3.

[52] M. McGuire and K. Plataniotis, *Estimating position of mobile terminal from path loss measurements with survey data*, Wireless Communications and Mobile Computing **3** (2003), no. 1, 51–62.

[53] M. McGuire, K.N. Plataniotis, and A.N. Venetsanopoulos, *Location of mobile terminals using time measurements and survey points*, Communications, Computers and signal Processing, 2001. PACRIM. 2001 IEEE Pacific Rim Conference on, vol. 2, 26-28 Aug. 2001, pp. 635–638vol.2.

[54] M. McGuire, K.N. Plataniotis, and A.N. Venetsanopoulos, *Data fusion of power and time measurements for mobile terminal location*, IEEE Transactions on Mobile Computing **4** (2005), 142 – 153.

[55] Geoffrey McLachlan and Thriyambakam Krishnan, *The em algorithm and extensions*, John Wiley & Sons, New York, 1996.

[56] Christian Musso, Nadia Oudjane, and François Le Gland, *Improving regularized particle filters, in sequential monte carlo methods in practice*, Springer-Verlag, New York, 2001.

[57] S.C. Nardone and V.J. Aidala, *Observability criteria for bearings-only tracking.*, IEEE Transactions on Aerospace and Electronic Systems (1981), 162–166.

[58] S.C. Nardone and M.L. Graham, *A closed-form solution to bearings-only target motion analysis*, Oceanic Engineering, IEEE Journal of **22** (1997), no. 1, 168–178.

[59] Slobodan Pajic and Kevin A. Clements, *Power System State estimation via Globally Convergent Methods*, IEEE Transactions on Power Systems **20** (2005), no. 4, 1683–1689.

[60] B. Pannetier, K. Benameur, V. Nimier, and M. Rombaut, *Vs-imm using road map information for a ground target tracking*, Information Fusion, 2005 8th International Conference on, vol. 1, 25-28 July 2005, p. 8pp.

[61] B. Pannetier, V. Nimier, and M. Rombaut, *Multiple ground target tracking with a gmti sensor*, Multisensor Fusion and Integration for Intelligent Systems, 2006 IEEE International Conference on, Sept. 2006, pp. 230–236.

[62] M. Pent, M.A. Spirito, and E. Turco, *Method for positioning gsm mobile stations using absolute time delay measurements*, Electronics Leters **33** (1997), no. 24, 2019–2020.

[63] Hongfeng Qin, Jianguo Huang, and Qunfei Zhang, *A novel joint estimator of direction-of-arrival and time-delay for multiple source localization*, IEEE Int. Conf. Neural Networks & Signal Processing (2003), 1294–1297.

[64] J. Riba and A. Urruela, *A non-line-of-sight mitigation technique based on ml-detection*, Acoustics, Speech, and Signal Processing, 2004. Proceedings. (ICASSP '04). IEEE International Conference on, vol. 2, 17-21 May 2004, pp. ii–153–6vol.2.

[65] Branco Ristic, Sanjeev Arulampalam, and Neil Gordon, *Beyond the kalman filter: Particle filters for tracking applications*, 2004.

[66] X. Rong Li and V. Jilkov, *A survey of maneuvering target tracking part I: dynamics models*, IEEE transactions on Aerospace and Electronic Systems **39** (2003), no. 4, 1333–1364.

[67] David Salmond, Martin Clark, Richard Vinter, and Simon Godsill, *Ground target modelling, tracking and prediction with road networks*, Information Fusion, 2007 10th International Conference on, 9-12 July 2007, pp. 1–8.

[68] A.H. Sayed, A. Tarighat, and N. Khajehnouri, *Network-based wireless location: challenges faced in developing techniques for accurate wireless location information*, IEEE Signal Processing Magazine **22** (2005), 24 – 40.

[69] Mark J. Schervish, *Theory of statistics*, Springer, 1995.

[70] D. Schulz, W. Burgard, D. Fox, and A.B. Cremers, *Tracking multiple moving targets with a mobile robot using particle filters and statistical data association*, Proceedings of the IEEE International Conference on Robotics and Automation, vol. 2, 2001, pp. 1665 – 1670.

[71] M. Silventoinen and T. Rantalainen, *Mobile Station Locating in GSM*, Wireless Communications System Symposium, IEEE (1995), 53–59.

[72] M.I. Silventoinen and T. Rantalainen, *Mobile station emergency locating in gsm*, IEEE International Conference on Personal Wireless Communications (1996), 232 – 238.

[73] A. Sinha, T. Kirubarajan, and Y. Bar-Shalom, *Maximum likelihood angle extractor for two closely spaced targets*, Radar Conference, 2001. Proceedings of the 2001 IEEE, 1-3 May 2001, pp. 345–350.

[74] M.A. Spirito, *Mobile station location with heterogeneous data*, IEEE Vehicular Technology Conference **4** (2000), 1583 – 1589.

[75] M.A. Spirito and A.G. Mattioli, *Preliminary experimental results of a gsm mobile phones positioning system based on timing advance*, Veh. Technol. Conf. **4** (1999), 2072–2076.

[76] P. Stoica and A. Nehorai, *Music, maximum likelihood, and the cramer-rao bound*, IEEE Transactions on Acoustics, Speech and Signal Processing **37** (1989), no. 5, 720–741.

[77] Niklas Svenzen, *Real time implementation of map aided positioning using a bayesian approach*, Master's thesis, Linköpings Universitet, 2002.

[78] Zhijun Tang and U. Ozguner, *Pf-hmap: A target track maintenance approach for mobile sensor platforms with intermittent and regional measurements*, Decision and Control, 2006 45th IEEE Conference on, 13-15 Dec. 2006, pp. 6757–6762.

[79] Chen Tsung-Yu, Chiu Chien-Ching, and Tu Ting-Chieh, *Mixing and combining with aoa and toa for the enhanced accuracy of mobile location*, Personal Mobile Communications Conference, no. 492, April 2003, pp. 276 – 280.

[80] A.-J. van der Veen, M.C. Vanderveen, and A.J. Paulraj, *Joint angle and delay estimation using shift-invariance properties*, IEEE Signal Processing Letters **4** (1997), 142 – 145.

[81] Michaela C. Vanderveen, *Estimation of parametric channel models in wireless communication networks*, Ph.D. thesis, Stanford University, 1997.

[82] Michaela C. Vanderveen, Constantinos B. Papadias, and Arogyaswami Paulraj, *Joint angle and delay estimation (jade) for multipath signals arriving at an antenna array.*, IEEE Communications Letters **1** (1997), no. 1.

[83] S. Venkatraman and J. Caffery, *A statistical approach to non-line-of-sight BS identification*, International Symposium on Wireless Personal Multimedia Communications **1** (2002), 296 – 300.

[84] S. Venkatraman and Jr. Caffery, J., *Hybrid toa/aoa techniques for mobile location in non-line-of-sight environments*, Wireless Communications and Networking Conference, 2004. WCNC. 2004 IEEE, vol. 1, 21-25 March 2004, pp. 274–278Vol.1.

[85] S. Venkatraman, Jr. Caffery, J., and H.-R. You, *Location using los range estimation in nlos environments*, Vehicular Technology Conference, 2002. VTC Spring 2002. IEEE 55th, vol. 2, 6-9 May 2002, pp. 856–860vol.2.

[86] Saipradeep Venkatraman, James Caffery, and HeungRyeol You, *A Novel ToA Location Algorithm Using LoS Range Estimation for NLoS Environments*, IEEE Transactions on Vehicular Technology **53** (2004), no. 5, 1515–1524.

[87] J. Vermaak, S.J. Gogsill, and P. Perez, *Monte carlo filtering for multitarget tracking and data association*, IEEE Transactions on aerospace and electronic systems **41** (2005), no. 1, 309–332.

[88] G. R. Walsh, *Methods of optimization*, John Wiley & Sons, London, 1975.

[89] Wei Wang, Ji-Yan Huang, Qun Wan, and Wan-Lin Yang, *Location of mobile terminals based on ls-svm with survey points in nlos environment*, Telecommunications, 2007. ConTel 2007. 9th International Conference on, 13-15 June 2007, pp. 307–310.

[90] Sung-Shik Woo, Heung-Ryeol You, and Jong-Seog Koh, *The nlos mitigation technique for position location using is-95 cdma networks*, Vehicular Technology Conference, 2000. IEEE VTS-Fall VTC 2000. 52nd, vol. 6, 24-28 Sept. 2000, pp. 2556–2560vol.6.

[91] C. F. J. Wu, *On the convergence properties of the em algorithm*, Ann. Statist. **11** (1983), 95–103.

[92] Dongdong Wu, Tongyu Zhu, Weifeng Lv, and Xin Gao, *A heuristic map-matching algorithm by using vector-based recognition*, Computing in the Global Information Technology, 2007. ICCGI 2007. International Multi-Conference on, March 2007, pp. 18–18.

[93] M.P. Wylie-Green and S.S. Wang, *Observed time difference (otd) estimation for mobile positioning in is-136 in the presence of bts clock drift*, IEEE Vehicular Technology Conference **4** (2001), 2677 – 2681.

[94] Li Xiong, *A selective model to suppress nlos signals in angle-of-arrival (aoa) location estimation*, IEEE International Symposium on Personal, Indoor and Mobile Radio Communications **1** (1998), 461 – 465.

[95] C. Yang, M. Bakich, and E. Blasch, *Nonlinear constrained tracking of targets on roads*, Information Fusion, 2005 8th International Conference on, vol. 1, 25-28 July 2005, p. 8pp.

[96] George P. Yost and Panchapakesan Shankari, *Errors in Automatic Location Identification Using Timing Advance.*, Proceedings of 1998 IEEE Vehicular Technology Conference, Canada (1998), 1955–1958.

[97] George P. Yost and Panchapakesan. Shankari, *Improvement in estimation of time of arrival (TOA) from timing advance (TA)*, International Conference on Universal Personal Communications **2** (1998), 1367–1372.

[98] Chen Yung-Fang and Yen Szu-Lung, *Smart antenna with joint angle and delay estimation for the geolocalization, smart uplink and downlink beamforming*, IEEE ICSP **1** (2002), 393 – 397.